ABSTRACT

Title of Dissertation:	THE REDOX HISTORY OF THE EARTH'S MANTLE: EVIDENCE FROM ULTRAMAFIC LAVAS
	Robert William Nicklas, Doctor of Philosophy in Geology, 2019
Dissertation directed by:	Research Scientist Dr. Igor S. Puchtel, Department of Geology

In order to determine the evolution of the redox state of the mantle, the oxygen fugacities of sixteen mantle-derived komatiitic and picritic systems, ranging in age from 3.55 Ga to present day, were determined using the redox-sensitive partitioning of V between olivine and komatiitic/picritic magma, a method refined by this study. The oxygen fugacity data for the studied systems was determined to reflect that of their respective mantle source regions. The dataset defines a well-constrained trend indicating an increase in oxygen fugacity of the bulk convecting mantle of 1.33±0.43 ΔFMQ log units from 3.48 to 1.87 Ga, and nearly constant oxygen fugacity from 1.87 Ga to the present. The oxygen fugacity data for the 3.55 Ga Schapenburg komatiites, the mantle source region of which was shown to have been isolated from mantle convection within the first 30 Ma of the Solar System history, plot well above the trend defined by the data for the contemporaneous lavas. This anamolous data point likely reflects preservation of early-formed magma ocean redox heterogeneities until at least the Paleoarchean.

The observed increase in the oxygen fugacity of the mantle requires admixture of a likely geochemically detectable amount of oxidized material. Three mechanisms were considered to account for the observed change in mantle redox state. The first two mechanisms: recycling of altered oceanic crust and venting of oxygen from the core due to inner core crystallization, were found to be unfeasible due to the large mass of recycled crust required, and the likely young age of the inner core, respectively. The third accessible mantle oxidation mechanism: convection-driven homogenization of an initially redox-heterogeneous mantle, is the most likely given available geochemical constraints. The new data presented here provide evidence for the mantle having triggered the Great Oxidation Event at ~2.4 Ga. We have additionally determined the Os isotopic and HSE systematics of 89 Ma komatiites from Gorgona Island, Colombia. The subset of these Gorgona samples that were also analyzed for oxygen fugacity shows BSE-like Os isotopes and HSE abundances in their mantle source, showing that their oxygen fugacity is likely representative of the mantle at 89 Ma.

THE REDOX HISTORY OF THE EARTH'S MANTLE: EVIDENCE FROM ULTRAMAFIC LAVAS

by

Robert William Nicklas

Dissertation submitted to the Faculty of the Graduate School of the
University of Maryland, College Park, in partial fulfillment
of the requirements for the degree of
Doctor of Philosophy in
Geology
2019

Advisory Committee:
Professor Richard J. Walker, Chair
Research Scientist Igor S. Puchtel
Associate Research Scientist Richard D. Ash
Associate Professor Sarah Penniston-Dorland
Professor James Farquhar
Professor Alice Mignerey (Dean's Representative)

© Copyright by
Robert William Nicklas
2019

Foreword

This dissertation contains substantial material that has been previously published in peer-reviewed journals. Chapters 2, 3 and 4 were all previously published and principally written by the author of this dissertation. Inclusion of these publications in this dissertation has been approved by the doctoral committee, who certify that the student was the primary author of all included publications.

Dedication

To my mother and father and to Martin

Acknowledgements

Firstly, I would like to acknowledge the careful mentorship and endless support of my advisor, Dr. Igor S. Puchtel. I am grateful to call him mentor, colleague, and friend. Additionally, I have benefited from the academic and social support of numerous members of the UMD Isotope Geochemistry Lab. I have also been immensely benefited from the mass spectrometry skills and career advice of Dr. Richard Ash, who has been instrumental to all my data gathering efforts. A large amount of the HSE and Os data in Chapter 5 was gathered by Kyle Ludwig during the course of his senior thesis at UMD, and his work is gratefully acknowledged. This study utilized my advisor's komatiite sample collection that he assembled over the 35 years of his scientific career. We also received additional komatiite and picrite samples from Drs. Eero Hanski, Alan Brandon, Alexander Samsonov, Pedro Waterton, Graham Pearson, Euan Nisbet, Matt Jackson and the Smithsonian National Museum of Natural History. Dr. Hanski is also thanked for his guidance during the fieldwork in Finland in the summer of 2016. Drs. Ariel Anbar and Christy Till are thanked for their advice and support of the FESD group studying the GOE. Finally, thanks to my family that have made this journey ever so much smoother, including my parents Randy and Lisa Nicklas, my brothers Paul and Tommy Nicklas, to my boyfriend Martin Molina Fructuoso, and friends John Cooke, Erwan Michard, Joe Schools, Scott Wipperfurth, Al Greaney, Angela Marusiak, Connor Hilton, Kayleigh Harvey, Shahan Haq, Daniel Eldridge and many others, I offer my sincerest thanks. My time at UMD has been made so much better by you all.

Table of Contents

List of Figures:

List of Tables:

Chapter 1: Introduction and Goals

1.1. Introduction

1.2. Background

1.2.1 The Great Oxidation Event (GOE)

1.2.2 Hadean Mantle Oxidation

1.2.3 Proxies for Mantle fO_2

1.2.4 Highly Siderophile Elements (HSEs) and the Re-Os Isotope System in Komatiites

1.3. Research Goals

1.1. Introduction

Oxygen fugacity (fO_2) is a fundamental intensive variable in igneous systems, along with such variables as temperature, pressure, and volatile content. It is perhaps best understood as the amount of molecular oxygen (O_2) that would be in equilibrium with a system at a given temperature and pressure, if that system were to be at equilibrium. Like all equilibria, oxygen fugacity is affected by temperature and pressure and is, thus, not often quoted as an absolute value. Instead, it is normally expressed relative to a mineral assemblage buffer, such as the nickel-nickel oxide (NNO) buffer (**1**), the fayalite-magnetite-quartz (FMQ) buffer (**2**), or the iron-wüstite (IW) buffer (**3**).

(1) $2Ni + O_2 \rightarrow 2NiO$

(2) $3Fe_2SiO_4 + O_2 \rightarrow 2Fe_3O_4 + SiO_2$

(3) $2Fe + O_2 \rightarrow 2FeO$

Oxygen fugacity in natural systems, from chondrites to mantle rocks to surface samples, varies by ~20 orders of magnitude, so quoting fO_2 as log units relative to a buffer has become a common practice (e.g., ΔNNO, ΔFMQ, ΔIW units). Oxygen fugacity controls the behavior of redox sensitive elements, such as Fe, Cr, V, and Mo, and the speciation of volcanic gases, such as H_2S, SO_2, CO_2, CO and CH_4. Like temperature and pressure, oxygen fugacity is thought to vary as a function of depth within the mantle. This variation is caused by a series of pressure-driven equilibrium reactions; a review of oxygen fugacity as a function of mantle depth is found in Frost and McCammon (2008).

The oxygen fugacity of the mantle is known to have increased by ~4 log units between core formation and the earliest rock record (Frost et al., 2013). Several studies have attempted to correlate mantle fO_2 with major changes in the oxidation state of the atmosphere, but none have succeeded in resolving the change in average mantle fO_2 to better than 1.0 log units and all concluded that mantle fO_2 has remained constant since ~4.3 Ga e (Canil, 1997; Canil and Fedortchouk, 2001; Delano, 2001; Li and

Lee, 2004; Trail et al. 2011; Rollinson et al. 2017) . This study has largely been motivated by the pioneering work of Kasting et al. (1993) and Holland (2002), who hypothesized that changes in mantle redox can control the oxidation state of the atmosphere.

Lavas from plumes or spreading centers are significantly more reduced than those from arc environments (Carmichael, 1991; Parkinson and Arcelus, 1999) and, thus, the present day uppermost mantle is heterogeneous with respect to fO_2. This study develops, applies and refines a method using ultramafic and mafic volcanic rocks that aims to constrain the bulk mantle fO_2 to within 0.3 log units, and attempts to correlate changes in mantle fO_2 with major events in Earth history. We succeed in showing that mantle fO_2 has increased by ~1.3 log units from 3.48 to 1.87 Ga, and has remained nearly constant since then.

1.2. Background

1.2.1. The Great Oxidation Event (GOE)

The Archean-Proterozoic boundary is marked by one of the most profound changes in the Earth's surficial environment: the irreversible rise of molecular oxygen in the atmosphere, known as the Great Oxidation Event (GOE). Between 2.4 and 2.3 Ga, the concentration of molecular oxygen in the Earth's atmosphere rose dramatically from below 10^{-5} atm to approximately 1% of the present-day atmospheric level (Roscoe, 1969). The disappearance of mass independent fractionation of sulfur isotopes in the sedimentary record (Farquhar et al., 2000) is seen by many (Lyons et al., 2014) as the proverbial "smoking gun" for the rise of atmospheric oxygen. Mass-independent fractionation of sulfur will only be preserved in the rock record in the absence of ozone (O_3) and atmospheric modeling has shown that the critical level of molecular oxygen necessary for ozone production is ~10^{-5} atm (Pavlov and Kasting, 2002).

As oxidative photosynthesis produces O_2, it is tempting to conclude that the GOE was caused by the emergence of oxygenic photosynthesis (Fischer et al., 2016). However, multiple lines of geochemical and genomic evidence are consistent with biological O_2 production originating well before 2.4 Ga (e.g., Lyons et al., 2014), and arguably as early as ~ 3.0 Ga (Planavsky et al., 2014). The reason for the time lag of several hundred million years between the onset of photosynthesis and the accumulation of atmospheric oxygen has been the subject of large amounts of scrutiny in the literature (i.e. Kasting et al., 1993, Holland, 2002, 2009; Catling 2001; Sleep, 2001). The GOE thus likely represents a point at which one or more of the sources or sinks of atmospheric O_2 changed significantly, altering the Archean atmospheric equilibrium. Numerous theories have been proposed to explain this important shift in atmospheric chemistry, including escape of H_2 to space in a methane-rich atmosphere (Catling et al., 2001), increased flux of sulfur and carbon from subduction of sediments (Holland, 2009), a switch from sub-aqueous to sub-areal volcanism (Kump and Barley, 2007), the rise of felsic continental crust (Lee et al., 2016) and formation of a large igneous province (LIP) (Ciborowski and Kerr, 2016). Furthermore, atmospheric box modeling (Holland, 2002) has shown that as small as a 0.5 ΔFMQ log unit change in the oxidation state of volcanic gases, which reflect the oxidation state of their host magmas (Gerlach et al., 1993), would be sufficient to trigger the GOE, emphasizing the important role of mantle redox in controlling the oxygen content in the atmosphere. Therefore, the purpose of this dissertation research was to attempt to constrain the fO_2 of the mantle to better than 0.5 log units across geologic time, and, thus, evaluate a possible mantle trigger for the GOE.

1.2.2. Hadean Mantle Oxidation

The Earth possesses a core made primarily of Fe-Ni alloy. For such a core to form, the early Earth must have had a low enough oxygen fugacity (i.e., near the IW buffer) for liquid Fe metal to be in

equilibrium with silicate melt. The current upper mantle is generally thought to be within a log unit of the FMQ buffer (Cottrell and Kelley, 2011; Berry et al. 2018), implying that the Earth's mantle must have been oxidized at least ~6 log units from the IW buffer to its current state early in its history (Frost et al,. 2013). Furthermore, core segregation models based on the abundances of siderophile elements, such as V, Co and Ni in the mantle require the Earth's mantle to have been increasing in fO_2 during core formation in order to explain the observed partitioning of these elements (Wade and Wood, 2005). One of the most commonly accepted mechanisms for oxidation of the mantle during core formation involves the preference of the high-pressure phase bridgemanite (Mg-Perovskite) for Fe^{3+} over Fe^{2+} (Wade and Wood, 2005; Frost and McCammon, 2008). Bridgemanite is the main stable mantle phase between 670 and 2700 km, comprising up to 93% of the mantle at those depths (Murakami *et al.,* 2012). Due to bridgemanite's preference for Fe^{3+}, Fe^{2+} will disproportionate (react with itself) to produce Fe^{3+} and Fe metal **(4)**.

(4) $3FeO \rightarrow Fe_2O_3 + Fe$

This reaction in and of itself does not change the oxygen fugacity of the mantle, but if some of the Fe metal produced by this reaction is lost to the core in down-going metal diapirs, the lower mantle then becomes oxidized and is no longer in redox equilibrium with the core. Mixing of oxidized lower mantle material into the upper mantle likely then oxidized the bulk mantle to the value we measure today. If the lower and upper mantles were not well mixed after loss of disproportionated Fe metal, redox heterogeneities would persist in the mantle.

1.2.3 Proxies for Mantle fO_2

The most common method for determining fO_2 of modern igneous rocks uses the $Fe^{+3}/\Sigma Fe$ ratio in minerals and glasses. Fe is the most abundant redox-sensitive element in igneous rocks and well-

established equilibrium thermodynamic equations, such as those of Sack et al. (1980) or Kress and Carmichael (1991), relate $Fe^{+3}/\Sigma Fe$ of minerals and glasses to fO_2. X-ray absorption near edge structure (XANES) spectroscopy has been extensively used to accurately determine $Fe^{+3}/\Sigma Fe$ in MORB glasses (Cottrell and Kelley, 2011) and in glasses from island arc basalts (Kelley and Cottrell, 2009; 2012). Glass is easily altered, however, and its $Fe^{+3}/\Sigma Fe$ can be changed by interaction with the modern oxidized atmosphere of the Earth. Thus, this method is not appropriate for determining fO_2 of altered rocks.

Numerous geochemical proxies have been developed to constrain the fO_2 of ancient igneous rocks, including V/Sc ratio in Archean basalts and eclogites (Li and Lee, 2004; Aulbach and Viljoen, 2015; Aulbach and Stagno, 2016), Cr content in basalts (Delano, 2001), Ce anomalies in zircon (Trail et al., 2011; Scaillet and Gaillard, 2011), $Fe^{+3}/\Sigma Fe$ ratios of ophiolitic chromitites (Rollinson et al., 2017) and $\delta^{57}Fe$ in komatiites (Hibbert et al., 2012). We use the experimental data of Canil (1997) and Canil and Fedortchouk (2001) which established that the partitioning of V into liquidus olivine in komatiitic systems is strongly dependent on magma oxidation state and only very weakly dependent on temperature and magma composition. The experimental calibration relating $D_V^{olivine/melt}$ to fO_2 is shown as **Fig. 1.1.**

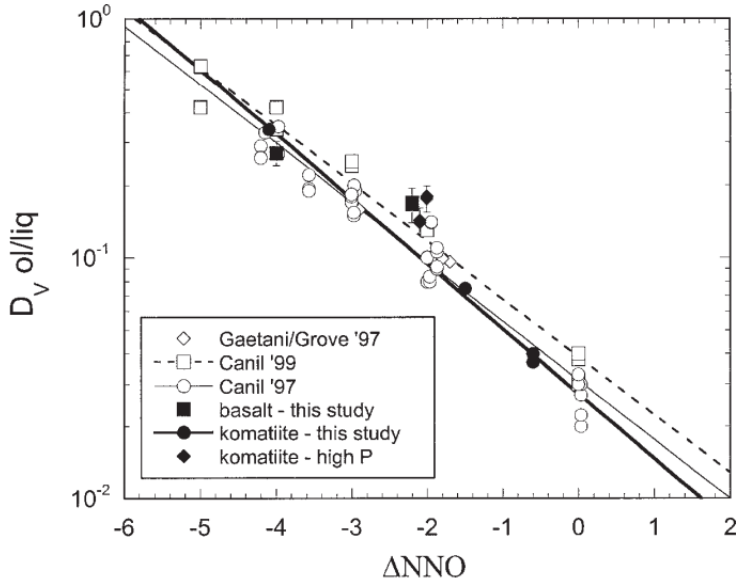

Figure 1.1. Experimental data relating $D_v^{olivine/melt}$ to fO_2 expressed as ΔNNO log units. Filled symbols are for basalts and komatiites from Canil and Fedortchouk (2001), and open symbols are data from Canil, 1997, Canil et al. 1999 and Gaetani and Grove (1997). Vertical arrays of data show the very minor effect of temperature and composition on $D_v^{olivine/melt}$ at constant oxygen fugacity.

While many previous studies (Canil, 1997, 1999; Delano, 2001; Canil and Fedortchouk, 2001; Li and Lee, 2004; Berry et al., 2008; Trail et al., 2011; Hibbert et al., 2012; Rollinson et al., 2017) examining mantle oxygen fugacity from the Archean to the present have found no change, these studies quoted uncertainties ranging from ±2.0 to ±1.0 ΔFMQ log units. In contrast, other, more recent studies, have argued that there has been a resolvable increase in mantle fO_2 from the mid-Archean to the present day (Aulbach and Stagno, 2016; Aulbach et al. 2017). More accurate data and a different approach are, therefore, necessary to further constrain the change in the mantle oxidation state from the Archean to the present.

1.2.4. Highly Siderophile Elements (HSE) and the ^{187}Re-^{187}Os Isotope System.

The eight highly siderophile elements (HSE: Re, Os, Ru, Rh, Ir, Pd, Pt, and Au) are highly depleted in the bulk silicate earth (BSE) relative to chondrites (Sun, 1982). They are termed "highly

siderophile" as they are known to partition very strongly into the metallic phase during core formation, with $D^{metal/silicate} \geq 10^4$. Unexpectedly, the abundances of the HSE in the mantle are enriched by approximately two orders of magnitude compared to values derived from low P-T core-mantle partitioning (Chou et al., 1978). This fact, and the observation that these elements show broadly chondritic ratios relative to one another in the mantle, have led to the conclusion that the HSE were added to the mantle in a post-core formation "late accretion" of chondritic material that constituted ~0.5% of the BSE mass (Kimura et al., 1974; Chou et al., 1983).

The HSE behave differently during mantle processes, with Os, Ir and Ru being compatible during mantle melting, and Rh, Pt, Pd, Re, and Au being moderately to highly incompatible (Barnes et al., 1985). All of the HSE are also strongly chalcophile in silicate-sulfide systems (Mungall and Brenan, 2014). HSE are often plotted on CI chondrite normalized spider diagrams in the order of increasing incompatibility during mantle melting, in a manner similar to the Rare Earth Elements (REE). An example spider diagram for peridotites from the 6 Ma Taitao ophiolite from Schulte et al. (2009) is shown in **Fig. 1.2.** The HSEs are valuable tracers of mantle processes (Walker, 2016) and characterizing their abundances and ratios is important for determining the mantle source region of a studied melt, the degree of sulfide saturation of melts and the degree of mantle mixing at the time of melting.

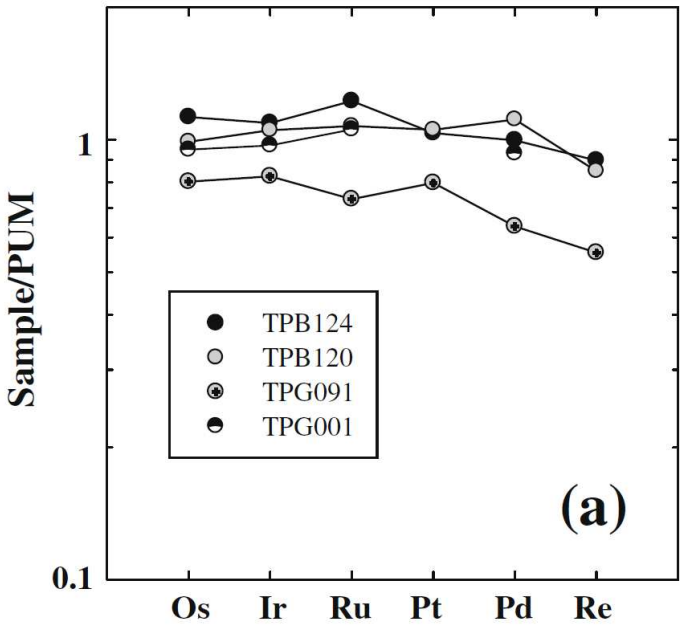

Figure 1.2: Abundances of HSE in peridotites from the 6 Ma Taitao ophiolite, Chile (Schulte et al., 2009). CI chondrite normalized (normalizing values from Horan et al. (2003)).

The ^{187}Re-^{187}Os system is a long-lived radiogenic isotope system ($\lambda = 1.666 * 10^{-11}$ yr^{-1}; (Smoliar et al., 1996)) that is effectively used for dating mantle processes. Both Re and Os are the HSE, but they are greatly fractionated from each other during mantle melting, as they show strongly differing compatibilities. Re is highly incompatible, while Os is strongly compatible during mantle melting. The BSE maintains a broadly chondritic $^{187}Re/^{188}Os$ ratio of 0.401 (Meisel et al., 1996), while continental crust reaches values of ~50 (Esser and Turkien, 1993). Os isotopic composition is normally reported relative to a chondritic reference using $\gamma^{187}Os$ **(5)** notation.

(5) $\gamma^{187}Os = (((^{187}Os/^{188}Os)_{sample}/(^{187}Os/^{188}Os)_{chondritic})-1)*100$

The Re-Os system is highly useful for dating komatiites, as Re and Os are fractionated from each other during komatiite differentiation, and komatiites have relatively high Os concentrations (Walker et al., 1988). The Re-Os system has also been used extensively to characterize the source regions of

komatiites from throughout the world (Walker et al. 1988, 1999; Puchtel et al. 2004; 2005; 2009a, b, 2014; 2016; Hanski et al. 2001; 2004; Gangopadhyay and Walker, 2003; Gangopadhyay et al., 2005; 2006).

1.3. Research Goals

The main goals of the performed PhD research were to characterize the oxygen fugacity (fO_2) of sixteen suites of komatiites and picrites ranging in age from 3.55 billion years ago to the present day, and to relate the fO_2 of the lavas to the oxygen fugacity of their mantle source regions. These data were then used to chart an increase in the fO_2 of the bulk convecting mantle of ~1.3 log units from 3.48 to 1.87 billion years ago, information on which can be found in Chapters 2-4. The causes of the observed mantle oxidation trend and the implications of this trend for the evolution of the atmosphere were modeled, and are described in Chapter 4. Additionally, the abundances of the HSE and the Os isotopic systematics of thirteen whole rock samples of the 89 million year old Gorgona komatiites were determined, and are discussed in Chapter 5. HSE and Os isotopic data were also available for all sample suites except for the Kevitsa Dikes, and the Winnipegosis and Gorgona Island komatiites, and, thus, these data were gathered for the Gorgona samples to provide important geochemical context to the fO_2 data. Finally, Chapter 6 contains conclusions and synthesis of all the data included in this dissertation, and implications for the chemical evolution of the Earth's mantle.

References for Chapter 1

-Aulbach S., Woodland A. B., Vasilyev P., Galvez M. E. and Viljoen K. S., 2017. Effects of low-pressure igneous processes and subduction of $Fe^{+3}/\Sigma Fe$ and redox state of mantle eclogites from Lace (Kaapvaal Craton). *Earth Planet. Sci. Lett.* **474**, 283–295.

-Aulbach, S., and Stagno, V., 2016. Evidence for reducing Archean ambient mantle and its effects on the carbon cycle. Geology **44**: 751-754.

-Barnes, S-J., Naldrett, A. J., Gorton, M. P. 1985. The origin of the fractionation of platinum-group elements in terrestrial magmas. Chem. Geol. **53**: 303–23

-Berry, A. J., Stewart, G. A., O'Neill, H. St.C., Mallmann, G., Mosselmans, J.F.W., 2018. A re-assesment of the oxidation state of iron in MORB glasses. Earth Planet. Sci. Lett. **483**: 114-123.

-Buick, R., 2008. When did oxygenic photosynthesis evolve? Philosophical Transactions of the Royal Society B: Biological Sciences, **363**(1504): 2731-2743.

-Buick, R., 1992. The antiquity of oxygenic photosynthesis: evidence from stromatolites in sulfate-deficient Archaean lakes. Science **255**: 74–77.

-Canil, D., 1997. Vanadium partitioning and the oxidation state of Archaean komatiite magmas. Nature **389** (6653): 842-845.

-Canil, D., 2002. Vanadium in peridotites, mantle redox and tectonic environments: Archean to present. Earth and Planetary Science Letters **195**(1-2): 75-90.

-Canil, D., Fedortchouk, Y., 2001. Olivine-liquid partitioning of vanadium and other trace elements, with applications to modern and ancient picrites. Canadian Mineralogist **39**: 319-330.

-Catling, D. C., Zahnle, K. J., McKay, C. P., 2001. Biogenic Methane, Hydrogen Escape, and the Irreversible Oxidation of Early Earth. Science **293** (5531): 839-843.

- Chou, C-L., 1978. Fractionation of siderophile elements in the earth's upper mantle. Proc. Lunar Planet. Sci. Conf., 9th, pp. 219–30

-Chou, C., Shaw, D. M., & Crocket, J. H., 1983. Siderophile trace elements in the Earth's oceanic crust and upper mantle. Journal of Geophysical Research, **88**(S02).

- Cottrell, E., Kelley, K. A., 2011. The oxidation state of Fe in MORB glasses and the oxygen fugacity of the upper mantle. Earth and Planetary Science Letters **305** (3-4): 270-282..

- Delano, J. W., 2001. Redox History of the Earth's Interior since ~3900 Ma: Implications for Prebiotic Molecules. Origins of life and evolution of the biosphere **31** (4-5): 311-341.

- Esser, B. K., Turekian, K. K. 1993. The osmium isotopic composition of the continental crust. Geochimica et Cosmochimica Acta **57**: 3093–104

-Fischer W. W., Hemp J. and Johnson J. E. (2016) Evolution of oxygenic photosynthesis. *Ann. Rev. Earth Planet. Sci.* **44**, 647–683.

- Farquhar, J., Bao, H., Thiemens, M., 2000. Atmospheric influence of Earth's earliest sulfur cycle. Science **289** (5480): 756-758.

- Frost, D. J., McCammon, C. A. 2008. The redox state of Earth's mantle. Annual Review of Earth and Planetary Sciences. Palo Alto, Annual Reviews. **36:** 389-420.

-Frost D. J., Mann U., Asahara Y., Rubie D. C., 2013. The redox state of the mantle during and just after core formation. Philosophical Transactions of the Royal Society of London **366**(1883): 4315-4337.

-Gangopadhyay, A., & Walker, R. J., 2003. Re–Os systematics of the ca. 2.7-Ga komatiites from Alexo, Ontario, Canada. Chemical Geology **196**(1-4): 147-162.

-Gangopadhyay, A., Walker, R. J., Hanski, E., & Solheid, P. A., 2006. Origin of Paleoproterozoic Komatiites at Jeesiorova, Kittila Greenstone Complex, Finnish Lapland. Journal of Petrology, **47**(4): 773-789.

-Gangopadhyay, A., Sproule, R. A., Walker, R. J., & Lesher, C. M., 2005. Re-Os systematics of komatiites and komatiitic basalts at Dundonald Beach, Ontario, Canada: Evidence for a complex alteration history and implications of a late-Archean chondritic mantle source. Geochimica Et Cosmochimica Acta, **69**(21): 5087-5098.

-Gerlach, T. M., 1993. Oxygen buffering of Kilauea volcanic gases and the oxygen fugacity of Kilauea basalt. Geochimica et Cosmochimica Acta **57**: 795-814.

- Hanski, E., Huhma, H., Rastas, P., Kamanetsky, V. S., 2001. The Palaeoproterozoic Komatiite-Picrite Association of Finnish Lapland. Journal of Petrology **42**(5): 855-876.

- Hanski, E., Walker, R. J., Huhma, H., Polyakov, G. V., Balykin, P. A., Hoa, T. T., & Phuong, N. T., 2004. Origin of the Permian-Triassic komatiites, northwestern Vietnam. Contributions to Mineralogy and Petrology, **147**(4): 453-469.

- Hibbert, K., Williams, H., Kerr, A., & Puchtel, I. 2012. Iron isotopes in ancient and modern komatiites: Evidence in support of an oxidised mantle from Archean to present. Earth and Planetary Science Letters, **321-322**: 198-207.

- Holland, H. D., 2002. Volcanic gases, black smokers, and the great oxidation event. Geochimica et Cosmochimica Acta **66** (21): 3811-3826.

- Holland, H. D. 2009. Why the atmosphere became oxygenated: A proposal. Geochimica Et Cosmochimica Acta, **73**(18): 5241-5255.

-Horan, M.F., Walker, R.J., Morgan, J.W., Grossman, J.N., Rubin, A.E., 2003. Highly siderophile elements in chondrites. Chemical Geology, **196**(1–4): 5–20.

-Kasting, J. F., Eggler, D. H., Raeburn, S. P., 1993. Mantle redox evolution and the oxidation state of the Archean atmosphere. Journal of Geology **101**: 245-257.

- Li, Z. X. A., Lee, C. T. A., 2004. The constancy of upper mantle fO_2 through time inferred from V/Sc ratios in basalts. Earth and Planetary Science Letters **228** (3-4): 483-493.

- Lyons, T. W., Reinhard, C. T., Planavsky, N. J., 2014. The rise of oxygen in Earth's early ocean and atmosphere. Nature **506** (7488): 307-315.

- Meisel T., Walker R. J., Morgan J. W., 1996. The osmium isotopic composition of the Earth's primitive upper mantle. Nature **383**: 517–20.

-Mungall, J. E., Brenan, J. M., 2014. Partitioning of platinum-group elements and Au between sulfide liquid and basalt and the origins of mantle-crust fractionation of the chalcophile elements. *Geochimica et Cosmochimica Acta,* **125**: 265-289.

-Murakami, M., Ohishi, Y., Hirao, N., & Hirose, K., 2012. A perovskitic lower mantle inferred from high-pressure, high-temperature sound velocity data. Nature, **485**(7396): 90-94.

-Nicklas, R.W., Puchtel, I.S., Ash, R.D., Piccoli, P.M., Hanski, E., Nisbet, E.G., Waterton, P., Pearson, D.G., and Anbar, A.D., 2019. Secular Mantle Oxidation across the Archean-Proterozoic Boundary: Evidence from V Partitioning in Komatiites and Picrites. *Geochimica et Cosmochimica Acta* **250**: 49-75.

-Planavsky N. J., Asael D., Hofmann A., Reinhard C. T., Lalonde S. V., Knudsen A., Wang X., Ossa Ossa F., Pecoits E., Smith A. J. B., Beukes N. J., Bekker A., Johnson T. M., Konhauser K. O., Lyons T. W. and Rouxel O. J. (2014) Evidence for oxygenic photosynthesis half a billion years before the Great Oxidation Event. *Nature Geosci.* **7**, 283.

- Puchtel, I. S., Blichert-Toft, J., Touboul, M., Horan, M. F., Walker, R. J., 2016. The coupled ^{182}W-^{142}Nd record of early terrestrial mantle differentiation. Geochemistry, Geophysics, Geosystems.

- Puchtel I. S., Walker R. J., Touboul M., Nisbet E. G. and Byerly G.R., 2014. Insights into Early Earth from the Pt–Re–Os isotope and Highly Siderophile Element abundance systematics of Barberton komatiites. Geochimica et Cosmochimica Acta **125:** 394–413.

- Puchtel, I. S., Walker, R. J., Brandon, A. D., Nisbet, E. G., 2009a. Pt-Re-Os and Sm-Nd isotope and HSE and REE systematics of the 2.7 Ga Belingwe and Abitibi komatiites. Geochimica et Cosmochimica Acta **73** (20): 6367-6389.

- Puchtel, I. S., Walker, R. J., Anhaeusser, C. R., Gruau, G., 2009b. Re–Os isotope systematics and HSE abundances of the 3.5 Ga Schapenburg komatiites, South Africa: Hydrous melting or prolonged survival of primordial heterogeneities in the mantle? Chemical Geology **262**(3-4): 355-369.

-Puchtel, I. S., Brandon, A. D., Humayun, M., Walker, R. J., 2005. Evidence for the early differentiation of the core from Pt-Re-Os isotope systematics of 2.8-Ga komatiites. Earth and Planetary Science Letters **237** (1-2): 118-134.

- Puchtel, I. S., Humayun, M., Campbell, A., Sproule, R., Lesher, C. M., 2004. Platinum group element geochemistry of komatiites from the Alexo and Pyke Hill areas, Ontario, Canada. Geochimica et Cosmochimica Acta **68** (6): 1361-1383.

-Rollinson, H., Adetunji, J., Lenaz, D., Szilas, K., 2017. Archean chromatites show constant $Fe^{+3}/\Sigma Fe$ in Earth's athenospheric mantle since 3.8 Ga. Lithos **282-283**: 316-325.

-Schlute, R. F., Schilling, M., Anma, R., Farquhar, J., Horan, M. F., Komiya, T., Piccoli, P. M., Pitcher, L., Walker, R. J., 2009. Chemical and chronological complexity in the convecting upper mantle: Evidence from the Taitao Ophiolite, southern Chile. Geochimica et Cosmochimica Acta **73**: 5793-5819.

- Sleep, N. H., 2001. Oxygenating the Atmosphere. Nature, **15**: 317-319.

- Trail, D., Watson, E. B., & Tailby, N. D., 2011. The oxidation state of Hadean magmas and implications for early Earth's atmosphere. Nature, **480**(7375): 79-82.

- Wade, J. & Wood, B. J. 2005 Core formation and the oxidation state of the Earth. Earth and Planetary Science Letters, **236**: 78–95.

-Walker, R. J., Storey, M., Kerr, A. C., Tarney, J., & Arndt, N. T., 1999. Implications of 187Os isotopic heterogeneities in a mantle plume: Evidence from Gorgona Island and Curaçao. Geochimica Et Cosmochimica Acta, **63**(5): 713-728.

-Walker, R. J., Shirey, S. B., & Stecher, O., 1988. Comparative Re-Os, Sm-Nd and Rb-Sr isotope and trace element systematics for Archean komatiite flows from Munro Township, Abitibi Belt, Ontario. Earth and Planetary Science Letters **87**(1-2): 1-12.

Chapter 2: High-Precision Determination of the Oxidation State of Komatiite Lavas using Vanadium Liquid-Mineral Partitioning

Note: This chapter has been previously published in the following publication:

Nicklas R. W., Puchtel I. S. and Ash R. D. (2016) High-precision determination of the oxidation state of komatiite lavas using vanadium liquid-mineral partitioning. *Chem. Geol.* **433**, 36–45.

Abstract for Chapter 2

Oxygen fugacity of the mantle (fO_2) is an important intensive variable in Earth sciences that is largely unconstrained throughout Earth history. Oxygen fugacity of modern basalts is determined by examining the Fe^{+3}/Fe^{+2} ratios of fresh volcanic glass, but this method cannot be applied to older lavas that have experienced post-magmatic alteration and/or metamorphism.

Here, we report the newly developed analytical techniques that, using the published experimental petrology data, have enabled us to determine the fO_2 of mantle-derived lavas with a precision of better than 0.10 log fO_2 units. This new method uses the partitioning behavior of the redox-sensitive transition metal vanadium between olivine and/or chromite and komatiitic melt as oxybarometers. In order to obtain accurate and precise results, a series of whole-rock samples was collected across differentiated komatiitic basalt Victoria's Lava Lake in Fennoscandia. Special attention was paid to ensure that the lava contained magmatic olivine and chromite that were in equilibrium with the emplaced melt composition, and that no re-equilibration has occurred during the lava differentiation. Vanadium and other transition metal abundances in the whole-rock samples were determined using standard addition solution ICP-MS technique with a precision of better than 5% (2SD), and in liquidus olivine and chromite by laser ablation ICP-MS, with a precision of better than 5% (2SE). The MgO and transition metal abundances in the emplaced komatiitic basalt lava were precisely calculated using several independent approaches; these approaches provided consistent results that agreed within the uncertainty of the method. The partition coefficients $D_V^{Ol,\ Chr\text{-}Liq}$ were then calculated and used to determine the fO_2 of the lava lake to be −0.24±0.04 and −0.21±0.03 ΔNNO log units, respectively (2SE). The two independent estimates are identical within the respective uncertainties and attest to the accuracy of the method; the average value of −0.22±0.04 ΔNNO log units (2SD) represents our best estimate for the redox state of the lava lake. Corrected for 4% crustal contamination, the redox state of the original

komatiite is calculated to be −0.29±0.04 ΔNNO log units. The new method provides a high-resolution tool for constraining the evolution of the redox state of the mantle over Earth's history.

2.1. Introduction

Oxygen fugacity (fO_2) is an important intensive variable in igneous petrology that controls the behavior of redox-sensitive elements, such as Fe, V, and Cr, during igneous differentiation. Unlike many other important variables, oxygen fugacity of the mantle is not well constrained throughout Earth's history. Previous attempts to constrain the evolution of mantle oxygen fugacity have relied on variations in Cr and V contents (Canil, 1997, 1999, 2002; Delano, 2001) and V/Sc ratios (Li and Lee, 2004) of mantle-derived mafic and ultramafic rocks. These studies concluded that, within ~0.5-1.0 log units, oxygen fugacity of the mantle has remained essentially constant since at least the early Archean. The 1.0 log fO_2 unit is in itself a very large change in oxygen fugacity and a more precise method for determining the oxidation state of the Archean and post-Archean mantle is needed. Accurate and precise determination of the variations in oxygen fugacity of the mantle throughout Earth's history may also hold the answer to one of the most debated questions in the Earth sciences of why oxygen abundance suddenly rose in the atmosphere at the Archean-Proterozoic boundary (Holland, 2002).

The work of Canil (1997) and Canil and Fedortchouk (2001) demonstrated that the partitioning of V between liquidus olivine and ultramafic melt is a strong function of fO_2, with little to no dependence on temperature and melt composition. Further work (Canil, 1999; 2002) demonstrated that the partitioning of V between liquidus chromite and melt was also a strong function of fO_2, although this partitioning is significantly affected by the Cr/Al ratio of the system. However, no accurate and precise combined data for V and Cr partitioning between olivine, chromite and natural mafic and ultramafic liquids have been reported by far. This is partly due to the scarcity of well-preserved ultramafic lavas in the ancient geological record that would retain primary magmatic minerals suitable for this type of study, and partly

due to the lack of appropriate analytical techniques at the time these studies took place, that would have allowed precise and accurate determination of V abundances in liquidus olivine, chromite, and the ultramafic magmas with which these mineral phases were in equilibrium.

Here, we report the newly developed analytical techniques that, using the experimental petrology data of Canil (1997, 1999, 2002) and Canil and Fedortchouk (2001), enabled us to determine the fO_2 of komatiite lavas with a precision of better than 0.10 log fO_2 units. It should be noted, however, that the precision of this method is very case-specific. In addition to our ability to measure V and other transition metal abundances in whole-rock samples and liquidus olivines and chromites with a sufficiently high degree of precision, it depends heavily on the availability of sufficient amounts of fresh liquidus olivine and/or chromite grains that were in equilibrium with the emplaced komatiite lava, and on the availability and the degree of alteration of samples with a wide range of chemical compositions collected across a single differentiated komatiitic lava flow. If these requirements are not met, it may become impossible to determine fO_2 of a komatiite system with any reasonable degree of precision.

The lavas that this method has been developed for are komatiites, ultramafic volcanic rocks having an MgO content of >18% (Arndt and Nisbet, 1982). Komatiites are thought to be the result of either deep, hot, anhydrous melting in mantle plumes (Campbell et al., 1989), with degrees of melting of up to 60% (Arndt, 1976), or lower-temperature, hydrous melting in a subduction zone environment (Parman *et al.*, 2004). The very high temperatures (up to 1600°C) and low viscosity of dry komatiitic melts enabled them to reach the surface rapidly, with little or no fractionation *en route*. Once on the surface, komatiite lava flows crystallized only olivine, and some minor chromite at the later stages of differentiation, forming olivine cumulate layers overlain by a zone of olivine– and pyroxene spinifex–textured rocks. Most komatiites are confined to Archean terrains, but Proterozoic and Phanerozoic komatiite occurrences have also been reported (see review in Arndt *et al.*, 2008). Although all komatiites are

altered to some degree, in many instances they preserve original, magmatic mineralogy, and some have even been characterized as "uniquely" (Nisbet *et al.*, 1987) and "remarkably" (Puchtel *et al.*, 1996) fresh, by Archean standards.

2.2. Geological background and samples

For this study, we chose the remarkably fresh komatiitic basalt lavas of the Victoria's Lava Lake located within the *ca.* 2.4 Ga Vetreny Belt in SE Fennoscandia (Puchtel *et al.*, 1996, 1997). The 250 km long Vetreny Belt is considered to be part of the oldest known large igneous province that formed in a continental rift setting, during the interaction of a mantle plume with the Archean continental crust of the Karelian granite-greenstone terrain (Puchtel *et al.*, 1997). Modeling involving lithophile trace element and Nd isotopic data has shown that komatiitic magmas parental to the Victoria's Lava Lake contained *ca.* 27% MgO, and were derived from a long-term LREE-depleted mantle source (Puchtel *et al.*, 1997, 2016). These authors concluded that the chemical evolution of the primary komatiite magmas *en route* to the surface was controlled by a combination of ~50% fractional crystallization and ~4.0±0.4% assimilation of tonalites from the adjacent ~3.2 Ga Vodla Block. Puchtel *et al.* (2016) reported Re-Os and Sm–Nd isochron ages for the lava lake of 2407±6 and 2403±32 Ma, respectively.

The lava lake is a ~110 m-deep sequence of komatiitic basalt, which filled a large topographic depression following eruption, and was estimated to have emplaced with *ca.* 15 wt.% MgO (Puchtel *et al.*, 1996, 2016). After emplacement, the lava lake underwent differentiation and developed a prominent internally layered structure comprised of three main units (from the top down): an upper chilled margin, a spinifex zone, and a cumulate zone (**Fig. 2.1**).

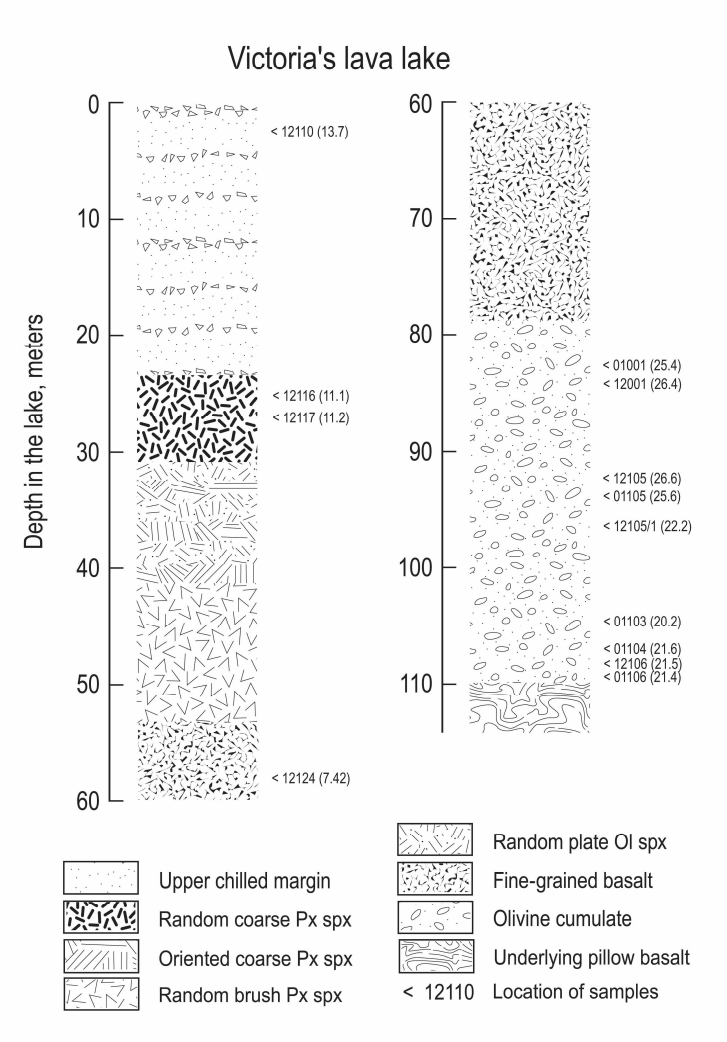

Figure 2.1. Schematic integrated section through the Victoria's Lava Lake showing textural variations within the lake and location of the samples analyzed in this study. The MgO contents of the individual samples (wt.%) are shown in parentheses.

The rocks are characterized by a superb state of preservation; the metamorphic grade did not exceed the prehnite-pumpellyite facies and most magmatic minerals are well preserved. For this study, we used the same set of samples collected across several sections of the lava lake and studied by Puchtel *et al.* (2016). The locations of the samples are shown on the integrated section of the lava lake in **Fig. 2.1**.

2.3. Analytical techniques

2.3.1. Sample selection

2.3.1.1. Whole-rock samples. In order to obtain accurate estimates of emplaced lava composition for a given komatiite lava flow, and to monitor the behavior of petrogenetically important elements during post-magmatic alteration and metamorphism, we studied samples with the widest possible range of MgO contents. In differentiated komatiite lava units, the most MgO-poor horizons are located at the bottom of spinifex-textured zones, and the most MgO-rich parts are usually located in the lower half of cumulate zones. We also included an upper chilled margin sample, since these normally represent the composition of the emplaced lava from which liquidus olivine crystallized. We, therefore, included samples collected across the entire section of the lava lake, with the MgO contents ranging from 7.4% to 27% (**Fig. 2.1.**).

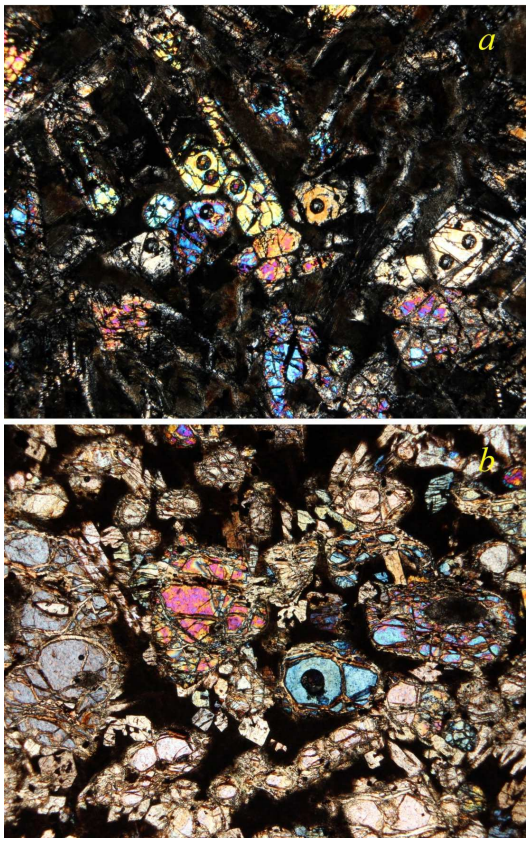

Figure 2.2. Photomicrographs of the upper chilled margin sample 12110 (**a**) and the olivine cumulate sample 12105 (**b**) showing the type of solid equant olivine grains analyzed in this study. Clearly visible are rounded laser ablation pits within the grains analyzed. The fields of view are 3.0×2.5 mm; cross-polarized light.

2.3.1.2. Olivine and chromite. In order to determine V abundances in the liquidus olivine and chromite in equilibrium with the emplaced komatiite lava composition, solid, equant olivine and chromite grains from both the upper chilled margin and the cumulate zone of the lava lake were analyzed in this study **(Fig. 2.2.).** Based on electron probe analyses, olivines from the chilled margin and the cumulate zone were shown to be in equilibrium with the emplaced lava composition (Puchtel *et al.*, 1996). Chips of the chilled margin sample 12110 and olivine cumulates 12001, 12105, and 12105/1 approximately 10 mm across were mounted in epoxy, and polished. Pure solid equant chromite grains were separated from the chilled margin sample 12110 and the olivine cumulate samples 12001 and 12105 using conventional magnetic and heavy liquid separation techniques and were also mounted in epoxy and polished.

2.3.2. Determination of the emplaced lava composition

Accurate determination of the composition of the emplaced komatiite lava is crucial for evaluating V partitioning behavior between liquidus olivine, chromite and the melt from which they crystallized. In order to calculate the MgO content of the emplaced lava, Puchtel *et al.* (1996, 2016) used several independent approaches.

The first approach used the composition of the upper chilled margin as a proxy for the parental liquid composition. This approach is based on the fact that upper chilled margins of komatiite lava flows likely crystallized rapidly. Consistent with this, they usually do not show evidence of differentiation after emplacement, although some may contain a small amount of olivine phenocrysts (Arndt, 1986).

The second approach is based on the well-established relationship between the composition of olivine and that of the liquid from which it crystallized (Roeder and Emslie, 1970; Beattie *et al.*, 1991). The maximum average MgO and minimum FeO contents of the cores of the cumulate olivine grains and olivine phenocrysts in the upper chilled margin of the Victoria's Lava Lake were determined and the

composition of the komatiite liquid in equilibrium with these olivine compositions was estimated using the partition coefficients from Beattie et al. (1991). Further, the compositions of the chilled margin derived from approach (1) and that of the emplaced lava derived from approach (2) were tested for consistency.

Finally, the third approach required calculation of the average MgO content of liquidus olivine in equilibrium with the emplaced lava by means of regressing the abundances of the elements that are incompatible with olivine, against the MgO contents; the intersections with the MgO axis corresponded to the average MgO content in the liquidus olivine. The average calculated MgO content of the liquidus olivine was then used to back-calculate the MgO content of the emplaced lava using approach (2). The MgO contents obtained using the three independent approaches were then averaged to yield the MgO content of the emplaced komatiite lava.

2.3.3. Analysis of major and minor elements in whole-rock samples

Major-element analyses of whole rock komatiite samples were carried out at Franklin & Marshall College on fused glass discs using a Phillips 2404 XRF spectrometer, following the procedure of Mertzman (2000). Typical accuracy of the analyses was ~1% relative for major elements with concentrations >0.5% and ~5% relative for the other major elements. In this study, we used the major element data obtained by Puchtel *et al.* (2016) for the set of samples studied here.

2.3.4. Electron microprobe analysis of olivine and chromite

Major element analyses of olivines were performed on polished thin sections using the *JEOL JXA 8900 R* electron probe microanalyzer at the *Center for Microanalysis*, University of Maryland. Special attention was paid to select and analyze only early-crystallized, solid equant grains that were likely in equilibrium with the emplaced Victoria's Lava Lake lava. Operating conditions were 15 KeV

accelerating potential, a 20 nA focused electron beam current, and a 10 μm spot size. Major element analyses of epoxy-mounted chromite separates were performed under the same conditions. These electron probe data were then used for data normalization purposes for the laser ablation analysis, as specified below.

2.3.5. Analysis of transition metal abundances in whole-rock samples

The abundances of the transition metals in whole-rock samples were determined using the standard addition solution inductively-coupled plasma mass-spectrometry technique (SA ICP-MS). Between 25 and 35 mg of sample powder, 0.5 mL double-distilled conc. HNO_3 and 3 mL double-distilled conc. HF were weighed out in 15 mL screw-cap Savillex Teflon vials, sealed using Teflon tape, and kept on a hotplate at 200ºC for 48 hours. The vials were then opened, the sample solutions evaporated to dryness, 0.5 mL of distilled SeaStar $HClO_4$ was added to the dry residue to convert fluorides into perchlorides. The vials were sealed again and kept on the hotplate at 200ºC for 48 hours. The vials were then opened and the sample solutions dried down on the hotplate at 230ºC. This step was followed by re-dissolution of the residue in 2-3 mL of 6*M* HCl to convert it into the chloride form, and dried down. This step was repeated twice. The dry residue was then taken up in ~10 grams of 0.8*M* HNO_3 and this stock solution was used for preparing spiked aliquots used for the ICP-MS measurements. A standard addition spike was prepared, containing concentrated mixed solutions of Sc, V, Cu, Co, Ga, Y, and Zr. Three aliquots of each sample, each containing 0.5-1.0 mL of sample stock solution, were prepared, one containing no spike, one with the amount of spike 2× the estimated amount of element present in the sample aliquot, and one with the amount of spike 4× the estimated amount of element present in the sample aliquot. One total analytical blank (TAB) was also prepared and measured with every batch of 6 samples. Approximately 100 mg of 500 ppb In solution was added to each sample aliquot and the TAB solutions

to monitor and correct for the signal drift during the analysis, and the three mixed solutions for each sample were diluted to 10 grams using 0.8*N* HNO_3.

The sample solutions were analyzed on a *ThermoFinnigan Element2* sector field inductively-coupled plasma mass-spectrometer (ICP-MS) at the *Plasma Laboratory,* Department of Geology, University of Maryland. Prior to analysis, the instrument was thoroughly tuned to maximize sensitivity and minimize oxide production, and mass-calibrated. The intensities of selected isotopes of each element were measured in both low- and medium resolution modes. The raw data were reduced using an in-house Excel macro. The in-run uncertainties on the concentrations were typically better than 2% for all elements (2SE). The external precision of the analysis was determined via the analysis of USGS standard reference materials (SRM) BIR-1, BHVO-1, and BCR-1; for most elements, including V, it was between 2 and 5% (2SD) and included the uncertainty introduced by sample powder heterogeneity **(Tables 2.1.-2.3., Fig. 2.3.)**. The largest of the 2SD uncertainties (5%) obtained for the three USGS SRM was used as a measure of uncertainty on the transition metal abundances for the individual whole-rock samples. These 2SD uncertainties were further used for the ISOPLOT regression calculations.

Table 2.1. Transition metal abundances (ppm) in USGS SRM BIR-1 obtained via the SA ICP-MS analysis technique. The GEOREM preferred values and the uncertainties (±2SD) are listed at the bottom.

SRM	Sc	V	Cu	Ga	Y	Zr
BIR1-01	44.2	323	125	16.0	15.2	16.9
BIR1-02	42.8	310	122	15.7	14.5	16.0
BIR1-03	43.9	316	126	16.1	14.8	15.5
BIR1-04	44.8	322	126	16.2	15.0	15.9
BIR1-05	43.1	313	123	15.5	14.6	17.0
BIR1-06	43.3	317	122	15.5	14.7	16.7
BIR1-07	45.3	331	131	15.6	14.7	16.1
BIR1-08	42.7	326	130	15.6	15.2	16.0
BIR1-09	43.0	310	126	15.5	14.6	16.3
BIR1-10	44.8	333	135	17.1	15.1	17.0
BIR1-11	42.5	307	119	14.9	14.6	15.5
BIR1-12	44.8	335	132	17.0	15.5	16.1
BIR1-13	43.7	315	131	16.1	15.2	16.0
BIR1-14	46.1	319	133	17.0	15.5	16.2
BIR1-15	46.4	322	144	16.9	15.9	16.6
BIR1-16	46.3	323	121	16.8	15.5	19.9
BIR1-17	44.6	319	113	16.3	14.9	15.7
BIR1-18	45.0	333	127	16.1	15.4	16.5
BIR1-19	45.1	335	130	16.5	15.1	16.1
BIR1-20	44.7	331	130	16.6	15.3	16.7
BIR1-21	44.9	326	125	16.3	14.8	17.2
BIR1-22	43.5	320	125	15.8	14.9	15.7
Average (±2SD)	44.3±2.3	322±17	127±13	16.1±1.2	15.0±0.8	16.4±1.9
±2SD (%)	5.2	5.3	10	7.3	5.0	11
GEOREM (±2SD)	**43±4**	**319±36**	**119±16**	**15.3±1.6**	**15.6±1.8**	**14.0±0.2**

Table 2.2. Transition metal abundances (ppm) in USGS SRM BCR-1 obtained via the SA ICP-MS analysis technique. The GEOREM preferred values and the uncertainties (±2SD) are listed at the bottom.

SRM	Sc	V	Cu	Ga	Y	Zr
BCR1-01	32.07		16.1	21.9	32.7	182
BCR1-02	33.37	396	16.0	22.6	34.8	197
BCR1-03	33.45	397	15.7	22.5	34.4	188
BCR1-04	31.93	404		22.5	33.9	186
BCR1-05	32.84	394	15.8	22.4	34.5	193
BCR1-06	33.22	401	15.7	22.6	34.2	195
BCR1-07	32.71	399	16.2	22.5	34.1	187
BCR1-08	33.09	396	15.9	22.3	35.0	196
BCR1-09	33.06	402	15.9	22.6	35.3	198
BCR1-10	32.46	401	16.3	22.3	34.0	185
BCR1-11	32.64	392	15.8	22.0	33.3	187
BCR1-12	32.82	399	15.8	22.6	33.6	192
BCR1-13	31.83	389	15.8	21.9	33.1	184
BCR1-14	33.04	398	16.1	22.5	34.2	191
BCR1-15	32.89	398	16.0	22.5	34.3	192
BCR1-16	32.43	408	16.9	22.4	34.1	190
BCR1-17	32.98	393	15.6	22.0	33.1	183
Average (±2SD)	32.8±1.0	398±10	16.0±0.6	22.3±0.5	34.0±1.4	190±10
2SD (%)	2.9	2.4	3.9	2.4	4.1	5.3
GEOREM (±2SD)	**32±4**	**410±40**	**21±6**	**23±4**	**36±4**	**189±18**

Table 2.3. Transition metal abundances (ppm) in USGS SRM BHVO-1 obtained via the SA ICP-MS analysis technique. The GEOREM preferred values and the uncertainties (±2SD) are listed at the bottom.

SRM	Sc	V	Cu	Ga	Y	Zr
BHVO1-01	33.1	315	153	22.0	25.2	189
BHVO1-02	32.3	309	152	22.2	25.1	177
BHVO1-03	32.8	311	143	22.5	26.2	185
BHVO1-04	32.0	301	147	21.1	25.2	165
BHVO1-05	31.9	306	155	21.6	25.0	166
BHVO1-06	31.5	303	142	21.6	24.5	169
Average (±2SD)	32.3±1.1	306±9	149±11	21.8±1.0	25.2±1.1	175±20
2SD (%)	3.5	2.8	7.2	4.7	4.3	12
GEOREM (±2SD)	**31±4**	**318±30**	**137±18**	**21±4**	**26±4**	**174±18**

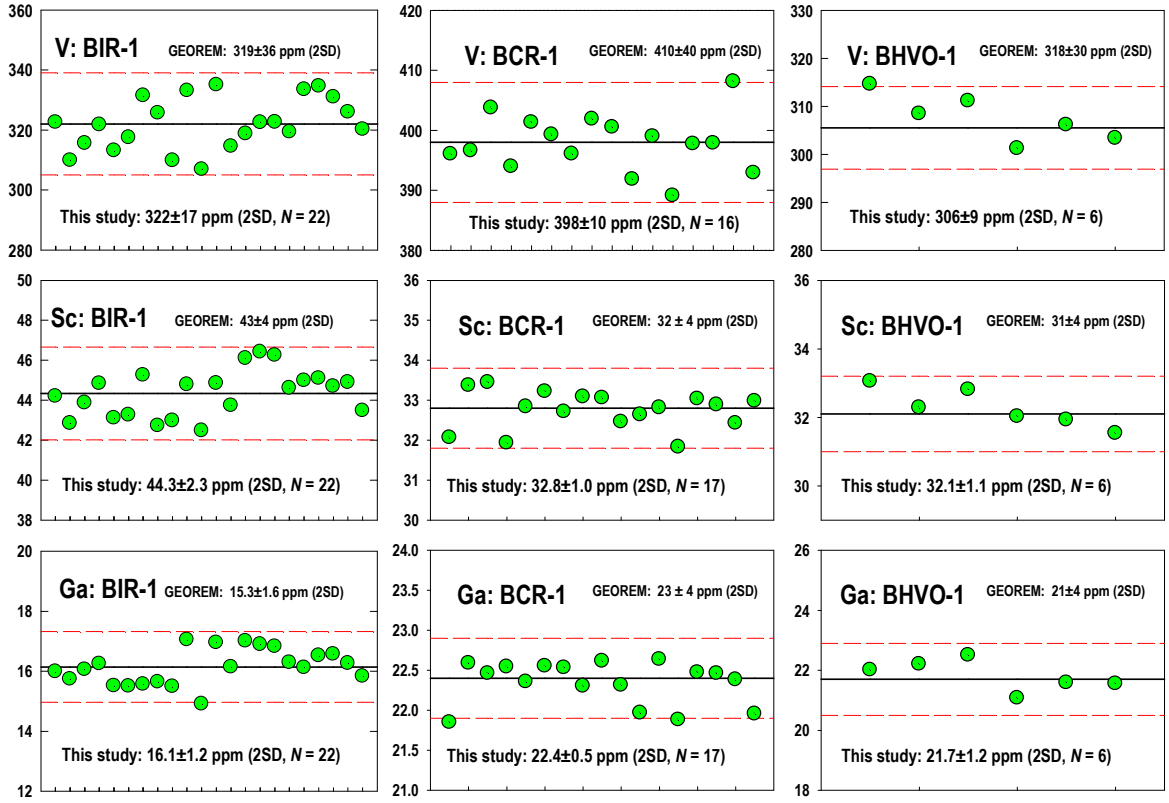

Figure 2.3. Vanadium, Sc, and Ga abundances in replicate digestions of the USGS standards BIR-1, BHVO-1, and BCR-1 determined using standard addition solution ICP-MS. The external reproducibility (2SD) is listed for each element. The GEOREM preferred values for each standard are provided for reference.

2.3.6. Laser ablation analysis of liquidus olivine and chromite

Several chips (~1 cm across) of the chilled margin sample 12110 and of olivine cumulates 12001, 12105, and 12105/1, as well as pure chromite separates from these samples, were selected for analysis. A total of 133 olivine grains and 139 chromite grains were analyzed using a *UP213 New Wave* laser-ablation system coupled to the *ThermoFinnigan Element2* ICP-MS at *the Plasma Laboratory,* Deparment of Geology, University of Maryland. The quintupled Nd-YAG laser operated at ~60% power and 7 Hz with fluence controlled between 2-4 J/cm^2 (~60% laser power). The spot size of each analysis varied between 55 and 100 μm for the olivines and 25-40 μm for the chromites, depending on

the size of the grains being analyzed. Only solid, equant olivine and chromite grains containing no visible inclusions were selected for analysis (**Fig. 2.2.**). Replicate analyses of the USGS SRM BHVO-2G and BCR-2G were performed with each set of 12-16 spots analyzed. The raw data were reduced using the in-house *LAMTRACE* software, using either the FeO abundances for liquidus olivine in equilibrium with the emplaced komatiite lava or average FeO for the population of chromite grains for each particular sample obtained from the electron microprobe analyses, as normalizing values.

Based on the available major and minor element abundance data for the studied olivine and chromite (e.g., Puchtel et al., 1996, and this study), variations in the abundances of these elements within individual samples are estimated to not exceed 5% relative, implying rather homogenous compositions of the solid equant olivine and chromite grains selected for analysis. Based on this observation, it is assumed that all the variations in V and other transition metal abundances in the studied populations of olivine and chromite grains within the same samples reflect the analytical uncertainty of the LA-ICP-MS analysis. As such, the 2SE was used as the measure of the uncertainty on the calculated average concentrations of transition metals in either olivine or chromite for the individual samples (**Figs. 2.4. and 2.5.**). For V concentrations, these uncertainties were ~5% for the olivine, and between 2 and 3% for the chromite. For the ISOPLOT regression calculations, the 2SD uncertainty on the average transition metal abundances in the studied olivine and chromite samples was used.

2.4. Results

2.4.1. Compositions of the emplaced komatiitic basalt lava and of the liquidus olivine and chromite

Transition metal abundance data for the whole-rock samples analyzed in this study are presented in **Table 2.4.**, and for the liquidus olivines and chromites in **Table 2.5**. The V abundances in the

individual olivine and chromite grains analyzed in this study are also plotted in **Figs. 2.4. and 2.5.**, respectively.

Table 2.4. MgO (wt. %) and transition metal (ppm) abundances in whole rock samples from the Victoria's Lava Lake and in the calculated emplaced lava composition.

Sample	Sc	V	Cu	Ga	Y	Zr	MgO	LOI
12110	32.6	189	90.3	12.5	12.6	53.7	13.7	2.25
12116	35.9	212	97.3	13.6	13.6	54.9	11.1	0.75
12117	35.5	208	98.3	13.4	13.7	55.0	11.2	0.58
12124	39.3	228	107	15.1	15.2	61.7	7.42	0.25
01001_B	22.6	131	59.6	8.10	7.98	31.2	25.4	2.78
12001	22.4	135	60.0	8.15	7.80	31.7	26.4	2.99
01103_B	28.2	161	71.4	10.0	10.4	37.4	20.2	1.49
01104_B	26.7	155	73.4	9.86	10.0	40.0	21.6	1.27
01105_B	23.2	138	58.9	8.40	8.33	37.0	25.6	2.80
12105	22.6	133	57.8	7.92	7.70	30.6	26.6	3.21
01106_B	27.7	155	68.2	9.40	9.77	36.4	21.4	1.42
12106	27.3	153	68.7	9.71	9.32	36.4	21.5	1.06
Slope	-1.232±30	-0.1815±41	-0.3953±90	-2.778±62	-2.755±62			
Intercept	54.77±0.98	49.59±0.48	49.31±0.49	48.51±0.47	48.27±0.46			
MSWD	3.4	1.2	0.82	0.45	0.67			
Emplaced lava	32.4±1.0	192±4	87.3±1.9	12.1±0.3	12.1±0.3	*	14.8±0.3	

Note. Analyses were re-calculated on an anhydrous basis using the loss on ignition (LOI) data from Puchtel et al. (2016). The transition metal abundances in the emplaced lava were calculated using ISOPLOT regressions for each element versus the calculated MgO content of the emplaced lava from this study. The uncertainties used in the regression analyses were as follows: for the transition metals, 5% (2SD) as derived from the external reproducibility of analyses of USGS SRM BIR-1, BCR-1, and BHVO-1; for MgO, 1% (2SD) as derived from the long-term reproducibility of analyses of USGS SRM BIR-1 and BCR-1 (Puchtel et al., 2016).

Table 2.5. Transition metal abundances in liquidus olivines and chromites from the Victoria's Lava Lake.

Sample	Sc	V	Cu	Ga	Y
12110 Olivine (N = 14)	5.84±0.18	7.82±0.39	4.25±0.19	0.239±0.067	0.122±0.025
12001 Olivine (N = 24)	6.02±0.45	7.31±0.39	2.62±0.67	0.115±0.043	0.093±0.010
12105 Olivine (N = 48)	6.12±0.21	7.21±0.36	2.87±0.42	0.097±0.017	0.093±0.009
12105/1 Olivine (N = 47)	4.66±0.14	7.18±0.36	2.72±0.43	0.149±0.048	0.079±0.010
12110 Chromite (N = 11)	10.1±4.8	1378±40	12.1±3.9	37.4±8.8	1.76±1.05
12001 Chromite (N = 64)	7.10±0.97	1395±28	9.47±3.15	19.6±0.8	0.407±0.554
12105 Chromite (N = 64)	7.12±0.67	1394±25	9.26±2.04	17.3± 0.5	0.092±0.060

Note. The data were obtained using the laser ablation ICP-MS technique. Each datum represents averages of multiple analyses performed on several mounts, as specified in the text. The uncertainties are 2SE.

The average V abundances in the liquidus olivines are 7.82±0.39 ppm in the chilled margin sample 12110 and 7.31±0.39, 7.21±0.36, and 7.18±0.36 ppm in the olivine cumulate samples 12001, 12105, and 12105/1, respectively (2SE). The average V abundances in the liquidus chromites are 1378±40 ppm in the chilled margin sample 12110, and 1395±28 and 1394±25 ppm in the olivine cumulate samples 12001 and 12105, respectively (2SE). It is important to note that the average V abundances for both olivines and chromites are identical between different cumulate samples collected across the lava lake. Even more importantly, the average V abundances in both olivine and chromite grains from the chilled margin and the cumulate zone samples are also identical, within their respective uncertainties.

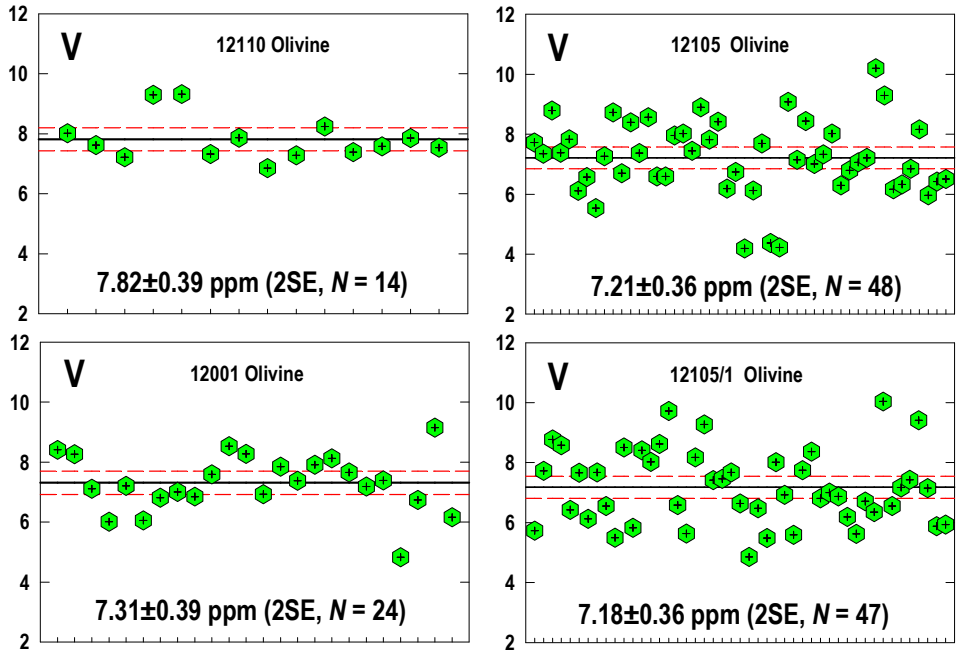

Figure 2.4. Laser ablation ICP-MS data for cores of solid, equant olivine grains from the chilled margin sample 12110 and olivine cumulate samples 12001, 12105, and 12105/1. The uncertainty on the concentrations is 2SE. Note the consistency of the average V abundances between samples collected from different parts of the lava lake.

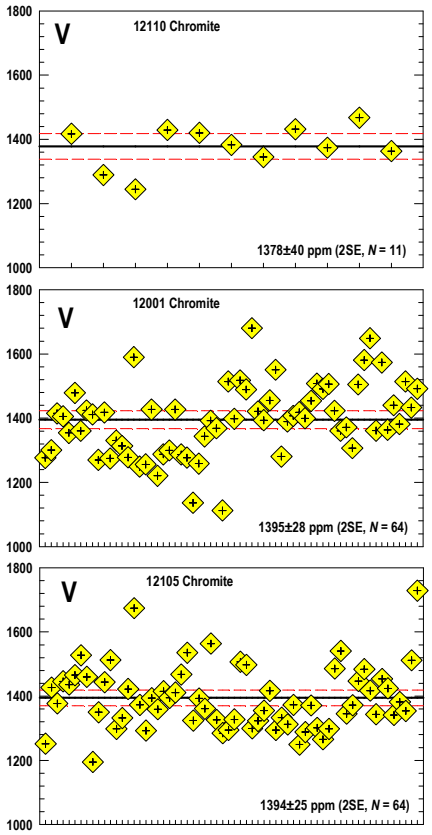

Figure 2.5. Laser ablation ICP-MS data for solid, equant chromite grains from the chilled margin sample 12110 and olivine cumulate samples 12001 and 12105. The uncertainty on the concentrations is 2SE. Note that, similarly to the olivine grains analyzed, chromite grains from the different parts of the lava lake have average V concentrations that are identical within the uncertainty.

Plotted in **Fig. 2.6.** are variations in lithophile trace element and transition metal abundances (ppm) *vs.* MgO contents (wt. %) in the whole-rock samples and liquidus olivines in equilibrium with the emplaced komatiite lava. The data form tight linear correlations for all elements analyzed; these linear correlations coincide with olivine control lines for the corresponding elements, indicating that olivine was the only major liquidus phase controlling variations of these elements over the entire range of the lava lake compositions. These correlations also attest to immobile behavior during secondary alteration and metamorphism of the lava lake, of all the transition metals analyzed in this study. This conclusion is

consistent with the findings of Puchtel et al. (1996, 2016) regarding immobile behavior of lithophile trace and highly siderophile elements that those authors studied.

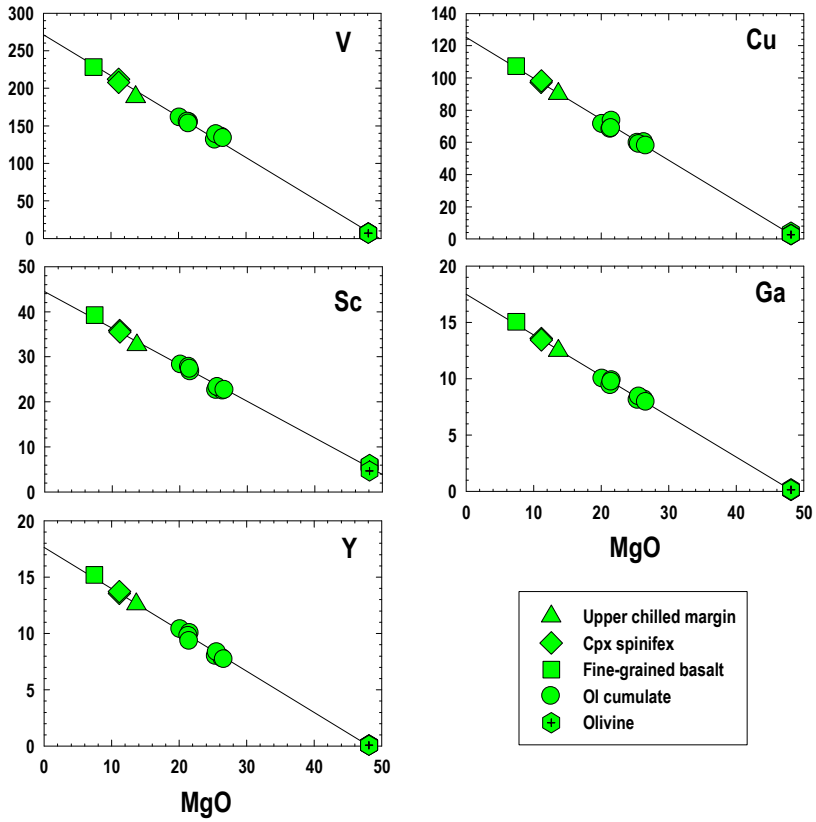

Figure 2.6. Concentrations of selected lithophile trace elements and transition metals (ppm) plotted against MgO contents (wt.%) for the whole rock samples and liquidus olivines of the Victoria's Lava Lake. All data plot on the tight, well constrained trends corresponding to olivine control lines, indicating that olivine was the only major fractionating phase controlling variations of these elements during differentiation of the lava lake, and that the samples fully retained their primary, igneous signatures with respect to concentrations of these elements.

In order to estimate the composition of the emplaced komatiitic basalt lava, several independent approaches were used, as outlined in the section on Analytical Techniques. Samples 91110, 01110/1, and 12110/1 collected from the upper chilled margin of the lava lake (Puchtel et al., 1996; 2016) are glassy rocks composed of ~15% euhedral olivine phenocrysts in a quenched groundmass of olivine microphenocrysts, cruciform and euhedral chromite grains, and devitrified glass. This part of the lava

lake must have crystallized very quickly. It did not undergo any post-eruption differentiation and is interpreted to have a bulk composition very similar to that of the komatiitic basalt liquid from which the lava lake formed. The average MgO content of the three samples is 14.65±0.04 wt. % MgO (2SD).

The second approach to estimate the composition of the emplaced komatiitic basalt lava was based on the relationship between the composition of olivine and that of the liquid from which it crystallized (Beattie et al., 1991). The most magnesian olivines ($Fo_{88.7\text{-}88.9}$) were documented in the upper and lower chilled margins of the lava lake (Puchtel et al., 1996). Using a $D^{Mg\text{-}Fe}_{Ol\text{-}Liq} = 0.31$ (Beattie et al., 1991) and the Mg/Fe ratio in the emplaced komatiite lava from Puchtel et al. (1996; 2016), these olivines were calculated to have been in equilibrium with a liquid containing 15.0±0.4 wt. % MgO (2SD).

Finally, the liquidus olivine composition was inferred using an indirect approach based on the general differentiation trends established for the lava lake. In the plots of MgO versus an element that is excluded from the olivine crystal lattice, the analytical data for samples containing different proportions of olivine crystallized from the emplaced komatiitic basalt lava must plot on the mixing lines, a.k.a. olivine control lines. The intercepts of these regression lines with the MgO axis correspond directly to the average composition of liquidus olivine. Using regressions for the incompatible lithophile trace element data from Puchtel et al. (1996; 2016), the average MgO content of the liquidus olivine has been calculated to be 47.8±0.5% MgO. Recalculating for the olivine stoichiometry, this gives an olivine composition of $Fo_{88.7}$, in excellent agreement with the results of the olivine microprobe studies. This result also implies equilibrium between liquidus olivine and the emplaced lava in terms of the Mg-Fe relationship. Thus, the three independent approaches yield an average MgO content of the emplaced komatiitic basalt lava of 14.8±0.3 wt. % (2SD).

Using the estimated MgO content of the emplaced komatiitic basalt lava of 14.8±0.3 wt. % and ISOPLOT regression analysis, we calculated abundances of the transition metals in the emplaced

komatiitic basalt lava; these data are reported in **Table 2.4**. These calculations gave the V content of 192±4 ppm. The average V contents of the liquidus olivines and chromites from the lava lake are calculated to be 7.38±0.30 and 1389±11 ppm, respectively, and the average Sc abundances are calculated to be 5.66±0.67 and 7.6±1.1 ppm, respectively. These data, thus, yielded the following liquidus mineral/komatiitic basalt melt partition coefficients for V and Sc: $D_V^{Ol\text{-}Liq} = 0.0385\pm0.0009$ and $D_V^{Chr\text{-}Liq} = 7.25\pm0.16$; $D_{Sc}^{Ol\text{-}Liq} = 0.174\pm0.006$ and $D_{Sc}^{Chr\text{-}Liq} = 0.236\pm0.007$. It is noteworthy that there are substantial differences in V and Sc partitioning behavior between olivine, chromite, and komatiitic melt. As a result, fractionation of chromite and olivine may have appreciable effect on the V/Sc ratio in the komatiitic and basaltic systems. In this study, we did not use the V/Sc systematics of the Victoria's Lava Lake to evaluate its redox state.

2.4.2. Evaluation of the redox state of the Victoria's Lava Lake system

Having determined the V partition coefficients between the liquidus olivine, chromite and the komatiitic basalt melt of the Victoria's Lava Lake, we used the experimental calibrations of Canil (1997, 1999; 2002) and Canil and Fedortchouk (2001) to evaluate the oxidation state of the komatiite system. Regressions of the experimental data yielded $\log(D_v^{Ol\text{-}Liq}) = -0.2416\times\Delta NNO - 1.4796$ ($r^2=0.94$) for the olivines (Canil, 1997; Canil and Fedortchouk, 2001), and $D_V^{Chr\text{-}Liq} = -5.442*(\Delta NNO)+6.1143$ ($r^2=0.97$) for the chromites (Canil, 1999). Though partitioning behavior of V has been shown to have little to no dependence on temperature, pressure, or melt composition, $D_V^{Chr\text{-}Liq}$ is known to depend strongly on the Cr/Al ratio of the system (Canil, 2002). For our calculations, we used the experimental calibration curve for komatiitic composition "komv" of Canil (1999). This composition was selected due to the fact that, among all experimental compositions studied by Canil (1999, 2002), it had the Cr/Al ratio that was most similar to that of the emplaced komatiitic basalt of the lava lake.

The fO_2 value calculated from the V partitioning data for the olivines is, thus, −0.24±0.04 ΔNNO log units, and the fO_2 value calculated from the V partitioning data for the chromite is −0.21±0.03 ΔNNO log units. The two independently obtained fO_2 values overlap within the respective uncertainties; the average fO_2 value of −0.22±0.04 (2SD) represents our best estimate for the redox state of the Victoria's Lava Lake.

2.5. Discussion

2.5.1. Effects of secondary alteration, re-equilibration, and crustal contamination

2.5.1.1. Secondary alteration

All komatiite lavas are altered to a greater or lesser degree as a result of interaction with seawater, as almost all were erupted subaqueously including the Victoria's Lava Lake, and also by subsequent metamorphism. Secondary alteration may result in post-magmatic re-distribution of petrogenetically important elements, including V, which, in turn, may have affected the estimates for V (and other transition metal) abundances in the emplaced komatiite lava. One way to test whether an element has been affected by postmagmatic processes is to plot its abundances against indices of magmatic differentiation, such as the MgO content (Arndt, 1986). Since the only liquidus phase present in komatiite lavas over a large range of temperatures and compositions is olivine, accompanied by minor chromite in lavas with less than 20-24% MgO depending on the oxidation state of the system (Barnes, 1998), samples with primary, magmatic distribution of the elements of interest should plot on olivine control lines. In case of the Victoria's Lava Lake, immobile behavior of most major, minor, and trace elements has been well documented (*e.g.,* Puchtel *et al.*, 1996, 2016). In this study, abundances of all transition metals are strongly inversely correlated with MgO content and follow olivine control lines (**Fig. 2.6.**), providing evidence for immobile behavior of these elements during alteration.

2.5.1.2. Mineral re-equilibration

The method to determine the redox state of a komatiite system used in this study requires liquidus olivine and chromite to be in equilibrium with the emplaced komatiite lava. Although olivine and chromite phenocrysts found in the upper chilled margins of komatiite lava flows likely preserve their original V partitioning characteristics due to the very quick solidification of this part of the lava flows (*e.g.,* Arndt, 1986), olivine and chromite from cumulate parts, which take longer to crystallize, may experience re-equilibration with the residual liquid (Barnes, 1998). In this study, several lines of evidence indicate that V re-equilibration between the olivine, chromite, and the komatiitic liquid played a very minor role during differentiation and crystallization of the Victoria's Lava Lake.

First, we analyzed only cores of solid, equant grains that were shown to be in equilibrium with the emplaced komatiite lava for major elements (Puchtel *et al.*, 1996). These cores of olivine and chromite grains, analyzed in samples collected across the lava lake, have similar V abundances between the samples, and little variations among the grains from the same samples, reflected in rather small uncertainties on the averages for individual samples.

Second, both olivine and chromite grains in the chilled margin sample 12110 have average V abundances identical to those of olivine and chromite grains in samples from the cumulate portion of the lava lake. Since the upper chilled margin of the lava lake most likely crystallized almost instantaneously as a result of intensive heat dissipation caused by turbulent flow and interaction with seawater (Huppert *et al.*, 1984; Huppert and Sparks, 1985b), as also evidenced by its essentially glassy texture (Puchtel *et al.*, 1996), it is very unlikely that the olivine and chromite grains from the cumulate zone of the lava lake would have retained the same V abundances as the olivine and chromite phenocrysts from the upper chilled margin, should any re-equilibration have taken place.

Finally, the consistency of the independent estimates of the redox state of the Victoria's Lava Lake system calculated on the basis of the olivine and chromite oxybarometers strongly argue against any late re-equilibration.

2.5.1.3. Crustal contamination

Due to their extremely high liquidus temperatures, in many instances exceeding 1600ºC, and low viscosities, komatiitic magmas are known to be able to assimilate up to 40% of country rocks on their way to the surface (Huppert and Sparks, 1985a) and up to 10% *via* thermal erosion after emplacement (Huppert and Sparks, 1985b). Due to one- to two orders of magnitude lower concentrations of lithophile trace elements in komatiitic magmas compared to upper crustal materials, crustal contamination may result in substantial changes in lithophile trace element and isotopic parameters of original komatiite magmas. Based on lithophile trace element data, Puchtel *et al.* (1996, 2016) calculated that the emplaced lava of the Victoria's Lava Lake was derived from a komatiite magma containing ca. 27% MgO *via* the combination of ca. 50% fractional crystallization and assimilation of 4.0±0.4% felsic crustal material of the adjacent Vodla Block tonalites. Although fractionation of olivine and minor chromite is not expected to cause any changes in the redox state of the original komatiite magma, the effects of assimilation of the tonalites must be evaluated and accounted for.

For the purpose of modeling, we assumed simple mixing between a tonalite endmember and the original komatiite magma parental to the Victoria's Lava Lake komatiitic basalt. As an estimate for the redox state of the tonalite endmember, we used an average fO_2 (+0.5 ΔNNO log units) of the andesitic continental crust produced at modern island arcs (Carmichael, 1991). Using the fO_2 of the contaminated Victoria's Lava Lake komatiite of −0.22±0.04 ΔNNO log units, addition of 4.0 wt. % of the tonalitic endmember is calculated to result in an increase in the oxygen fugacity of the original komatiite lava by 0.07 ΔNNO log units. Even though the redox state of the Archean continental crust is currently not very

well constrained and may slightly differ from the redox state of the modern continental crust, it was likely less oxidized due to the more reducing atmosphere in the Archean compared to the present. As such, this shift in the redox state of the original komatiite magma of 0.07 ΔNNO log units represents the maximum estimate. Assuming a rather conservative 50% uncertainty on this estimate from the range in crustal fO_2, crustal contamination is calculated to increase the oxidation state of the Victoria's Lave Lake system by 0.07±0.04 ΔNNO log units. Corrected for the effects of crustal contamination, the estimated redox state of the komatiite system is, thus, calculated to be −0.29±0.04 ΔNNO log units.

2.5.2. The significance of the redox data for the Victoria's Lava Lake

Based on the argument presented above, we conclude that the redox state of the Victoria's Lava Lake komatiite system of −0.29±0.04 ΔNNO log units, calculated on the basis of the combined olivine and chromite oxybarometers and corrected for crustal contamination, represents our best estimate for the redox state of the Victoria's Lava Lake primary komatiite magma. The uncertainty on this estimate is at least a factor of 10 smaller than those reported in the previous studies (Canil, 1997; Delano, 2001; Li and Lee, 2004).

Even though the absolute uncertainty on the estimate for the redox state of a komatiite system reached in this study is ca. 0.04 ΔNNO log units, it still can be affected by the absolute uncertainties on the experimental calibrations of both the olivine and chromite oxybarometers, which can be as large as 0.20 ΔNNO log units (Canil, 1999; Canil and Fedortchouk, 2001). However, since uncertainties on the relative estimates for redox states of different komatiite systems are insensitive to the uncertainties in the experimental calibrations, this method provides a high-resolution, accurate tool for constraining the evolution of mantle oxygen fugacity over Earth's history.

2.6. Concluding remarks

Komatiites represent a valuable tool for studying Earth's interior, especially during the first 2 billion years of Earth's history. This study reports details of a newly developed high-resolution method for determining redox state of komatiite lavas with a precision of better than 0.10 ΔNNO log units.

The new method uses the partitioning behavior of the redox-sensitive transition metal vanadium between olivine, chromite and komatiitic melt as oxybarometers, and the experimental calibrations of Canil (1997), Canil and Fedortchouk (2001) and Canil (1999, 2002). In order for this methodology to produce accurate and precise results, several important conditions must be met.

First, V must be shown to be immobile during secondary alteration and metamorphism of the selected komatiite lava. This is accomplished via systematic collection of a series of samples across differentiated komatiite lava flow(s), obtaining high-precision whole-rock major element and V (and other transition metal) concentration data using standard addition ICP-MS, and regressing these data against indices of magmatic differentiation (e.g., MgO content) to establish the magmatic nature of the variations in V abundances across the lava flows. Second, MgO, V, and other transition metal abundances in the emplaced komatiite lava must be precisely calculated using several independent approaches; these approaches should provide consistent results that must agree within the uncertainty of the method. Third, the komatiite lavas of interest must contain sufficient amounts of liquidus olivine and/or chromite and these must be shown to be in equilibrium with the emplaced komatiite lava. A special attention must be paid to ensure that no re-equilibration has occurred during differentiation of the komatiite lava units, which can be achieved via analyzing only cores of solid, equant olivine and/or chromite grains from both upper chilled margins and cumulate layers of lava flows and closely monitoring the consistency between their chemical compositions. Finally, laser ablation ICP-MS analyses of the olivine and/or chromite grains must be performed to determine V (and other transition

metal) concentrations with the highest possible precision and accuracy, which is achieved via analyzing sufficiently large number of inclusion-free grains.

The independent olivine and chromite oxybarometers studied here yielded results that overlapped within the respective uncertainties, attesting to the accuracy of the redox data obtained for the lava lake.

Even though the uncertainty on the oxygen fugacity of a komatiite system reached in this study is ca. 0.04 ΔNNO log units, it still can be affected by the absolute uncertainty on the experimental calibrations of the olivine and chromite oxybarometers, which can be as large as 0.20 ΔNNO log units (Canil, 1999; Canil and Fedortchouk, 2001). However, since uncertainties on the relative estimates for redox states of different komatiite systems are insensitive to the uncertainties in the experimental calibrations, this method provides a high-resolution tool for constraining evolution of the redox state of the mantle over Earth's history.

Acknowledgments for Chapter 2

This study was supported by NSF FESD Type I Grant #1338810 "The Dynamics of Earth System Oxygenation" (lead PI is A.D. Anbar, I.S. Puchtel is a co-PI). This source of support is gratefully acknowledged. We thank Cin Ty Lee, Dante Canil, and Fabrice Gaillard for constructive reviews that helped improve the original version of the manuscript, and Catherine Chauvel for editorial handling. We also thank Valentina Puchtel for help with sample preparation for the ICP-MS analyses.

References for Chapter 2

-Arndt, N.T., 1976. Melting relations of ultramafic lavas (komatiites) at one atmosphere and high pressure. Yearbook of Carnegie Inst. Wash. **75**: 555-562.

-Arndt, N.T., 1986. Differentiation of komatiite flows. Journal of Petrology **27**(2): 279-301.

-Arndt, N.T., Lesher, C.M., and Barnes, S.J. (2008). Komatiite. Cambridge, UK, Cambridge University Press.

-Arndt, N.T., and Nisbet, E.G. (1982). What is a komatiite? Komatiites. Arndt, N.T. and Nisbet, E.G. London, George Allen and Unwin**:** 19-28.

-Barnes, S.J., 1998. Chromite in komatiites, I. Magmatic controls on crystallization and composition. Journal of Petrology **39**(10): 1689-1720.

-Barnes, S.J., Hill, R.E.T., and Gole, M.J., 1988. The Perseverance ultramafic complex, Western Australia: the product of a komatiite lava river. Journal of Petrology **29**(2): 305-331.

-Beattie, P., Ford, C., and Russell, D., 1991. Partition coefficients for olivine-melt and orthopyroxene-melt systems. Contributions to Mineralogy and Petrology **109**(2): 212-224.

-Campbell, I.H., Griffiths, R.W., Hill, R.I. (1989). Melting in an Archean Mantle Plume: heads it's basalts, tails it's komatiites. Nature **339**: 697-699.

-Canil, D., 1997. Vanadium partitioning and the oxidation state of Archaean komatiite magmas. Nature **389**(6653): 842-845.

-Canil, D., 1999. Vanadium partitioning between orthopyroxene, spinel and silicate melt and the redox states of mantle source regions for primary magmas. Geochimica et Cosmochimica Acta **63**(3-4): 557-572.

-Canil, D., and Fedortchouk, Y., 2001. Olivine-liquid partitioning of vanadium and other trace elements, with applications to modern and ancient picrites. Canadian Mineralogist **39**: 319-330.

-Canil, D., 2002. Vanadium in peridotites, mantle redox and tectonic environments: Archean to present. Earth and Planetary Science Letters **195**(1-2): 75-90.

-Carmichael, I.S.E., 1991. The redox states of basic and silicic magmas: a reflection of their source regions? Contributions to Mineralogy and Petrology **106**(2): 129-141.

-Cottrell, E., and Kelley, K.A., 2011. The oxidation state of Fe in MORB glasses and the oxygen fugacity of the upper mantle. Earth and Planetary Science Letters **305**(3-4): 270-282.

-Cottrell, E., Kelley, K.A., Lanzirotti, A., and Fischer, R.A., 2009. High-precision determination of iron oxidation state in silicate glasses using XANES. Chemical Geology **268**(3-4): 167-179.

-Delano, J.W., 2001. Redox History of the Earth's Interior since ~3900 Ma: Implications for Prebiotic Molecules. Origins of life and evolution of the biosphere **31**(4-5): 311-341.

-Farquhar, J., Bao, H., and Thiemens, M., 2000. Atmospheric influence of Earth's earliest sulfur cycle. Science **289**(5480): 756-758.

-Huppert, H.E., and Sparks, R.S.J., 1985a. Cooling and contamination of mafic and ultramafic magmas during ascent through continental crust. Earth and Planetary Science Letterrs **74**(4): 371-386.

-Huppert, H.E., and Sparks, R.S.J., 1985b. Komatiites I: Eruption and flow. Journal of Petrology **26**(3): 694-725.

-Huppert, H.E., Sparks, R.S.J., Turner, J.S., and Arndt, N.T., 1984. Emplacement and cooling of komatiite lavas. Nature **309**(5963): 19-22.

-Li, Z.X.A., and Lee, C.T.A., 2004. The constancy of upper mantle fO_2 through time inferred from V/Sc ratios in basalts. Earth and Planetary Science Letters **228**(3-4): 483-493.

-Lyons, T.W., Reinhard, C.T., and Planavsky, N.J., 2014. The rise of oxygen in Earth's early ocean and atmosphere. Nature **506**(7488): 307-315.

-Mertzman, S.A., 2000. K-Ar results from the southern Oregon - northern California Cascade range. Oregon Geology **62**(4): 99-122.

-Nisbet, E.G., Arndt, N.T., Bickle, M.J., Cameron, W.E., Chauvel, C., Cheadle, M., Hegner, E., Kyser, T.K., Martin, A., Renner, R., and Roedder, E., 1987. Uniquely fresh 2.7 Ga komatiites from the Belingwe greenstone belt, Zimbabwe. Geology **15**(12): 1147-1150.

-Parman, S.W., Grove, T.L., Dann, J.C., and de Wit, M.J., 2004. A subduction origin for komatiites and cratonic lithospheric mantle. South African Journal of Geology **107**(1-2): 107-118.

-Puchtel, I.S., Haase, K.M., Hofmann, A.W., Chauvel, C., Kulikov, V.S., Garbe-Schönberg, C.D., and Nemchin, A.A., 1997. Petrology and geochemistry of crustally contaminated komatiitic basalts from the Vetreny Belt, southeastern Baltic Shield: Evidence for an early Proterozoic mantle plume beneath rifted Archean continental lithosphere. Geochimica et Cosmochimica Acta **61**(6): 1205-1222.

-Puchtel, I.S., Hofmann, A.W., Mezger, K., Shchipansky, A.A., Kulikov, V.S., and Kulikova, V.V., 1996. Petrology of a 2.41 Ga remarkably fresh komatiitic basalt lava lake in Lion Hills, central Vetreny Belt, Baltic Shield. Contributions to Mineralogy and Petrology **124**: 273-290.

-Puchtel, I.S., Touboul, M., Blichert-Toft, J., Walker, R.J., Brandon, A.D., Nicklas, R.W., Kulikov, V.S., and Samsonov, A.V., 2016. Lithophile and siderophile element systematics of the mantle at the Archean-Proterozoic boundary: Evidence from 2.4 Ga komatiites. Geochimica et Cosmochimica Acta **180:** 227-255.

-Roeder, P.L., and Emslie, R.F., 1970. Olivine-liquid equilibrium. Contributions to Mineralogy and Petrology **29**(4): 275-282.

Chapter 3: Redox state of the Archean mantle: Evidence from V partitioning in 3.5–2.4 Ga komatiites.

Note: This chapter has been previously published in the following publication:

Nicklas R. W., Puchtel I. S. and Ash R. D., (2018). Redox state of the Archean mantle: Evidence from V partitioning in 3.5–2.4 Ga komatiites. *Geochim. Cosmochim. Acta* **222**, 447–466.

Abstract for Chapter 3

Oxygen fugacity of the mantle is a crucial thermodynamic parameter that controls such fundamental processes as planetary differentiation, mantle melting, and possible core-mantle exchange. Constraining the evolution of the redox state of the mantle is of paramount importance for understanding the chemical evolution of major terrestrial reservoirs, including the core, mantle, and atmosphere. In order to evaluate the secular evolution of the redox state of the mantle, oxygen fugacities of six komatiite systems, ranging in age from 3.48 to 2.41 Ga, were determined using high-precision partitioning data of the redox-sensitive element vanadium between liquidus olivine, chromite and komatiitic melt. The calculated oxygen fugacities range from −0.11±0.30 ΔFMQ log units in the 3.48 Ga Komati system to +0.43±0.26 ΔFMQ log units in the 2.41 Ga Vetreny system. Although there is a slight hint in the data for an increase in the oxygen fugacity of the mantle between 3.48 and 2.41 Ga, these values generally overlap within their respective uncertainties; they are also largely within the range of oxygen fugacity estimates for modern MORB lavas of +0.60±0.30 ΔFMQ log units that we obtained using the same technique. Our results are consistent with the previous findings that argued for little change in the mantle oxygen fugacity since the early Archean and indicate that the mantle had reached its nearly-present day redox state by at least 3.48 Ga.

3.1. Introduction

The oxidation state of the mantle is a crucial thermodynamic parameter that controls such fundamental processes as planetary differentiation, mantle melting, and volcanic outgassing (Canil *et al.*, 1994; Kump *et al.*, 2001; Holland, 2002; Williams *et al.*, 2004; Frost *et al.*, 2008; Frost and McCammon, 2008; Cottrell and Kelley, 2011; Evans, 2012; Kelley and Cottrell, 2012; Lee *et al.*, 2016). It is quantified in terms of oxygen fugacity ($\Delta\log f\mathrm{O_2}$) relative to mineral assemblage buffers, which is determined in mantle-derived igneous rocks and then extrapolated to their mantle sources. There are a few approaches that can be used to determine $f\mathrm{O_2}$ of igneous rocks. In pristine samples, it can be determined using mineral $\mathrm{Fe^{2+}}/\Sigma\mathrm{Fe}$ equilibria (Canil *et al.*, 1994; Cottrell *et al.*, 2009). In Archean rocks, this approach cannot be used as the $\mathrm{Fe^{2+}}/\Sigma\mathrm{Fe}$ equilibria are usually affected by seawater alteration and metamorphism. Thus, alternative methods are required, including determination of iron stable isotopic composition of rocks and minerals (Williams *et al.*, 2005; Williams *et al.*, 2009; Dauphas, 2009), quantifying ratios of redox sensitive elements, such as V, to redox insensitive elements, such as Sc, in whole-rock samples (Li and Lee, 2004; Aulbach and Viljoen, 2015; Aulbach and Stagno, 2016), or using partitioning behavior of redox-sensitive elements, *e.g.,* V or Cr, during magmatic differentiation (Canil, 1997; Canil and Fedortchouk, 2001; Delano, 2001).

Although most studies, that largely concentrated on the upper-derived mantle rocks, have concluded that the mantle $f\mathrm{O_2}$ has remained constant within ~1.0 log unit since at least the early Archean (Canil, 1997; Canil and Fedortchouk, 2001; Delano, 2001; Li and Lee, 2004; Berry *et al.*, 2008; Trail *et al.*, 2011; Hibbert *et al.*, 2012), some researchers have argued for an increase in modern upper mantle $f\mathrm{O_2}$ since the early Archean by as much as 1.5 log units (e.g., Aulbach and Viljoen, 2015; Aulbach and Stagno, 2016). Resolving this controversy is crucial for understanding the chemical evolution of major terrestrial reservoirs, including the mantle and atmosphere. In order to segregate the core, the early

mantle must have been reducing enough to be in equilibrium with metallic Fe (Frost and McCammon, 2008), likely close to −2.3 ΔIW log units (Wade and Wood, 2005). The five orders of magnitude increase in the fO_2 of the present-day upper mantle is postulated to be the result of Fe^{2+} disproportionation into Fe metal and Fe^{+3} in Mg-perovskite, the lower mantle's dominant phase, and subsequent loss of Fe metal to the core during the magma ocean stage of the evolution of the planet (Wade and Wood, 2005; Frost *et al.*, 2008; Frost and McCammon, 2008). Mass balance calculations indicate that all of the mantle's Fe^{3+} could readily have been generated from a single disproportionation event (Williams *et al.*, 2012). As a result, the post-magma ocean mantle would likely have consisted of a relatively reduced upper mantle and a relatively oxidized lower mantle, which subsequently were homogenized to form the modern oxidized mantle. The need for disproportionation to oxidize the upper mantle has been disputed by Hirschmann (2012) and Zhang et al. (2017). These authors asserted that if Fe^{+3} coordination number increases above 7 GPa, an oxidized upper mantle is a natural consequence of a magma ocean. However, no experimental data yet exist to show that Fe^{+3} increases in coordination above 7 GPa. Thus, the timing and duration of this homogenization process, and even if Fe disproportionation is necessary to oxidize the mantle to its present day oxidation state, remain the subject of academic debate.

In order to further constrain the evolution of the redox state of the mantle in the Archean, we determined the fO_2 of six komatiite systems ranging in age from 3.48 to 2.41 Ga using partitioning behavior of the redox-sensitive element V between liquidus olivine, chromite and komatiite liquid. Komatiites are high-temperature ultramafic lavas that are generally thought to be the result of high-degree (up to 50%) anhydrous partial melting in mantle plumes (Campbell *et al.*, 1989; Herzberg, 1992). Due to their very low viscosities and extremely high temperatures, komatiitic melts ascended very quickly to the surface without significant fractionation (Huppert *et al.*, 1984; Huppert and Sparks, 1985),

which renders them useful samples for determining the oxygen fugacity of the upper mantle. Komatiites are largely restricted to the Archean, but are also known to occur in the Proterozoic and Phanerozoic.

Komatiites were likely not the dominant constituent of the Archean greenstone belt volcanic packages, with the bulk of Archean volcanism being represented by basalts (e.g., Condie, 2001), although in some greenstone belt sequences, the proportion of komatiites was as high as 25-30% (e.g., deWit and Ashwal, 1997; Condie, 2001). The question, thus, naturally arises: why use komatiites as probes of upper mantle fO_2 and not basalts? Other studies have used geochemical databases for basalts (Delano, 2001; Li and Lee, 2004), due to the massive amounts of literature data available. There are, however, several advantages to using komatiites as probes of upper mantle redox state.

First, it has been well established that the modern uppermost mantle, especially the mantle lithosphere, is heterogeneous with respect to oxygen fugacity (e.g. Wood et al., 1990; Cottrell and Kelley, 2013; Brounce et al., 2014; 2015), and this heterogeneity is evident in a ~6.0 log fO_2 unit difference in oxygen fugacity between island arc- and non-arc basalts (Carmichael, 1991). The idea that arc basalts were derived from more oxidized mantle sources has been challenged, however, by Lee *et al.* (2005), who showed that arc basalts and MORB display similar V/Sc. Whether or not the source region of arc basalts is more oxidized than that of MORB is still the subject of active debate (Lee et al., 2005, Kelley and Cottrell, 2012). Regardless of this, the tectonic environment of emplacement of Archean basalts cannot always be unambiguously established due to poor preservation of both magmatic features of the lavas and stratigraphy of Archean greenstone belts. A large body of isotope and geochemical data has been accumulated for the komatiite systems that were selected for this study, and a strong argument has been put forward in favor of uniform, mantle plume origin for these komatiite systems (McDonough and Ireland 1993; Kareem, 2005; Berry et al., 2008; Connolly et al., 2011; Puchtel et al., 2004, 2009;

2013; 2016a), thus avoiding the potential uncertainty from comparing different tectonic environments of lava emplacement.

Second, work on two separate modern OIB systems demonstrated a strong correlation between measured $Fe^{3+}/\Sigma Fe$ and sulfur content of volcanic glasses (Kelley and Cottrell, 2012; Moussallam et al., 2014, 2016). Sulfur is present in silicate melts as either S^{-2} or S^{+6} species; degassing of sulfur as SO_2 can have, therefore, a strong reducing post-emplacement effect on a lava. Degassing of sulfur has been shown to be one of the main controls on the evolution of fO_2 in lavas after their emplacement, with differentiation (Kelley and Cottrell, 2012; Grocke et al., 2015) and degassing of H_2O (Waters and Lange, 2016) or CO_2 (Moussallam et al., 2016) all having negligible effects. All of the komatiites studied here have been shown to be sulfur-undersaturated and volatile-poor (Puchtel et al., 2004, 2009; 2013; 2016a), whereas most modern MORB lavas have been shown to be sulfur- and vapor-saturated upon emplacement (e.g., Mathez, 1976; Bottinga and Javoy, 1990; Le Voyer et al., 2014), and so likely were many Archean basalts. Further, since most Archean basalts do not contain/preserve olivine, the V partitioning behavior in olivine cannot be used to determine their redox state.

The pioneering work to explore the redox-sensitive nature of V in komatiitic lavas has been done by Canil (1997, 1999) and Canil and Fedortchouk (2001). These authors constrained the bulk V partition coefficients in several komatiite systems by means of comparing the slopes of bulk fractionation trends for V with those for redox-insensitive elements (e.g., Sc, Zr, Y, Ti), for which the bulk partition coefficients were experimentally determined, and then used these bulk V partition coefficients and experimentally determined dependence of V partitioning on oxygen fugacity to constrain the redox states of these komatiite systems with a precision of ~1.5 ΔNNO log units.

Our newly developed analytical techniques that use the combined experimental data set of Canil (1997) and Canil and Fedortchouk (2001) and directly determined partitioning behavior of V between

liquidus olivine, chromite and komatiitic liquid, enabled us to determine the fO_2 of komatiite lavas with a precision of ca. ~0.30 log fO_2 units. In this study, we present results for the six komatiite systems studied, and discuss implications for the evolution of the redox state of the upper mantle.

3.2. Geological background and samples

In this study, whole-rock samples and liquidus olivine and chromite from a number of differentiated lava flows within six komatiite systems have been analyzed for trace metal abundances. These komatiite systems are the 3.48 Ga Komati and 3.26 Ga Weltevreden Formations (Fms.) from the Barberton Greenstone Belt (GB) in the Kaapvaal Craton, South Africa, the 2.72 Ga Pyke Hill and Alexo localities in the Abitibi GB, Canadian Shield, the 2.69 Ga Belingwe GB in the Rhodesian Craton, South Africa, and the 2.41 Ga Vetreny Belt in the Fennoscandian Shield.

3.2.1. The 3.48 Ga Komati and 3.26 Ga Weltevreden komatiite systems

The 3.48 Ga Komati Fm. is the komatiite type locality (Viljoen and Viljoen, 1969) situated within the Barberton GB in the Kaapvaal Craton, South Africa that contains a 3.6-3.2 Ga sequence of well-preserved supracrustal rocks. The lowermost section of the ~15 km sequence consists of the Onverwacht Group containing a total of seven Fms. (Lowe and Byerly, 1999). A thin felsic tuff layer within the Komati formation contains magmatic zircon with an age of 3482 ± 5 Ma (Armstrong et al. 1990). The Komati Fm. itself is divided into an upper 1.3 km-thick section of komatiitic basalts and a lower 1.8 km-thick section of komatiites (Viljoen et al. 1983; Dann, 2000). In this study, we analyzed the sample powders prepared by Puchtel et al. (2013), along with olivine, for a series of spatially closely associated komatiite lava flows (see Fig. 1 in Puchtel et al. 2013) within the lower Komati Fm. Solid equant olivine grains studied at this locality came from the cumulate portions of the lava flows. The

metamorphic grade of the komatiite lavas at the type locality did not exceed the lower greenschist facies, with the majority of cumulate samples preserving up to 60% of their magmatic mineralogy.

The 3.26 Ga Weltevreden Fm. is the youngest within the Onverwacht Group, and is dated by the Re-Os method to 3266 ± 8 Ma (Connolly et al., 2011), consistent with the age of the underlying volcanics and overlying sediments. Located on the northern limb of the Barberton GB, the Weltevreden Fm. consists of a several thousand meter thick sequence of komatiitic lavas, tuffs, and sills. The lava flows vary in thickness between 10 and 500 m. In this study, we analyzed sample powders prepared by Puchtel et al. (2013) for three differentiated komatiite lava flows (see Fig. 2 in Puchtel et al. (2013)). The metamorphic grade of these lava flows did not exceed prehnite-pumpellyite facies. Additional field, petrological, and geochemical information on both localities can be found in Kareem (2005), Connolly et al. (2011), Stiegler et al. (2012), and Puchtel et al. (2013).

3.2.2. The 2.72 Ga Pyke Hill and Alexo komatiite systems

The 2.72 Ga Pyke Hill and Alexo komatiite systems are located within contemporaneous volcanic sequences that belong to the Kidd-Munro Assemblage of the Abitibi GB, Superior Craton, Canada (Pyke et al. 1973; Arndt, 1986a). The komatiites have been dated using the Re-Os system to 2737 ± 16 Ma (Puchtel et al., 2009). The Pyke Hill samples were obtained from a ~100 m long drill core, which intersected a number of thin differentiated lava flows. Sample powders for the 2.9 m thick lava flow PH-I prepared by Puchtel et al. (2004) were used in this study (see Fig. 1 in Puchtel et al. (2004)). The metamorphic grade in the area did not exceed the prehnite-pumpellyite facies (Arndt et al. 1977); the cumulate portion of the lava flow preserved up to 50% of its magmatic mineralogy.

The Alexo samples, previously studied by Puchtel et al. (2004), came from a ~400 m drill core. In this study, we used the powders prepared by Puchtel et al. (2004) for the 18 m thick differentiated lava flow (see Fig. 1 in Puchtel et al. (2004)). The cumulate zone of the flow preserved up to 40% of its

magmatic mineralogy. More detailed information on the geochemistry and petrology of the studied komatiite samples from the Pyke Hill and Alexo localities can be found in Puchtel et al. (2004, 2009).

3.2.3. The 2.69 Ga Belingwe komatiite system

The 2.69 Ga Belingwe komatiite system is located within the Belingwe GB, an ~ 8 km thick sequence of supracrustal rocks in the Rhodesian Craton, Zimbabwe (Nisbet et al. 1977, 1987). The second-lowest formation within the GB is the ~1 km thick Reliance Formation, a mafic-ultramafic volcanic sequence. The middle section of the Reliance formation (400 m) contains komatiite lava flows, whereas the upper and lower sections of the Formation are composed of basalts. Komatiites within the Reliance formation have been dated by the Pb-Pb whole-rock method to 2692 ± 9 Ma (Chauvel et al. 1993). In this study, we utilized sample powders prepared by Puchtel et al. (2009) for a single differentiated lava flow, named Tony's Flow, sampled in both surface outcrops and the drill core (see Fig. 1 in Puchtel et al., 2009). These komatiites are among the best-preserved komatiites found on Earth (Nisbet et al., 1987). Additional information on the geochemistry and petrology of the Belingwe komatiite system can be found in Nisbet et al. (1987), Renner et al. (1994), and Puchtel et al. (2009).

3.2.4. The 2.41 Ga Vetreny Belt komatiite system

The 250 km long Vetreny Belt in SE Fennoscandia is considered to be part of one of the oldest known large igneous provinces that formed in a continental rift setting, during the interaction of a mantle plume with the Archean continental crust of the Karelian granite-greenstone terrain (Puchtel et al., 1997). A komatiitic basalt lava containing ca. 15% MgO flowed into a large topographic depression and formed a ~110 m thick differentiated sequence, now known as the Victoria's Lava Lake. This komatiitic sequence, metamorphosed to the prehnite-pumpellyite facies, is also among the best preserved in the Precambrian record (Puchtel et al., 1996; 2016a). This lava has been interpreted to be derived from 50% fractional crystallization of an original komatiite magma that contained 27% MgO,

accompanied by ca. 4% contamination by 3.21 Ga upper crustal rocks of the adjacent Vodla Block TTG complex (Puchtel et al., 2016a). These authors reported Re–Os and Sm–Nd isochron ages for the lava lake of 2407±6 and 2403±32 Ma, respectively. Additional geochemical and petrological data on the Victoria's Lava Lake can be found in Puchtel et al. (1996, 2016a). The partitioning behavior of V between liquidus olivine, chromite and emplaced komatiitic basalt lava during differentiation of the lava lake has been studied in detail by Nicklas et al. (2016). The data obtained in their study have been presented here together with some additional data for the lava lake, along with the data for the other five komatiite systems, for the sake of completeness and consistency.

3.3. Analytical Techniques

3.3.1. Determination of the composition of the emplaced komatiite lavas

Accurate determination of the V content of the emplaced komatiite lava is crucial for estimating V partition coefficient between liquidus olivine, chromite and the komatiite melt from which they crystallized. In order to determine the V content of the emplaced lava, its MgO content must first be determined. Three independent approaches were used in several previous studies to determine the MgO contents of the emplaced lavas for each of the six komatiite systems. These approaches have been developed by Arndt (1986) and Barnes et al. (1988) and have been widely used in the follow-up studies of komatiites.

The first approach uses the composition of the chilled margins of a lava flow as a proxy for the emplaced lava composition. This approach is based on the observation that chilled margins of komatiite lava flows crystallized rapidly (e.g., Huppert and Sparks, 1985). Consistent with this, they usually contain little to no cumulus olivine, although many contain 2-5% by volume of olivine phenocrysts with skeletal crystal habits indicative of their crystallization *in situ* (e.g., Arndt et al., 1977; Arndt, 1986b). Normally, if chilled margins of a komatiite lava flow are well preserved, their composition can be used

to directly determine the composition of the emplaced komatiite lava; the other two approaches are complementary and generally serve as independent tests of the results obtained using the first approach.

The second approach is based on the well-established Fe-Mg relationship between the composition of olivine and that of the liquid from which it crystallized (Roeder and Emslie, 1970; Beattie et al., 1991). The maximum average MgO and minimum average FeO contents of the cores of equant olivine grains in the cumulate portions of lava flows and olivine phenocrysts in the chilled margins (where available) were determined, and the compositions of the komatiite liquids in equilibrium with these olivine compositions were estimated using the partition coefficient $D^{Ol\text{-}Liq}_{Mg\text{-}Fe} = 0.30$ from Beattie et al. (1991). Further, the compositions of the chilled margins derived from approach (1) and those of the emplaced lavas derived from approach (2) were tested for consistency.

Finally, the third approach requires estimating the average MgO content of liquidus olivine in equilibrium with the emplaced lava by means of regressing the abundances of the elements that are excluded from the olivine crystal lattice (i.e., elements that are highly incompatible in olivine) against the MgO contents; the intersections with the MgO axis correspond to the average MgO content in the liquidus olivine. The average MgO content of the liquidus olivine is then used to back-calculate the MgO content of the emplaced lava using approach (2).

All three approaches gave consistent results for the komatiite systems studied here; the average maximum MgO and minimum FeO contents in the liquidus olivine, as well as calculated MgO and FeO contents in the emplaced komatiite lavas for each komatiite system with their respective uncertainties (2 standard deviations, 2SD) are presented in Tables 4 and 5. After the MgO contents of the emplaced komatiite lavas have been calculated, the V (and other trace metal) contents in the emplaced komatiite lavas were calculated via regressing measured trace metal abundances in whole-rock samples and olivine against the MgO contents using ISOPLOT (Ludwig, 2003). For additional details on the

protocol for estimating the MgO and trace metal contents of the emplaced komatiite lavas for the studied komatiite systems and the associated uncertainties of the method, the reader is referred to the publications by Puchtel et al. (2004, 2009, 2013, 2016a) and Nicklas et al. (2016). Additional background information used in the calculations is presented in the online Supplementary Tables A1-A6.

3.3.2. Analysis of major and minor element abundances in the whole-rock samples

Major element analyses of the whole-rock komatiite samples were carried out at Franklin & Marshall College on fused glass discs using a Phillips 2404 XRF spectrometer, following the procedure of Mertzman (2000). Typical accuracy of the analyses was ~2% relative (2SD) for major elements with concentrations >0.5% and ~5% relative for the rest of the major elements and for minor elements, as indicated by the analysis of the USGS standard reference materials (SRM) BIR-1 and BCR-1 as unknowns (Puchtel et al., 2016a). We used the major element data obtained by Puchtel et al. (2004, 2009, 2013, 2016a) for the same sets of komatiite sample powders further studied here.

3.3.3. Analysis of trace metal abundances in the whole-rock samples

The abundances of the trace metals in the whole-rock samples were determined using the standard addition solution inductively-coupled plasma mass-spectrometry technique (SA ICP-MS), and following the protocol detailed in Nicklas et al. (2016). Approximately 50 mg of sample powder, 0.5 mL double-distilled conc. HNO_3 and 3 mL double-distilled conc. HF were placed in 15 mL screw-cap Savillex Teflon vials, tightly sealed using Teflon tape, and kept on a hotplate at 200ºC for 48 hours. The vials were then opened, the sample solutions evaporated to dryness, and 0.5 mL of distilled SeaStar $HClO_4$ was added to the dry residue to convert fluorides into perchlorides. The vials were sealed again and placed on the hotplate at 200ºC for 24 hours. The vials were then opened and the sample solutions dried down on the hotplate at 230ºC. This step was followed by re-dissolution of the residue in 3-4 mL of 6*M*

HCl on the hotplate to convert it into the chloride form, and dried down. This step was repeated until clear solution with no visible residue was obtained upon re-dissolution in 6*M* HCl. The dry residue was then taken up in ~10 grams of 0.8*M* HNO_3 (with the exact weight recorded) and this stock solution was used for preparing spiked aliquots for the ICP-MS measurements. A standard addition mixed spike was prepared, containing concentrated solutions of Sc, V, Cu, Ga, Y, and Zr. Three aliquots of each sample, each containing 0.5-1.0 g of sample stock solution (with the exact weight recorded), were prepared, one containing no spike, one with the amount of spike containing ~2× the estimated amount of element present in the sample aliquot, and one with the amount of spike containing ~4× the estimated amount of element present in the sample aliquot, with the exact weights of the spike recorded. One total analytical blank (TAB) was also prepared and measured with every batch of 6 samples. Approximately 500 mg of 500 ppb In solution (with the exact weight recorded) was added to each sample aliquot and the TAB solutions to monitor and correct for the signal drift during the analysis, and the one sample- and two sample-spike solutions for each sample were diluted to 10 grams using 0.8*N* HNO_3.

The sample solutions were analyzed on a *ThermoFinnigan Element2* sector field ICP-MS at the *Plasma Laboratory (PL),* Department of Geology, University of Maryland. Prior to analysis, the instrument was thoroughly tuned to maximize sensitivity and minimize oxide production, and mass-calibrated. The intensities of selected isotopes of each element were measured in both low- and medium resolution modes. The raw data were reduced using an in-house Excel macro. The in-run precision (i.e., 2SE) was typically between 1 and 2% relative for all elements. The external precision and accuracy (i.e., 2SD) of the procedure was determined via the analysis of the USGS SRM BIR-1 and BHVO-1, which were digested and run on a regular basis throughout the entire analytical campaign; the V and Sc abundance data for these SRM are presented in **Fig. 3.1**. The uncertainties on V and Sc concentrations were between 3 and 5% (2SD), and the obtained average concentrations were in perfect agreement with

the GeoREM reference values for these SRM **(Fig. 3.1.)**. The largest of the 2SD uncertainties (i.e., 5%) obtained from analyses of the two USGS SRM were used as a measure of uncertainty on the obtained trace metal abundances in the whole-rock samples. These 2SD uncertainties were further used in the ISOPLOT regression calculations to determine the trace metal abundances in the emplaced lavas for each komatiite system. For additional details on the development of the high-precision trace metal analysis in komatiites, the reader is referred to the publication by Nicklas et al. (2016).

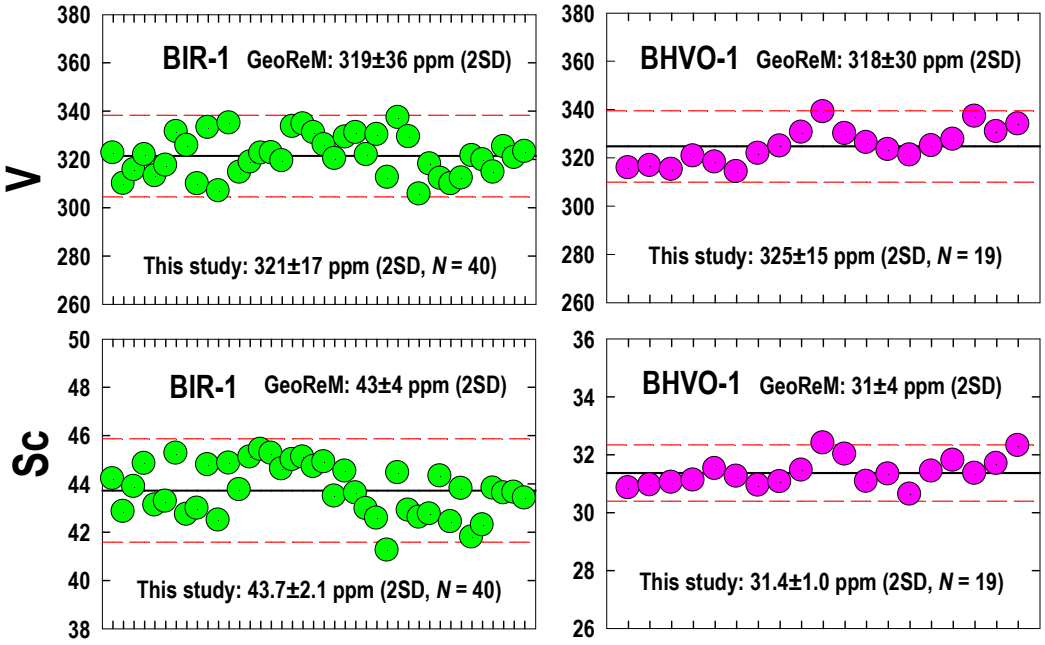

Figure 3.1. Vanadium and Sc abundances (ppm) in replicate digestions of the USGS SRM BIR-1 and BHVO-1 determined using the standard addition solution ICP-MS technique over the course of the entire analytical campaign. The external reproducibility of the analysis (2SD) is listed for each element and was 4.9% and 4.0% relative for V and Sc, respectively; this uncertainty has been used as the measure of uncertainty on the trace element abundance data for the whole-rock komatiite samples analyzed in this study. The GeoREM preferred values for each SRM are provided for reference.

3.3.4. Laser ablation ICP-MS analysis of liquidus olivine and chromite

Rock chips ~10 mm across or polished thin sections of the olivine cumulate samples (B_{2-4} subzones) from each komatiite system, as well as of the chilled margin samples TN01 (Belingwe) and 12110

(Vetreny) and of spinifex-textured samples PH04 (Pyke Hill) and ALX26 (Alexo), and pure chromite separates from the Vetreny komatiite system, the only system where chromite was a liquidus phase in addition to olivine, were selected for analysis. The chromite separates were mounted in epoxy and the mounts were polished prior to the analysis.

The olivine and chromite grains were analyzed using an *UP213 New Wave* laser-ablation system coupled to the *ThermoFinnigan Element2* ICP-MS at *the PL*. The quintupled Nd-YAG laser operated at 7 Hz with fluence controlled between 2-4 J/cm^2 (~60% laser power). The spot size of each analysis varied between 55 and 100 μm depending on the size and homogeneity of the grains being analyzed. Except for the spinifex-textured samples PH04 and ALX26, where cores of skeletal platy olivine grains were studied, only solid, equant olivine and chromite grains containing no visible inclusions were selected for analysis. Photomicrographs of magmatic olivines from chilled margin (a), olivine spinifex (b), and olivine cumulate samples (c) of the type that were selected for analysis are shown in **Fig. 3.2.**

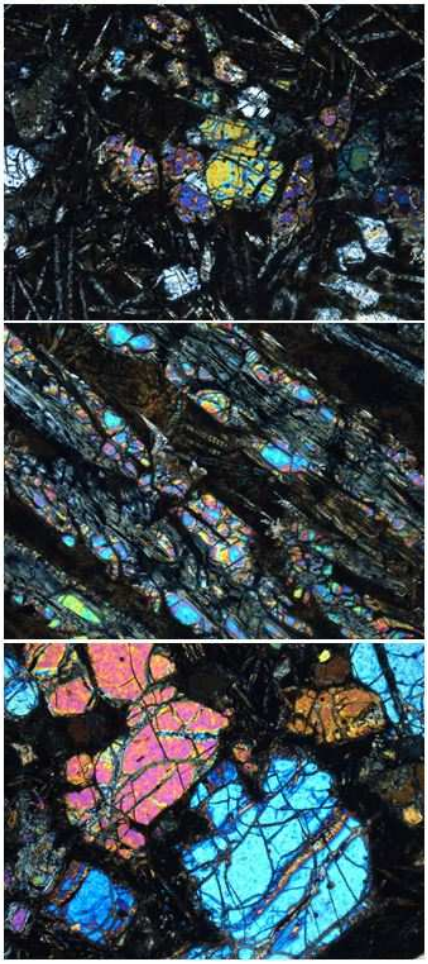

Figure 3.2. Photomicrographs of the upper chilled margin sample TN01 (**a**), spinifex-textured sample PH04 (**b**), and the olivine cumulate sample ZV77 (**c**) showing the type of olivine grains analyzed in this study. Only sufficiently large areas of olivine grains free from cracks and inclusions were analyzed. The fields of view are 3.0×2.5 mm; cross-polarized light.

Replicate analyses of the USGS SRM BHVO-2G and BCR-2G were performed with each set of 12-16 spots analyzed. The raw data were reduced using the *LAMTRACE* software and the average FeO abundances for the olivine and chromite as normalizing values. These average FeO abundances were derived from the previous studies of the six komatiite systems (Puchtel et al. 2004; 2009; 2013; 2016a), as well as from this study, and are presented in Table 5 and in the online Supplementary **Tables A1-A6**.

In order to assess the uncertainty on the trace metal concentration data obtained by the laser ablation ICP-MS analysis of olivine, a single grain of San Carlos olivine has been analyzed using the same

protocol utilized in the analysis of komatiitic olivine in this study, and the data are presented in **Fig. 3.3**. The uncertainties for both V and Sc were ~5% (2SD). Because variations in trace metal abundances in the studied populations of olivine grains within individual samples were >5% (2SD), and, thus, likely reflect small natural compositional variability between individual grains, the 2SD was used as a measure of the uncertainty on the calculated average concentrations of trace metals in olivine and chromite for the individual samples.

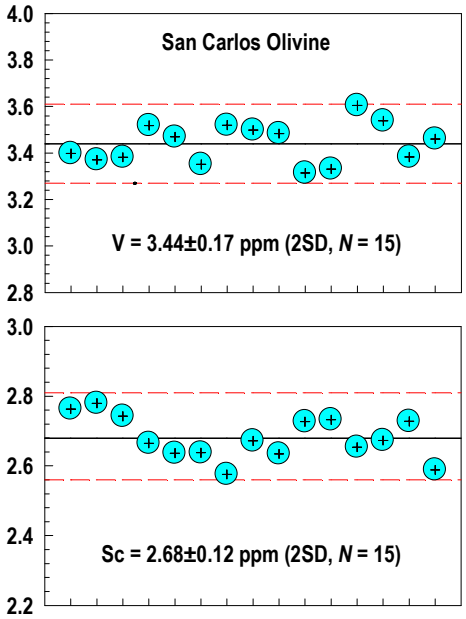

Figure 3.3. Vanadium and Sc abundances (ppm) in a single grain of San Carlos olivine determined by the laser ablation ICP-MS technique. The external reproducibility of the analysis (2SD) is listed for each element and was 5.0% and 4.6% relative for V and Sc, respectively.

3.4. Results

3.4.1. Trace metal abundances in the liquidus olivine and chromite

Average concentrations of V, Sc, Ga, Y, and Cu in olivine and chromite from the studied six komatiite systems are listed in **Table 3.1.;** the full sets of the LA ICP-MS analysis data are presented in the online Supplementary **Tables A1-A6**.

Table 3.1. Average trace metal abundances in olivine and chromite from the studied komatiite systems

Locality	Sample	*N*	Sc	V	Cu	Ga	Y
Komati	BV03 Ol cum	10	2.79±1.36	5.29±4.05	3.03±3.45	0.268±0.243	n.d.
	BV10 Ol cum	12	2.77±1.58	5.10±2.87	2.75±2.79	0.277±0.334	n.d.
	BV13 Ol cum	12	2.95±1.29	5.47±2.13	2.88±1.87	0.233±0.434	n.d.
	BV15 Ol cum	12	3.05±1.77	5.64±3.21	3.48±1.12	0.294±0.328	n.d.
	BV16 Ol cum	12	2.83±1.04	5.25±2.81	3.87±2.09	0.214±0.280	n.d.
Weltevreden	501-1 Ol cum	36	3.03±1.34	4.89±1.94	1.93±0.55	0.088±0.112	0.077±0.133
	501-8 Ol cum	43	4.10±1.53	4.62±1.51	1.96±0.49	0.077±0.092	0.061±0.117
	12-6 Ol cum	16	5.77±0.68	4.65±0.84	2.06±0.38	0.090±0.050	0.050±0.076
	12-8 Ol cum	16	5.60±0.60	4.93±0.62	2.39±0.39	0.079±0.010	0.038±0.015
Pyke Hill	PH04 Ol spx	16	4.37±1.16	5.44±1.27	2.11±0.39	0.079±0.024	0.061±0.037
	PH18 Ol cum	25	3.78±1.14	5.83±1.08	1.88±0.49	0.101±0.042	0.085±0.035
	PH19 Ol cum	16	6.65±1.94	5.62±1.07	2.23±0.54	0.151±0.072	0.135±0.094
	PH20 Ol cum	20	4.62±1.21	5.59±1.68	1.84±0.80	0.207±0.270	0.127±0.161
Alexo	ALX26 Ol spx	49	5.79±2.03	5.84±0.86	3.31±0.60	0.112±0.036	0.067±0.034
	ALX19 Ol cum	74	4.43±0.93	5.95±1.22	2.76±0.79	0.077±0.064	0.065±0.061
	ALX20 Ol cum	39	4.33±1.70	5.62±0.96	2.43±0.75	0.069±0.041	0.052±0.040
Belingwe	TN01 Ol chill	13	4.88±0.71	5.68±1.32	2.71±0.76	0.076±0.068	0.080±0.086
	ZV10 Ol cum	23	5.11±0.93	5.81±1.29	2.94±0.62	0.082±0.042	0.091±0.092
	ZV77 Ol cum	24	6.23±1.43	5.69±1.62	2.82±0.57	0.115±0.054	0.115±0.123
Vetreny	12110 Ol chill	14	5.84±0.68	7.82±1.45	4.25±0.71	0.194±0.089	0.114±0.071
	12110 Chr chill	11	7.75±4.38	1378±133	10.8±9.6	33.8±18.0	1.76±2.98
	12001 Ol cum	24	6.02±2.23	7.31±1.92	2.36±2.19	0.115±0.209	0.093±0.047
	12001 Chr cum	64	6.65±2.85	1395±225	7.72±9.17	19.6±6.5	0.105±0.310
	12105 Ol cum	74	6.12±1.09	7.21±2.52	2.83±1.90	0.096±0.116	0.093±0.064
	12105 Chr cum	64	6.82±2.21	1394±198	8.05±7.03	17.3±3.8	0.073±0.283
	12105/1 Ol cum	48	4.66±0.95	7.18±2.48	2.59±2.33	0.123±0.272	0.079±0.068

Note. *N* - number of olivine grains analyzed in a given sample. The uncertainties are 2SD. Data for the individual LA-ICP-MS analyses for each of the komatiite system are provided in the online Supplementary Tables A1-A6. n.d. – not determined.

Vanadium concentrations in olivine are low relative to those in the emplaced komatiite and komatiitic basalt lavas and vary in a narrow range, between 4.6 and 7.8 ppm, indicating incompatible behavior of V in olivine. Average V abundances in olivine within individual komatiite systems show even less variability, from ±2% in the Vetreny system up to ±8% in the Komati system, as measured by the 2SD uncertainty on the averages for each of the system (**Table 3.5.**). It is also important to note that

V concentrations in olivine from the chilled margin samples 12110 (Vetreny) and TN01 (Belingwe), as well as from the spinifex-textured samples PH04 (Pyke Hill) and ALX26 (Alexo), are identical, within their respective uncertainties, to those in olivine from the cumulate samples of the same komatiite systems.

Vanadium concentrations in cumulus chromite from the Vetreny komatiite system studied by Nicklas et al. (2016) are high relative to those in the emplaced komatiitic basalt lava, indicating compatible behavior of V in chromite, with averages ranging between 1378 ppm (upper chilled margin sample 12110) and 1395 ppm (cumulate sample 12001).

3.4.2. Trace metal abundances in the whole-rock samples

The abundances of V, Sc, Ga, Cu, Y, and Zr in the whole-rock samples from the six komatiite systems are listed in **Tables 3.2.** and **3.3.**; the V and Sc abundances are also plotted as a function of MgO contents in **Figs. 3.4.-3.6**.

Table 3.2: Trace metal abundances in the early Archean komatiites from the Komati and Weltevreden Formations of the Barberton Greenstone Belt, South Africa

Locality	Sample	MgO	LOI	Sc	V	Cu	Ga	Y	Zr	Lithology
Komati	**BV02**	29.4	6.44	18.3	104	37.6	4.88	7.09	24.4	CM
	BV04A	29.5	6.96	18.2	106	82.8	4.89	7.11	24.3	Ol spx
	Replicate			17.7	109	78.0	4.72	6.96	23.0	Ol spx
	BV05	28.2	6.23	19.3	112	34.1	5.12	7.90	25.3	Ol spx
	Replicate			19.0	114	36.9	5.06	7.74	24.6	Ol spx
	BV06	25.3	4.29	21.3	124	46.5	5.49	8.66	28.3	Ol spx
	Replicate			21.8	125	48.4	5.62	8.89	29.5	Ol spx
	BV08	27.8	6.44	19.7	110	22.7	5.11	7.92	26.8	Ol spx
	BV01	33.1	7.52	15.3	85.7	47.5	3.91	5.84	18.0	Ol cum
	BV03	35.3	5.79	13.3	75.4	26.2	3.48	5.17	16.8	Ol cum
	Replicate			13.8	80.8	26.8	3.59	5.28	16.9	Ol cum
	BV04B	31.3	7.82	16.9	97.3	48.4	4.25	6.66	23.3	Ol cum
	Replicate			16.4	99.9	46.5	4.14	6.56	21.0	Ol cum
	BV10	34.1	7.05	15.3	86.0	9.13	3.86	6.04	19.1	Ol cum
	BV13	36.1	7.55	13.2	74.1	4.90	3.04	4.67	16.1	Ol cum
	BV15	36.7	7.22	12.8	70.7	5.95	3.18	4.47	15.6	Ol cum
	BV16	34.9	7.36	14.5	75.9	4.37	3.62	5.34	17.2	Ol cum
Weltevreden	**564-6**	31.0	8.87	19.7	104	27.8	4.60	4.09	8.60	CM
	501-3	31.0	7.85	19.6	104	27.7	4.21	3.73	8.00	Ol spx
	501-4	34.0	10.3	17.4	92.0	22.1	3.61	3.43	7.12	Ol spx
	564-4	28.8	7.89	21.0	112	14.9	4.84	4.47	10.5	Ol spx
	12-2	28.9	8.08	20.8	108	28.8	5.03	4.25	10.4	Ol spx
	501-1	42.7	10.7	10.4	53.5	2.27	2.31	1.99	4.14	Ol cum
	501-7	41.7	10.1	11.8	58.8	3.36	2.48	2.17	4.44	Ol cum
	501-8	42.4	9.85	11.0	55.8	3.37	2.26	2.02	4.55	Ol cum
	501-9	42.1	9.79	11.6	57.8	2.99	2.34	2.18	4.60	Ol cum
	501-10	41.5	6.85	11.2	57.8	2.66	2.38	2.10	6.49	Ol cum
	564-2	41.0	8.73	11.3	55.9	16.23	2.19	1.88	4.50	Ol cum
	564-3	41.4	8.37	11.6	59.3	10.21	2.22	1.93	4.19	Ol cum
	12-6	40.7	9.36	11.6	59.8	3.50	2.05	2.08	4.33	Ol cum
	12-8	42.0	10.3	11.1	53.7	2.40	2.24	1.95	4.76	Ol cum

Note. Here and in Table 3, the abundances of both MgO (wt. %) and trace metals (ppm) are re-calculated on an anhydrous basis using the LOI (wt. %) values from Puchtel et al. (2004; 2009; 2013; 2016a). CM – chilled margin, Ol spx – olivine spinifex, Ol cum – olivine cumulate samples. Additional major element data are provided in the online Supplementary Tables A1-A6.

Table 3.3. Trace metal abundances in late Archean komatiites from the Abitibi and Belingwe greenstone belts and in early Proterozoic komatiitic basalts from the Vetreny Belt

Locality	Sample	MgO	LOI	Sc	V	Cu	Ga	Y	Zr	Lithology
Pyke Hill	**PH23**	27.5	6.73	24.1	144	21.0	7.93	8.27	17.3	CM
	PH04	29.1	6.62	24.6	141	49.4	7.24	7.09	15.7	Ol spx
	PH13	24.2	5.74	29.5	177	37.3	9.88	10.3	24.2	Ol spx
	Replicate			29.6	173	38.4	9.86	10.4	23.6	Ol spx
	PH14	23.5	5.67	29.7	180	33.0	9.53	10.3	24.0	Ol spx
	PH17	28.8	6.29	23.6	138	23.4	7.78	7.93	18.3	Ol cum
	PH18	30.3	5.93	21.9	130	43.6	7.14	7.33	17.1	Ol cum
	PH19	32.6	6.37	20.5	120	15.7	6.56	6.71	15.8	Ol cum
	PH20	32.4	7.15	20.3	119	5.67	6.38	6.59	16.1	Ol cum
	PH22	29.2	6.63	22.6	134	27.4	7.38	7.58	17.4	Ol cum
Alexo	**ALX21**	26.7	6.60	28.6	164	42.3	8.10	8.35	18.5	CM
	ALX02	25.5	6.02	29.1	172	62.4	8.34	8.51	18.3	Ol spx
	ALX07	23.7	5.91	29.7	176	19.8	8.95	8.75	19.0	Ol spx
	ALX12	20.7	4.80	32.2	194	174	9.51	9.93	22.4	Ol spx
	ALX14	25.7	6.46	28.3	164	334	8.63	7.93	17.8	Ol spx
	ALX15	27.1	6.39	26.4	151	48.7	7.55	7.57	15.8	Ol spx
	ALX26	30.0	7.16	22.7	129	46.3	6.86	6.70	16.9	Ol spx
	ALX18	39.7	11.4	13.8	74.9	2.94	3.57	3.51	7.74	Ol cum
	ALX19	36.4	7.79	17.1	97.9	27.4	4.61	4.70	9.76	Ol cum
	ALX20	35.4	7.62	18.5	106	26.6	5.19	5.10	11.0	Ol cum
Belingwe	**TN01**	24.0	6.61	30.2	165	65.4	7.95	7.52	16.7	CM
	TN03	20.3	3.85	33.0	185	75.8	8.78	8.33	18.4	Ol spx
	TN05	19.5	3.30	33.7	190	79.5	9.15	8.60	19.1	Ol spx
	TN06	18.1	2.95	34.1	191	74.2	9.26	8.74	19.8	Ol spx
	ZV14	16.5	2.79	37.8	214	84.0	10.2	10.2	21.4	Ol spx
	TN09	28.3	2.47	24.5	134	51.1	6.38	5.93	13.2	Ol cum
	TN16	31.0	3.07	22.0	120	46.6	5.62	5.26	10.8	Ol cum
	TN19	30.3	2.68	21.7	120	45.6	5.59	5.26	11.8	Ol cum
	ZV10	27.5	2.16	25.0	135	52.5	6.44	6.14	15.5	Ol cum
Vetreny	**12110/1**	14.6	2.23	32.1	187	84.3	12.2	12.5	52.7	CM
	12110	13.7	2.25	33.6	197	n.d.	n.d.	13.5	52.3	CM
	Replicate			32.6	196	83.3	12.5	12.6	53.7	CM
	12101	10.1	0.74	37.1	218	99.7	13.8	14.2	56.9	Cpx spx
	12116	11.1	0.75	35.9	220	97.3	13.6	13.6	54.9	Cpx spx
	12117	11.2	0.58	35.7	214	n.d.	n.d.	15.3	54.7	Cpx spx
	Replicate			35.5	216	98.3	13.4	13.7	55.0	Cpx spx
	12124	7.42	0.25	40.1	237	n.d.	n.d.	15.9	60.9	Cpx spx
	Replicate			39.3	237	107	15.1	15.2	61.7	Cpx spx
	01001	25.4	2.78	22.6	131	59.6	8.10	7.98	31.2	Ol cum
	12001	26.4	2.99	23.3	139	n.d.	n.d.	8.25	31.9	Ol cum
	Replicate			22.4	140	60.0	8.15	7.80	31.7	Ol cum
	01103	20.2	1.49	28.2	161	71.4	10.0	10.4	37.4	Ol cum
	01104	21.6	1.27	26.7	155	73.4	9.86	10.0	40.0	Ol cum
	01105	25.6	2.80	23.2	138	58.9	8.40	8.33	37.0	Ol cum
	12105	26.6	3.21	23.5	141	n.d.	n.d.	8.18	31.5	Ol cum
	Replicate			22.6	139	57.8	7.92	7.70	30.6	Ol cum

	01106	21.4	1.42	27.7	155	68.2	9.40	9.8	36.4	Ol cum
	12106	21.5	1.06	27.3	153	68.7	9.71	9.3	36.4	Ol cum

Note. n.d. – not determined. Additional major element data are provided in the online Supplementary Tables A1-A6.

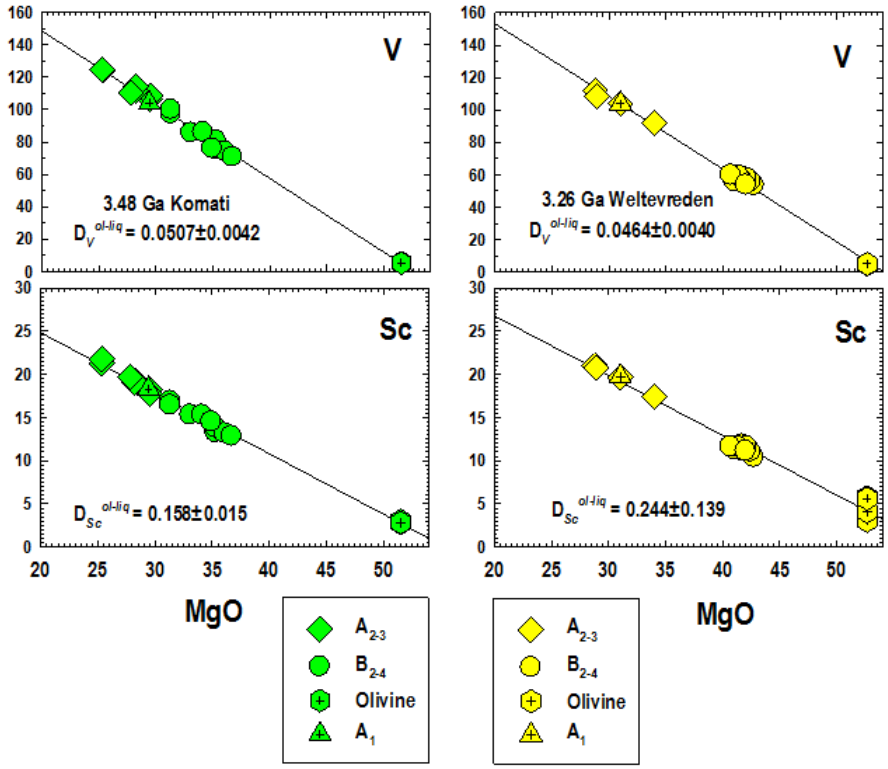

Figure 3.4. Vanadium and Sc (ppm) abundances in komatiite whole-rock samples and olivine from the 3.48 Ga Komati and 3.26 Ga Weltevreden komatiite systems plotted against MgO contents (wt. %). A_1 – upper chilled margin, A_{2-3} – spinifex-textured zone, and B_{2-4} – cumulate zone. The composition of the upper chilled margin zone approximates that of the emplaced lava. The details of the method for calculating the D_V^{Ol-Liq} values for each system here and in Figs. 5 and 6 are given in the text. The uncertainties here and in Figs. 5 and 6 are propagated 2SD uncertainties.

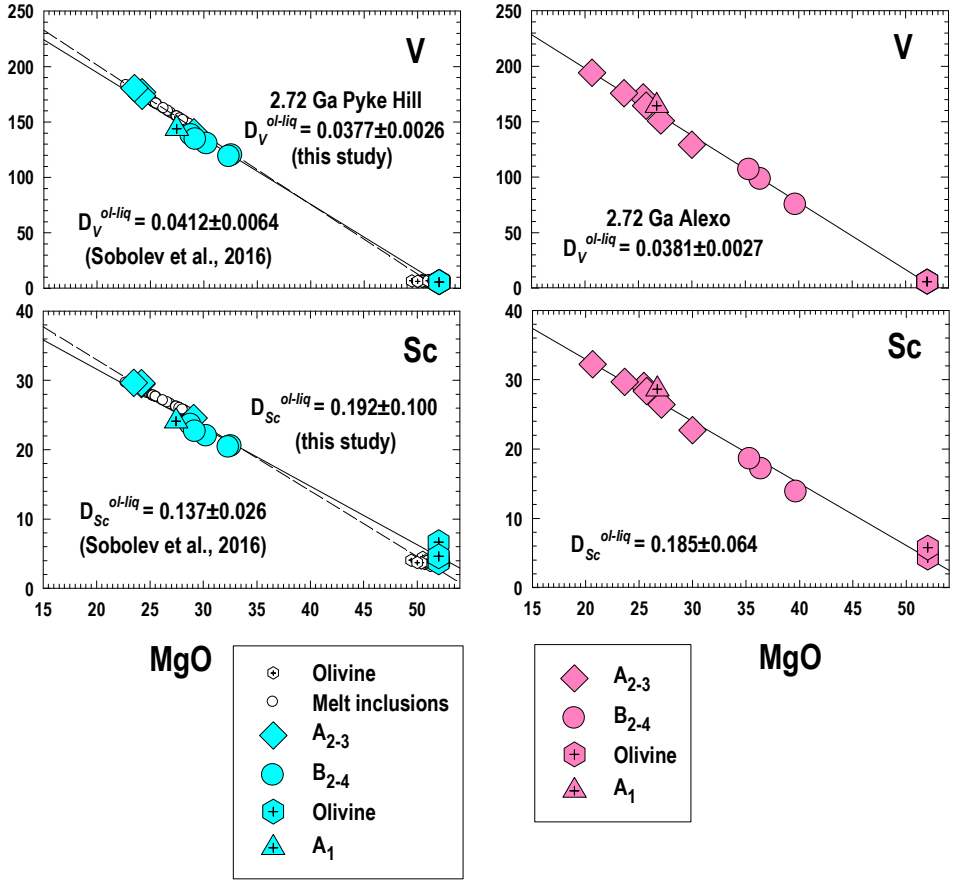

Figure 3.5. Vanadium and Sc (ppm) abundances in komatiite whole-rock samples and olivine from the 2.72 Ga Pyke Hill and Alexo komatiite systems plotted against MgO contents (wt. %). A_1 – upper chilled margin, A_{2-3} – spinifex-textured zone, and B_{2-4} – cumulate zone. Data from Sobolev et al. (2016) for the Pyke Hill komatiite system are shown as open symbols. The calculated partition coefficients for V and Sc for both data sets are within error of each other.

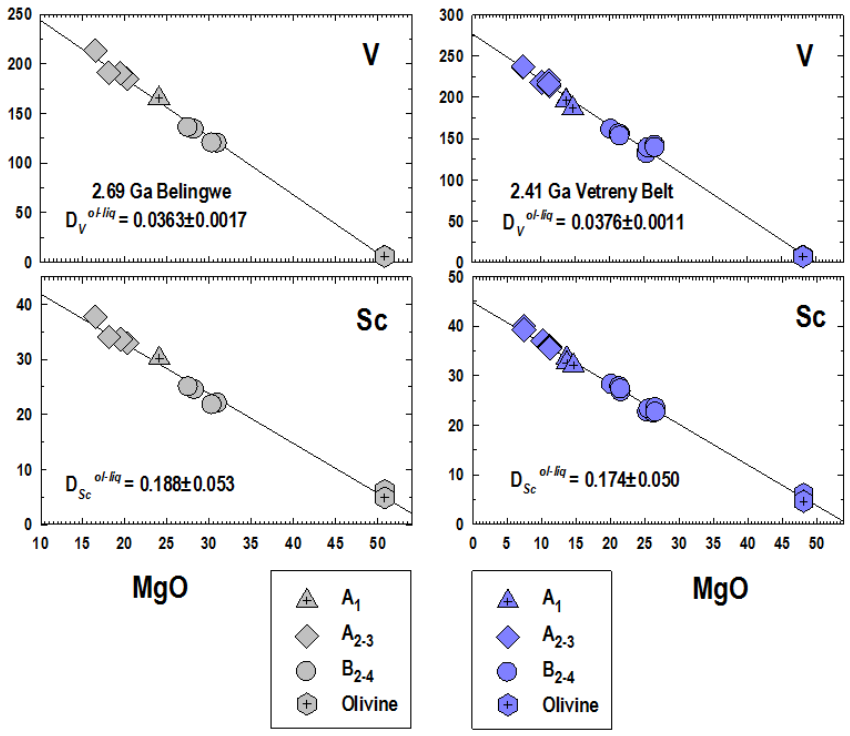

Figure 3.6. Vanadium and Sc (ppm) abundances in komatiite whole-rock samples and olivine from the 2.69 Ga Belingwe and 2.41 Ga Vetreny komatiite systems plotted against MgO contents (wt. %). A_1 – upper chilled margin, $A_{2\text{-}3}$ – spinifex-textured zone, and $B_{2\text{-}4}$ – cumulate zone.

Both V and Sc abundances (and also Ga and Y – not shown) are strongly inversely correlated with the MgO contents and plot on the regression lines that pass through the measured olivine compositions for each individual komatiite system, thus exhibiting incompatible behavior over the entire range of compositions present in the studied lavas. This also indicates that these regression lines represent olivine control lines. This observation, in turn, attests to the immobile behavior of both V and Sc (and also Ga, Y, and Zr) during seafloor alteration and metamorphism of the studied komatiite systems and provides evidence for olivine being the only major fractionating phase that controlled variations in the abundances of these elements. Notable exceptions are samples 01001, 12001, 01105, and 12105 from the 2.41 Ga Vetreny komatiite system, which plot slightly above the olivine control line in the MgO vs. V diagram (**Fig. 3.6.**). These samples also plot on the olivine+chromite fractionation trend in the MgO

vs. Cr diagram (Puchtel et al., 2016a) indicating presence of ca. 2% liquidus chromite in these samples. Because V is compatible in chromite, it is most likely that the deviation of these samples from the olivine control line in the MgO vs. V diagram is due to the presence of cumulus chromite. Although the effect was apparently small, these samples were not included in the follow-up regression calculations to estimate the V abundances in the emplaced komatiite lavas from the Vetreny komatiite system.

3.4.3. Estimation of the V and Sc abundances in the emplaced komatiite lavas

The calculated MgO and FeO contents in the emplaced komatiite lavas and the average maximum MgO and average minimum FeO contents in the liquidus olivine in equilibrium with the respective emplaced komatiite lavas from the six komatiite systems are listed in **Tables 3.4.** and **3.5.** and in the online Supplementary **Tables A1-A6**. The calculated MgO contents in the emplaced komatiite lavas vary between 29.4±0.5 and 31.4±0.9 wt. % in the early Archean Komati and Weltevreden systems, respectively, decrease to 27.5±0.7 to 24.5±0.5 wt. % in the late Archean Abitibi (Pyke Hill and Alexo) and Belingwe komatiite systems, and further decrease to 14.8±0.5 wt. % in the early Proterozoic Vetreny system.

Table 3.4. The calculated MgO, FeO, V, and Sc abundances and V/Sc ratios in the emplaced komatiite lavas from the studied komatiite systems

Locality	MgO	FeO	V (ppm)	Sc (ppm)	V/Sc
Komati	29.4±0.5	12.2±0.2	105.5±3.0	18.2±0.8	5.80±0.30
Weltevreden	31.4±0.9	9.80±0.30	102.8±6.0	19.0±1.8	5.43±0.58
Pyke Hill	27.5±0.7	10.6±0.4	149.1±5.5	25.3±2.4	5.88±0.61
Pyke Hill*	26.2±3.2	10.2±0.7	162.3±20.3	27.1±3.1	5.99±1.01
Alexo	27.5±0.7	10.6±0.4	151.8±5.9	26.3±2.3	5.78±0.65
Belingwe	24.5±0.5	11.6±0.5	157.9±6.4	28.8±2.5	5.49±0.52
Vetreny	14.8±0.5	10.5±0.7	192.3±4.5	32.5±1.1	5.92±0.24

Note. The calculated MgO and FeO abundances (wt. %) in the emplaced komatiite lavas (uncertainties are 2SD) have been adopted from the following sources: Komati – Puchtel et al. (2013); Weltevreden – Connolly et al. (2011); Pyke Hill and Alexo – Puchtel et al. (2004); Belingwe – Puchtel et al. (2009); Vetreny – Puchtel et al. (1996; 2016a). The background data and the calculation details are

provided in the text and in the online Supplementary Tables A1-A6. The V and Sc abundances in the emplaced komatiite lavas and the uncertainties on the V and Sc abundances and V/Sc ratios were derived from ISOPLOT regression calculations and are propagated 2SD uncertainties. Pyke Hill* represent the data for trapped melt inclusions in olivine derived from Sobolev et al. (2016); the MgO and FeO abundances are the averaged abundances corrected by Sobolev et al. (2016) for the Fe-Mg exchange. The V and Sc abundances and the V/Sc ratio were derived via ISOPLOT regression analysis of the data for both melt inclusions and host olivine presented in Table 3.5.

Table 3.5. Maximum average MgO and minimum average FeO (wt. %) and average V and Sc abundances in liquidus olivine and chromite and calculated D_v and D_{Sc} and fO_2 in the komatiite systems studied

Locality	MgO	FeO	V (ppm)	Sc (ppm)	V/Sc	$D_v^{Ol\text{-}Liq}$, $D_v^{Chr\text{-}Liq}$	$D_{Sc}^{Ol\text{-}Liq}$, $D_{Sc}^{Chr\text{-}Liq}$	fO_2 (ΔNNO)	fO_2(ΔFMQ)
Komati	51.5±0.5	6.40	5.35±0.42	2.88±0.24	1.86±0.21	0.0507±0.0042	0.158±0.015	−0.83±0.30	−0.11±0.30
Weltevreden	52.6±0.7	4.94	4.77±0.32	4.62±2.60	1.03±0.58	0.0464±0.0040	0.244±0.139	−0.67±0.30	+0.05±0.30
Pyke Hill	52.0±0.6	6.00	5.62±0.32	4.85±2.50	1.16±0.60	0.0377±0.0026	0.192±0.100	−0.31±0.28	+0.41±0.28
Pyke Hill*	50.9±0.6	6.00	6.69±0.61	3.70±0.56	1.81±0.32	0.0412±0.0064	0.137±0.026	−0.46±0.37	+0.26±0.37
Alexo	52.0±0.6	6.00	5.81±0.34	4.85±1.63	1.20±0.41	0.0381±0.0027	0.185±0.064	−0.33±0.28	+0.38±0.28
Belingwe	50.8±1.0	7.60	5.73±0.14	5.40±1.44	1.06±0.28	0.0363±0.0017	0.188±0.053	−0.24±0.27	+0.48±0.27
Vetreny, Ol	48.1±0.4	10.5	7.23±0.14	5.66±1.35	1.28±0.37	0.0376±0.0011	0.174±0.050	−0.30±0.26	+0.43±0.26
Vetreny, Chr	2.69	33.7	1389±19	7.65±1.86	182±44	7.22±0.20	0.235±0.050	−0.36±0.15	+0.37±0.15

Note. The sources of the FeO and MgO abundance data (wt. %) are as follows: Komati – Puchtel et al. (2013); Weltevreden – Connolly et al. (2011); Pyke Hill and Alexo – Puchtel et al. (2004); Belingwe – Renner et al. (1994); Vetreny – Puchtel et al. (1996). Pyke Hill* data represent the averaged data for olivine derived from Sobolev et al. (2016). The $D_v^{Ol\text{-}Liq}$, and fO_2 values were calculated using the same protocol applied to the data from this study. All the uncertainties in both studies are the 2SD propagated uncertainties calculated using the standard protocol outlined in Harris (2010).

Using the calculated MgO contents in the emplaced komatiite lavas and regressing the trace element abundances obtained in this study for the whole rock samples and olivine against the MgO contents using ISOPLOT (Ludwig, 2003), trace element abundances in the emplaced komatiite lavas for each individual komatiite system have been calculated; these abundances, with their respective propagated

2SD uncertainties, are presented in **Table 3.4**. The V and Sc abundances in the emplaced komatiite lavas vary from 102.8±6.0 to 105.5±3.0 and 18.2±0.8 to 19.0±1.8 ppm, respectively, in the early Archean komatiite systems, and 149.1±5.5 to 157.9±6.4 and 25.3±2.4 to 28.8±2.5 ppm, respectively, in the late Archean komatiite systems. The emplaced komatiitic lava from the early Proterozoic Vetreny system contained 192.3±4.5 ppm V and 32.5±1.1 ppm Sc.

3.4.4. Evaluation of the redox state of the komatiite systems

3.4.4.1. Vanadium and Sc partitioning between olivine, chromite and emplaced komatiite lavas

The average V and Sc concentrations in the liquidus olivine and chromite, with their respective propagated 2SD uncertainties, are presented in **Table 3.5**. Using these values and the estimated V and Sc abundances in the emplaced komatiite lavas (**Table 3.4.**), partition coefficients for V and Sc between liquidus olivines and emplaced komatiite lavas for the studied komatiite systems were obtained; these data are listed in **Table 3.5.** and also presented in the MgO vs. V and MgO vs. Sc variation diagrams (**Figs. 3.4.-3.6.**). Uncertainties on the emplaced komatiite lava and average olivine compositions were propagated in quadrature to determine the uncertainties on the $D_V^{Ol\text{-}Liq}$ for the individual komatiite systems using the standard protocols listed in Harris (2010).

These $D_V^{Ol\text{-}Liq}$ values do not show any correlation with the geochemical types of the komatiite lavas studied (Al-depleted/enriched or Al-undepleted). However, these *D* values do exhibit a resolvable secular trend, decreasing from 0.0507±0.0042 in the 3.48 Ga Komati system to 0.0464±0.0040 in the 3.26 Ga Weltevreden system and further to 0.0377±0.0026 and 0.0381±0.0027 in the 2.72 Ga Abitibi systems and then essentially level off in the 2.69 Ga Belingwe (0.0363±0.0017) and 2.41 Ga Vetreny systems (0.0376±0.0011). The $D_{Sc}^{Ol\text{-}Liq}$ values range between 0.159±0.015 and 0.244±0.139 and are identical, within the uncertainties, in all the komatiite systems studied.

Having determined the V partition coefficients between the liquidus olivine (for the six komatiite systems), liquidus chromite (for the Vetreny system) and the emplaced komatiite lavas, we used the combined experimental calibrations of Canil (1997) and Canil and Fedortchouk (2001) for olivine and Canil (1999) for chromite to evaluate the oxidation states of these komatiite systems. Although additional experiments are available in Mallmann and O'Neill (2009), these experiments were performed on compositions different from those of komatiites and were thus not used in this study. Other determinations of $D_V^{Ol\text{-}Liq}$, such as those found in Canil (2002), are more relevant to the pressures and temperatures of mantle melting and were thus not used in the regressions. One experimental data point listed in Canil and Fedortchouk (2001) was obtained at a very high oxygen fugacity of ΔNNO = +6.6; such conditions are extreme and totally irrelevant to conditions under which komatiites form; in addition, this data point is an outlier on the experimental calibration curve of Canil and Fedortchouk (2001) and was, thus, excluded from our compilation. Regressions of the experimental data that we compiled from the above two publications (excluding the outlier) yielded the following equations:

$$\log(D_v^{Ol\text{-}Liq}) = (-0.250\pm0.023)\times\Delta NNO - (1.501\pm0.064)\ (r^2 = 0.94) \qquad (1)$$

$$D_v^{Chr\text{-}Liq} = (-5.77\pm0.59)\times\Delta NNO + (5.13\pm0.79)\ (r^2 = 0.97) \qquad (2)$$

Uncertainties on the slopes and intercepts of equations (1) and (2) are derived from the 95% confidence interval of the regression of the experimental data and experimental uncertainties using ISOPLOT (Ludwig, 2003). The uncertainties shown in equations (1) and (2) were propagated in quadrature through the determination of fO_2 from $D_V^{Ol\text{-}Liq}$ and $D_V^{Chr\text{-}Liq}$. The data listing the results of the experiments and associated uncertainties from Canil (1997) and Canil and Fedortchouk (2001) are included in Supplementary Table A7.

Partitioning behavior of V between olivine and komatiitic liquid has been shown in these studies to have little to no dependence on temperature and melt composition and, therefore, no corrections for

either of these factors have been made. Although a vanadium-in-olivine oxybarometer that takes into account the effects of temperature and composition is available in Mallmann and O'Neill (2013), their version of this oxybarometer requires the precise knowledge of CaO, Na_2O, and K_2O abundances in the emplaced lavas. However, it has been shown in the previous studies that in the majority of these komatiite systems, both Ca and alkalis were mobile during seafloor alteration and metamorphism. Estimation of SiO_2, CaO, Na_2O and K_2O concentrations of emplaced lavas using ISOPLOT regressions results in large uncertainties for these elements due to the significant scatter of the data in the MgO vs. element plots. This in turn results in large uncertainties in the fO_2 estimates using the Mallmann and O'Neill (2013) oxybarometer, in most cases exceeding 0.60 log fO_2 units. The composition-independent oxybarometer (1), thus, minimizes uncertainty and is most relevant for this study.

Unlike $D_V^{Ol\text{-}Liq}$, $D_V^{Chr\text{-}Liq}$ has been shown to depend strongly on the Cr/Al ratio of the system (Canil, 2002). For our calculations, we used the experimental calibration curve for komatiitic composition "komv" of Canil (1999). This composition was selected due to the fact that, among all compositions studied by Canil (1999; 2002), it had the Cr/Al ratio that was most similar to that of the emplaced komatiitic basalt of the Vetreny system.

For ease of comparison to previously published data for mantle-derived rocks, all of the oxygen fugacity values have been converted from ΔNNO log units to the more commonly used ΔFMQ log units using the standard thermodynamic values for each mineral buffer assemblage listed in Lindsley (1991). The fO_2 values calculated from the V partitioning data for the olivine and chromite are listed in **Table 3.5.** and plotted as a function of the age of the komatiite systems in **Fig. 3.7a**.

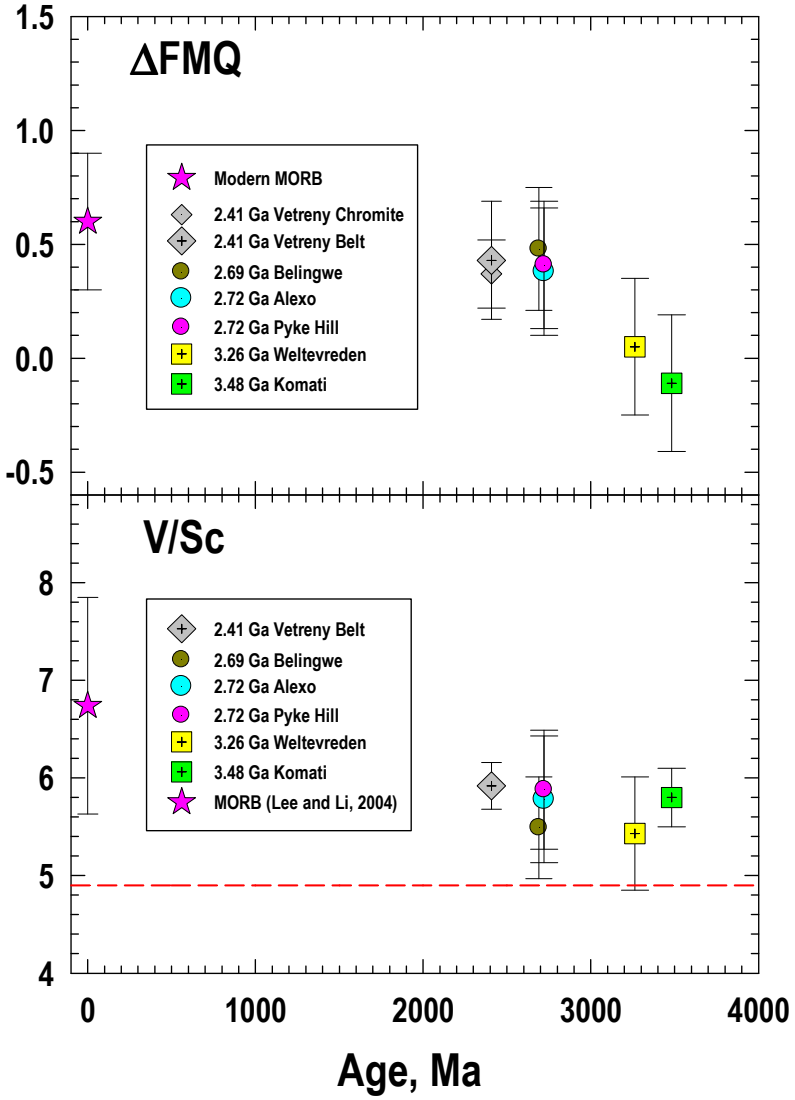

Figure 3.7a. The estimated oxygen fugacity (fO_2) relative to the Fayalite-Magnetite-Quartz (FMQ) buffer for the studied komatiite systems plotted as a function of their ages. The uncertainties shown are determined by the propagated 2SD uncertainties on the calculated $D_V^{Ol\text{-}Liq}$ and $D_V^{Chr\text{-}Liq}$ and the 95% confidence interval error on the regression of the combined experimental data of Canil (1997) and Canil and Fedortchouk (2001). The fO_2 estimates for modern MORB were calculated using the V partitioning between olivine and basaltic melt and the V abundance data for the four olivine/glass pairs from Kelley and Cottrell (2012) and Mallmann and O'Neill (2013). The MORB value of +0.60±0.30 ΔFMQ log units is the average of the four estimates with the uncertainty reflecting the 2SD of those estimates propagated to account for the uncertainty in experimental calibration in equation (1). **b**. The V/Sc ratios of the studied komatiite systems plotted as a function of their ages. Data for modern MORB are from Li and Lee (2004). The horizontal dashed line shows the estimated primitive upper mantle value (PUM) of Lee et al. (2005). See text for additional details.

The early Archean komatiite systems are characterized by somewhat lower calculated fO_2 values of −0.11±0.30 ΔFMQ log units for the 3.48 Ga Komati and +0.05±0.30 ΔFMQ log units for the 3.26 Ga Weltevreden systems compared to the late Archean and early Proterozoic systems (i.e., +0.43±0.26 ΔFMQ log units for the 2.41 Ga Vetreny system), which provides a hint for a slight increase in the mantle oxygen fugacity from 3.48 to 2.41 Ga. However, the calculated fO_2 values in all six komatiite systems are essentially the same within their respective uncertainties. Also plotted in this diagram is an estimate of the redox state for modern East Pacific Rise MORB obtained using the V abundance data for the olivine-glass pairs from Kelley and Cottrell (2012) and Mallmann and O'Neill (2013) and the equation (1) above. The calculated MORB fO_2 values are +0.59±0.26 ΔFMQ log units (Mallmann and O'Neill, 2013) and +0.68±0.33, +0.63±0.33 and +0.50±0.33 ΔFMQ log units (Kelley and Cottrell, 2012). Thus, the calculated average MORB value is +0.60±0.15 ΔFMQ log units (2SD), but in light of the inherent uncertainty of the experimental calibration (1), the true uncertainty on this value is estimated at 0.30 ΔFMQ log units. It has been shown that the redox data obtained using the oxybarometers relying on the partitioning behavior of V are systematically offset by up to 1 log unit from the oxygen fugacity data calculated using the $Fe^{+3}/\Sigma Fe$ equilibria (e.g., Mallmann and O'Neill, 2013). Therefore, although there exist reliable data on fO_2 estimates for MORB obtained using the $Fe^{+3}/\Sigma Fe$ ratio of MORB glasses (i.e., Bezos and Humler, 2005, Cottrell and Kelley, 2011), for the sake of consistency we calculated and compared the oxygen fugacities of the Archean komatiite systems and MORB using the same methodology, i.e., from $D_V^{Ol\text{-}Liq}$ and equation (1). The calculated fO_2 values for all komatiite systems are largely within the uncertainty of the range of the average fO_2 value for modern MORB lavas of +0.60±0.30 ΔFMQ log units obtained.

Recently, Sobolev et al. (2016) presented precise estimates of redox state of the Abitibi komatiite system using V partitioning between olivine and the trapped silicate melt of inclusions in olivine. Their

data are listed in **Tables 3.4. and 3.5.** and plotted in **Fig. 3.5.** together with our data for this komatiite system. The Sobolev et al. (2016) samples came from the surface outcrops, whereas our samples came from the 254-257 m deep interval of a drill core, therefore, sampling different lava flows. However, both trends overlap within their respective uncertainties. The olivines studied by Sobolev et al. (2016) appear to be on average less MgO-rich (the average MgO and FeO contents are 51.0±1.6 and 6.0±1.0 wt. %, respectively; 2SD) than olivines from our study. These olivines can be shown to be in equilibrium with komatiite liquid containing 26.2±3.2 wt.% MgO and 10.2±0.7 wt.% FeO (2SD), which are the average MgO and FeO abundances in their komatiite liquid of fluid inclusions corrected for Fe-Mg exchange. Using the protocol developed here and applying it to the Sobolev et al. (2016) dataset, we calculated the fO_2 value of +0.26±0.37 ΔFMQ log units (2SD), which is within uncertainty, to the value obtained for this komatiite system in our study (+0.41±0.28 ΔFMQ log units), thus providing an independent test of the accuracy of the analytical techniques used in this study.

3.4.4.2. Variations in V/Sc in the emplaced komatiite lavas

Variations in V/Sc ratios in Archean basalts as a function of age have been used to study the evolution of the oxidation state of the Archean upper mantle (e.g., Li and Lee, 2004). Because V becomes more incompatible with an increase in fO_2 of the system, and Sc partitioning is independent of fO_2, the higher the fO_2 of the system during melting, the higher the V/Sc should be in the melt. Li and Lee (2004) estimated the V/Sc in the global compilation of MORB lavas to be 6.7±1.1 (2SE), which is equivalent to −0.3±1.0 ΔFMQ log units for the modern upper mantle. They have also shown that Archean basalts have an average V/Sc = 6.3±1.2 (2SE) and concluded that the fO_2 of the modern upper mantle and that of the sources of Archean basalts were the same within the cited uncertainties.

In this study, the sensitivity of the V/Sc system to the small-scale changes in fO_2 in the komatiite mantle sources, as implied by the olivine-komatiite liquid V partitioning data obtained, was examined.

The studied komatiite systems have calculated V/Sc ratios that are identical within the uncertainties (**Fig. 3.7b.**) and are at the lower end of the MORB estimates of Li and Lee (2004).

It is important to note that, since komatiites are high melt-fraction lavas, they are expected to show less variation in V/Sc with oxygen fugacity than basalts, with their V/Sc ratios closer to those of their mantle source regions. Indeed, all of the studied komatiites plot above, but close to, the estimate for the primitive mantle V/Sc ratio from Lee et al. (2005).

The calculated V/Sc ratios for the studied komatiite systems define an essentially flat trend through time, interpretation of which is complicated by several additional factors. First, komatiitic basalts of the Vetreny system have been shown to be derived from a komatiitic magma with 27% MgO via 50% fractional crystallization and 4% assimilation of tonalites from the adjacent Vodla Block (Puchtel et al., 2016a). While addition of 4% of material of Archean tonalitic crust (V = 138 ppm, V/Sc = 6.3, Rudnick and Fountain, 1995) is not expected to have any measurable effect on the V/Sc ratio of the original komatiite magma due to the similar V/Sc ratio and V content in the latter, fractionation of 50% olivine is expected to have some effect. Scandium is more compatible in olivine than V; as a result, liquidus olivine has lower V/Sc ratios than the komatiite magma from which it crystallized (average V/Sc = 1.14±0.14 in olivine from the late Archean Al-undepleted komatiites, i.e. lavas derived from partial melting in the spinel peridotite stability field, **Table 3.5.**). Our calculations indicate that 50% olivine fractionation from the original komatiite magma with 27% MgO to form the Vetreny emplaced komatiitic basalt with 14.8 wt. % MgO would result in a slight decrease in the V/Sc in the original komatiite magma from 5.9 to 5.7; however, this value is still identical to the V/Sc ratio in the late Archean komatiite systems in this study.

Another complicating factor is the difference in melting histories of the early and late Archean komatiite systems. The Komati komatiites are Al-depleted and have been interpreted to be derived via

melting in equilibrium with residual majorite garnet (e.g., Jahn et al., 1982; Puchtel et al., 2013), whereas the Weltevreden komatiites are Al-enriched (Puchtel et al., 2013) and were likely the products of re-melting of majorite-enriched residual mantle (e.g., Ohtani, 1988; 1990; Robin-Popieul et al., 2012). The late Archean and early Proterozoic komatiite systems, on the other hand, are Al-undepleted and formed via melting in equilibrium with garnet-free residue. Although Sc and V appear to be similarly compatible in majorite garnet (e.g., Ohtani et al., 1989), their partitioning behavior in garnet is currently not well constrained and even small variations in $D_{V,Sc}^{Maj\text{-}Liq}$ may cause fractionation of the V/Sc during partial melting in the garnet stability field. Due to these limitations, we did not consider any further the V/Sc systematics of the studied komatiite systems for the purpose of constraining their redox state.

3.5. Discussion

3.5.1. The effects of alteration, mineral-melt re-equilibration, and crustal contamination on the redox state of the studied komatiite systems

3.5.1.1. Secondary alteration

All studied komatiite lavas have been modified to a greater or lesser degree as a result of seafloor alteration and subsequent metamorphism. Secondary alteration may have resulted in post-magmatic re-distribution of petrogenetically important elements, including V, which, in turn, may have affected the estimates for V (and other trace metals) abundances in the emplaced komatiite lavas. This post-magmatic re-distribution, however, can be easily recognized in the trace metal vs. MgO variation diagrams (**Figs. 3.4.-3.6.**). Element mobility will result in the data for the affected element plotting off the olivine control lines, which is not observed. Although abundances of Cu do plot with significant scatter for such systems as Komati, Weltevreden, Pyke Hill, and Alexo (but not for Belingwe or Vetreny), V, Sc, Ga, Y, and Zr exhibit strong inverse correlations with the indices of magmatic differentiation and plot on trends that coincide with olivine control lines, attesting to the immobile

behavior of these elements during post-magmatic processes. This conclusion is consistent with the observed immobile behavior of lithophile trace elements reported by Puchtel et al. (2004; 2009; 2013; 2016a) for these komatiite systems.

3.5.1.2. Late-stage re-equilibration of the liquidus olivine and chromite

The method to determine the redox state of komatiite systems used in this study requires liquidus olivine and chromite to be in equilibrium with the emplaced komatiite lava. Although olivine phenocrysts found in chilled margins of komatiite lava flows most likely preserved their original V partitioning signature due to the almost instantaneous solidification after emplacement (Huppert et al., 1984; Huppert and Sparks, 1985; Arndt, 1986b), olivine from cumulate zones, which take much longer to crystallize, may have experienced re-equilibration with the residual liquid. Nicklas et al. (2016) in their study of the ca. 100-m deep Victoria's Lava Lake showed that V contents of olivine and chromite from the cumulate zone and the upper chilled margin were identical. This strongly suggests that re-equilibration between olivine, chromite and the residual liquid played a negligible role during the evolution of the lava lake. Here, we use the same line of reasoning to argue that this was also the case for the thinner komatiite lava flows from the other five komatiite systems.

First, as was also the case with the Victoria's Lava Lake, we analyzed only cores of solid, equant olivine and chromite grains that were previously shown to be in equilibrium with the emplaced komatiite lavas for major elements (Puchtel et al. 2004; 2009; 2013). These cores of olivine and chromite grains, analyzed in samples collected across the individual lava flows, have similar average V abundances between the samples within the same lava flows, and limited compositional variations among the grains within the same samples (**Table 3.1.**). Second, similarly to the Victoria's Lava Lake, skeletal olivine phenocrysts in the chilled margin sample TN01 of the ~14-m thick Tony's Flow of the Belingwe system have average V abundances identical to those of solid equant olivine grains in samples

from the cumulate portion of this flow. Since the upper chilled margin of Tony's Flow most likely crystallized almost instantaneously as a result of intensive heat dissipation caused by turbulent flow and interaction with seawater (Huppert et al., 1984; Huppert and Sparks, 1985), it is very unlikely that the olivine grains from the cumulate zone of Tony's Flow would have retained the same V abundances as the skeletal olivine phenocrysts from the upper chilled margin, should any re-equilibration have taken place.

Finally, all studied komatiite units are substantially thinner compared to the Victoria's Lava Lake. As a result, it likely took these flows far less time to crystallize, which gives olivine grains from the cumulate portions of these lava flows much greater chances to avoid any late re-equilibration.

The precision of the method used in this study is further confirmed by the excellent agreement between calculated oxygen fugacities for the individual komatiite systems that were presumably derived from the same mantle plume (i.e., the 2.72 Ga Pyke Hill and Alexo systems). A supporting piece of evidence for the adequate accuracy of the calculated fO_2 values comes from the excellent agreement between the estimates derived from the independent olivine- and chromite-based oxybarometers for the Vetreny komatiite system (Nicklas et al., 2016) and from the consistency of the independent estimates of the fO_2 for the Abitibi system from our study and that of Sobolev et al. (2016).

3.5.1.3. Crustal contamination

As was modeled by Nicklas et al. (2016), due to the difference in the redox state of upper crustal rocks and komatiite magmas, crustal contamination can have a measurable effect on the oxidation state of the hybrid komatiitic melts. Further, Nicklas et al. (2016) estimated that in the Victoria's Lava Lake, 4% crustal contamination could have resulted in the increase of the fO_2 of the primary komatiite magma by 0.07 ΔFMQ log units. This increase, however, is within the uncertainty on the estimated fO_2 of the Vetreny system and, therefore, no correction has been applied to the fO_2 value obtained. Moreover, it

has been also noted that continental arc basalts do not exhibit any correlation between the degree of crustal contamination and their fO_2 (Grocke et al., 2016); although komatiites form in different environment than arc basalts, this observation provides additional support to our approach.

In the case of the five remaining komatiite systems, the possibility of crustal contamination has been carefully evaluated in the previous studies of lithophile trace element abundances and isotope systematics (Puchtel et al., 2004; 2009; 2013). These studies have concluded that crustal contamination did not play a significant role in the evolution of these komatiite systems; therefore, no further corrections for the changes in the redox state of the studied komatiite systems due to crustal contamination have been made, or are otherwise warranted.

3.5.2. The significance of the calculated fO_2 of the studied komatiite systems

It is important to note that the studied early Archean komatiite systems have higher MgO contents compared to their late Archean counterparts, and, thus, must have formed in a hotter mantle. In order to evaluate the significance of the calculated fO_2 of the studied komatiite systems, it is important to evaluate the effect of secular cooling of the mantle (e.g., Nisbet et al., 1993; Herzberg, 1995; Herzberg and Gazel, 2009) on the calculated oxygen fugacities. Decrease in mantle temperatures will result in increased Fe^{+3} activity in mantle spinel, and, thus, higher mantle oxygen fugacity in the spinel peridotite stability field, due to the temperature dependence of mantle mineral redox equilibria (Sack et al., 1980; Ballhaus et al., 1991; Ballhaus, 1993; Frost and McCammon, 2008). The extent to which the ambient upper mantle cooled over ~760 Ma, from 3.48 Ga to 2.41 Ga, is not well established, but most likely was less than 100°C (Herzberg et al., 2010). Using the experimental upper mantle oxybarometer of Ballhaus et al. (1991), we estimated the change in oxygen fugacity that would be caused by decrease in the mantle potential temperature by 100°C, from 1800°C to 1700°C, assuming a constant pressure of 7.5 GPa, a X^{spinel}_{Al} of 0.4 and $X^{olivine}_{Fe}$ of 0.1. Our calculations indicate that this decrease in temperature

would be equal to an increase of 0.06 ΔFMQ log units in oxygen fugacity, which is smaller than the uncertainty on the fO_2 estimates for all komatiite systems in this study. Moreover, based on the parameterization by Herzberg et al. (2010), there might have been a small increase in the mantle potential temperatures between 3.5 and 3.3 Ga, as also evidenced by the higher MgO content of the emplaced komatiite lavas from the 3.26 Ga Weltevreden komatiite system compared to that of the 3.48 Ga Komati system. We conclude, therefore, that secular change in the mantle potential temperature between 3.48 and 2.41 Ga must have had no measurable effect on the calculated oxygen fugacities for the studied komatiite systems.

Another issue to address is the difference in the depth of melting for the studied komatiite systems and its effect on the calculated fO_2. It has been argued that the oxygen fugacity of the mantle decreases with increasing depth due to pressure dependence of the garnet-fayalite-ferrosilite-O_2 equilibrium (Woodland and Koch, 2003). However, although melting in the early Archean plumes that gave rise to the studied komatiite systems most likely started at greater depths due to higher temperatures in the early Archean mantle, as indicated by their Al-depleted/enriched signatures, the depths at which the plumes originated are not well constrained and there is no reason to believe that early Archean plumes originated at greater depths than their late Archean counterparts. For example, some modern lavas (i.e., Hawaii) have been shown to be derived from plumes that might have originated at the core-mantle boundary (e.g., Brandon et al., 1999; Mundl et al., 2017). Moreover, depth of mantle plume initiation should have no effect on the fO_2 of the emplaced komatiite lava due to the fact that the komatiite melts likely remained in equilibrium with the mantle residue well past the depth of plume initiation. Although there are complicating factors in linking fO_2 during generation of the komatiite melt to fO_2 of that melt upon emplacement (such as the pressure dependence of molar volume in redox reactions), the FMQ redox buffer closely follows the redox evolution of a decompressing melt, so that the oxygen fugacity

values expressed in ΔFMQ terms retain their validity through decompression melting (Kress and Carmichael, 1991, Kelley and Cottrell, 2012). This is one of the reasons the FMQ buffer has been previously used as a reference point for determining the upper mantle oxygen fugacity (e.g., Kelley and Cottrell, 2012). Additionally, the obtained redox data for the Archean komatiite systems were compared to the fO_2 of modern-day MORB in an attempt to minimize the different effects of decompression melting on the calculated oxygen fugacities.

Two additional factors that have been shown to have an effect on the oxygen fugacity of a magma are fractional crystallization and volatile degassing. Although olivine fractionation is known to be able to change the oxygen fugacity of mafic magmas (Cottrell and Kelley, 2011), due to their very low viscosities and high temperatures, komatiite magmas experience little to no differentiation prior to emplacement, as evidenced by a generally small amount of olivine phenocrysts present in upper chilled margins of komatiite lava flows, usually not exceeding 2-5% by volume (e.g., Arndt, 1986b; Arndt et al., 2008). Degassing of sulfur is also likely to be only a minor control on the measured fO_2 values, as all the studied komatiites have been shown to be sulfur undersaturated (Puchtel et al., 2004, 2009; 2013; 2016a). Based on these multiple lines of evidence, we, therefore, conclude that the data presented in **Fig. 3.7.** likely closely reflects the redox state of the convecting upper mantle source regions of the studied komatiites.

3.5.3. Relationship between Mantle Oxidation State and rise of Oxygen in the Atmosphere

The Great Oxidation Event (GOE) is one of the most significant events in the history of Earth's atmosphere; it involves the rise of the concentration of O_2 from less than 10^{-5} atm to ~1% of the present-day atmospheric level (Lyons et al., 2014). Many previous studies of upper mantle redox evolution focused on finding a connection between changes in upper mantle redox and the GOE (Canil, 1997; Holland, 2002; Li and Lee, 2004; Aulbach and Stagno, 2016). Although the GOE has been linked to the

evolution of photosynthetic life, it is likely that oxygenic photosynthesis evolved ~300 Ma prior to the GOE and, thus, a non-evolutionary trigger for the permanent oxygenation of the terrestrial atmosphere seems to be necessary (Buick, 2008).

Reducing volcanic gases, such as CO, H_2S and H_2, are a major sink for atmospheric oxygen, and the proportion of these gases relative to oxidizing volcanic gases, such as CO_2, SO_2, and H_2O, is controlled by fO_2 of the gases. Volcanic gas fO_2 is largely buffered by the fO_2 of the degassing lava during cooling (Gerlach, 1993; Kasting et al. 1993). This link is complicated, however, by the effect of degassing pressure on the oxidation state of the gases evolved (Gaillard et al., 2011). Composition of these gases provides an important link between upper mantle redox and the composition of the atmosphere. Atmospheric models have shown that an increase of ~0.50 log units in the oxidation state of mantle sources of volcanoes could have reduced the volcanic gas sink for O_2 and would be sufficient to trigger the GOE (Holland, 2002). There is no significant difference in the estimates for the redox state between the 3.48 – 2.41 Ga komatiite systems presented in this study or those for the modern MORB lavas, although there is a slight hint in the data for a possible secular change in mantle oxidation from the Paleoarchean to the present day. Therefore, at this point, it still cannot be determined conclusively whether changes in the upper mantle redox, if any, were an important trigger for the GOE.

3.5.4. Implications for the timing of the initial mantle oxidation event

As mentioned previously, the five orders of magnitude increase in the fO_2 of the present-day upper mantle compared to the redox state of the Hadean mantle immediately following core formation is postulated to be the result of Fe^{2+} disproportionation into Fe metal and Fe^{3+} in Mg-perovskite, the lower mantle's dominant phase, and subsequent loss of Fe metal to the core during the magma ocean stage of the evolution of the planet (Wade and Wood, 2005; Frost *et al.*, 2008; Frost and McCammon, 2008). As a result of the disproportionation reactions, the post-magma ocean mantle would likely have been redox-

stratified into a reduced upper mantle and an oxidized lower mantle. This stratification could have been subsequently erased by means of Mg-perovskite releasing Fe^{+3} into the upper mantle acting as an "oxygen pump" (Wade and Wood, 2005) via mantle convection, high-energy impacts, and stagnant-lid tectonic processes to form the modern oxidized mantle. The timing and duration of this homogenization process are not well constrained; based on the results of this study, it may be concluded that the mantle had reached its near present-day redox state at least by 3.48 Ga, the age of the oldest komatiite system studied.

Mantle domains showing anomalies of short-lived isotopic systems (i.e., ^{182}W) that were isolated from the rest of the mantle ~30 Ma into the Earth's history and were sampled by plume-derived lavas, have been shown to persist into the Archean (Touboul et al., 2012; Puchtel et al., 2016b, 2017) and even to modern times (Rizo et al., 2016; Mundl et al., 2017). These isotopic heterogeneities provide evidence that the mantle has never been fully homogenized for these isotopic systems. It is, thus, possible that the initial redox stratification of the mantle has also been at least partially preserved. None of the komatiite systems studied here have been shown to have been derived from mantle domains that were isolated from the bulk mantle during the initial stages of planetary differentiation, but komatiitic systems that preserved short-lived isotopic anomalies, such as the 3.55 Ga Schapenburg komatiitic system (Puchtel et al., 2016b), would be good candidates to search for the presence of primordial redox heterogeneities in the mantle.

3.6. Conclusions

Oxygen fugacity has been determined for six komatiite systems using V partitioning between liquidus olivine, chromite and host komatiitic lavas, with a precision of ca. 0.30 fO_2 log units. The obtained fO_2 values range between −0.11±0.30 ΔFMQ log units in the 3.48 Ga Komati system to +0.43±0.26 ΔFMQ log units in the 2.41 Ga Vetreny system. These values are, thus, largely

indistinguishable, within their respective uncertainties, from each other and from our average estimate for modern MORB of +0.60±0.30 ΔFMQ log units, although there is a slight hint in the data for a possible secular trend of increasing upper mantle oxygen fugacity in the Archean. These results indicate that the primordial mantle redox stratification that is postulated to have been formed immediately following core formation, has been largely homogenized by 3.48 Ga, i.e., by the time the oldest studied komatiite system formed.

Acknowledgments for Chapter 3

This study was supported by NSF FESD Type I Grant #1338810 "The Dynamics of Earth System Oxygenation" (lead PI is A.D. Anbar, I.S. Puchtel is a co-PI). This source of support is gratefully acknowledged. We thank Valentina Puchtel for help with sample preparation. We also thank Mark Fornace (undergraduate assistant), Valentina Puchtel, and William F. McDonough for their assistance in the initial development of the standard addition technique, which was supported by NSF grant EAR-0739006 (to W.F.M.). The final version of this manuscript greatly benefited from constructive, thorough reviews by Elizabeth Cottrell, Paolo Sossi, Fabrice Gaillard, and Cin-Ty Lee. Editorial handling by Dmitri Ionov is gratefully acknowledged. Supporting data are included in Supplementary Tables A1-A7; additional data can be obtained from the authors upon request.

References for Chapter 3

-Armstrong, R. A., Compston, W., DeWit, M. J., Williams, I. S., 1990. The stratigraphy of the 3.5-3.2 Ga Barberton greenstone belt revisited: A single zircon ion microprobe study. Earth and Planetary Science Letters **101** (1): 90-106.

-Arndt, N.T., Lesher, C.M., and Barnes, S.J., 2008. Komatiite. Cambridge, UK, Cambridge University Press, 467 pp.

-Arndt, N. T., 1986a. Spinifex and swirling olivines in a komatiite lava lake, Munro Township, Canada. Precambrian Research **34**(2): 139-155.

-Arndt, N. T., 1986b. Differentiation of komatiite flows. Journal of Petrology **27** (2): 279-301.

-Arndt N. T., Naldrett A. J., and Pyke D. R., 1977. Komatiitic and iron-rich tholeiitic lavas of Munro Township, northeast Ontario. *J. Petrol.* **18:** 319–369.

-Aulbach, S., and Stagno, V., 2016. Evidence for a reducing Archean ambient mantle and its effects on the carbon cycle. Geology.

-Aulbach, S., and Viljoen, K.S., 2015. Eclogite xenoliths from the Lace kimberlite, Kaapvaal craton: From convecting mantle source to palaeo-ocean floor and back. Earth and Planetary Science Letters **431**: 274-286.

-Ballhaus, C., 1993. Redox states of lithospheric and asthenospheric upper mantle. Contributions to Mineralogy and Petrology **114** (3): 331-348.

-Ballhaus, C., Berry, R. F., Green, D. H., 1991. High pressure experimental calibration of the olivine-orthopyroxene-spinel oxygen geobarometer: implications for the oxidation state of the upper mantle. Contributions to Mineralogy and Petrology **107** (1): 27-40.

-Barnes, S. J., Hill, R. E. T., Gole, M. J., 1988. The Perseverance ultramafic complex, Western Australia: the product of a komatiite lava river. Journal of Petrology **29** (2): 305-331.

-Beattie, P., Ford, C., Russell, D., 1991. Partition coefficients for olivine-melt and orthopyroxene-melt systems. Contributions to Mineralogy and Petrology **109** (2): 212-224.

-Berry, A.J., Danyushevsky, L.V., O'Neill, H.S.C., Newville, M., and Sutton, S.R., 2008. Oxidation state of iron in komatiitic melt inclusions indicates hot Archaean mantle. Nature **455**(7215): 960-U42.

-Bezos A., & Humler, E., 2005. The $Fe^{+3}/\Sigma Fe$ ratios of MORB glasses and their implications for mantle melting. Geochimica et Cosmochimica Acta **69**(3): 711-725.

-Bottinga, Y., & Javoy, M., 1990. MORB degassing: Bubble growth and ascent. Chemical Geology, **81**(4): 255-270.

-Brandon, A. D., Norman, M. D., Walker, R. J., Morgan, J. W., 1999. ^{186}Os-^{187}Os systematics of Hawaiian picrites. Earth and Planetary Science Letters **174** (1-2): 25-42.

-Brounce, M., Kelley, K. A., Cottrell, E., & Reagan, M. K., 2015. Temporal evolution of mantle wedge oxygen fugacity during subduction initiation. Geology,**43**(9): 775-778.

-Brounce, M. N., Kelley, K. A., & Cottrell, E., 2014. Variations in $Fe^{+3}/\Sigma Fe$ of Mariana Arc Basalts and Mantle Wedge fO2. Journal of Petrology, **55**(12): 2513-2536.

-Buick, R., 2008. When did oxygenic photosynthesis evolve? Philosophical Transactions of the Royal Society B: Biological Sciences, **363**(1504): 2731-2743.

-Campbell, I.H., Griffiths, R.W., and Hill, R.I., 1989. Melting in an Archaean mantle plume: head it's basalts, tails it's komatiites. Nature **339**(6227): 697-699.

-Canil, D., 1997. Vanadium partitioning and the oxidation state of Archaean komatiite magmas. Nature **389**(6653): 842-845.

-Canil, D., 1999. Vanadium partitioning between orthopyroxene, spinel and silicate melt and the redox states of mantle source regions for primary magmas. Geochimica et Cosmochimica Acta **63** (3-4): 557-572.

-Canil, D., 2002. Vanadium in peridotites, mantle redox and tectonic environments: Archean to present. Earth and Planetary Science Letters **195**(1-2): 75-90.

-Canil, D., and Fedortchouk, Y., 2001. Olivine-liquid partitioning of vanadium and other trace elements, with applications to modern and ancient picrites. Canadian Mineralogist **39**: 319-330.

-Canil, D., O'Neill, H.S.C., Pearson, D.G., Rudnick, R.L., McDonough, W.F., and Carswell, D.A., 1994. Ferric iron in peridotites and mantle oxidation states. Earth and Planetary Science Letters **123**(1-3): 205-220.

-Carmichael, I. S., 1991. The redox states of basic and silicic magmas: A reflection of their source regions? Contr. Mineral. and Petrol., **106**(2): 129-141.

-Chauvel, C., Dupré, B., Arndt, N. T., 1993. Pb and Nd isotopic correlation in Belingwe komatiites and basalts. The Geology of the Belingwe Greenstone Belt, Zimbabwe. A study of the evolution of Archaean continental crust. Bickle, M. J. and Nisbet, E. G. Rotterdam/Brookfield, A.A. Balkema**:** 167-174.

-Condie, K., 2001. Mantle Plumes and Their Record in Earth History. Cambridge, Cambridge University Press

-Connolly, B. D., Puchtel, I. S., Walker, R. J., Arevalo, R. J., Piccoli, P. M., Byerly, G. R., Robin-Popieul, C., Arndt, N. T., 2011. Highly Siderophile Element systematics of the 3.3 Ga Weltevreden komatiites, South Africa: implications for early Earth history. Earth and Planetary Science Letters **311** (3-4): 253-263.

-Cottrell, E., and Kelley, K. A., 2013. Redox heterogeneity in mid-ocean ridge basalts as a function of mantle source. Science **340**(6138): 1314-1317.

-Cottrell, E., and Kelley, K.A., 2011. The oxidation state of Fe in MORB glasses and the oxygen fugacity of the upper mantle. Earth and Planetary Science Letters **305**(3-4): 270-282.

-Cottrell, E., Kelley, K.A., Lanzirotti, A., and Fischer, R.A., 2009. High-precision determination of iron oxidation state in silicate glasses using XANES. Chemical Geology **268**(3-4): 167-179.

-Dann, J. C., 2000. The 3.5 Ga Komati Formation, Barberton Greenstone Belt, South Africa, Part I: New maps and magmatic architecture. South African Journal of Geology **103** (1): 47-68.

-Dauphas, N., 2009. Iron isotopes may reveal the redox conditions of mantle melting from Archean to Present. Earth and Planetary Science Letters **288**: 255-267.

-Delano, J.W., 2001. Redox History of the Earth's Interior since ~3900 Ma: Implications for Prebiotic Molecules. Origins of life and evolution of the biosphere **31**(4-5): 311-341.

-de Wit, M. J., Ashwal, L. D., Eds. 1997. Greenstone Belts. Oxford, Clarendon Press.

-Evans, K.A., 2012. The redox budget of subduction zones. Earth-Science Reviews **113**(1-2): 11-32.

-Frost, D.J., Mann, U., Asahara, Y., and Rubie, D.C., 2008. The redox state of the mantle during and just after core formation. Philosophical Transactions of the Royal Society **366**(1883): 4315-4337.

-Frost, D.J., and McCammon, C.A. 2008. The redox state of Earth's mantle. Annual Review of Earth and Planetary Sciences. Palo Alto, Annual Reviews. **36:** 389-420.

-Gaillard, F., Scaillet, B., Arndt, N. T. 2011. Atmospheric oxygenation caused by a change in volcanic degassing pressure. Nature **478**: 229-233.

-Gerlach, T. M., 1993. Oxygen buffering of Kilauea volcanic gases and the oxygen fugacity of Kilauea basalt. Geochimica et Cosmochimica Acta **57**: 795-814.

-Grocke, S. B., Cottrell, E., Silva, S. D., & Kelley, K. A., 2016. The role of crustal and eruptive processes versus source variations in controlling the oxidation state of iron in Central Andean magmas. Earth and Planetary Science Letters, **440:** 92-104.

-Harris, D. C., 2010. Quantitative chemical analysis. New York, NY: Freeman.

-Herzberg, C., Condie, K., Korenaga, J., 2010. Thermal history of the Earth and its petrological expression. Earth and Planetary Science Letters **292** (1-2): 79-88.

-Herzberg, C.T., 1992. Depth and degree of melting of komatiites. Journal of Geophysical Research **97**(B4): 4521-4540.

-Hibbert, K.E.J., Williams, H.M., Kerr, A.C., and Puchtel, I.S., 2012. Iron isotopes in ancient and modern komatiites: Evidence in support of an oxidised mantle from Archean to present. Earth and Planetary Science Letters **321-322**: 198-207.

-Hirschmann, M.M., 2012. Magma ocean influence on early atmosphere mass and composition. Earth and Planetary Science Letters **341-344**: 48-57.

-Holland, H.D., 2002. Volcanic gases, black smokers, and the great oxidation event. Geochimica et Cosmochimica Acta **66**(21): 3811-3826.

-Huppert, H.E., and Sparks, R.S.J., 1985. Komatiites I: Eruption and flow. Journal of Petrology **26**(3): 694-725.

-Huppert, H.E., Sparks, R.S.J., Turner, J.S., and Arndt, N.T., 1984. Emplacement and cooling of komatiite lavas. Nature **309**(5963): 19-22.

-Jahn, B., Gruau, G., & Glikson, A. Y., 1982. Komatiites of the Onverwacht Group, S. Africa: REE geochemistry, Sm/Nd age and mantle evolution. Contr. Mineral. and Petrol. **80**(1): 25-40.

-Kareem, K., 2005. Komatiites of the Weltevreden Formation, Barberton Greenstone Belt, South Africa: Implications for the chemistry and temperature of the Archean mantle. Department of Geology and Geophysics. Baton Rouge, Louisiana State University. **Doctor of Philosophy:** 233.

-Kasting, J. F., Eggler, D. H., Raeburn, S. P., 1993. Mantle redox evolution and the oxidation state of the Archean atmosphere. Journal of Geology **101**: 245-257.

-Kelley, K.A., and Cottrell, E., 2012. The influence of magmatic differentiation on the oxidation state of Fe in a basaltic arc magma. Earth and Planetary Science Letters **329-330**: 109-121.

-Kress, V.C., and Carmichael, I.S.E., 1991. The compressibility if silicate liquidus containing Fe_2O_3 and the effect of composition, temperature, oxygen fugacity and pressure on their redox states. Contrb Mineral Petrol **103**: 82-92.

-Kump, L.R., Kasting, J.F., and Barley, M.E., 2001. Rise of atmospheric oxygen and the "upside-down" Archean mantle. Geochemistry, Geophysics, Geosystems **2**(1).

-Lee, C. A., 2005. Similar V/Sc Systematics in MORB and Arc Basalts: Implications for the Oxygen Fugacities of their Mantle Source Regions. Journal of Petrology **46**(11): 2313-2336.

-Lee, C.-T.A., Yeung, L.Y., McKenzie, N.R., Yokoyama, Y., Ozaki, K., and Lenardic, A., 2016. Two-step rise of atmospheric oxygen linked to the growth of continents. Nature Geoscience **9**: 417-424.

-Le Voyer, M., Cottrell, E., Kelley, K. A., Brounce, M., & Hauri, E. H., 2015. The effect of primary versus secondary processes on the volatile content of MORB glasses: An example from the equatorial Mid-Atlantic Ridge (5°N-3°S). Journal of Geophysical Research: Solid Earth **120**(1): 125-144.

-Li, Z.X.A., and Lee, C.T.A., 2004. The constancy of upper mantle fO_2 through time inferred from V/Sc ratios in basalts. Earth and Planetary Science Letters **228**(3-4): 483-493.

-Lindsley, D. H. (Ed.). 1991. Oxygen Barometry of Spinel Peridotites. In B.R. Frost (Author), Reviews in Mineralogy and Geochemistry (Vol. 25, 417-432). Mineralogical Society of America.

-Lowe, D. R., Byerly, G. R., 1999. Stratigraphy of the west-central part of the Barberton Greenstone Belt, South Africa. Geological Evolution of the Barberton Greenstone Belt. Lowe, D. R. and Byerly, G. R. Boulder, Geological Society of America, Special Paper 329**:** 1-36.

-Ludwig, K. R., 2003, ISOPLOT 3.00. A geochronological toolkit for Microsoft Excel, Berkeley Geochronol. Cent. Spec. Publ., 4, 70 pp.

-Lyons, T. W., Reinhard, C. T., Planavsky, N. J., 2014. The rise of oxygen in Earth's early ocean and atmosphere. Nature **506** (7488): 307-315.

-Mallmann, G., & O'Neill, H. S., 2013. Calibration of an Empirical Thermometer and Oxybarometer based on the Partitioning of Sc, Y and V between Olivine and Silicate Melt. Journal of Petrology **54**(5): 933-949.

-Mallmann, G., & O'Neill, H. S., 2009. The Crystal/Melt Partitioning of V during Mantle Melting as a Function of Oxygen Fugacity Compared with some other Elements (Al, P, Ca, Sc, Ti, Cr, Fe, Ga, Y, Zr and Nb), Journal of Petrology **50**(9): 1765-1794.

-Mathez, E. A. 1976. Sulfur solubility and magmatic sulfides in submarine basalt glass. Journal of Geophysical Research **81**(23): 4269-4276.

-McDonough, W. F., Ireland, T. R. 1993. Intraplate origin of komatiites inferred from trace elements in glass inclusions. Nature **365**: 432-434.

-Mertzman, S. A., 2000. K-Ar results from the southern Oregon - northern California Cascade range. Oregon Geology **62** (4): 99-122.

-Moussallam, Y., Edmonds, M., Scaillet, B., Peters, N., Gennaro, E., Sides, I., & Oppenheimer, C., 2016. The impact of degassing on the oxidation state of basaltic magmas: A case study of Kīlauea volcano. Earth and Planetary Science Letters, **450**: 317-325.

-Moussallam, Y., Oppenheimer, C., Scaillet, B., Gaillard, F., Kyle, P., Peters, N., Hartley M., Berlo K., Donovan, A. , 2014. Tracking the changing oxidation state of Erebus magmas, from mantle to surface, driven by magma ascent and degassing. Earth and Planetary Science Letters, **393:** 200-209.

-Mundl, A., Touboul, M., Jackson, M. G., Day, J. M., Kurz, M. D., Lekic, V., Helz, R., Walker, R. J., 2017. Tungsten-182 heterogeneity in modern ocean island basalts. Science **356**(6333): 66-69.

-Nicklas, R. W., Puchtel, I. S., Ash, R. D., 2016. High-precision determination of the oxidation state of komatiite lavas using vanadium liquid-mineral partitioning. Chemical Geology **433**: 36-45.

-Nisbet, E. G., Arndt, N. T., Bickle, M. J., Cameron, W. E., Chauvel, C., Cheadle, M., Hegner, E., Kyser, T. K., Martin, A., Renner, R., Roedder, E., 1987. Uniquely fresh 2.7 Ga komatiites from the Belingwe greenstone belt, Zimbabwe. Geology **15** (12): 1147-1150.

-Nisbet, E.G., Bickle, M.J., and Martin, A., 1977, The mafic and ultramafic lavas of the Belingwe Greenstone Belt, Rhodesia: Journal of Petrology **18**: 521-566.

-Ohtani, E., 1988. Chemical stratification of the mantle formed by melting in the early stage of the terrestrial evolution. Tectonophysics **154** (3-4): 201-210.

-Ohtani, E., Kawabe, I., Moriyama, J., Y., N., 1989. Partitioning of elements between majorite garnet and melt and implications for petrogenesis of komatiite. Contributions to Mineralogy and Petrology **103** (3): 263-269.

-Puchtel, I. S., Touboul, M., Blichert-Toft, J., Walker, R. J., Brandon, A. D., Nicklas, R. W., Kulikov, V. S., and Samsonov, A. V., 2016a. Lithophile and siderophile element systematics of the Earth's mantle at the Archean-Proterozoic boundary: Evidence from 2.4 Ga komatiites. Geochimica et Cosmochimica Acta, **180**: 227–255.

-Puchtel, I. S., Blichert-Toft, J., Touboul, M., Horan, M. F., Walker, R. J., 2016b. The coupled ^{182}W-^{142}Nd record of early terrestrial mantle differentiation. Geochemistry, Geophysics, Geosystems. **17** (6): 2168-2193.

-Puchtel, I. S., Blichert-Toft, J., Touboul, M., Walker, R. J., Byerly, G., Nisbet, E. G., Anhaeusser, C. R., 2013. Insights into early Earth from Barberton komatiites: Evidence from lithophile isotope and trace element systematics. Geochimica et Cosmochimica Acta **108**: 63-90.

-Puchtel, I. S., Haase, K. M., Hofmann, A. W., Chauvel, C., Kulikov, V. S., Garbe-Schönberg, C. D., Nemchin, A. A., 1997. Petrology and geochemistry of crustally contaminated komatiitic basalts from the Vetreny Belt, southeastern Baltic Shield: Evidence for an early Proterozoic mantle plume beneath rifted Archean continental lithosphere. Geochimica et Cosmochimica Acta **61** (6): 1205-1222.

-Puchtel, I. S., Hofmann, A. W., Mezger, K., Shchipansky, A. A., Kulikov, V. S., Kulikova, V. V., 1996. Petrology of a 2.41 Ga remarkably fresh komatiitic basalt lava lake in Lion Hills, central Vetreny Belt, Baltic Shield. Contributions to Mineralogy and Petrology **124**: 273-290.

-Puchtel, I. S., Humayun, M., Campbell, A., Sproule, R., Lesher, C. M., 2004. Platinum group element geochemistry of komatiites from the Alexo and Pyke Hill areas, Ontario, Canada. Geochimica et Cosmochimica Acta **68** (6): 1361-1383.

-Puchtel, I. S., Walker, R. J., Brandon, A. D., Nisbet, E. G., 2009. Pt-Re-Os and Sm-Nd isotope and HSE and REE systematics of the 2.7 Ga Belingwe and Abitibi komatiites. Geochimica et Cosmochimica Acta **73** (20): 6367-6389.

-Pyke, D.R., Naldrett, A.J. and Eckstrand, O.R., 1973. Archean ultramafic flows in Munro Township, Ontario. Geol. Soc. Am. Bull., **84**: 955-978.

-Renner, R., Nisbet, E. G., Cheadle, M. J., Arndt, N. T., Bickle, M. J., Cameron, W. E., 1994. Komatiite flows from the Reliance Formation, Belingwe Belt, Zimbabwe: I. Petrography and mineralogy. Journal of Petrology **35** (2): 361-400.

-Rizo, H., Walker, R. J., Carlson, R. W., Horan, M. F., Mukhopadhyay, S., Manthos, V., Francis, D., Jackson, M. G., 2016. Preservation of Earth-forming events in the tungsten isotopic composition of modern flood basalts. Science **352** (6287): 809-812.

-Robin-Popieul, C. C. M., Arndt, N. T., Chauvel, C., Byerly, G. R., Sobolev, A. V., Wilson, A., 2012. A New Model for Barberton Komatiites: Deep Critical Melting with High Melt Retention. Journal of Petrology **53** (11): 2191-2229.

-Roeder, P. L., Emslie, R. F., 1970. Olivine-liquid equilibrium. Contributions to Mineralogy and Petrology **29** (4): 275-282.

-Rudnick, R. L., & Fountain, D. M., 1995. Nature and composition of the continental crust: A lower crustal perspective. Rev. Geophys. **33**(3): 267-309.

-Sack, R. O., Carmichael, I. S. E., Rivers, M., Ghiorso, M. S., 1980. Ferric-ferrous equilibria in natural silicate liquids at 1 bar. Contributions to Mineralogy and Petrology **75** (4): 369-376.

-Sobolev, A. V., Asafov, E. V., Gurenko, A. A., Arndt, N. T., Batanova, V. G., Portnyagin, M. V., Garbe-Schoenberg, D., Krasheninnikov, S. P., 2016. Komatiites reveal a hydrous Archaean deep-mantle reservoir. Nature, **531**(7596): 628-632.

-Stiegler, M. T., Cooper, M., Byerly, G. R., Lowe, D. R., 2012. Geochemistry and petrology of komatiites of the Pioneer Ultramafic Complex of the 3.3 Ga Weltevreden Formation, Barberton greenstone belt, South Africa. Precambrian Research **212**: 1-12.

-Touboul, M., Puchtel, I. S., Walker, R. J., 2012. ^{182}W Evidence for Long-Term Preservation of Early Mantle Differentiation Products. Science **335**: 1065-1069.

-Trail, D., Watson, E.B., and Tailby, N.D., 2011. The oxidation state of Hadean magmas and implications for early Earth's atmosphere. Nature **480**(7375): 79-82.

-Viljoen, M. J., Viljoen, R. P., 1969. The geology and geochemistry of the Lower Ultramafic Unit of the Onverwacht Group and a proposed new class of igneous rocks. Geological Society of South Africa Special Publication **2**: 55-86.

-Viljoen, M. J., Viljoen, R. P., Smith, H. S., Erlank, A. J., 1983. Geological, textural and geochemical features of komatiitic flows from the Komati Formation. Geological Society of South Africa Special Publication **9**: 1-20.

-Wade, J., and Wood, B.J., 2005. Core formation and the oxidation state of the Earth. Earth and Planetary Science Letters **236**(1-2): 78-95.

-Waters, L. E., Lange, R. A., 2016. No effect of H_2O degassing on the oxidation state of magmatic liquids. Earth and Planetary Science Letters, **447**: 48-59.

-Wood, B. J., Bryndzia, L. T., & Johnson, K. E., 1990. Mantle Oxidation State and Its Relationship to Tectonic Environment and Fluid Speciation. Science **248**(4953): 337-345.

-Woodland, A., & Koch, M., 2003. Variation in oxygen fugacity with depth in the upper mantle beneath the Kaapvaal craton, Southern Africa. Earth and Planetary Science Letters **214**(1-2): 295-310.

-Williams, H.M., McCammon, C.A., Peslier, A.H., Halliday, A.N., Teutsch, N., Levasseur, S., and Burg, J.-P., 2004. Iron Isotope Fractionation and the Oxygen Fugacity of the Mantle. Science **304**(5677): 1656-1659.

-Williams, H.M., Nielsen, S.G., Renac, C., Griffin, W.L., O'Reilly, S.Y., McCammon, C.A., Pearson, N., Viljoen, F., Alt, J.C., and Halliday, A.N., 2009. Fractionation of oxygen and iron isotopes by partial melting processes: Implications for the interpretation of stable isotope signatures in mafic rocks. Earth and Planetary Science Letters **283**(1-4): 156-166.

-Williams, H.M., Peslier, A.H., McCammon, C., Halliday, A.N., Levasseur, S., Teutsch, N., and Burg, J.P., 2005. Systematic iron isotope variations in mantle rocks and minerals: The effects of partial melting and oxygen fugacity. Earth and Planetary Science Letters **235**(1-2): 435-452.

-Williams, H.M., Wood, B.J., Wade, J., Frost, D.J., and Tuff, J., 2012. Isotopic evidence for internal oxidation of the Earth's mantle during accretion. Earth and Planetary Science Letters **321-322**: 54-63.

-Zhang, H.L., Hirschmann, M.M., Cottrell, E., Withers, A.C., 2017. Effect of pressure on $Fe^{+3}/\Sigma Fe$ ratio in mafic magma and consequences for magma ocean redox gradients. Geochimica et Cosmichimica Acta **204**: 83-103.

Chapter 4: Secular mantle oxidation across the Archean Proterozoic boundary: Evidence from V partitioning in komatiites and picrites

Note: This chapter has been previously published in the following publication:

Nicklas R. W., Puchtel I. S., Ash R. D., Piccoli P. M., Hanski E., Nisbet E. G., Waterton P., Pearson D. G. and Anbar A. D. (2019) Secular Oxidation across the Archean-Proterozoic boundary: Evidence from V partitioning in komatiites and picrites. *Geochim. Cosmochim. Acta* **250**: 49-75.

Abstract for Chapter 4

The oxygen fugacities of nine mantle-derived komatiitic and picritic systems ranging in age from 3.55 Ga to modern day were determined using the redox-sensitive partitioning of V between liquidus olivine and komatiitic/picritic melt. The combined set of the oxygen fugacity data for the systems from this study and the six komatiite systems studied by Nicklas et al. (2018), all of which likely represent large regions of the mantle, defines a well-constrained trend indicating an increase in oxygen fugacity of the lavas of ~1.3 ΔFMQ log units from 3.48 to 1.87 Ga, and a nearly constant oxygen fugacity from 1.87 Ga to the present. The oxygen fugacity data for the 3.55 Ga Schapenburg komatiite system, the mantle source region of which was previously argued to have been isolated from mantle convection within the first 30 Ma of the Solar System history, plot well above the trend and were not included in the regression. These anomalously high oxygen fugacity data likely reflect preservation of early-formed magma ocean redox heterogeneities until at least the Paleoarchean.

The observed increase in the oxygen fugacity of the studied komatiite and picrite systems of ~1.3 ΔFMQ log units is shown to be a feature of their mantle source regions and is interpreted to indicate secular oxidation of the mantle between 3.48 and 1.87 Ga. Three mechanisms are considered to account for the observed change in the redox state of the mantle: (1) recycling of altered oceanic crust, (2) venting of oxygen from the core due to inner core crystallization, and (3) convection-driven homogenization of an initially redox-heterogeneous primordial mantle. It is demonstrated that none of the three mechanisms alone can fully explain the observed trend, although mechanism (3) is best supported by the available geochemical data. These new data provide further evidence for mantle involvement in the dramatic increase in the oxygen concentration in the atmosphere leading up to the Great Oxidation Event at ~2.4 Ga.

4.1. INTRODUCTION

The oxidation state of the mantle is an important intensive thermodynamic parameter that controls the geochemical behavior of redox-sensitive elements in igneous systems (Herd, 2008), and that may be intimately linked to the oxidation state of the atmosphere (Holland, 2002).

Due to its large variation in natural systems, and to minimize the relative effects of temperature and pressure, the oxidation state of the mantle is quantified in terms of log units ($\Delta\log f\mathrm{O_2}$) relative to various mineral assemblage buffers, such as the nickel-nickel oxide (NNO) and the fayalite-magnetite-quartz (FMQ) buffers. There are several methods that are currently used to determine $f\mathrm{O_2}$ of igneous rocks and their mantle sources, including using experimentally calibrated equilibria (Sack et al., 1980; Ballhaus et al., 1991) in pristine mantle- and mantle-derived igneous rocks, utilizing measurements of $\mathrm{Fe^{3+}/\Sigma Fe}$ in spinels (Canil et al., 1994) or fresh volcanic glasses, respectively (Cottrell et al., 2009). For most samples in the geological record, however, this approach cannot be used, as the $\mathrm{Fe^{2+}/\Sigma Fe}$ ratio of minerals and glasses can be readily reset during alteration and metamorphism, although volcanic glass can be preserved as olivine-hosted melt inclusions in rocks as old as 2.69 Ga (e.g., Berry et al., 2008). Additionally, the $\mathrm{Fe^{3+}/\Sigma Fe}$ of volcanic glasses can be affected by syn-eruptive processes, such as sulfur degassing (Moussallam et al., 2014, 2016).

Because of the inapplicability of the $\mathrm{Fe^{2+}/\Sigma Fe}$ oxybarometer to altered samples, alternative methodology has been used, including determination of the stable Fe isotopic composition in rocks and minerals (Williams et al., 2005; Williams et al., 2009; Dauphas, 2009), quantification of ratios of redox-sensitive to redox-insensitive elements (Li and Lee, 2004; Aulbach and Viljoen, 2015; Aulbach and Stagno, 2016), or modeling partitioning behavior of redox-sensitive elements, such as V or Cr, during magmatic differentiation (Canil, 1997; Canil and Fedortchouk, 2001; Delano, 2001; Mallmann and O'Neill, 2009, 2013; Nicklas et al., 2016, 2018).

Most studies have concluded that mantle fO_2 has remained constant since at least the early Archean (Canil, 1997; Canil and Fedortchouk, 2001; Delano, 2001; Li and Lee, 2004; Berry et al., 2008; Trail et al., 2011; Hibbert et al., 2012). Recently, however, some researchers have argued for an increase in fO_2 of the upper mantle since the early Archean by as much as ~0.9 log units (e.g., Aulbach and Viljoen, 2015; Aulbach and Stagno, 2016; Shu et al., 2016; Aulbach et al., 2017a), while others have reported data that suggest the possibility of an increase in fO_2 of the mantle during the Archean (Nicklas et al., 2018). Because even small changes in mantle redox conditions can have large effects on the chemical evolution of major terrestrial reservoirs, such as the atmosphere, further constraints on mantle redox evolution are necessary.

Nicklas et al. (2016, 2018) determined the fO_2 of six Archean komatiite systems ranging in age from 3.48 to 2.41 Ga and showed that their entire range of oxygen fugacities was within the uncertainties of that for modern MORB at the 2-sigma uncertainty level. However, the data defined a distinct trend indicative of an increase in mantle fO_2 with time at the 1-sigma uncertainty level. In this study, we determined the fO_2 of nine additional komatiite and picrite systems. With the exception of the 3.55 Ga Schapenburg komatiite system, all the new systems are post-Archean in age.

Our use of ultramafic lavas to ascertain mantle fO_2 deserves justification because the vast majority of mantle-derived post-Archean volcanism is basaltic in nature. We argue that komatiites and picrites provide unique insights into mantle fO_2 for several reasons. First, it has been shown that island arc basalts can be up to ~6.0 log fO_2 units more oxidized than MORB or OIB (Carmichael, 1991) and this high fO_2 is likely a result of subduction-related metasomatism in their mantle wedge source region (Kelley and Cottrell, 2012; Brounce et al., 2014). We, therefore, avoided the potential complicating factor of including subduction-related lavas and, instead, opted for rocks that have been argued to be derived from anhydrous melting in hot mantle upwellings, or plumes. Second, work on two separate

modern OIB systems demonstrated a strong correlation between measured $Fe^{3+}/\Sigma Fe$ and sulfur content of volcanic glasses, with degassing of SO_2 having a reducing effect on the melt (Kelley and Cottrell, 2012; Moussallam et al., 2014, 2016). Based on the results of previous studies that demonstrated incompatible behavior of Pd and Pt in sulfur-undersaturated systems (i.e. Brügmann et al., 1987; Puchtel et al., 2016a), the level of saturation of sulfur species, if any, can be detected and corrected for in all the systems studied. In contrast, MORB lavas have been shown to be, to various degrees, sulfide- and vapor-saturated upon emplacement (e.g., Mathez, 1976; Bottinga and Javoy, 1990; Le Voyer et al., 2014), and their oxygen fugacities were likely affected by sulfur degassing. The komatiite and picrite systems we selected for this study were mostly produced by large degrees of partial melting of the mantle and, therefore, the compositions of the studied lavas are chemically similar to those of their mantle sources. Although the mantle source regions sampled by spreading ridges are not necessarily directly analogous to the mantle source regions tapped by anomalously hot plumes, comparing oxidation states of plume lavas serves as a valid proxy for the evolving oxidation state of the mantle. Even if there are differences in redox state between plume source mantle and ridge source mantle, there is no *a priori* reason why the relative difference between those two sources should change with time. This allows for the comparison of plume lavas to one another in order to constrain the redox evolution of the bulk mantle.

The method we applied in this study relies on the redox-sensitive nature of V partitioning between liquidus olivine and komatiitic and picritic magmas. The method was developed by Nicklas et al. (2016, 2018) and utilizes experimental data from Canil (1997) and Canil and Fedortchouk (2001). It was previously applied to six Archean komatiite systems by Nicklas et al. (2016, 2018), and the results of those studies will be considered in concert with the new current results in order to constrain the redox evolution of the mantle since the early Archean.

4.2. GEOLOGICAL BACKGROUND OF RESEARCH TARGETS

In this study, whole-rock samples and near-liquidus olivine from nine komatiite and picrite systems have been analyzed for trace metal abundances. These include the 3.55 Ga Schapenburg komatiites from the Barberton Greenstone Belt (BGB) in the Kaapvaal Craton, South Africa, the 2.06 Ga Lapland komatiites and the 1.98 Ga Onega Plateau picrites in the Fennoscandian Shield, the 1.87 Ga Winnipegosis komatiites of the Superior Craton, Canada, the 0.251 Ga Song Da komatiites, Vietnam, the 0.089 Ga komatiites of Gorgona Island, Colombia, the 0.062 Ga picrites of Padloping Island, Canada, and modern picrites from the Kilauea Iki lava lake in Hawaii and the Western Rift Zone of Iceland.

4.2.1. The 3.55 Ga Schapenburg komatiite system, Barberton Greenstone Belt, South Africa

The Schapenburg Greenstone Remnant (SGR) is a 12×2.5 km sequence of alternating volcanic and marine sedimentary rocks in the Kaapvaal Craton, South Africa (Anhauesser and Robb, 1980). The sequence is correlated with the lowermost formations of the Onverwacht Group of the Barberton BGB (Viljoen and Viljoen, 1969). The Onverwacht Group contains, among others, the 3.48 Ga Komati and 3.26 Ga Weltevreden Formations, which were previously studied for their fO_2 by Nicklas et al. (2018). The volcano-sedimentary sequence of the SGR is cyclic in nature, consisting of komatiites, komatiitic basalts, and banded iron formations (Anhauesser and Robb, 1980).

The SGR komatiites are typical Al-depleted komatiites (Al_2O_3/TiO_2 = 10.0±0.8, Gd/Yb_N = 1.57±0.03) and are also slightly depleted in LREE (La/Sm_N = 0.93±0.04). Using the Re-Os system, the SGR samples have been directly dated at 3550 ± 87 Ma (Puchtel et al., 2016a). The petrology and geochemistry of the Schapenburg komatiites have been studied using both outcrop samples (Lecuyer et al., 1994; Blichert-Toft et al., 2004; Puchtel et al., 2009) and in drill core samples (Puchtel et al., 2016a).

The sample powders analyzed in this study are those prepared by Puchtel et al. (2016a); all samples came from a single differentiated komatiite lava flow.

The SGR komatiites are of particular interest as they display negative ^{182}W and ^{142}Nd anomalies ($\mu^{182}W$ =-8.4 ± 4.5, $\mu^{142}Nd$ =-4.9 ± 2.8), due to their derivation from an early-formed (within the first 30 Ma of the Solar System history) mantle source that experienced fractionation of lower mantle phases, such as Ca-perovskite and bridgmanite (Puchtel et al., 2016a). The long-lived ^{147}Sm-^{143}Nd and ^{176}Lu-^{176}Hf systems (initial $\varepsilon^{143}Nd$ = +2.4 ± 0.1, initial $\varepsilon^{176}Hf$ = +5.7 ± 0.3) are decoupled, plotting off the terrestrial mantle array at 3.55 Ga, also likely due to early lower-mantle magma ocean processes (Puchtel et al., 2016a). The SGR mantle source has been calculated to contain 29±5% of the total HSE abundances estimated for the modern BSE, indicating that the SGR source region did not receive the full complement of chondritic late accretion component (Puchtel et al., 2016a). Finally, the initial $\gamma^{187}Os$ value of +3.7 ± 0.2 indicates derivation from a source with a long-term supra-chondritic Re/Os established early in Earth's history. Additional information on the SGR komatiites can be found in Anhaeusser (1983, 1991), Anhaeusser and Robb (1980), Lecuyer et al. (1994), Blichert-Toft et al. (2004), and Puchtel et al. (2009, 2016a).

4.2.2. The 2.06 Ga Lapland komatiite system, Fennoscandian Shield

The geology of Finnish Lapland is dominated by the Paleoproterozoic Central Lapland Greenstone Belt (CLGB), consisting of a thick succession of metamorphosed supracrustal rocks ranging in age from ca. 2.5 to 1.9 Ga (Hanski and Huhma, 2005). The Savukoski Group, in the upper section of the CLGB, consists of fine-grained sedimentary rocks overlain by Ti-rich komatiites and picrites, which have been associated with mantle plume activity (Hanski et al., 2001). The komatiites of this group have been directly dated at 2056±25 Ma using the Sm-Nd method on primary clinopyroxenes (Hanski et al., 2001). This age is consistent with the U-Pb zircon age of 2058±4 Ma obtained for the Kevitsa mafic-ultramafic

intrusion cutting phyllites of the Savukoski Group (Mutanen and Huhma, 2001). The Kevitsa intrusion is cut by ultramafic dikes, termed "Kevitsa dikes", which have very similar chemical and isotopic compositions to those of komatiitic lavas of the Savukoski Group, including unique hump-shaped chondrite-normalized REE patterns (Hanski et al., 2001), and it was argued, based on several lines of evidence, that the dikes served as feeding magma conduits to the komatiites (Huhma et al., 2018). The CLGB komatiites have yet to show preservation of igneous olivine, and were, thus, unsuitable for this study. However, unlike the CLGB komatiites, the Kevitsa dikes display excellent preservation of igneous minerals (**Fig. 4.1a.)**. The studied dike is >40 m in thickness and is characterized by internal differentiation related to fractionation of olivine, with a coarse-grained olivine-enriched central part and finer-grained chilled zones near contacts with the host rocks. The chilled margins of the dike consist of glassy, olivine phenocryst-poor komatiite. Additional information on the CLGB komatiites and Kevitsa dikes can be found in Hanski et al. (2001) and Huhma et al. (2018).

Figure 4.1.a. Photomicrograph of thin section sample KD08 from the Lapland komatiite system. A large olivine phenocryst is shown with two 100 micron LA-ICP-MS pits in its core.

4.2.3. The 1.98 Ga Onega Plateau picrite system, Fennoscandian Shield

The Onega Plateau is a large (~35,000 km^2) continental flood basalt province within the central Karelian Province of the Fennoscandian Shield (Puchtel et al., 1998a). The flood basalts are divided into two sequences, the lower Jatulian sequence, ~700 m in thickness, and the upper Ludikovian sequence, which is further subdivided into the lower ~1800-m-thick Zaonega suite and the upper ~700-m-thick Suisaarian suite (Puchtel et al., 1998a). It has been proposed by those authors that the Onega Plateau was emplaced rapidly onto submerged continental crust in a single starting mantle plume environment, with a plume head being ~2000 km in diameter. The samples chosen for this study come from the Konchozero sill, which served as a feeding magma conduit to the Suisaarian suite picrites. The sill ranges in thickness from a few tens of meters at its periphery to over 200 m in its central zone. The sill has a 4- to 6-m-thick glassy chilled margin close to its contact with the country rocks, and displays significant variation in the abundance of olivine within the sill, demonstrating internal differentiation after emplacement (Puchtel et al., 1998b). Both the Konchozero sill and the Suisaarian suite picrites have elevated $(Nb/Th)_N$ of 1.4-2.4 and $(Nb/La)_N$ of 1.1-1.3, and a positive initial ε_{Nd} value of +3.2±0.1, indicating that they did not experience any significant crustal contamination (Puchtel et al., 1998a). The Konchozero sill has been dated at 1969±18 Ma by the Re-Os isochron method on whole-rock samples and primary minerals, which is consistent with the Sm-Nd and Pb-Pb isochron ages of 1988±34 Ma and 1985±57 Ma, respectively, determined for the same samples (Puchtel et al., 1998b). Although the Suisaarian suite picrites do not preserve igneous olivine due to seafloor alteration and prehnite-pumpellyite facies metamorphism, a number of Ol-Cpx cumulate samples from the Konchozero sill that show good preservation of olivine have recently been identified. These samples were the ones selected for our study, and new sample powders and thin sections were prepared. Additional information on both the Onega Plateau picrites and the Konchozero sill rocks can be found in Puchtel et al. (1998a,b).

4.2.4. The 1.87 Ga Winnipegosis komatiite system, Canadian Shield

The Winnipegosis Komatiite Belt (WKB) is located on the western edge of the Archean Superior Craton, Manitoba, Canada, and is spatially associated with the Thompson Nickel Belt, with both belts comprising parts of the larger Paleoproterozoic Circum-Superior Belt (Hulbert et al., 1994). The latter belt consists of a 3000-km-long band of bimodal felsic-mafic volcanism along the western and northern edges of the Superior Craton (Baragar and Scoates, 1981), and has been interpreted as a tectonically emplaced large igneous province (LIP) (Ernst and Bleeker, 2010). The ~150×30-km-sized WKB is covered by a 120-to -500-m-thick sequence of Paleozoic sedimentary rocks and is dominated by komatiitic basalts and komatiites, with minor carbonate and shale sediments (McGregor, 2011). Due to the lack of surface exposure of the WKB, all samples of the belt were collected from drill core. The komatiites are remarkably well preserved, having only experienced sub-greenschist facies metamorphism and minimal aqueous alteration (Waterton et al., 2017) and retain large equant olivine phenocrysts (**Fig. 4.1b.)**. The komatiites belong to the Al-undepleted type (Al_2O_3/TiO_2 = 17.2±1.1, Gd/Yb_N = 1.13±0.04) and are dominated by massive olivine-porphyritic flows (Waterton et al., 2017). U-Pb zircon dating of basaltic flows within the WKB yielded a weighted average $^{207}Pb/^{206}Pb$ age of 1870±7 Ma (Waterton et al., 2017). For this study, we used samples representing several massive Ol-porphyritic komatiite lava flows. Additional information on the WKB komatiites can be found in Hulbert et al. (1994), McGregor (2011), and Waterton et al. (2017).

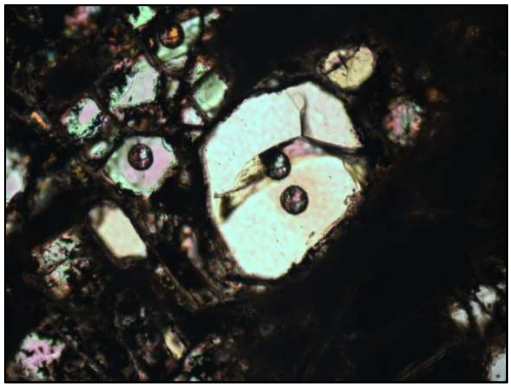

Figure 4.1.b. Photomicrograph of thin section sample RP-8 from the Winnipegosis komatiite system. Olivine phenocrysts are shown with 80 micron LA-ICP-MS pits. Both images were taken with cross-polarized light using 120 micron thick slides, and have a field of view of 3.0 x 2.5 mm.

4.2.5. The 251 Ma Song Da komatiite system, Vietnam

The Song Da Zone (SDZ) is a Permian supracrustal belt ~20 × 250 km in size in northwestern Vietnam running parallel to the Red River Fault (Polyakov et al., 1991; Hanski et al., 2004). The SDZ is closely associated with the Emeishan LIP in SW China, and likely formed in the SW part of the Emeishan LIP before being displaced ~600 km southeast by the Red River Fault (Chung et al., 1997, 1998). The Emeishan LIP has been Ar-Ar dated at 251.2–252.8 Ma (Lo et al., 2002). The SDZ consists of carbonate and siliciclastic sediments surrounding a central band of mafic-ultramafic volcanic rocks (Polyakov et al., 1991). Flows of MgO-rich lavas within this central band have been termed either komatiites (Hanski et al., 2004) or picrites (Wang et al., 2007; Anh et al., 2011). In this study, following Hanski et al. (2004), we refer to them as komatiites, consistent with the presence of clinopyroxene spinifex textures in these lavas. Komatiites in the SDZ experienced greenschist facies metamorphism and relatively minor aqueous alteration, with ~75% of their olivine phenocrysts preserved (Hanski et al., 2004). A Re-Os isochron obtained on whole-rock komatiite samples yielded an age of 270±21 Ma and a chondritic initial $\gamma^{187}Os$ value of +0.02±0.40 (Hanski et al., 2004). The initial $\varepsilon^{143}Nd$ values of the komatiites range from +3 to +8 reflecting varying, but small (2–3%), degrees of contamination with

Proterozoic silicic basement material, as indicated by their moderate depletion in the highly incompatible lithophile trace elements ($La/Sm_N = 0.58\pm0.34$). The Song Da komatiites are typical Al-undepleted komatiites, with $Al_2O_3/TiO_2 = 20\pm5$ and $Gd/Yb_N = 0.97\pm0.23$ (Hanski et al., 2004). Komatiite whole-rock samples from the Na Muoi River region were analyzed in this study. More information on komatiites from the SDZ can be found in Polyakov et al. (1991), Hanski et al. (2004), Wang et al. (2007), and Anh et al. (2011).

4.2.6. The 89 Ma Gorgona komatiite system, Colombia

Gorgona is a ~2 × 8 km island off the Pacific coast of Colombia (Echeverria, 1980). High-MgO lavas found on Gorgona were first recognized to be Phanerozoic equivalents of Archean komatiites by Gansser et al. (1979) and Echeverria (1980), making them one of the rare examples of true Phanerozoic komatiites, and the youngest komatiites yet discovered. They are transitional between the Al-undepleted and Al-depleted types of komatiites ($Al_2O_3/TiO_2 = 18.5\pm0.9$, $Gd/Yb_N = 1.24\pm0.04$) and have coupled radiogenic $\varepsilon^{143}Nd$ and $\varepsilon^{176}Hf$ systematics (Thompson et al., 2003) and, thus, plot on the terrestrial array for these two isotopic systems. They have initial $\varepsilon^{186}Os$ and $\gamma^{187}Os$ ranging from 0 to +0.7 and from 0 to +12, respectively (Walker et al., 1999; Brandon et al., 2003), implying a substantial long-term heterogeneity in Re/Os and Pt/Os in the source of these lavas. Lead isotope data have shown resolvable differences between komatiites exposed on the east coast of the island and those exposed on the west coast (Dupre and Echeverria, 1984). Isotopic and trace element data imply that at least three, and possibly four, separate end member compositions were present in the mantle source region of the Gorgona lavas to explain the large diversity of geochemical signatures found on the island (Kerr, 2005).

Ar-Ar dating of Gorgona basalts has yielded a weighted mean age of 88.9±1.2 Ma (Sinton et al., 1998), while a Re-Os isochron on the Gorgona basalts yielded an age of 89.2±5.2 Ma (Walker et al., 1999). Due to the significant Os and Pb isotopic heterogeneity recognized within Gorgona komatiites,

we have selected two komatiite groups from Gorgona Island for analysis, one on the eastern and another on the western side, and have determined the oxygen fugacity of each of the two groups. We analyzed samples collected by Revillon et al. (2000) (western group) and Echeverria (1980) (eastern group). All the samples studied were obtained as rock slabs from the Smithsonian National Museum of Natural History. They are characterized by superb state of preservation of primary minerals, and presence of abundant olivine phenocrysts. Additional geochemical information on the Gorgona komatiites is available in Echeverria (1980), Dupr*é* and Echeverria (1984), Kerr et al. (1996), Walker et al. (1999), Revillon et al. (2000, 2002), Serrano et al. (2011) and Kerr (2005).

4.2.7. The 62 Ma Padloping Island picrites

Padloping Island is a ~6 × 2 km island located off the coast of southeastern Baffin Island, Nunavut, Canada (Clarke and Upton, 1971). The picrite lavas located on Padloping Island are genetically closely associated with those on Disko Island off the west coast of Greenland, as well as those from the Faroe Islands and the British Tertiary Volcanic Province, indicating a common plume origin for these lavas, which likely formed during the first interaction of the present-day Iceland plume with the lithosphere (White and McKenzie, 1989; Robillard et al., 1992). The total thickness of the exposed lava sequence does not exceed 750 m (Francis, 1985), and the lowermost 350 m of the sequence consist of subaqueously erupted lavas (Robillard et al., 1992). The Padloping picrites have not experienced any significant alteration due to their very young age (Clarke and Upton, 1971). The lavas have not been directly dated, but their magnetic polarization belongs to Chron27n (Deutsch et al., 1971), making it possible to correlate them with the Anaanaa member in west Greenland dated at 61.7–62.0 Ma (Pedersen et al., 2002). Samples from Padloping Island have been found to be among the lavas having the highest $^{3}He/^{4}He$ ratios on Earth, indicating that they sampled a primordial, undegassed reservoir (Stuart et al., 2003; Starkey et al., 2009). The lavas also possess very primitive Pb isotope compositions

(Jackson et al., 2010), although it has been suggested that this was the result of crustal contamination with Archean gneisses (Dale, 2016). It has been recently recognized that the Padloping Island lavas have a large positive $\mu^{182}W$ anomaly, providing further evidence that the picrites sampled a mantle domain that was isolated from the convecting mantle within the first ~50 Ma of Earth's history (Rizo et al., 2016). However, the ^{146}Sm-^{142}Nd isotope system shows no anomaly in the Padloping Island picrites, indicating a decoupling of these short-lived isotopic systems in the mantle source of the lavas (De Leeuw et al., 2017). The average initial $^{187}Os/^{188}Os = 0.1272\pm0.0007$ determined for the lavas is chondritic, which indicates that the picrites had a negligible amount of ancient recycled crust in their source region (Dale et al., 2009), as would be expected for lavas sampling a very primitive source. Although samples from Padloping Island have not previously been the subject of oxygen fugacity measurements, the correlated Anaanaa unit in west Greenland has been determined to have an fO_2 close to $\Delta FMQ = +0.28$, based on the oxidation state of Fe in volcanic glasses (Larsen and Pedersen, 2002). We analyzed sample powders and thin sections previously studied by Kent et al. (2004), Dale et al. (2009) and Jackson (2010). These samples were taken from subaqueously erupted pillow-textured picritic lava flows exposed on the northeastern shore of Padloping Island, in the lowermost 350 m of the volcanic sequence. Additional information on the Padloping Island picrites can be found in Clarke and Upton (1971), Francis (1985), Kent et al. (2004), Dale et al. (2009) and Starkey et al. (2009).

4.2.8. The 1959 Kilauea Iki lava lake, Hawaii

The Kilauea Iki lava lake erupted over a four-week interval in 1959 (Richter and Moore, 1966), and has subsequently cooled and internally differentiated as a closed system. It has been extensively utilized as an excellent natural laboratory for studying igneous differentiation; the lava lake was drilled and sampled by the USGS throughout the 1960s, as it cooled and crystallized. The lava lake is picritic in composition, with the emplaced parental magma containing ~15 wt. % MgO (Wright, 1973). The lavas

are strongly LREE-enriched, with La/Sm_N = 1.7±0.1 and they show steeply sloping chondrite-normalized REE patterns, with La/Yb_N = 5.6±0.5 (Helz, 2012), a feature common to many ocean island basalts. We utilized a set of surface outcrop samples that we collected in 2015 from across the upper chilled margin of the lava lake. The oxygen fugacity of the lava lake, corrected for sulfur degassing, has been previously estimated to be ~ΔNNO = 0 (Moussallam et al., 2016), using the $Fe^{+3}/\Sigma Fe$ ratio of melt inclusions, and this estimate will be further used to inter-calibrate our fO_2 data with the fO_2 data determined using the $Fe^{+3}/\Sigma Fe$ method. Background geochemical data on the Kilauea-Iki lava lake can be found in Pitcher et al. (2009) and Helz (2012).

4.2.9. Western Rift Zone picrites, Iceland

Iceland represents an important modern-day example of mantle plume-induced magmatic activity. The majority of Icelandic igneous rocks, including picrites, show isotopic evidence for recycled oceanic crust in their mantle source region (Hemond et al., 1993). There is also a primordial, undegassed component in many Icelandic lavas, as evidenced by their elevated $^3He/^4He$ ratios relative to MORB (Kurz et al., 1985). We selected Icelandic picrites for our study as another modern analogue to compare with Archean plume lavas. This study utilized thin sections and sample powders from Maelifell and Dagmalafell volcanoes, two spatially associated volcanoes in the Western Rift Zone (WRZ) of SW Iceland previously studied by Brandon et al. (2007). These samples have been shown to have moderately elevated $^3He/^4He$ (11.5–17.2) relative to MORB, and slightly elevated initial $^{187}Os/^{188}Os$ ratios (0.13305–0.13335), indicating that both a primordial and a recycled component are present in their mantle source region (Brandon et al., 2007). More information on the Western Rift Zone samples used in this study can be found in Brandon et al. (2007).

4.3. ANALYTICAL TECHNIQUES

The protocols we used to determine the oxygen fugacity of the studied komatiite and picrite systems closely follow those used by Nicklas et al. (2016, 2018), and are briefly summarized in the sections below.

4.3.1. Sample selection, crushing procedure, and major and minor element abundances

In this study, we either used the sample powders already available from previous studies, or prepared new powders. In the case of the Onega Plateau picrites, the Lapland, Song Da and Gorgona komatiites, and the Kilauea Iki lava lake, new sample powders were prepared. The protocol for preparation of these samples followed that described by Puchtel et al. (2016b). Hand specimens, between 200 and 500 g in size, were cut into slabs, abraded on the cut surfaces using SiC sandpaper to remove saw marks, crushed in an alumina jaw crusher, and finely ground using an alumina shatterbox and alumina disk mill.

The major- and minor element analyses for the whole-rock samples were carried out at Franklin & Marshall College, Lancaster, Pennsylvania, USA on fused glass discs using a Phillips 2404 XRF spectrometer, following the procedure of Mertzman (2000). Typical precision of the analyses was ~2% relative (2SD) for major elements with concentrations >0.5% and ~5% relative for the rest of the major elements and for minor elements, as indicated by the analysis of the USGS Geologic Reference Materials BIR-1 and BCR-1 as unknowns (Puchtel et al., 2016b).

4.3.2. Analysis of trace element abundances in the whole-rock samples

The abundances of the trace metals in the whole-rock samples were determined using the standard addition solution inductively-coupled plasma mass-spectrometry technique (SA ICP-MS), and following the protocols detailed in Nicklas et al. (2016) and Nicklas et al. (2018). The sample solutions were analyzed on a *ThermoFinnigan Element2* sector field ICP-MS at the *Plasma Laboratory (PL),* Department of Geology, University of Maryland in medium resolution (MR) mode. The external

precision (i.e., 2SD) of the procedure was previously found to be 5% or better for all the elements of interest (Nicklas et al., 2016, 2018), and this value was used as the uncertainty on V concentrations for all error propagation calculations. For additional details on the development of the high-precision trace metal analysis in komatiites, the reader is referred to Nicklas et al. (2016, 2018).

4.3.3. Electron probe microanalysis of liquidus olivine

Major element analyses of olivines were performed on polished thin sections using the *JEOL JXA 8900 R* electron probe microanalyzer at the *Advanced Imaging and Microscopy Laboratory (AIMLab)*, University of Maryland. Special attention was paid to select and analyze only early-crystallized, equant grains. Operating conditions were 15 keV accelerating potential, 20 nA beam current, and 10 μm spot size. These electron probe data were then used for data normalization purposes for the laser ablation analysis, and to calculate the emplaced lava composition of each system, as described in Section 3.4.

4.3.4. Determination of the composition of the emplaced komatiite lavas

All the whole-rock samples studied, except for the upper chilled margin samples, have likely fractionated olivine post-emplacement and, therefore, the MgO contents of these whole-rock samples do not reflect that of the emplaced lava from which the olivine phenocrysts formed, due to addition or subtraction of cumulate olivine. Calculation of the emplaced lava MgO content for each komatiite and picrite system allows us to estimate the abundances of incompatible elements, most importantly V, in the emplaced lavas. The approach we used to calculate the emplaced lava MgO content was developed by Arndt (1986a) and Barnes et al. (1988) and has been widely used in follow-up studies of komatiites. This approach is based on the well-established Fe-Mg relationship between the composition of olivine and that of the liquid from which it crystallized (Roeder and Emslie, 1970; Beattie et al., 1991). The highest MgO and lowest FeO contents of the cores of equant olivine grains, as determined via EPMA (see section 3.3), and the compositions of the komatiite liquids in equilibrium with these olivine

compositions, were estimated using the partition coefficient $D^{Ol\text{-}Liq}_{Mg\text{-}Fe} = 0.30$ from Beattie et al. (1991). The whole-rock FeO contents of chilled margin samples from each komatiite system were used as a proxy for emplaced lava FeO content. For additional details on this protocol, the reader is referred to the publications by Puchtel et al. (2004, 2009, 2013, 2016b) and Nicklas et al. (2016, 2018).

4.3.5. Laser ablation ICP-MS analysis of liquidus olivine

Olivine grains were studied in polished thin sections in all komatiite and picrite systems except for the Western Gorgona and Schapenburg komatiites, and Kilauea Iki and Padloping Island picrites, for which polished rock chips mounted in epoxy were used.

The olivine grains were analyzed using an *UP213 New Wave* laser-ablation system coupled to the *ThermoFinnigan Element2* ICP-MS at *the PL*. The quintupled Nd-YAG laser operated at 7 Hz with fluence controlled between 2–4 J/cm^2 (~60% laser power). The analyses were conducted in low resolution (LR) mode, as this has been found to provide adequate resolution for V analyses in olivine (Aulbach et al.., 2017b). Before each analysis, the surface was ablated briefly to remove surface contamination, and the signal was allowed to drop to the baseline level before the analysis was begun. The spot size of each analysis varied between 55 and 100 μm depending on the size and homogeneity of the grains analyzed. Only equant olivine grains containing no visible inclusions were selected for analysis. Typically, the small size of the olivine grains permitted only one laser spot per each grain. Photomicrographs of the olivines from the Lapland komatiitic dike (a) and a massive komatiite sample from Winnipegosis (b) of the type that were selected for analysis are shown in **Fig. 4.1.** Replicate analyses of the USGS Microanalytical Reference Materials BHVO-2G and BCR-2G were performed with each set of 12–16 spots analyzed. The raw data were reduced using the *LAMTRACE* software and the lowest FeO abundances for the olivine in each komatiite and picrite system, determined by EPMA analysis, were used as normalizing values. The 2SD of the mean was used as a measure of the

uncertainty on the calculated average concentrations of trace metals in olivine for the individual samples.

4.4. RESULTS

4.4.1. Trace metal abundances in the liquidus olivine

Average concentrations of V, Sc, Ga, Y, and Cu in olivine from the nine studied systems are listed in **Table 4.1.;** the full sets of the LA-ICP-MS analysis data are presented in the online Supplementary **Tables S1-S9**. Vanadium concentrations in olivine are low relative to those in the emplaced komatiite and picrite lavas and vary in a narrow range, between 3.43 and 10.7 ppm, indicating incompatible behavior of V in olivine. Vanadium abundances in olivine within individual komatiite systems show differences in variability, from ~0.93% (2SD) in the Schapenburg system, up to ~24% in the Icelandic picrite system (**Table 4.1.**). The average Sc abundances in olivine are slightly more variable, from ~6.8% (2SD) in the Winnipegosis system, up to ~42% in the Schapenburg system. The V/Sc ratios in the olivines vary from 0.69±0.09 (2SD) in the Song Da system, up to 1.6±0.4 in the Onega Plateau lavas. The Ga and Y concentrations in olivine are very consistent within a single system, but Cu concentrations are highly variable both within individual samples and between samples within the same komatiite/picrite system, possibly reflecting the presence of Cu-rich inclusions in olivine that are heterogeneously distributed within the flow, and/or remobilization of Cu during metamorphic alteration (Waterton et al., 2017). This conclusion is further supported by the instability of the Cu signal during LA-ICP-MS analyses compared to that of the other trace elements.

Table 4.1. Average trace metal abundances (in ppm) in olivine from the studied systems

System	Sample	*N*	Sc	V	Cu	Ga	Y
Schapenburg	**SCH1.10-1**	34	3.69±1.05	3.30±1.04	1.93±2.09	0.06±0.05	0.15±0.27
	SCH1.10-2	23	2.74±0.83	3.32±0.82	2.23±1.90	0.06±0.04	0.14±0.25
Lapland	**KD-05**	50	4.70±1.77	5.53±1.88	3.76±1.74	0.21±0.09	0.08±0.04
	KD-06	31	3.72±0.65	5.76±1.45	3.57±1.16	0.20±0.11	0.09±0.03
	KD-08	36	3.87±0.97	5.37±1.83	2.83±3.53	0.21±0.10	0.08±0.05
	KD-09	26	3.92±1.30	5.49±1.30	2.76±3.22	0.23±0.09	0.07±0.04
	KD-10	15	3.67±1.00	5.31±0.81	2.52±2.72	0.19±0.07	0.07±0.04
Onega Plateau	**689-4**	32	5.84±1.85	10.0±4.8	6.95±5.06	0.30±0.17	0.63±0.51
	689-5	32	6.87±1.51	10.6±5.7	4.58±6.05	0.31±0.20	0.68±0.46
Winnipegosis	**RP-01**	30	4.12±0.57	4.71±0.86	3.02±3.25	0.25±0.17	0.08±0.03
	RP-02	32	4.27±0.75	4.85±0.87	1.85±1.71	0.24±0.12	0.08±0.03
	RP-08	48	3.93±0.69	4.84±0.83	2.96±2.48	0.18±0.12	0.07±0.03
	RP-11	48	4.05±0.57	4.95±0.89	3.11±1.83	0.19±0.12	0.07±0.03
Song Da	**VS 6-1-1**	47	8.79±2.46	5.67±2.19	10.8±6.5	0.31±0.17	0.13±0.08
	VS 6-1-2	32	7.73±2.24	5.55±2.50	12.6±4.9	0.32±0.23	0.12±0.06
	VS 6-1-3	47	8.24±2.35	5.83±2.06	10.9±5.5	0.28±0.14	0.13±0.10
Eastern Gorgona	**GOR153-1**	32	4.82±0.86	6.98±1.01	4.42±0.57	0.35±0.21	0.10±0.04
	GOR153-2	46	5.66±1.03	7.07±0.93	4.49±0.93	0.44±0.29	0.12±0.06
Western Gorgona	**GOR538-1**	47	6.69±1.19	7.16±1.12	4.54±0.87	0.25±0.10	0.13±0.04
	GOR538-2	47	5.98±0.91	7.07±1.14	4.64±1.51	0.23±0.15	0.13±0.04
	GOR538-3	47	6.38±1.30	7.18±1.17	4.56±1.64	0.25±0.09	0.13±0.03
Padloping	**AK-6**	22	7.09±1.03	10.1±1.8	8.67±1.65	0.23±0.06	0.13±0.04
	DB-9	31	6.58±0.90	8.50±2.25	6.93±1.16	0.21±0.09	0.12±0.05
	PI-20	32	7.24±1.63	9.18±2.37	4.54±1.59	0.21±0.22	0.13±0.12
Kilauea Iki	**15H-1**	30	5.73±0.55	5.43±0.73	3.86±0.48	0.20±0.08	0.13±0.03
	15H-2	13	4.95±0.72	5.57±0.44	4.21±1.67	0.25±0.10	0.15±0.05
	15H-3	31	6.09±1.39	5.59±0.82	3.82±0.49	0.20±0.06	0.11±0.02
	15H-4	32	4.88±1.06	5.64±0.63	3.78±0.29	0.17±0.03	0.12±0.03
Iceland	**ICE4A**	56	7.78±2.34	5.06±1.70	4.05±1.45	0.16±0.08	0.07±0.03
	ICE4B	8	7.20±0.70	5.35±1.35	4.14±0.30	0.19±0.07	0.08±0.02
	ICE5	16	6.14±1.22	5.65±1.35	4.30±0.88	0.17±0.05	0.06±0.01

Note. N - number of olivine grains analyzed in each given sample. The uncertainties are 2SD. Data for the individual LA-ICP-MS analyses for each of the komatiite and picrite systems are provided in the online Supplementary Tables S1-S9.

4.4.2. Trace metal abundances in the whole-rock samples

The abundances of V, Sc, Ga, Cu, Y, and Zr in the whole-rock samples from the nine komatiite and picrite systems are listed in **Tables 4.2., 4.3. and 4.4.**; the V abundances are also plotted as a function of MgO contents in **Figs. 4.2.-4.4.**

Table 4.2. Trace metal abundances in whole-rock samples from the Schapenburg, Lapland, and Onega Plateau systems.

System	Sample	MgO	LOI	Sc	V	Cu	Ga	Y	Zr	Lithology
Schapenburg	**SCH1.1**	26.5	4.15	19.2	138	319	5.47	6.91	10.3	Ol spx
	Replicate			19.4	139	313	5.44	6.99		
	SCH1.2	27.9	5.12	17.8	117	35.8	5.03	6.28	11.0	Ol spx
	Replicate			17.5	115	34.8	5.02	6.16		
	SCH1.3	26.7	3.52	19.2	126	94.8	5.20	7.12	14.0	Ol spx
	Replicate			19.2	126	94.8	5.16	7.07		
	SCH1.4	26.9	3.39	20.2	125	26.9	5.30	7.08	10.7	Ol spx
	Replicate			20.2	125	26.9	5.26	7.07		
	SCH1.5	25.9	2.80	19.3	130	152	5.41	7.27	11.4	Ol spx
	Replicate			19.3	130	151	5.36	7.12		
	SCH1.6	24.8	2.48	20.6	151	301	5.54	7.90	15.0	Ol spx
	SCH1.8	28.7	4.13	18.5	120	2.14	4.42	6.76	7.64	CM
	Replicate			18.2	123	2.17	4.33	6.74		
	SCH1.9	32.3	7.09	14.8	91.7	0.598	3.65	5.12	9.86	Ol cum
	Replicate			14.9	90.9	0.811	3.73	5.30		
	Replicate			14.9	91.6	0.718	3.63	5.10		
	SCH.10	36.0	8.27	12.6	78.4	0.593	3.18	4.03	8.04	Ol cum
	Replicate			12.6	78.0	0.867	3.16	4.04		
	Replicate			12.7	78.7	0.850	3.22	4.07		
Lapland	**KD-05**	22.6	0.63	30.4	238	114	11.8	10.9	31.9	KD
	KD-06	22.3	0.55	29.3	228	111	11.5	10.7	30.0	KD
	KD-08	25.2	1.40	26.6	210	104	10.5	9.36	27.3	KD
	KD-09	28.3	1.47	24.9	172	86.0	8.52	7.50	19.3	KD
	KD-10	28.3	2.15	25.3	180	n.d.	n.d.	n.d.	21.0	KD
	KD-11	24.2	1.25	28.4	223	108	11.1	10.0	29.3	KD
	KD-12	21.2	1.01	31.2	255	119	12.6	11.9	35.2	KD
	KD-13	20.2	1.22	31.7	258	123	12.9	11.9	36.5	KD
Onega Plateau	**689-1**	21.7	6.11	24.5	250	60.5	13.6	12.9	83.6	Pic
	689-3	30.6	8.19	19.4	160	104	7.56	7.83	46.8	Pic
	689-4	31.2	7.74	18.4	143	90.8	7.38	8.38	50.5	Pic
	689-5	31.7	7.61	19.1	147	68.9	6.85	7.22	39.9	Pic
	689-6	29.5	7.70	23.0	162	147	7.69	7.72	44	Pic
	9702	13.6	5.30	28.3	340	114	17.1	19.7	124	Pic
	9704	29.3	7.30	20.8	164	232	7.52	7.41	43.2	Pic
	9705	30.3	7.95	22.4	170	243	7.81	7.88	44.7	Pic

Note. Here and in Tables 3 and 4, the abundances of both MgO (wt. %) and trace metals (ppm) are re-calculated on an anhydrous basis using measured LOI (wt. %) values. CM – chilled margin, Ol spx – olivine spinifex, Ol cum – olivine cumulate, Pic – picrite, KD – komatiitic dike. The rest of the major element data are provided in the online Supplementary Tables S1–S9. n.d. - not detected.

Table 4.3. Trace metal abundances in whole-rock samples from the Winnipegosis, Song Da and Gorgona Island komatiite systems.

System	Sample	MgO	LOI	Sc	V	Cu	Ga	Y	Zr	Lithology
Winnipegosis	**RP-01**	24.2	2.93	27.1	n.d.	73.3	9.06	9.67	25.0	MK
	RP-04	20.3	3.73	29.2	211	83.7	10.5	10.9	29.3	MK
	RP-05	23.0	3.24	28.6	193	80.2	9.56	10.2	26.6	MK
	RP-08	25.3	3.05	26.2	177	72.6	8.72	9.19	24.1	MK
	RP-09	22.0	2.70	29.5	197	82.2	9.87	10.5	27.6	MK
	RP-11	24.0	2.36	26.2	183	75.2	9.09	9.40	25.1	MK
	RP-12	22.8	2.54	27.5	196	83.1	9.56	10.0	26.3	MK
	RP-14	21.4	4.31	30.5	205	n.d.	10.0	10.9	28.2	MK
	RP-17	20.6	4.12	30.3	204	92.6	10.1	11.0	29.5	MK
Song Da	**P 9/86**	26.8	5.25	27.2	180	81.7	8.77	10.2	17.7	MK
	Replicate			27.0	177	82.7	8.87	10.0	17.5	MK
	P 11/86	32.6	8.55	23.1	140	61.5	7.27	8.30	17.1	MK
	Replicate			21.9	139	59.1	7.09	8.04	16.3	MK
	B6887	33.5	6.33	21.6	122	59.9	6.22	7.83	14.3	Ol cum
	Replicate			22.0	122	56.8	6.18	7.83	13.4	Ol cum
	VS 5-1	21.4	3.96	34.8	227	114	12.0	14.4	24.4	MK
	Replicate			31.8	237	121	12.0	14.7	24.1	MK
	VS 6-1	22.6	2.23	33.0	207	100	11.0	13.6	22.8	Ol cum
	Replicate			31.7	214	112	11.4	13.8	22.7	Ol cum
	VS 6-2	14.3	4.55	43.2	261	45.7	14.5	15.8	27.0	MK
	Replicate			40.3	251	47.4	13.9	15.0	25.5	MK
Eastern Gorgona	**GOR152**	15.3	2.80	37.7	307	146	14.6	15.3	33.1	CM
	GOR153	23.8	3.29	29.3	227	107	10.9	11.4	24.8	Ol cum
	GOR155	15.4	5.97	38.9	314	155	14.4	15.6	31.9	Ol spx
	GOR156	17.7	3.09	35.0	284	134	13.6	14.3	30.9	Ol spx
	GOR157	12.1	3.15	42.0	346	158	16.3	17.3	36.5	Ol spx
	GOR159	18.7	2.69	34.2	276	133	13.4	13.8	29.2	Ol spx
	GOR160	17.8	5.07	35.7	289	132	14.0	14.4	30.9	Ol spx
Western Gorgona	**GOR537**	17.2	1.83	35.2	293	137	13.8	14.5	29.9	Ol spx
	GOR538	25.7	2.88	27.3	221	99.5	10.1	10.4	21.8	Ol cum
	GOR539	18.3	4.21	33.3	266	135	13.0	13.4	28.2	Ol spx
	GOR540	18.0	4.64	36.6	298	123	13.2	13.2	26.4	Ol spx

Note. CM – chilled margin, Ol spx – olivine spinifex, Ol cum – olivine cumulate, MK – massive komatiite. Additional major element data are provided in the online Supplementary Tables S1–S9. n.d. – not detected.

Table 4.4. Trace metal abundances in whole-rock picrite samples from the Kilauea Iki lava lake, the Western Rift Zone of Iceland, and Padloping Island.

System	Sample	MgO	LOI	Sc	V	Cu	Ga	Y	Zr	Lithology
Kilauea Iki	**H15-1_1**	11.7	-0.48	29.7	311	119	19.7	22.0	150	MP
	Replicate			30.1	309	126	19.3	22.0	148	MP
	15H-1_2	11.6	-0.48	30.3	310	124	19.5	22.1	151	MP
	H15-2_1	17.6	-0.39	25.8	259	106	16.2	18.4	124	MP
	15H-2_2	17.8	-1.50	25.0	248	106	15.7	17.7	120	MP
	H15-3_1	12.1	-0.50	29.5	301	106	19.0	20.7	145	MP
	Replicate			29.7	305	107	19.3	21.4	148	MP
	15H-3_2	12.4	-0.47	29.8	304	111	19.0	21.4	148	MP
	H15-4_1	15.7	-0.56	26.4	275	107	17.2	19.1	129	MP
	15H-4_2	16.3	-0.54	26.9	273	105	17.0	19.0	130	MP
Iceland	**ICE4A**	25.3	n.d.	34.2	191	72.3	9.40	8.91	15.3	MP
	ICE4B	23.9	n.d.	35.0	200	71.3	9.69	9.04	15.4	MP
	ICE5	18.8	n.d.	38.1	225	83.0	11.8	9.67	14.0	MP
	Replicate	18.8	n.d.	38.6	224	83.1	11.9	9.80	14.0	MP
Padloping	**AK-6**	25.0	2.73	28.7	200	92.8	9.96	11.6	26.1	MP
	DB-9	23.0	1.41	30.0	216	99.3	10.9	12.6	34.9	MP
	PI-20	19.5	0.79	36.1	249	93.3	12.4	15.3	45.9	MP

Note. The remainder of the major element data are provided in the online Supplementary Tables S1-S9. MP- massive picrite.

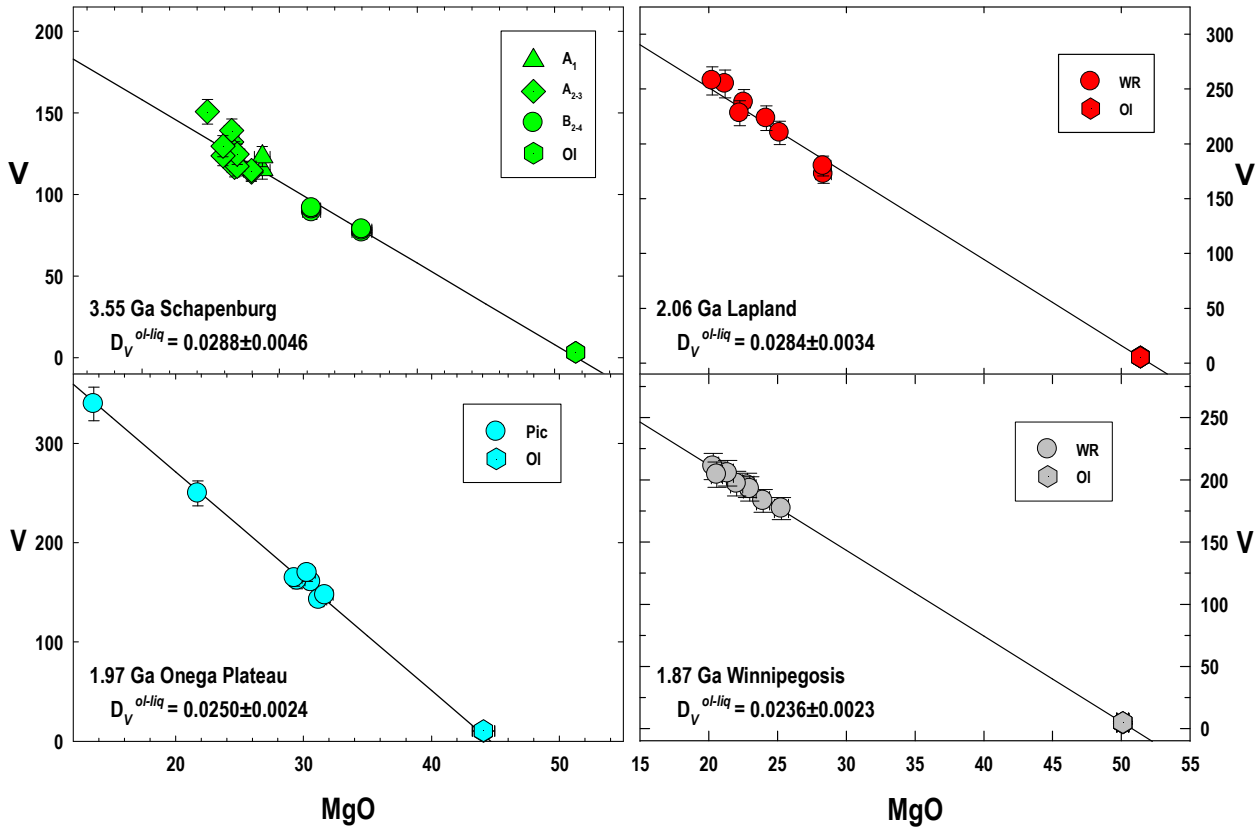

Figure 4.2. Vanadium (ppm) abundances in whole-rock samples and olivine from the 3.55 Ga Schapenburg komatiite, 2.06 Ga Lapland komatiite, 1.97 Onega Plateau picrite, and 1.87 Ga Winnipegosis komatiite systems plotted against MgO contents (wt. %). A_1 - upper chilled margin, A_{2-3} - spinifex zone, B_{2-4} - cumulate zone, WR - whole rock, and Ol - olivine. The composition of the upper chilled margin zone approximates that of the emplaced lava. The details of the protocol for calculating the $D_V^{Ol\text{-}Liq}$ values for each system here and in Figs. 3–4 are given in the text. The uncertainties here and in Figs. 3 and 4 are propagated 2SD uncertainties.

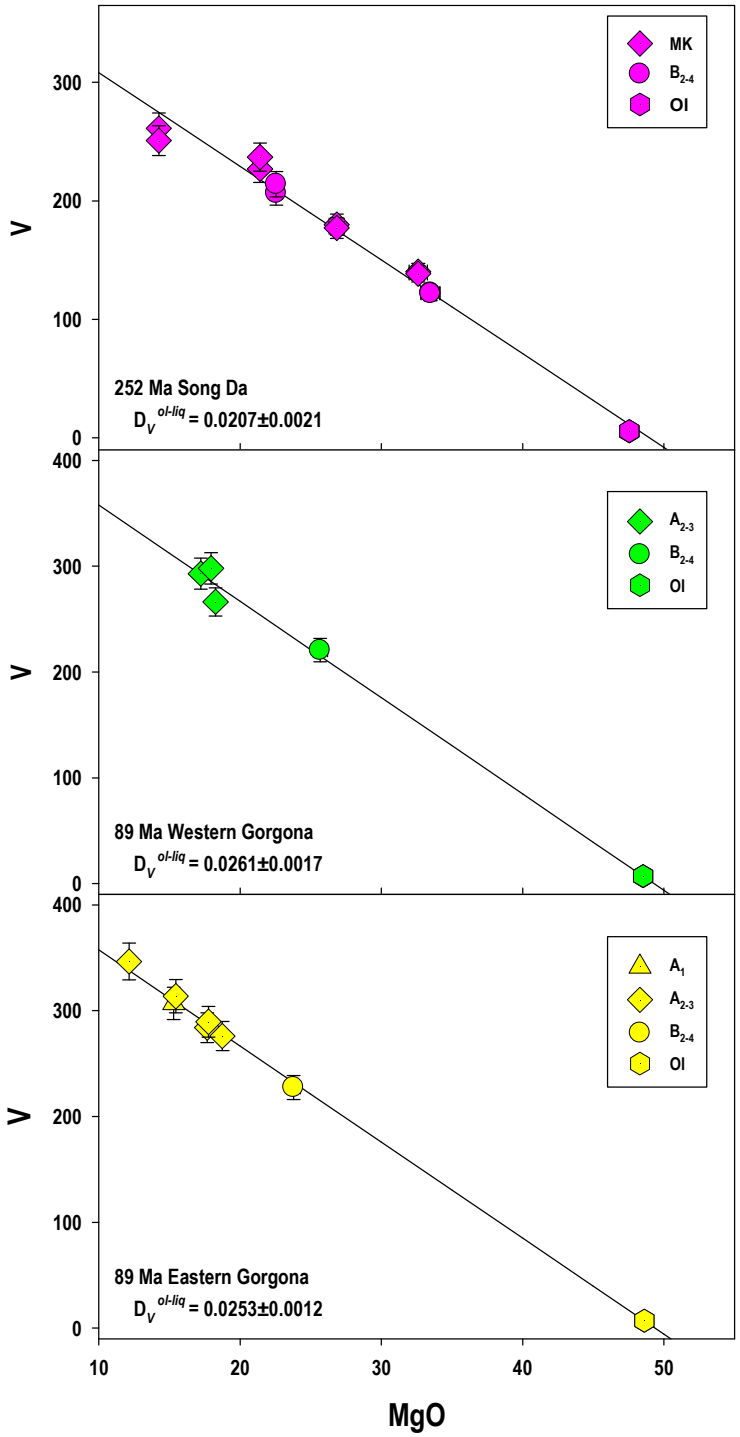

Figure 4.3. Vanadium (ppm) abundances in komatiite whole-rock samples and olivine from the 251 Ma Song Da komatiite system and from two flows of the 89 Ga Gorgona komatiite system plotted against MgO contents (wt.%). A_1 - upper chilled margin, A_{2-3} - spinifex zone, B_{2-4} - cumulate zone, MK – massive komatiites, and Ol - olivine.

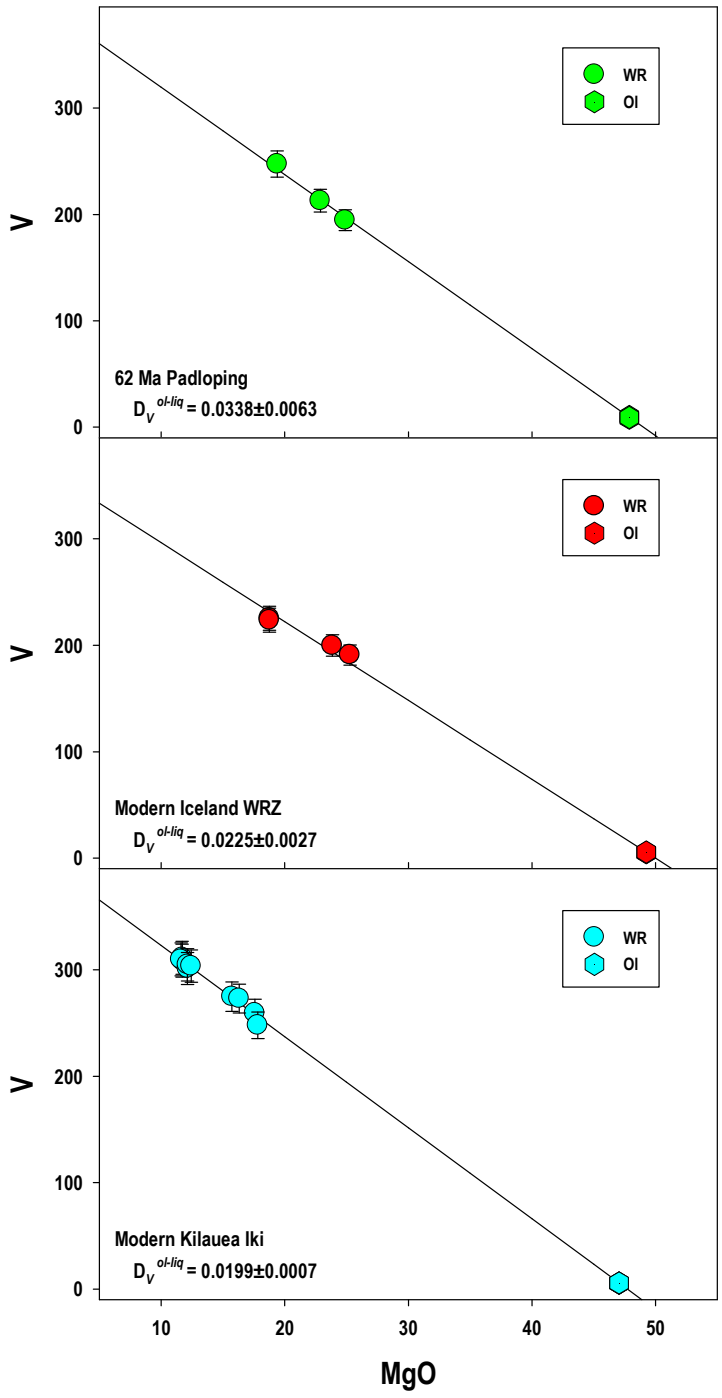

Figure 4.4. Vanadium (ppm) abundances in whole-rock samples and olivine from the 62 Ma Padloping Island picrites, as well as picrites from the 1959 eruption of Kilauea Iki and the Western Rift Zone (WRZ) of Iceland plotted against MgO contents (wt.%). WR - whole rock, Ol - olivine.

Vanadium abundances (and also Ga and Sc – not shown) are strongly inversely correlated with MgO contents, thus exhibiting incompatible behavior over the entire range of compositions present in the studied lavas. These regression lines pass through the measured olivine compositions for each individual system, indicating that these regression lines represent olivine control lines. The Y abundances (not shown) display similarly incompatible well-constrained behavior in all but the Iceland picrites, where the Y data are more scattered (MSWD = 10). Cu and Zr plot with considerably more scatter, and show deviations from linear behavior in the Onega Plateau and Schapenburg systems for Cu, and the Padloping Island, Onega Plateau and Schapenburg systems for Zr. These deviations from olivine control lines for Y, Zr and Cu are most likely due to seafloor alteration and metamorphism, or fractionation of another significant phase hosting these elements in the systems, or both. These observations attest to the immobile behavior of V, Sc and Ga, the most petrogenetically important elements in this study, on the whole-rock scale (and also Y, Cu, and Zr in most cases) since crystallization of the studied systems and provide evidence for olivine being the only major fractionating phase that controlled variations in the abundances of these elements in the studied komatiite and picrite systems.

4.4.3. Estimation of the V and Sc abundances in the emplaced komatiite lavas

The FeO content, as well as the calculated MgO content, of each of the emplaced lavas are listed in **Table 4.5.**, and errors on the emplaced MgO content of each system are propagated in quadrature to calculations of concentrations of incompatible elements in the emplaced lavas. The average maximum MgO and average minimum FeO contents in the liquidus olivine used to calculate the emplaced lava MgO content in each of the nine systems are listed in **Table 4.6.** and in the online Supplementary **Tables S1-S9**. The calculated MgO contents in the emplaced lavas vary between 21.1±2.5 and 28.6±2.8

wt.% in the Precambrian komatiite systems, then decrease to 7.95±0.28 – 19.3±1.6 wt.% in the picrite and Phanerozoic komatiite systems.

Table 4.5. The measured FeO and calculated MgO abundances (wt.%), along with calculated V, and Sc abundances (ppm) and V/Sc ratios in emplaced lavas from the studied komatiite and picrite systems.

	FeO	MgO	V (ppm)	Sc (ppm)	V/Sc
Schapenburg	11.7	28.6±2.8	115±18	17.8±2.3	6.47±1.34
Lapland	9.00	27.4±2.4	193±19	25.4±2.4	7.60±1.04
Onega Plateau	9.00	7.95±0.28	411±23	38.9±8.7	10.6±2.4
Winnipegosis	11.2	21.1±2.5	205±18	29.6±2.4	6.91±0.82
Song Da	11.0	14.3±1.0	274±25	40.3±2.6	6.80±0.75
Eastern Gorgona	11.4	18.8±1.1	278±12	34.5±1.7	8.04±0.53
Western Gorgona	11.4	19.3±1.6	273±17	33.4±2.2	8.17±0.73
Padloping	10.4	15.5±1.4	274±15	37.5±2.4	7.31±0.62
Kilauea Iki	11.8	15.0±0.6	280±5	27.5±0.7	10.2±0.3
Iceland	9.89	17.9±1.3	238±12	40.5±2.2	5.88±0.44

Note. The background data and the calculation details are provided in the text and in the online Supplementary Tables S1-S9. The V and Sc abundances in the emplaced komatiite lavas and the uncertainties on the V and Sc abundances were derived from ISOPLOT regression calculations and are propagated 2SD uncertainties.

Table 4.6. Average maximum MgO and minimum FeO (wt.%) and average V and Sc abundances in liquidus olivine and calculated D_v and D_{Sc} and fO_2 in the systems studied

Locality	MgO	FeO	V (ppm)	Sc (ppm)	D_v^{Ol-Liq}	D_{Sc}^{Ol-Liq}	fO_2 (ΔNNO)	fO_2(ΔFMQ)
Schapenburg	51.54±0.54	6.32±0.50	3.31±0.03	3.22±1.34	0.0288±0.0046	0.181±0.079	0.16±0.38	0.88±0.38
Lapland	51.38±0.55	6.43±0.32	5.49±0.35	3.98±0.84	0.0284±0.0034	0.156±0.036	0.18±0.33	0.90±0.33
Onega Plateau	44.06±0.47	15.46±0.37	10.29±0.38	6.35±1.46	0.0250±0.0024	0.158±0.044	0.40±0.31	1.12±0.31
Winnipegosis	50.10±0.44	8.13±0.63	4.84±0.20	4.09±0.28	0.0236±0.0023	0.138±0.015	0.50±0.31	1.22±0.31
Song Da	47.55±0.35	11.36±0.38	5.68±0.28	8.26±1.06	0.0207±0.0021	0.205±0.030	0.73±0.32	1.45±0.32
Eastern Gorgona	48.62±0.31	8.86±0.26	7.02±0.13	5.24±1.19	0.0253±0.0012	0.152±0.035	0.38±0.27	1.10±0.27
Western Gorgona	48.53±0.52	8.64±0.39	7.14±0.12	6.35±0.71	0.0261±0.0017	0.190±0.025	0.33±0.28	1.05±0.28
Padloping	47.89±0.56	10.96±0.58	9.27±1.64	6.94±0.81	0.0338±0.0063	0.185±0.025	-0.12±0.41	0.60±0.41
Kilauea Iki	47.07±0.15	11.15±0.15	5.56±0.19	5.41±1.19	0.0199±0.0007	0.196±0.044	0.80±0.27	1.52±0.27
Iceland	49.26±0.33	9.42±0.39	5.36±0.59	7.04±1.66	0.0225±0.0027	0.174±0.042	0.59±0.34	1.31±0.34

Note. The D_v^{Ol-Liq} and fO_2 values were calculated using the protocol detailed in the text. All the uncertainties are the 2SD uncertainties propagated in quadrature.

Using the calculated MgO contents in the emplaced lavas for each system and regressing the trace element abundance data obtained in this study for the whole-rock samples and olivine against the MgO contents using ISOPLOT (Ludwig, 2003), Sc and V abundances in the emplaced komatiite lavas for each individual komatiite system have been calculated; these abundances, with their respective propagated 2SD uncertainties, are also presented in **Table 4.5**. The calculated V and Sc abundances vary from 115±18 to 278±12 and 17.8±2.3 to 40.3±2.6 ppm, respectively, in the komatiite systems, and 238±12 to 404±19 and 27.5±0.7 to 40.5±2.2 ppm, respectively, in the picrite systems.

4.4.4. Evaluation of the redox state of the komatiite and picrite systems

4.4.4.1. Vanadium and Sc partitioning between olivine and emplaced lavas

The average V and Sc concentrations in the liquidus olivine, with their respective propagated 2SD uncertainties, are presented in **Table 4.6**. Using these values and the estimated V and Sc abundances in the emplaced komatiite lavas (**Table 4.5.**), partition coefficients for V and Sc between liquidus olivine

and emplaced lavas for the studied komatiite and picrite systems were obtained; these data are listed in **Table 4.6.** and presented in the MgO vs. V variation diagrams (**Figs. 4.2.-4.4.**). Uncertainties on the komatiite lava and average olivine compositions were propagated in quadrature to determine the uncertainties on the $D_V^{Ol\text{-}Liq}$ for the individual systems.

The calculated $D_V^{Ol\text{-}Liq}$ values do not show any correlation with the petrologic types of the lavas studied (*e.g.,* komatiite or picrite). However, the *D* values do exhibit a trend with age of the systems, decreasing from 0.0284±0.0034 in the 2.06 Ga Lapland komatiite system to 0.0207±0.0021 and 0.0199±0.0007 in the 251 Ma Song Da and modern Kilauea Iki systems, respectively. The $D_{Sc}^{Ol\text{-}Liq}$ values range between 0.135±0.015 and 0.205±0.030 and do not appear to exhibit any secular trend, possibly varying as a result of temperature or melt composition effects.

Having determined the V partition coefficients between the liquidus olivine and the emplaced lavas for the nine systems, we used the combined experimental calibrations of Canil (1997) and Canil and Fedortchouk (2001) to evaluate the oxidation states of these komatiite and picrite systems. Regressions of experimental data compiled by Nicklas et al. (2018) from the above two publications yielded the following equation:

$$\log(D_v^{Ol\text{-}Liq}) = (-0.250\pm0.023)\times\Delta NNO - (1.501\pm0.064)\ (r^2 = 0.94) \qquad (1)$$

Uncertainties on the slopes and intercepts of equation (1) were derived from the 95% confidence interval of the regression of the experimental data and experimental uncertainties using ISOPLOT 3.00 (Ludwig, 2003). The uncertainties shown in equation (1) were propagated in quadrature through the determination of fO_2 from $D_V^{Ol\text{-}Liq}$. More information on the experimental regression shown in equation (1) can be found in Nicklas et al. (2018).

Although V partitioning oxybarometers that take into account abundances of other major elements, mostly alkalis, in the crystallizing melt do exist (e.g., Mallmann and O'Neill 2009, 2013), those

oxybarometers are not applicable to samples that experienced seafloor alteration and/or metamorphism, for which the primary abundances of fluid-mobile major elements (such as the alkalis) are difficult to constrain. Although the abundances of fluid-mobile elements are well constrained in some of the younger systems, there exists a systematic offset between the fO_2 values calculated using different oxybarometers (Mallmann and O'Neill, 2013) and as such, we have chosen to use only partitioning data from a single suite of experiments. As the experiments of Canil (1997) and Canil and Fedortchuok (2001) used bulk compositions close to that of the lavas studied here we have elected to use those experimental data. The composition-independent oxybarometer in equation (1) is derived from those data, and is used to facilitate comparison between the Archean and modern lavas. For ease of comparison to previously published data for mantle-derived rocks, all of the oxygen fugacity values have been converted from ΔNNO log units to the more commonly used ΔFMQ log units using the standard thermodynamic values for each mineral buffer assemblage listed in Wood (1991). The fO_2 values calculated from the V partitioning data are listed in **Table 4.6.** and plotted as a function of the age of the studied systems in **Fig. 4.5a**.

The early Archean Schapenburg komatiite system is characterized by an elevated calculated fO_2 value of +0.88±0.38 ΔFMQ log units, significantly higher than the spatially and temporally associated 3.48 Ga Komati system at −0.11±0.30 ΔFMQ log units (Nicklas et al., 2018). The Schapenburg system has been found to retain short lived ^{182}W and ^{142}Nd isotope anomalies (Puchtel et al., 2016a), while no such anomalies have been detected in the Komati system (Touboul et al., 2012). The Schapenburg system, therefore, likely sampled a region of the mantle that was anomalous with respect to both fO_2 and short-lived isotope systems, and, thus, does not represent the bulk of the mantle at 3.55 Ga. The lavas from the Padloping Island picrite system show the lowest measured fO_2 value at +0.60±0.41 ΔFMQ, which is within uncertainty of that estimated in the related Anaanaa unit of West Greenland at ~+0.28

ΔFMQ (Larsen and Pedersen, 2002). The Padloping lavas have also been shown to have large short-lived isotopic anomalies (Rizo et al., 2016) and were, therefore, also not used to characterize the mantle at 62 Ma. The significance of the obtained fO_2 values for these two systems is further addressed in Section 5.4.

The fO_2 values of the remaining komatiite and picrite systems vary between +0.90±0.33 ΔFMQ in the Lapland system, to +1.52±0.27 ΔFMQ in the Kilauea Iki system, and show a broad correlation with age. Data from this study, combined with the Archean komatiite data from Nicklas et al. (2018), define a secular trend in oxygen fugacity from 3.48 Ga to the present day, with an overall change in oxidation state of ~1.6 log units. The change is most marked from 3.48 to 1.87 Ga, with all systems postdating the Winnipegosis system having fO_2 values that are identical within errors. A linear least-squares ISOPLOT regression (MSWD = 2.4) of the fO_2 data from 3.48 to 1.87 Ga yields a slope of 0.80±0.20 log units ΔFMQ /Ga. This linear regression is plotted in **Fig. 4.5a**. The difference in oxygen fugacity between the Komati and Winnipegosis systems, which anchor the ends of the linear regression line, is 1.33±0.43 log units.

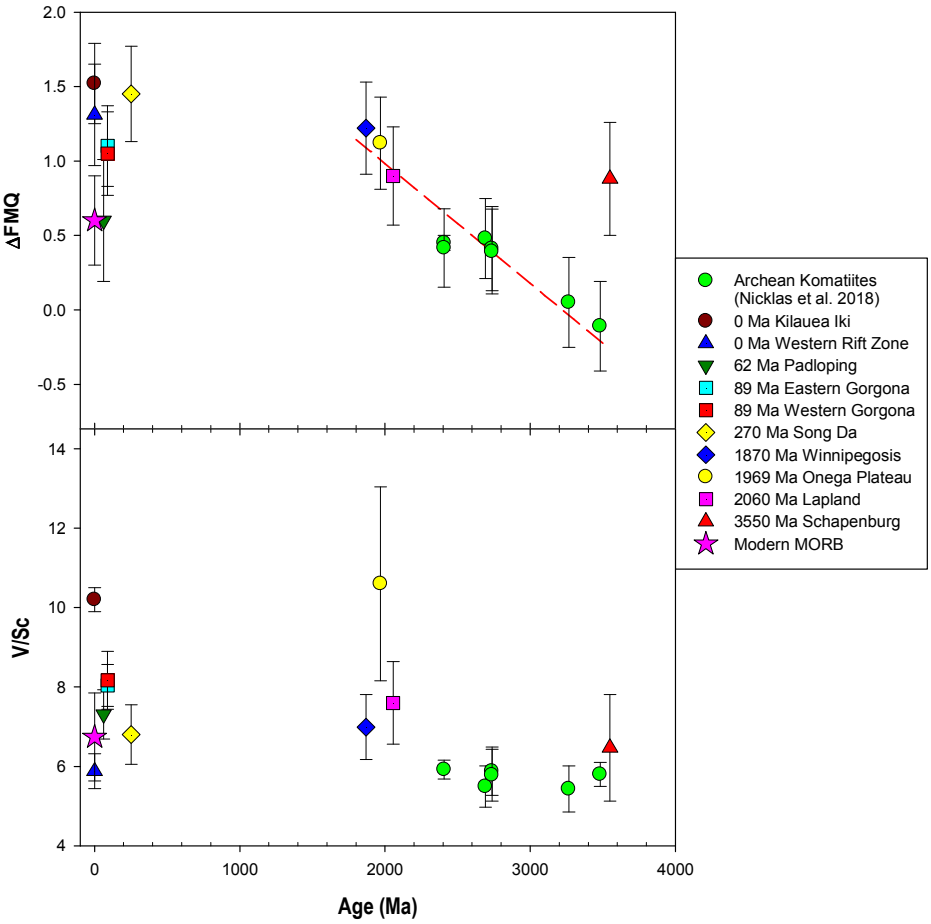

Figure 4.5.a. The calculated oxygen fugacity (fO_2) relative to the FMQ buffer for the studied komatiite and picrite systems plotted as a function of their ages. The uncertainties shown are determined by the propagated 2SD uncertainties on the calculated $D_V^{Ol\text{-}Liq}$ and the 95% confidence interval error of equation (1) in the text. The fO_2 estimates for modern MORB were calculated using the V partitioning of four olivine/glass pairs from Kelley and Cottrell (2012) and Mallmann and O'Neill (2013). The MORB value of +0.60±0.30 ΔFMQ log units is the average of the four estimates with the uncertainty reflecting the 2SD of those estimates propagated to account for the uncertainty in experimental calibrations in equation (1). The dotted red line is an ISOPLOT least-squares regression of all data from 3.48 to 1.87 Ga (MSWD = 2.4). See text for further details. **b**. The V/Sc ratios of the studied komatiite and picrite systems plotted as a function of their ages. Data for modern MORB are from Li and Lee (2004). See text for additional details.

Also plotted in **Fig. 4.5a.** is an estimate of the redox state for modern East Pacific Rise MORB obtained using V abundance data of the olivine-glass pairs from Kelley and Cottrell (2012) and Mallmann and O'Neill (2013) and equation (1) above at +0.60±0.15 ΔFMQ log units (2SD). It has been

shown that the redox data obtained using oxybarometers relying on the partitioning behavior of V are systematically offset by up to 1 log unit from the oxygen fugacity data obtained using the $Fe^{+3}/\Sigma Fe$ equilibria (e.g., Mallmann and O'Neill, 2013), so only MORB data determined using the same method as for the samples studied here are used for comparison. As most modern MORB are erupted at or close to sulfide saturation (Bottinga and Javoy, 1990; Le Voyer et al., 2014), and sulfur degassing can affect the redox state of a lava (Moussallam et al., 2014), the calculated MORB average likely represents a minimum fO_2 estimate. It is, thus, not surprising that the MORB average plots below most of the Phanerozoic systems studied. For more information on the calculations of the MORB average plotted in **Fig. 4.5a/** the reader is referred to Nicklas et al. (2018).

4.4.4.2. Variations in V/Sc in the emplaced komatiite and picrite lavas

Variations in V/Sc ratios in Archean basalts as a function of age have been used to study the evolution of the oxidation state of the Archean upper mantle (e.g., Li and Lee, 2004). Because V becomes more incompatible with an increase in fO_2 of the system, and Sc partitioning is independent of fO_2, the higher the fO_2 of the system during melting, the higher the V/Sc ratio should be in the melt. Li and Lee (2004) estimated the V/Sc in the global compilation of MORB lavas to be 6.7±1.1 (2SE), which is equivalent to −0.3±1.0 ΔFMQ log units for the modern upper mantle. They also estimated that Archean basalts have an average V/Sc = 6.3±1.2 (2SE) and concluded that the fO_2 of the modern upper mantle and that of the sources of Archean basalts were identical within the cited uncertainties.

We applied the V/Sc oxybarometer of Li and Lee (2004) to the komatiite and picrite systems from this study, by calculating the V/Sc ratios in the emplaced lavas of each system. The V/Sc ratios vary from 5.88±0.44 in the Icelandic picrites to 10.2±0.3 in Kilauea Iki lava lake. These V/Sc ratios, along with those determined for Archean komatiites in Nicklas et al. (2018), as well as the MORB range from

Li and Lee (2004), are plotted against age in **Fig. 4.5b**. No significant trend is observed, and all but the Kilauea Iki and Onega Plateau lavas plot within the range of modern MORB. The data obtained using the V/Sc oxybarometer, thus, provide no evidence for secular oxidation within our sampled systems. Similar oxybarometers utilizing the V/Ga and V/Y ratios (Mallmann and O'Neill, 2013; Laubier et al., 2014) also show no variation in the calculated fO_2 with time. The reasons for this and the implicit assumptions behind these oxybarometers are discussed below.

Firstly, it is important to note that, since komatiites and picrites are high melt-fraction lavas, they are expected to show less variation in V/Sc as a function of oxygen fugacity than basalts, with their V/Sc ratios being closer to those of their mantle source regions. Another complicating factor is the difference in melting histories of different komatiite and picrite systems, as the use of V/Sc as an oxybarometer relies on the assumption that the V/Sc in the source region of all the studied rocks was identical. However, previous melt depletion events at high oxygen fugacity would lower the V/Sc ratio of a mantle source region, leading to subsequent melts extracted from that source to give erroneously reduced values using this oxybarometer. Finally, V^{+3} and Sc^{+3} behave similarly during melting in the spinel stability field, but may have significantly different partition coefficients between solid and melt in the garnet stability field. Petrologic modeling has shown that melting in the garnet stability field will indeed impart a higher V/Sc ratio at constant fO_2 when compared to melting in the spinel stability field (Lee et al 2005; Aulbach and Stagno, 2016). Notably, the Kilauea Iki and Onega Plateau systems have much higher V/Sc ratios, at 10.2±0.3 and 10.0±1.7, respectively, than any of the other systems. It has been previously determined that both systems are primarily the result of melting in the garnet stability field (Puchtel et al., 1998a; Norman and Garcia, 1999), illustrating the possible effect of residual garnet on the V/Sc ratio of the melt. Due to these limitations, we did not consider any further the V/Sc systematics of the studied komatiite and picrite systems for the purpose of constraining their redox state.

4.5. DISCUSSION

4.5.1. The effects of alteration, mineral-melt re-equilibration, and crustal contamination on the redox state of the studied komatiite systems

4.5.1.1. Secondary alteration

The effect of secondary alteration on the determination of fO_2 of Archean komatiites has been previously addressed by Nicklas et al. (2016, 2018). Additionally, the effect of surface alteration on the chemistry of the Schapenburg komatiite flows has been previously addressed in Puchtel et al. (2016a). The Phanerozoic and Proterozoic samples studied here are mineralogically very well preserved, and metamorphic grade was uniformly sub-greenschist facies. Igneous textures are preserved in all of the studied Phanerozoic samples, and igneous minerals are very well preserved in the Song Da, Kilauea Iki, Gorgona, Iceland and Padloping lavas. The Schapenburg komatiite system and the Onega Plateau picrites are remarkably well preserved given their age, and the Lapland and Winnipegosis komatiite systems retain almost exclusively igneous minerals with little evidence for any secondary phases, indicating an excellent degree of preservation (**Fig. 4.1.)**.

Secondary alteration may result in re-distribution of petrogenetically important elements, including V, which, in turn, may have affected the estimates for V (and other trace metals) abundances in the emplaced lavas. This post-magmatic re-distribution on a whole-rock scale, however, can be easily recognized in the trace metal vs. MgO variation diagrams (**Figs. 4.2.-4.4.**). Element mobility will result in the data for the affected element plotting off the olivine control lines, which is not observed. Vanadium and Sc exhibit strong inverse correlations with MgO, with MSWD < 3.0 for all systems along with MgO intercepts close to the composition of liquidus olivine phenocrysts, and it is, thus, concluded that all komatiite and picrite systems probably retain primary, igneous distributions of these elements.

4.5.1.2 Late-stage re-equilibration of the liquidus olivine with host lava

The method we used to determine the redox state of the komatiite and picrite systems assumes that olivine was in chemical equilibrium with the emplaced lava. Although olivine phenocrysts found in chilled margins of komatiite lava flows most likely preserved their original V partitioning signature due to the almost instantaneous solidification after emplacement (Huppert et al., 1984; Huppert and Sparks, 1985; Arndt, 1986b), olivine from cumulate zones, which take much longer to crystallize, may have experienced re-equilibration with the residual liquid. In their study of the ~100-m-deep Victoria's lava lake, Nicklas et al. (2016) demonstrated that V contents of olivine from the cumulate zone and the upper chilled margin of the komatiitic lava lake were indistinguishable, which was taken as evidence that V re-equilibration between olivine and the residual liquid played a negligible role during the evolution of the lava lake. All samples, except for those from the Lapland, Onega Plateau, Kilauea Iki and Iceland systems, are from sub-aqueously erupted flows significantly thinner than the 100-m-deep lava lake, and thus re-equilibration was likely also negligible. The Lapland samples are sub-volcanic in nature, but still likely cooled relatively quickly, as the width of the Kevitsa dike from which they were collected was ~40 m. Similarly, the Onega Plateau samples analyzed come from the sub-volcanic Konchozero sill, which shows evidence for rapid solidification and cooling (Puchtel et al., 1998b). The samples from the Kilauea Iki and Iceland systems are sub-aerially erupted lavas that cooled quickly, albeit likely not as quickly as sub-aqueously erupted lavas, and thus also had little time for re-equilibration. In order to minimize the effect of re-equilibration, Kilauea Iki samples were taken from the upper chilled margin of the lava lake, which must have solidified rapidly. It is therefore likely that the olivine grains analyzed in this study retain their liquidus V and Sc concentrations in all the studied systems.

4.5.1.3. Crustal contamination

Crustal contamination can have an effect on the fO_2 of mantle-derived lavas due to assimilation of oxidized species in continental crust that was generated in an oxidized arc environment. The Gorgona,

Kilauea Iki and Iceland lavas are all known to have erupted in an oceanic environment and are thus not contaminated by continental crust. Of the komatiitic and picritic systems studied here that erupted onto continental crust, previous studies have found minimal crustal contamination, ranging from <1% in the Padloping Island picrites (Day, 2016), to 1–2% in the Song Da system (Hanski et al., 2004) to <3% in the Winnipegosis system (Waterton et al., 2017). The upper Onega Plateau picrites show no evidence for contamination with continental crust (Puchtel et al., 1998b). The degree of crustal contamination of the Lapland samples is also likely very low, as shown by their εNd values ranging from +3 to +4 and their strong depletion in LREE (Huhma et al., 2018). Based on their trace element and Nd isotopic systematics, it is also unlikely that the Schapenburg komatiites experienced any crustal contamination (Puchtel et al., 2009). In addition, the study of Grocke et al. (2016) observed no effect on fO_2 in continental arc lavas that had been variably contaminated by up to >30% continental crust, and, thus, it is unlikely that the low degree of contamination found in all of the studied systems had a measurable effect on the calculated fO_2 values.

4.5.2. The significance of the calculated fO_2 of the studied komatiite systems

4.5.2.1. The effect of temperature on V partitioning in ultramafic systems

The experimental studies of Mallmann and O'Neill (2013) and Laubier et al. (2014) showed a dependence of $D_V^{ol/melt}$ on the temperature of olivine crystallization. As the younger suites analyzed have, on average, lower liquidus temperatures, it is important to evaluate the effect of temperature on the partitioning of V in the komatiitic and picritic lavas studied. A decrease in temperature of ca. 100 °C would result in a change of ~0.1 log unit in the calculated oxygen fugacity using the Mallmann and O'Neill (2013) oxybarometer, which takes temperature into account. Although our suites show a large range in the emplaced lava MgO contents (7.95–28.6 wt.% MgO), this spread likely corresponds to a maximum of 400 °C difference in the liquidus temperatures. A 0.4 log unit oxidation is significantly

smaller than the observed range of ~1.6 log units. Furthermore, the MgO content of the lavas, a proxy for liquidus temperature, does not show a correlation with the calculated oxygen fugacity, as the lowest MgO samples from the Onega Plateau, at 7.95 wt.% MgO, have an fO_2 within uncertainty of those of the Lapland and Winnipegosis komatiites, which contained 27.4 and 21.1 wt.% MgO in their emplaced lavas, respectively, encompassing almost the entire spectrum of the MgO contents of the sample set, with minimal changes in fO_2.

4.5.2.2 The effect of mantle secular cooling on fO_2

It is generally accepted that the mantle has experienced secular cooling (Herzberg, 2010; Ganne and Feng, 2017; Aulbach and Arndt, 2019); as such, the older komatiite systems likely formed from a hotter mantle than their younger counterparts. In order to evaluate the significance of the calculated fO_2 of the studied komatiite systems, it is important to constrain the effects of secular cooling of the mantle (e.g., Nisbet et al., 1993; Herzberg, 2010) on the calculated oxygen fugacities. Decrease in mantle temperatures will result in increased Fe^{+3} activity in mantle spinel, and, thus, higher mantle oxygen fugacity in the spinel peridotite stability field due to the temperature dependence of mantle mineral redox equilibria (Ballhaus et al., 1991). The extent to which the mantle cooled over the past ~3.5 Ma is not well established, but was likely less than 150 °C (Ganne and Feng, 2017, Aulbach and Arndt, 2019). Using the experimental oxybarometer of Ballhaus et al. (1991), we estimated the change in oxygen fugacity that would be caused by decrease in the mantle potential temperature by 150 °C, from 1800°C to 1650 °C, assuming a constant pressure of 2.0 GPa, and constant X^{spinel}_{Fe+3} of 0.05, X^{spinel}_{Fe+2} of 0.55, X^{spinel}_{Al} of 0.4, and $X^{olivine}_{Fe}$ of 0.1. Our calculations indicate that this decrease in temperature would be equal to an increase of 0.02 ΔFMQ log units in oxygen fugacity, which is smaller than the uncertainty on the fO_2 estimates for all the magmatic systems in this study. We conclude, therefore, that secular change in the mantle potential temperature had no measurable effect on the calculated oxygen fugacities for the

studied systems, and that the trend observed in **Fig. 4.5a.** is not the result of mantle cooling, nor was the trend significantly dispersed by it.

4.5.2.3 The effects of depth of mantle melting and upwelling on fO_2

Another issue to address is the difference in the depth of melt segregation for the studied systems and its effect on the calculated fO_2. It has been argued that the oxygen fugacity of the mantle decreases with increasing depth due to pressure dependence of the garnet-fayalite-ferrosilite-O_2 equilibrium (Woodland and Koch, 2003). However, this calibration is only relevant until the depth of metal saturation, beyond which fO_2 shows comparatively little pressure dependence (Frost et al., 2008). Although melting in the studied plume lavas took place at depths that are not well constrained, there is no evidence that melts segregated at greater depths in older samples than in their younger counterparts. The Kilauea Iki lavas yielded fO_2 that is among the highest of the measured values, but were derived from melting well into the garnet stability field (Norman and Garcia, 1999), opposite to the predicted trend of Woodland and Koch (2003). In addition, the relationship between the depth of melting initiation and fO_2 is not straightforward due to the fact that the melts likely remained in equilibrium with the mantle residue well past the depth of melt initiation. The Al_2O_3/TiO_2 ratio has been shown to vary with depth of segregation of a komatiitic melt from its mantle residue (Nesbitt and Sun, 1976; Sossi et al., 2016), but there is no correlation between fO_2 and average Al_2O_3/TiO_2 ratio evident in our data.

The FMQ redox buffer follows the redox evolution of a decompressing melt within ~0.17 log units/GPa (Kress and Carmichael, 1991), so that oxygen fugacity values expressed in ΔFMQ terms largely retain their validity through decompression melting (Kelley and Cottrell, 2012). This difference is small enough that it is within uncertainty of most of the fO_2 determinations. This is one of the reasons that fO_2 of volcanic rocks relative to the FMQ buffer has been previously used as a reference point for

determining upper mantle oxygen fugacity (e.g., Kelley and Cottrell, 2012). Finally, the obtained redox data for the studied systems were compared to the fO_2 of modern-day MORB and plume lavas, as opposed to modern peridotites, in an attempt to minimize the differential effects of decompression on the calculated oxygen fugacities. We, therefore, conclude that differences in depth of melting are likely not the cause for the secular trend in oxygen fugacity observed in **Fig. 4.5a.**

4.5.2.4 The effects of magma degassing and differentiation on fO_2

Two additional factors that have been shown to have an effect on the oxygen fugacity of an evolving magma are fractional crystallization and volatile degassing. Olivine fractionation removes Fe^{+2} and, thus, changes the oxygen fugacity of mafic magmas evolving as closed systems (Cottrell and Kelley, 2011; Sossi et al., 2012). However, this effect is relatively minor for the magmas studied here, which experienced little differentiation prior to emplacement, as their high MgO contents show that they are close to composition of primary mantle melts. Moreover, the Winnipegosis and Song Da komatiite suites and the Onega Plateau picrites all have fO_2 values within error of each other but range in their emplaced lava MgO content from 7.95±0.28 to 21.1±2.5 wt.%. Theory predicts that lower-MgO lavas should exhibit higher fO_2, but the Padloping Island lavas are the most reduced lavas measured in this study, despite the fact that they are less MgO-rich than most of the others (**Tables 4.5., 4.6.**). We, thus, conclude that olivine fractionation had a negligible effect on the measured fO_2 values of the lavas.

Degassing of sulfur has been shown to have a strong control on the fO_2 of an evolving picritic (Moussallam et al., 2016) or phonolitic (Moussallam et al., 2014) magma. Sulfur is largely present as S^{-2} in mantle-derived magmas, which can be degassed as SO_2 according to the following equation from Metrich et al. (2009):

$$S^{-2} + 4Fe_2O_3 \rightarrow S^{+6}O_2 + 8FeO + 2O^{-2} \qquad (2)$$

Equation (2) shows that for each mole of sulfur degassed as SO_2, 8 moles of Fe^{+3} are reduced to Fe^{+2}. It has been demonstrated for Kilauea Iki lava lake that sulfur degassing had a resolvable reducing effect on the evolving magma, and the un-degassed picritic magma was estimated to have had an oxygen fugacity of ~ΔNNO = 0 (Moussallam et al., 2016). Our value of ΔNNO = +0.80±0.27 for Kilauea Iki is higher than this estimate, and may reflect rapid quenching of the uppermost section of the lava lake prior to extensive degassing, or alternatively, may reflect inter-calibration issues between the V partitioning and $Fe^{+3}/\Sigma Fe$ ratio oxybarometers.

The highly siderophile element abundance data indicate that the Schapenburg lavas were sulfide undersaturated (Puchtel et al., 2016a), and, thus, likely degassed little sulfur. Chalcophile elements, such as Cu, Pd and Pt, behaved incompatibly during differentiation of Gorgona komatiites (Brügmann et al., 1987), and this suite was, therefore, also sulfur-undersaturated. Although sulfide saturation depletes an evolving melt in sulfur, high-degree melts that never experienced sulfide saturation, like those studied here, did not experience sulfide saturation because they contained very low concentrations of sulfur. Sulfide undersaturation therefore requires the lack of significant sulfur degassing in the studied ultramafic rocks. Sulfur degassing in the Lapland and Onega Plateau systems was also likely relatively minor due to their subvolcanic nature. It is also worth noting that the Gorgona, Schapenburg and Winnipegosis komatiites erupted sub-aqueously, which likely minimized sulfur degassing. It is unknown what effect sulfur degassing had on the measured fO_2 of the Song Da komatiites and the Iceland and Padloping Island picrites. Unless initial conditions were extremely oxidizing, such as those found in arc basalts, degassing of sulfur has only been shown to cause reduction and not oxidation (Moussallam et al., 2014, 2016; Brounce et al., 2017), and, thus, the fO_2 values for these systems likely represent the minimum values. There is no *a priori* reason why the older systems would have degassed more sulfur than the younger systems, and, therefore, the observed trend of secular oxidation is likely

not caused by variable amounts of sulfur degassing. We, thus, conclude that the secular oxidation trend observed in our data likely represents oxidation of the mantle source regions of these lavas with time.

4.5.3. Mechanisms for oxidation of the mantle

Our data indicate an increase of 1.33±0.43 ΔFMQ log units over 1.6 Ga of Earth history, which is within uncertainties of the 0.93±0.55 ΔFMQ log unit difference between Archean and modern samples estimated by Aulbach and Stagno (2016) using the V/Sc oxybarometer. The conclusion that the Earth's mantle has oxidized since the Archean is also supported by the study of Aulbach et al. (2017a), which used $Fe^{+3}/\Sigma Fe$ ratios in eclogitic garnets to determine that subducted Archean oceanic crust was likely more reduced than the present-day oceanic crust. Additionally, Foley (2011) suggested that the lack of carbonatites in the geologic record prior to 2.7 Ga was the result of the mantle at that time being more reduced than the present-day mantle. Compared to our data, both of the Aulbach and Stagno (2016) dataset shows significantly lower absolute oxygen fugacity values in both Archean picrites and modern MORB. This is likely due to issues with inter-calibration of different oxybarometers, as discussed by Mallmann and O'Neill (2013), or due to differences in mantle melting processes between ridge and plume settings. Despite this, the agreement between the magnitude of our trend and the Aulbach and Stagno (2016) trend is remarkable, and offers further support to the notion that the mantle has experienced significant secular oxidation. In the following sections, we discuss the mechanisms that might have been responsible for the observed change in the redox state of the mantle.

An increase in the oxygen fugacity of the mantle of ca. 1.3 ΔFMQ log units is a significant change for a reservoir as large as the mantle, which comprises ~84% of the Earth's volume and ~68% of the Earth's mass. Changing the mantle's redox state by 1.3 ΔFMQ log units would require the addition of a large and likely geochemically detectable amount of oxidized material. Three possible scenarios are

considered as potential mechanisms for oxidizing the mantle: (1) recycling of oceanic crust, (2) venting of oxygen from the core, and (3) homogenization of early formed mantle heterogeneities. None of these mechanisms are mutually exclusive, and all may have contributed to the observed trend.

4.5.3.1. Recycling of oceanic crust

The most obvious explanation for an increase in the oxygen fugacity of the mantle comes from evaluating the effects of modern plate tectonic processes. Oceanic crust returning into the mantle at subduction zones is more oxidized than the crust emerging at spreading centers as a result of interaction with O_2 and H_2O on the Earth's surface. Serpentinization reactions reduce seawater to generate H_2 gas, which may subsequently be lost to space. The low molecular mass of the H_2 gas makes it one of the few volatile species to readily escape from the Earth's atmosphere, acting as a net oxidant to the entire Earth system (Catling et al., 2001). However, H_2 gas produced in an oxygenated atmosphere rapidly reacts with O_2 and, therefore, remains in the Earth system (Zahnle et al., 2013). As a consequence of serpentinization, Fe^{+2} in altered oceanic crust (AOC) is oxidized to Fe^{+3} to form magnetite, enriching the AOC package in Fe^{+3}. For example, serpentinites have $Fe^{3+}/\Sigma Fe$ of ~0.3 (Padron-Navarta et al., 2011), greatly in excess of the mantle value of 0.02–0.05 (Cottrell and Kelley, 2011). However, the amount of oxidized material that makes it into the deep mantle remains largely unknown. Some of that oxidized material is likely lost to generate the oxidized mantle wedge and the comparatively oxidized arc lavas (Parkinson and Arculus, 1999; Brounce et al., 2014).

Mass balance calculations indicate that subduction is a net oxidant for the mantle even today, after accounting for the oxidants lost in arc lavas and gases and those brought back up by MORB and OIB volcanism (Evans, 2012). The mass balance of various fluxes indicates that Fe^{3+} is the main oxidant making it through subduction zones to the deep mantle, while SO_4^{-2} and CO_3^{-2} are largely returned to the

surface in arc volcanoes (Evans, 2012). The net oxidation flux for the modern Earth's mantle is estimated at $46 \pm 12 \times 10^{12}$ mol/yr (Evans, 2012), similar to the earlier estimates (7.1×10^{12} moles of oxidant/year) which only took into account Fe^{3+} flux and also relied on an older understanding of serpentinization reactions (Lecuyer and Ricard, 1999).

Using the mantle oxidation equations of Evans (2012), and their estimated present-day subduction flux of oxidants, we tested the hypothesis of whether crustal recycling is a viable mechanism for mantle oxidation. Starting with the oxidation state of the Komati system of -0.11 ± 0.30 ΔFMQ log units at 3.48 Ga, we allow the mantle to mix in crust at present day rates up to 1.87 Ga, when the oxidation trend flattened out. Our calculations show that the mantle would have only been oxidized from -0.11 to +0.38 ΔFMQ log units over the ~1.6 Ga period, i.e., an increase in the redox state of the mantle of ~0.49 ΔFMQ log units, which falls short of the oxygen fugacity of the Winnipegosis komatiites by ~0.71 ΔFMQ log units.

For the sake of the modeling, we varied the subduction redox flux and the fraction of the mantle participating in the mixing. Increasing the subduction redox flux by a factor of ~4 results in a mantle oxidation of +1.22 ΔFMQ log units by 1.87 Ga, which is consistent with the oxidation state of the Winnipegosis komatiites. Reducing the fraction of the mantle participating in the mixing calculation to ~25% of the mantle's total mass achieves the same effect. One of the major weaknesses of this model is that there is no *a priori* reason why oxidation of the mantle would cease in the Paleoproterozoic, as oxidized slab material likely continued to be recycled into the mantle well past 1.87 Ga. Another weakness of this model is that with little agreement on the existence of modern-style plate tectonics in the Archean, there are no strong constraints on the crustal recycling rate during that period. The question of whether modern-style mobile-lid plate tectonics operated during the Archean has been the subject of much debate (e.g., Sizova et al., 2010; Moore and Webb, 2013; Gerya, 2014), but some mode of crustal

recycling must have existed during the Archean, and any such tectonic process could theoretically bring oxidized material back into the mantle. The altered oceanic crust in the early Earth was also likely less oxidized than the present day crust until ~800 Ma (Stolper and Kelley, 2018). The results of our modeling represent an upper limit on the amount of oxidation resulting from this mechanism, given the few constraints on the oxidation state of Archean altered oceanic crust and the possibly lower rates of crustal recycling in the Archean. It appears unlikely that the subduction redox flux at any time in Earth history was ~4 times greater than that of the present day and equally unlikely that ~75% of the mantle did not participate in convective mixing.

Based on all the arguments presented above, we conclude that the crustal recycling model is unlikely to account for the change in the redox state of the mantle of ~1.3 ΔFMQ log units required by the data. However, further work to quantify Precambrian crustal recycling rates and the oxidation state of deeply subducted slabs may affect this conclusion.

4.5.3.2. Venting of oxygen from the core

The second possible mechanism of progressive oxidation of the mantle involves venting of oxygen from the outer core into the lower mantle. The Earth's core contains substantial amounts of light elements, such as Si, S, and O (e.g., Birch, 1964; Badro et al., 2015). Initially, Earth's core is thought to have been entirely molten and, as the Earth cooled, the inner core began to crystallize and grew over time. It has been shown experimentally (Badro et al., 2007), through modeling (Badro et al., 2015), and via ab initio calculations (Alfe et al., 2002) that the solid metal of the inner core would preferentially exclude O, but would incorporate significant amounts of Si and S. Crystallization of the inner core, thus, enriches the outer core in dissolved O and, if the outer core were to become supersaturated with respect to O, some of this oxygen could have escaped into the lower mantle. This model removes the problems associated with the large amounts of recycled material required to oxidize the mantle, because the mass

of the outer core is similar in magnitude to the mass of the mantle. Using the present-day size of the inner core and the O concentration estimates of Alfe et al. (2002), the amount of oxygen added to the outer core from inner core crystallization is calculated to be ~10^{24} moles. This is ~0.25 moles oxygen/kg of the mantle mass, far more than is needed to oxidize the relatively reduced mantle by ~1.3 log units. However, this upper limit of oxygen released into the mantle does not take into account gradual inner core growth, and assumes that all of the oxygen released as the result of inner core crystallization is transferred to the mantle. Neither of these are safe assumptions. The maximum amount of oxygen that can be dissolved in the outer core is not experimentally constrained and likely varies with outer core temperature. It is also unknown whether a supersaturated outer core would lose molecular O_2 (a mantle oxidant) or FeO (a mantle reductant). Existing constraints indicate that FeO is the likely phase that would exsolve from an outer core supersaturated in oxygen (Humayun et al., 2004), making this mechanism invalid. However, additional high-pressure experimental data are necessary. In addition, the existence of chemical exchange between the core and mantle is still debated, based mostly on the available isotopic data for plume-derived lavas (Brandon et al., 1999; Brandon et al., 2003; Baker and Jensen, 2004; Brandon and Walker, 2005; Puchtel et al., 2005; Luguet et al., 2008; Ireland et al., 2011).

Perhaps the most central issue with this model is the fact that the timing of the onset of inner core crystallization is poorly constrained (e.g., Buffett, 2003). The overall oxidation trend revealed by the data from this study begins at 3.5 Ga and continues to 1.87 Ga, necessitating early inner core formation for outer core O saturation to be the driving mechanism behind the observed mantle oxidation trend. Models of core-mantle interaction based on geochemical evidence of leakage of Os from the outer core into the lower mantle require an early onset of inner core crystallization, ranging from 3.0 to 4.2 Ga (Brandon et al., 2003; Puchtel et al., 2005). In contrast, thermal history models favor a younger age for the inner core, e.g., ca. 1.0 Ga $^{+1.0}_{-1.5}$ (Labrosse et al., 2001). The presence of significant concentrations

of radioactive elements in the core (e.g., K), or the existence of a radioactive element-enriched "slab graveyard" at the core-mantle boundary could push the onset of inner core crystallization back to 3.0 Ga. Overall, there is little agreement among researchers on the timing of the onset of inner core crystallization; as such, the mechanism presented here remains largely speculative. Recent geochemical evidence for relatively sluggish mixing of the mantle (e.g., Touboul et al., 2012; Rizo et al., 2016; Puchtel et al., 2016a; Mundl et al., 2017) also contradicts this model. Oxygen leaving the outer core would escape into the lower mantle upward in all directions, and the upper and lower mantle need to be efficiently mixed in order to facilitate mantle oxidation.

As a further issue to account for in models of core-mantle interaction, any large-scale chemical exchange between the core and mantle would likely result in large enrichments in the highly siderophile elements (HSE), coupled enrichments in ^{186,187}Os (Brandon et al., 1999; Brandon et al., 2003; Ireland et al., 2011), and strongly negative μ^{182}W isotopic anomalies (Touboul et al., 2012) in plume-derived lavas that originated at the core-mantle boundary. However, large HSE enrichments have not been observed in the mantle sources of any of the magmatic systems studied here.

Tungsten isotopic anomalies have only been detected in the Kilauea Iki, Padloping Island and Schapenburg systems (Rizo et al., 2016; Mundl et al., 2017; Puchtel et al., 2016a). Mundl et al. (2017) concluded, however, that the negative μ^{182}W signal in the Kilauea Iki lave lake is unlikely to originate from the outer core. The source region of the Schapenburg komatiite system with a negative μ^{182}W anomaly is strongly depleted in the HSE relative to BSE and, thus, likely experienced no core-mantle exchange (Puchtel et al., 2016a), while the Padloping Island's positive μ^{182}W signal is opposite to what would be expected from addition of outer core material. The Schapenburg and Padloping Island systems were also excluded from the ISOPLOT regression calculations illustrated in **Fig. 4.5a.** There is, thus, no strong evidence, isotopic or otherwise, for addition of core material to the mantle source regions of any

of the studied systems, although it is possible that a light element, such as O, could vent to the mantle without entraining any other elements. Overall, better constraints on the maximum O content of the outer core, the timing of the onset of the inner core crystallization, and the mechanisms of core-mantle interaction are necessary to further determine the viability of this model.

4.5.3.3. Mixing of primordial mantle redox heterogeneities

According to the commonly accepted scenario of early Earth evolution, the silicate Earth melted and differentiated early in its history due to the energetic impacts associated with planetary accretion, and the release of heat associated with core formation (Matsui and Abe, 1986; Tonks and Melosh, 1993). This early differentiation facilitated the fractionation of short-lived isotope systems, isotopic anomalies of which are found in Precambrian and even in modern rocks (Touboul et al., 2012; Willbold et al., 2015; Rizo et al., 2016; Puchtel et al., 2016a, Mundl et al., 2017).

In order to segregate a core made of Fe-Ni alloy, the primordial mantle must have been reducing enough to be in equilibrium with metallic Fe, i.e., its redox state must have been close to the iron-wüstite (IW) buffer. The five orders of magnitude higher oxidation state of the present-day mantle than the IW buffer has been proposed to be the result of Fe (II) disproportionation reactions in the deep mantle and loss of Fe metal to the core in down-going metallic diapirs (Wood et al., 2006; Frost and McCammon, 2008). In this model, Fe^{2+} disproportionates to Fe^{3+} and Fe metal at high pressures in the lower mantle, which enables Fe^{3+} to enter the predominant bridgmanite crystal structure at these depths. Some of this disproportionated Fe metal was subsequently lost to the core, leaving a more oxidized lower mantle that was no longer in redox equilibrium with the core. The early terrestrial mantle would thus consist of a relatively reduced upper mantle sitting atop a relatively oxidized lower mantle. This model is supported

by the observation that the lunar mantle is highly reduced due to the fact that the pressures at the bottom of the lunar magma ocean were not high enough to stabilize bridgmanite (Frost et al., 2008).

The komatiite and picrite systems studied here may represent relatively deep mantle melts, but constraining the depth at which the respective mantle plumes that gave rise to these systems originated is difficult. Assuming all the systems were representative of the upper mantle in terms of their redox state at the time of their formation, then the upper mantle has presumably mixed with a more oxidized lower mantle to produce oxidation with time. It is unclear whether this process was continuous or episodic. As there is no mantle oxidation observed after 1.87 Ga, it is possible that the main homogenization event had already occurred by 1.87 Ga, possibly due to the initiation of mobile-lid plate tectonics at the Archean-Proterozoic boundary, which efficiently mixed away much, but not all, of the early-formed mantle isotopic heterogeneities (Debaille et al., 2013; Mundl et al., 2017). Since the heterogeneities produced by the ^{182}Hf-^{182}W isotope system persist to the present day, it is, thus, not unreasonable to suggest that early redox heterogeneities may have persisted well into the Paleoproterozoic. It is likely that the mantle has become more homogenous with time due to convective stirring, which makes progressive mixing between the upper and lower mantle a viable mechanism for explaining upper mantle oxidation.

A supporting argument for this mechanism is provided by the high fO_2 of the Schapenburg komatiite system relative to komatiite systems of similar age within the same craton, such as the 3.48 Komati and 3.26 Weltevreden systems (Nicklas et al., 2018). Isotopic constraints from both short- and long-lived isotope systems indicate that the mantle source region of the Schapenburg komatiites fractionated bridgmanite within the first ~30 Ma of solar system formation (Puchtel et al., 2016a). No such short-lived anomalies have been found in the source region of the other Kaapvaal Craton komatiites studied (Touboul et al., 2012; Puchtel et al., 2013; 2014). Thus, the Schapenburg source region was formed in

the lower mantle close to the time of core formation and was preserved until 3.55 Ga. The high oxidation state of the Schapenburg system likely reflects the loss of disproportionated Fe metal in its source region during an early magma ocean stage. Mixing between a theoretical "Schapenburg-type" mantle with high fO_2 and a "Komati-type" mantle with the low fO_2 could have resulted in the observed trend. Although the Schapenburg system is not as oxidized as some of the Phanerozoic systems, the "Schapenburg-type" endmember may have extended to higher fO_2 than observed in the Schapenburg komatiites. This mantle oxidation scenario has been previously advocated by Nicklas and Puchtel (2016), Aulbach and Stagno (2016) and Andrault et al. (2018). However, more investigation into the oxidation state of ultramafic rocks showing short-lived isotope anomalies, and into the thermodynamics of mixing mantle regions of different oxidation states, are needed to further constrain this model.

4.5.4. The Schapenburg and Padloping Island Systems and Early Earth Redox

As mentioned in the previous sections, both the Schapenburg komatiite and Padloping Island picrite systems show resolved anomalies in the short-lived ^{182}Hf -^{182}W isotope system. In addition to a negative ^{182}W anomaly, the Schapenburg komatiite system has a negative ^{142}Nd anomaly, as well as decoupled long-lived ^{176}Lu–^{176}Hf and ^{147}Sm–^{143}Nd systems, indicating fractionation of the lower mantle phases bridgmanite and Ca-perovskite very early in its mantle source region's history (Puchtel et al., 2016a). The Padloping Island picrites have the largest known terrestrial ^{182}W anomaly (Rizo et al., 2016), but do not show any resolvable anomaly in ^{142}Nd (De Leeuw et al., 2017). The lack of a ^{142}Nd anomaly rules out crystal-liquid silicate fractionation as a mechanism for generating the large ^{182}W anomalies in the Padloping Island picrites. Early metal-silicate fractionation could have produced large ^{182}W anomalies with no effect on the lithophile Sm-Nd isotope system, indicating that this is the likely mechanism for generating the source region of the Padloping Island lavas (Rizo et al., 2016).

Although both the Padloping Island and Schapenburg komatiite systems have short-lived isotope anomalies and are excluded from the regression of the fO_2 data in **Fig. 4.5a.**, the Schapenburg komatiites are characterized by a higher oxidation state relative to systems of the same age, while the Padloping Island lavas are within uncertainties of most other plume-derived Phanerozoic lavas, and also overlap with the range of modern MORB in terms of their fO_2. The Schapenburg source likely lost disproportionated Fe to the core early in its history, leading to the high oxidation state of Schapenburg lavas. There is no evidence for the Padloping source region being in the bridgmanite stability field during core-forming events, and thus it is not expected to show an elevated fO_2 value. Indeed, the equilibration of the Padloping Island source region with metal (Rizo et al., 2016) likely greatly lowered its fO_2, but this signature was possibly later diluted by ambient mantle to create a mantle region with large ^{182}W anomalies but only slightly lower fO_2 than the source regions of other plume lavas of the same age. These two magmatic systems illustrate that relationships between oxidation state and short-lived isotope anomalies in plume-derived lavas may not be straightforward.

4.5.5. Relationship between Mantle Oxidation State and Atmospheric O_2 content

The Great Oxidation Event (GOE) marked one of the most dramatic changes in the Earth's surficial environment. Molecular oxygen rose from trace levels in the Archean atmosphere ($< 10^{-6}$ atm) to become a small but significant constituent of the atmosphere in the Proterozoic, eventually rising to ~ 0.2 atm in the Phanerozoic. The exact timing and tempo of the GOE are complex, but it is denoted most clearly in the geochemistry of sulfur isotopes (Farquhar et al., 2000). Specifically, the disappearance of mass independent sulfur isotope fractionation ($\Delta^{33}S$) in sedimentary rocks, beginning between 2.461 and 2.308 Ga (Gumsley et al., 2017), is best-explained by the accumulation of sufficient atmospheric O_2 to

oxidize and homogenize isotopically fractionated atmospheric S reservoirs produced by UV-driven photochemistry (Ono, 2017).

The exact causes of the GOE remain unclear. Oxidative photosynthesis is the source of O_2 to the atmosphere, but also of organic carbon. In biological respiration, O_2 reacts with organic carbon, removing O_2 from the atmosphere. In fact, on an annual basis, O_2-producing photosynthesis and O_2-consuming respiration are in almost perfect equilibrium (Catling, 2014). Therefore, accumulation of O_2 in the atmosphere requires: (a) photosynthetic production of O_2; (b) burial of photosynthetically produced organic carbon for geologically significant periods of time, leaving behind unrespired O_2 in the surface environment; (c) that this net biogeochemical process produces O_2 at rates sufficient to overwhelm geological sinks of O_2, such as the oxidation of Fe^{2+} and other reductants in crustal rocks and hydrothermal systems, and the oxidation of reduced gases derived from the mantle.

It is likely that a decrease in the strength of geological sinks was a critical contributor to the GOE. Two lines of evidence are particularly important. First, although it is tempting to conclude that the GOE was caused by the proximal emergence of oxygenic photosynthesis (Fischer et al., 2016), multiple lines of geochemical and genomic evidence are consistent with biological O_2 production originating well before 2.4 Ga (e.g., Lyons et al., 2014), and arguably as early as ~ 3.0 Ga (Planavsky et al., 2014). Hence, it is highly unlikely that the GOE is a direct and simple consequence of biological evolution.

Second, the carbon isotope record in sedimentary rocks can be used to place constraints on the extent of burial of organic carbon through time (Schidlowski et al., 1988), and, hence, on whether there could have been a change in net biogeochemical production of O_2. A recent statistical re-examination of this record revealed that the fraction of carbon leaving the surface environment as organic carbon ("f_{org}") did, indeed, increase steadily through the Precambrian (Krissansen-Totton et al., 2015). However, the

extent of this increase does not appear to be sufficient to account for the O_2 accumulation represented by the GOE (Krissansen-Totton et al., 2015).

Attention, therefore, turns to the extent of O_2 consumed by geological sinks. Reactions with volcanic gases, such as CO, H_2S and H_2, are major sinks for atmospheric O_2. The reducing capacity of volcanic gases is controlled by their fO_2, which is, in turn, largely buffered by the fO_2 of the degassing lava during cooling (Gerlach, 1993; Kasting et al., 1993), making igneous and, therefore, mantle fO_2 an important factor in atmospheric evolution.

Although the relationship between mantle fO_2 and volcanic gas fO_2 is complicated by many factors, such as degassing pressures (e.g., Gaillard et al., 2011), it has been shown that an increase of ~0.50 log units in the oxidation state of the mantle sources of volcanoes between the Archean and Proterozoic could have reduced the sufficiently large volcanic gas O_2 sink to explain the GOE (Holland, 2002). This hypothesized shift is well within the range indicated by our data. Therefore, the data presented here suggest that the oxidation state of the atmosphere is most likely coupled to that of the deep Earth, with important implications for the GOE.

The idea that the GOE was triggered by homogenization of the mantle with an oxidized lower mantle component has been previously advocated (Nicklas and Puchtel, 2016; Aulbach and Stagno, 2016; Andrault et al., 2018), and this scenario is consistent with our data. We do not necessarily argue that the progressive mantle oxidation over time was the sole trigger of the GOE, as other important factors that affected geological O_2 sinks may have played a role, including the growth of felsic continents (Lee et al., 2016), the rise of subaerial volcanism (Kump and Barley, 2007), or large flood basalt events (Ciborwoski and Kerr, 2016).

4.6. CONCLUSIONS

Oxygen fugacity has been studied in nine komatiite and picrite systems ranging in age from 3.55 Ga to the present day using V partitioning between liquidus olivine and host lavas. These systems were considered together with the six komatiite systems previously studied by Nicklas et al. (2016; 2018). The systems dated from 3.48 Ga to 1.87 Ga define a secular trend of increasing oxygen fugacity of the mantle from −0.11±0.30 to +1.22± 0.31 ΔFMQ log units, a change of 1.33±0.43 ΔFMQ log units over 1.61 Ga of Earth's history. Several mechanisms for oxidation of the mantle are considered, including recycling oceanic crust, venting O from the outer core, and mixing in of primordial mantle redox heterogeneities.

Our modeling indicates that subducted redox fluxes ~4 times that of the present-day Earth are required to achieve the change in oxidation state observed in our data. Alternatively, having only <25% of the mantle participating in mixing with subducted slabs achieves the same effect. Both of these scenarios seem unlikely given the anoxic oceanic conditions in the Archean and the likely lack of modern-style plate tectonics during the same period.

Inner core crystallization is theoretically capable of delivering orders of magnitude more oxygen than that required to oxidize the mantle to the degree established in this study, provided that the outer core became supersaturated with respect to O and vented O into the lower mantle without causing collateral entrainment of any other geochemically detectable outer core material. The viability of this mechanism is contingent upon the early onset of inner core crystallization and the low solubility of O in the outer core, both of which are presently poorly constrained.

The iron disproportionation model of primordial mantle oxidation (Frost et al., 2008) requires that the lower mantle (bridgmanite stability field) became more oxidized than the upper mantle immediately following core formation. The observation that the source region of 3.55 Ga Schapenburg komatiites was in the bridgmanite stability field early in Earth history and was isolated from the convecting mantle

until the time of komatiite formation, and the fact that the system shows relatively high fO_2 indicate that lower mantle-derived primordial redox heterogeneities persisted well into the Archean. Mixing in of "Schapenburg-type" mantle with the accessible convecting mantle is a possible mantle oxidation mechanism. Additional data on the oxidation state of the early lower mantle and mantle mixing rates during the Archean are needed to better constrain this model, but we consider it the most plausible of the three mechanisms discussed here.

Due to difficulties with comparing the results of different oxybarometers, additional work using the V-partitioning oxybarometer is needed for well documented mantle-derived rocks of all ages in order to further constrain the redox evolution of the mantle. Most notably, only four MORB samples have been studied using this method and future work should focus on increasing the amount of available MORB data.

The temporal trend in mantle fO_2 documented in this study most likely points to the involvement of deep mantle oxidation in the surficial oxidation seen during the GOE. Although more modeling is necessary to clarify the relationship between the change in the oxidation state of the mantle and the GOE, it is evident that the mantle played an important role in this fundamental change in Earth's surficial environment.

ACKNOWLEDGEMENTS FOR CHAPTER 4

This study was supported by NSF FESD Type I Grant #1338810 "The Dynamics of Earth System Oxygenation" (lead PI is A.D. Anbar, I.S. Puchtel is a co-PI). This source of support is gratefully acknowledged. Eero Hanski acknowledges support from Academy of Finland Grant #281859. The authors wish to thank Nadezhda Tolstykh and Andrey Vishnevsky for providing the Song Da samples VS 5-1, VS 6-1 and VS 6-2, and Alan Brandon for providing the Icelandic samples ICE4A, ICE4B, and ICE5. We thank Valentina Puchtel for help with sample preparation. We also thank Mark Fornace

(undergraduate assistant), Valentina Puchtel, and William F. McDonough for their assistance in the initial development of the standard addition technique, which was supported by NSF grant EAR-0739006 (to W.F.M.). The support of the Maryland NanoCenter and its AIMLab is gratefully acknowledged. Finally, thorough reviews by Dr. Sonja Aulbach and Dr. Guilherme Mallmann, as well as comments by Associate Editor Dr. Munir Humayun, greatly improved the initial version of this manuscript.

References for Chapter 4

-Alfè D., Gillan M. and Price G. (2002) Composition and temperature of the Earth's core constrained by combining ab initio calculations and seismic data. *Earth Planet. Sci. Lett.* **195,** 91–98.

-Andrault D., Muñoz M., Pesce G., Cerantola V., Chumakov A., Kantor I., Pascarelli S., Ruffer R. and Hennet L. (2018) Large oxygen excess in the primitive mantle could be the source of the Great Oxygenation Event. *Geochem. Persp. Lett.* 6, 5–10 | doi: 10.7185/. 2018) geo chem let.1801.

-Anh T. V., Pang K. N., Chung S. L., Lin H. M., Hoa T. T., Anh T. T. and Yang H. J. (2011) The Song Da Magmatic Suite revisited: A petrologic, geochemical and Sr-Nd isotopic study of picrites, flood basalts and silicic volcanic rocks. *J. Asian Earth Sci.* **42**, 1341–1355.

-Anhaeusser C. R. (1983) The geology of the Schapenburg greenstone remnant and surrounding Archaean granitic terrane south of Badplaas, Eastern Transvaal.*Geol. Soc. S. Afr., Spec. Publ.* 9, 31–44.

-Anhaeusser C. R. (1991) Schapenburg greenstone remnant. In *Two Cratons and an Orogen—Excursion Guidebook and Review Articles for a Field Workshop Through Selected Archaean Terranes of Swaziland, South Africa and Zimbabwe* (ed. L. D. Ashwal). Univ. of the Witwatersrand, Johannesburg, South Africa. pp. 107–115.

-Anhaeusser C. R. and Robb L. J. (1980) Regional and detailed field and geochemical studies of Archaean trondhjemitic gneisses, migmatites and greenstone xenoliths in the southern part of the Barberton Mountain Land, South Africa. *Precambrian Res.* **11**, 373–397.

-Arndt N. T. (1986a) Spinifex and swirling olivines in a komatiite lava lake, Munro Township, Canada. *Precambrian Res.* **34**, 139–155.

-Arndt N. T. (1986b) Differentiation of komatiite flows. J. Petrol. **27**, 279–301.

-Aulbach S., and Arndt N. T. (2019) Eclogites as paleodynamic archives: Evidence for warm (not hot) and depleted (but heterogeneous) Archean ambient mantle. *Earth Planet. Sci. Lett.* **505,** 162-172.

-Aulbach S., Woodland A. B., Vasilyev P., Galvez M. E. and Viljoen K. S. (2017a) Effects of low-pressure igneous processes and subduction of $Fe^{+3}/\Sigma Fe$ and redox state of mantle eclogites from Lace (Kaapvaal Craton). *Earth Planet. Sci. Lett.* **474**, 283–295.

-Aulbach S., Sun J., Tappe S., Hofer H. and Gerdes A. (2017b) Volatile-rich metasomatism in the cratonic mantle beneath SW Greenland: Link to kimberlites and mid-lithospheric discontinuites. *J. Petrol.* **58**, 2311–2338.

-Aulbach S. and Stagno V. (2016) Evidence for a reducing Archean ambient mantle and its effects on the carbon cycle. *Geology* **44**, 751–754.

-Aulbach S. and Viljoen K. S. (2015) Eclogite xenoliths from the Lace kimberlite, Kaapvaal craton: From convecting mantle source to palaeo-ocean floor and back. *Earth Planet. Sci. Lett.* **431**, 274–286.

-Badro J., Fiquet G., Guyot F., Gregoryanz E., Occelli F., Antonangeli D. and D'astuto M. (2007) Effect of light elements on the sound velocities in solid iron: Implications for the composition of Earth's core. *Earth Planet. Sci. Lett.* **254**, 233–238.

-Badro J., Brodholt J. P., Piet H., Siebert J. and Ryerson F. J. (2015) Core formation and core composition from coupled geochemical and geophysical constraints. *Proc. Natl. Acad. Sci. USA* **112**, 12310–12314.

-Baker J. A. and Jensen J. K. (2004) ^{186}Os-^{187}Os enrichments in the Earth's mantle: core-mantle interaction or recycling of ferromanganese crusts and nodules? *Earth Planet. Sci. Lett.* **220**, 277–286.

-Ballhaus C., Berry R. F. and Green D. H. (1991) High pressure experimental calibration of the olivine-orthopyroxene-spinel oxygen geobarometer: implications for the oxidation state of the upper mantle. *Contrib. Mineral. Petrol.***107**, 27–40.

-Barnes S. J., Hill R. E. T. and Gole M. J. (1988) The Perseverance ultramafic complex, Western Australia: the product of a komatiite lava river. *J. Petrol.* **29**, 305–331.

-Baragar W. R. A. and Scoates R. F. J. (1981) The Circum-Superior Belt: A Proterozoic plate margin? In *Precambrian Plate Tectonics* (ed. A. Kröner, A.). Elsevier, Amsterdam. pp. 297–330

-Beattie P., Ford C. and Russell D. (1991) Partition coefficients for olivine-melt and orthopyroxene-melt systems. *Contrib. Mineral. Petrol.* **109**, 212–224.

-Berry A. J., Danyushevsky L. V., O'Neill H. St. C., Newville M. and Sutton S. R. (2008) Oxidation state of iron in komatiitic melt inclusions indicates hot Archaean mantle. *Nature* **455**, 960–963.

-Birch F. (1964) Density and composition of mantle and core. *J. Geophys. Res.* **69**, 4377–4388.

-Blichert-Toft J., Arndt N. T. and Gruau G. (2004) Hf isotopic measurements on Barberton komatiites: Effects of incomplete sample dissolution and importance for primary and secondary magmatic signatures. *Chem. Geol.* **207**, 261–275.

-Bottinga Y. and Javoy M. (1990) MORB degassing: Bubble growth and ascent. *Chem. Geol.* **81**, 255–270.

-Brandon A. D., Graham D. W., Waight T. and Gautason B. (2007) ^{186}Os and ^{187}Os enrichments and high-^{3}He/^{4}He sources in the Earth's mantle: Evidence from Icelandic picrites. *Geochim. Cosmochim. Acta* **71**, 4570–4591.

-Brandon A. D., Walker R. J. (2005). The debate over core-mantle interaction. *Earth Planet. Sci. Lett.* **232**, 211–225.

-Brandon A. D., Walker R. J., Puchtel I. S., Becker H., Humayun M. and Revillon S. (2003) ^{186}Os-^{187}Os systematics of Gorgona Island komatiites: Implications for early growth of the inner core. *Earth Planet. Sci. Lett.* **206**, 411–426.

-Brandon A. D., Norman M. D., Walker R. J. and Morgan J. W. (1999) ^{186}Os-^{187}Os systematics of Hawaiian picrites. *Earth Planet. Sci. Lett.* **174**, 25–42.

-Brounce M. N., Stolper E. and Eiler, J. (2017) Redox variations in Mauna Kea lavas, the oxygen fugacity of the Hawaiian plume, and the role of volcanic gases in Earth's oxygenation. *Proc. Natl. Acad. Sci*. **114**, 8997–9002.

-Brounce M. N., Kelley K. A. and Cottrell E. (2014). Variations in $Fe^{+3}/\Sigma Fe$ of Mariana Arc Basalts and Mantle Wedge fO_2. *J. Petrol.* **55**, 2513–2536.

-Brügmann G., Arndt N., Hofmann A. and Tobschall H. (1987). Noble metal abundances in komatiite suites from Alexo, Ontario and Gorgona Island, Colombia. *Geochim. Cosmochim. Acta* **51**, 2159–2169.

-Buffett B. A. (2003) The thermal state of Earth's core. *Science* **299**, 1675–1676.
Canil D. and Fedortchouk Y. (2001) Olivine-liquid partitioning of vanadium and other trace elements, with applications to modern and ancient picrites. *Can. Mineral.* **39**, 319–330.

-Canil D. (1997) Vanadium partitioning and the oxidation state of Archaean komatiite magmas. *Nature* **389**, 842–845.

-Canil D., O'Neill H. St. C., Pearson D. G., Rudnick, R., McDonough W. and Carswell, D. (1994) Ferric iron in peridotites and mantle oxidation states. *Earth Planet. Sci. Lett.* **123**, 205–220.

-Carmichael I. S. (1991) The redox states of basic and silicic magmas: A reflection of their source regions? *Contrib. Mineral. Petrol.* **106**, 129–141.

-Catling D. C. (2014) The Great Oxidation Event Transition. *Treatise on Geochemistry* **6**, 177–195.

-Catling D. C., Zahnle K. J. and McKay C. P. (2001). Biogenic methane, hydrogen escape, and the irreversible oxidation of early Earth. *Science* **293**, 839–843.

-Chung S. L., Lee T. Y., Lo C. H., Wang P. L., Chen C. Y., Nguyen T. Y., Tran T. H. and Wu G. Y. (1997) Intraplate extention prior to continental extrusion along the Ailao Shan-Red River shear zone. *Geology* **25**, 311–314

-Chung S.-L., Jahn B.-M., Genyao W., Lo C.-H. and Bolin C. (1998) The Emeishan Flood Basalt in SW China: A mantle plume initiation model and its connection with continental breakup and mass extinction at the Permian-Triassic boundary. In *Mantle Dynamics and Plate Tectonics in East Asia* (eds. M. F. J., Flower, S.-L. Chung, C.-H. Lo and T.-Y. Lee). AGU Geodynamics Series 27, 47–58.

-Ciborowski T. and Kerr A. C. (2016) Did mantle plume magmatism help trigger the Great Oxidation Event? *Lithos* **246–247**, 128–133.

-Clarke D. B. and Upton B. G. J. (1971) Tertiary basalts of Baffin Island: Field relations and tectonic setting. *Can. J. Earth Sci.* **8**, 248–258.

-Cottrell E. and Kelley K. A. (2011) The oxidation state of Fe in MORB glasses and the oxygen fugacity of the upper mantle. *Earth Planet. Sci. Lett.* **305**, 270–282.

-Cottrell E., Kelley K.A., Lanzirotti A. and Fischer R. A. (2009) High-precision determination of iron oxidation state in silicate glasses using XANES. *Chem. Geol.* **268**, 167–179.

-Dale C., Pearson D. G., Starkey N., Stuart F., Ellam R., Larsen L., Fitton J. M. and Macpherson C. (2009) Osmium isotopes in Baffin Island and West Greenland picrites: Implications for the $^{187}Os/^{188}Os$ composition of the convecting mantle and the nature of high $^{3}He/^{4}He$ mantle. *Earth Planet. Sci. Lett.* **278**, 267–277.

-Dauphas N. (2009) Iron isotopes may reveal the redox conditions of mantle melting from Archean to Present. *Earth Planet. Sci. Lett.* **288**, 255–267.

-Day J. M. D. (2016) Evidence against an ancient non-chondritic mantle source for North Atlantic Igneous Province lavas. *Chem. Geol.* **440**, 91–100.

-Debaille, V., O'Neill C., Brandon A. D., Haenecour P., Yin Q.-Z., Matielli N. and

-Treiman A. H. (2013) Stagnant-lid tectonics in early Earth revealed by ^{142}Nd variations in late Archean rocks. *Earth Planet. Sci. Lett.* **373**, 83–92.

-Delano J. W. (2001) Redox history of the Earth's interior since ~3900 Ma: Implications for prebiotic molecules. *Orig. Life Evol. Biosp*. **31**, 311–341.

-De Leeuw G. D., Ellam R., Stuart F. and Carlson R. (2017) ^{142}Nd/^{144}Nd inferences on the nature and origin of the source of high ^{3}He/^{4}He magmas. *Earth Planet. Sci. Lett.* **472**: 62–68.

-Deutsch E. R., Kristjansson L. G. and May B. T. (1971) Remanent magnetism of lower Tertiary lavas on Baffin Island. *Can. J. Earth Sci.* **8,** 1542–1552.

-Dupre B. and Echeverria L. M. (1984) Pb isotopes of Gorgona island (Colombia): isotopic variations correlated with magma type. *Earth Planet. Sci. Lett.* **67**, 186–190.

-Echeverria L.,(1980) Tertiary or Mesozoic komatiites from Gorgona Island, Colombia: Field relations and geochemistry. *Contrib. Mineral. Petrol.* 73, 253–266.

-Evans K. A. (2012) The redox budget of subduction zones. *Earth-Sci. Rev.* **113**, 11–32.

-Ernst R. and Bleeker W. (2010) Large igneous provinces (LIPs), giant dyke swarms, and mantle plumes: significance for breakup events within Canada and adjacent regions from 2.5 Ga to the present. *Can. J. Earth Sci.* **47**, 695**–**739.

-Farquhar J., Bao H. and Thiemens M. (2000) Atmospheric influence of Earth's earliest sulfur cycle. *Science* **289**, 756–758.

-Fischer W. W., Hemp J. and Johnson J. E. (2016) Evolution of oxygenic photosynthesis. *Ann. Rev. Earth Planet. Sci.* **44**, 647–683.

-Foley S. F. (2011) A reappraisal of redox melting in the Earth's mantle as a function of tectonic setting and time. *J. Petrol.* **52**, 1363–1391.

-Francis D. (1985) The Baffin–Bay lavas and the value of picrites as analogs of primary magmas. *Contrib. Mineral. Petrol.* 89, 144–154.

-Frost D., Mann U., Asahara Y. and Rubie D. (2008) The redox state of the mantle during and just after core formation. *Phil. Trans. Roy. Soc. A: Math. Phys. Eng. Sci.* **366**, 4315–4337.

-Frost D. J. and McCammon C. A. (2008) The redox state of Earth's mantle. *Ann. Rev. Earth Planet. Sci.* **36:** 389–420.

-Gaillard F., Scaillet B. and Arndt N. T. (2011) Atmospheric oxygenation caused by a change in volcanic degassing pressure. *Nature* **478**, 229–233.

-Ganne J. and Feng X. (2017) Primary magmas and mantle temperatures through time. *Geochem. Geophys. Geosyst.* **18**, 872–888.

-Gansser A., Dietrich V. J. and Cameron W. E. (1979) Paleogene komatiites from Gorgona Island. *Nature* **278**, 545–546

-Gerlach T. M. (1993) Oxygen buffering of Kilauea volcanic gases and the oxygen fugacity of Kilauea basalt. *Geochim. Cosmochim. Acta* **57**, 795–814.

-Gerya T. (2014) Precambrian geodynamics: Concepts and models. *Gondwana Res.* **25**, 442–463.

-Grocke S. B., Cottrell E., Silva S. D. and Kelley K. A. (2016) The role of crustal and eruptive processes versus source variations in controlling the oxidation state of iron in Central Andean magmas. *Earth Planet. Sci. Lett.* **440,** 92–104.

-Gumsley A. P., Chamberlain K. R., Bleeker W., Söderlund U., de Kock M. O., Larsson E. R. and Bekker A. (2017) Timing and tempo of the Great Oxidation Event. *Proc. Natl. Acad. Sci*. **114**, 1811–1816.

-Hanski E. and Huhma H. (2005) Central Lapland greenstone belt. In *Precambrian Geology of Finland – Key to the Evolution of the Fennoscandian Shield* (eds. M. Lehtinen, P. A. Nurmi, O. T. Rämö, O. T.). Elsevier Science B.V., Amsterdam. pp. 139–193.

-Hanski E., Walker R. J., Huhma H., Polyakov G. V., Balykin P. A., Hoa T. T. and Phuong N. T. (2004) Origin of the Permian-Triassic komatiites, northwestern Vietnam. *Contrib. Mineral. Petrol.* **147**, 453–469.

-Hanski E., Huhma H., Rastas P. and Kamenetsky V. S. (2001) The Palaeoproterozoic komatiite-picrite association of Finnish Lapland. *J. Petrol.* **42**, 855–876.

-Helz R. T. (2012) Trace Element Analyses of Core Samples from the 1967–1988 Drillings of Kilauea Iki Lava Lake, Hawaii. *U.S. Geol. Surv., Open-file Report* 2012–1050.

-Hemond C., Arndt N. T., Lichtenstein U., Hofmann A. W., Askarsson N. and Steinthorsson S. (1993) The heterogeneous Iceland plume: Nd–Sr–O isotopes and trace element constraints. *J. Geophys. Res.* **98**, 15833–15850.

-Herd C. D. (2008) Basalts as probes of planetary interior redox state. *Rev. Mineral. Geochem.* **68**, 527–553.

-Herzberg C., Condie K. and Korenaga J. (2010) Thermal history of the Earth and its petrological expression. *Earth Planet. Sci. Lett.* **292**, 79–88.

-Hibbert K. E. J., Williams H. M., Kerr A. C. and Puchtel, I. S. (2012) Iron isotopes in ancient and modern komatiites: Evidence in support of an oxidised mantle from Archean to present. *Earth Planet. Sci. Lett.* **321-322**, 198–207.

-Holland H. D. (2002) Volcanic gases, black smokers, and the great oxidation event. *Geochim. Cosmochim. Acta* **66**, 3811–3826.

-Huhma H., Hanski E., Kontinen A., Vuollo J., Mänttäri I. and Lahaye Y. (2018) Sm-Nd and U-Pb isotope geochemistry of the Paleoproterozoic mafic magmatism in eastern and northern Finland. *Geol. Surv. Finl., Bull.* 405.

-Hulbert L., Stern R., Kyser T. K., Pearson J., Lesher M. and Grinenko L., (1994) The Winnipegosis komatiite belt, central Manitoba. *Manitoba Mining and Minerals Convention* 1994, Program and Abstracts, p. 21.

-Humayun M., Qin L. and Norman M. D. (2004) Geochemical Evidence for Excess Iron in the Mantle Beneath Hawaii. *Science* **306**, 91–94.

-Huppert H. E. and Sparks R. S. J. (1985) Komatiites I: Eruption and flow. *J. Petrol.* **26**, 694–725.

-Huppert H. E., Sparks R. S. J., Turner J. S. and Arndt N. T. (1984) Emplacement and cooling of komatiite lavas. *Nature* **309**, 19–22.

-Ireland T. J., Walker R. J. and Brandon A. D. (2011) ^{186}Os–^{187}Os systematics of Hawaiian picrites revisited: New insights into Os isotopic variations in ocean island basalts. *Geochim. Cosmochim. Acta* **75**, 4456–4475.

-Jackson M. G., Carlson R. W., Kurz M. D., Kempton P. D., Francis D. and Blusztajn J. (2010) Evidence for the survival of the oldest terrestrial mantle reservoir. *Nature* **466**, 853–856.

-Kasting J. F., Eggler D. H. and Raeburn S. P. (1993) Mantle redox evolution and the oxidation state of the Archean atmosphere. *J. Geol.* **101**, 245–257.

-Kelley K. A. and Cottrell E. (2012) The influence of magmatic differentiation on the oxidation state of Fe in a basaltic arc magma. *Earth Planet. Sci. Lett.* **329-330**, 109–121.

-Kent A. J. R., Stolper E. M., Francis D., Woodhead J., Frei R. and Eiler J. (2004) Mantle heterogeneity during the formation of the North Atlantic Igneous Province: constraints from trace element and Sr–Nd–Os–O isotope systematics of Baffin Island picrites. *Geochem. Geophys. Geosyst.* 5, 2004GC000743.

-Kerr A. C. (2005) La Isla de Gorgona, Colombia: A petrological enigma? Lithos **84**, 77–101.

-Kerr A. C., Marriner G. F., Arndt N. T., Tarney J., Nivia A., Saunders A. D. and Duncan R. A. (1996) The petrogenesis of Gorgona komatiites, picrites and basalts: New field, petrographic and geochemical constraints. *Lithos* **37,** 245–260.

-Kress V. C. and Carmichael I. S. E. (1991) The compressibility of silicate liquidus containing Fe_2O_3 and the effect of composition, temperature, oxygen fugacity and pressure on their redox states. *Contrib. Mineral. Petrol.* **103**, 82–92.

-Krissansen-Totton J., Buick R. and Catling D. C. (2015) A statistical analysis of the carbon isotope record from the Archean to Phanerozoic and implications for the rise of oxygen. *Am. J. Sci*. **315**, 275–316.

-Kump L. R. and Barley M. E., 2007. Increased subaerial volcanism and the rise of atmospheric oxygen 2.5 billion years ago. *Nature* **448**, 1033–1036.

-Kurz M. D., Meyer P. S. and Sigurdsson H. (1985) Helium isotopic systematics within the neovolcanic zones of Iceland. *Earth Planet. Sci. Lett.* **74**, 291–305.
Labrosse S., Poirier J.-P. and Le Mouël J.-L. (2001) The age of the inner core. *Earth Planet. Sci. Lett.* **190**, 111–123.

-Laubier M., Grove T. L. and Langmuir C. H. (2014) Trace element mineral/melt partitioning for basaltic and basaltic andesitic melts: An experimental and laser ICP-MS study with application to the oxidation state of mantle source regions. *Earth Planet. Sci. Lett.* **392**, 265–278.

-Lécuyer C. and Ricard Y. (1999) Long-term fluxes and budget of ferric iron: Implication for the redox states of the Earth's mantle and atmosphere. *Earth Planet. Sci. Lett.* **165**, 197–211.

-Lecuyer C., Gruau G., Anhaeusser C. R. and Fourcade S. (1994) The origin of fluids and the effect of metamorphism on the primary chemical compositions of Barberton komatiites: New evidence from geochemical (REE) and isotopic (Nd, O, H, $^{39}Ar/^{40}Ar$) data. *Geochim. Cosmochim. Acta* **58**, 969–984.

-Lee C.-T. A., Yeung L. Y., McKenzie N. R., Yokoyama Y., Ozaki K. and Lenardic A. (2016) Two-step rise of atmospheric oxygen linked to the growth of continents. *Nature Geosci.* **9**, 417–424.

-Lee C.-T. A., Leeman W. P., Canil D., and Li Z.-X. A. (2005) Similar V/Sc Systematics in MORB and Arc Basalts: Implications for the Oxygen Fugacities of their Mantle Source Regions. Journal of Petrology **46**(11): 2313-2336.

-Le Voyer M., Cottrell E., Kelley K. A., Brounce M. and Hauri E. H. (2015) The effect of primary versus secondary processes on the volatile content of MORB glasses: An example from the equatorial Mid-Atlantic Ridge (5°N-3°S). *J. Geophys. Res.* **120**, 125–144.

-Li Z. X. A. and Lee C. T. A. (2004) The constancy of upper mantle fO_2 through time inferred from V/Sc ratios in basalts. *Earth Planet. Sci. Lett.* **228**, 483–493.

-Lo C.-H., Chung S.-L., Lee T.-Y. and Wu G. (2002) Age of the Emeishan flood magmatism and relations to Permian-Triassic boundary events. *Earth Planet. Sci. Lett.* **198,** 449–458

-Ludwig K. R. (2003) ISOPLOT 3.00. *A Geochronological Toolkit for Microsoft Excel*. Berkeley Geochronol. Cent. Spec. Publ. 4.

-Luguet A., Pearson D. G., Nowell G. M., Dreher S. T., Coggon J. A., Spetsius Z. V. and Parman S. W. (2008) Enriched Pt-Re-Os isotope systematics in plume lavas explained by metasomatic sulfides. *Science* **319**, 453–456.

-Lyons T. W., Reinhard C. T. and Planavsky, N. J. (2014) The rise of oxygen in Earth's early ocean and atmosphere. *Nature* **506**, 307–315.

-Mallmann G. and O'Neill H. St. C. (2013) Calibration of an empirical thermometer and oxybarometer based on the partitioning of Sc, Y and V between olivine and silicate melt. *J. Petrol.* **54,** 933–949.

-Mallmann G. and O'Neill H. St. C. (2009) The crystal/melt partitioning of V during mantle melting as a function of oxygen fugacity compared with some other elements (Al, P, Ca, Sc, Ti, Cr, Fe, Ga, Y, Zr and Nb). *J. Petrol.* **50**, 1765–1794.

-Mathez E. A. (1976) Sulfur solubility and magmatic sulfides in submarine basalt glass. *J. Geophys. Res*. **81**, 4269–4276.

-Matsui T. and Abe Y. (1986) Formation of a 'magma ocean' on the terrestrial planets due to the blanketing effect of an impact-induced atmosphere. *Earth Moon Planets.* **34**, 223–230.

-McGregor C. R. (2011) *Open File OF2011–1: GIS Compilation of Relogged Sub-Phanerozoic Precambrian Exploration Drillcore from the Thompson Nickel Belt, Eastern Flin Flon Belt and Winnipegosis Komatiite Belt* (Parts of NTS 63B, C, F, G, J, K).

-Mertzman S. A. (2000) K-Ar results from the southern Oregon - northern California Cascade range. *Oregon Geol*. **62**, 99–122.

-Métrich N., Berry A. J., O'Neill H. St. C. and Susini J. (2009) The oxidation state of sulfur in synthetic and natural glasses determined by X-ray absorption spectroscopy. *Geochim. Cosmochim. Acta* **73,** 2382–2399.

-Moore W. B. and Webb A. A. (2013) Heat-pipe Earth. *Nature* **501**, 501–505.

-Moussallam Y., Edmonds M., Scaillet B., Peters N., Gennaro E., Sides I. and Oppenheimer C. (2016) The impact of degassing on the oxidation state of basaltic magmas: A case study of Kīlauea volcano. *Earth Planet. Sci. Lett.* **450**, 317–325.

-Moussallam Y., Oppenheimer C., Scaillet B., Gaillard F., Kyle P., Peters N., Hartley M., Berlo K. and Donovan A. (2014) Tracking the changing oxidation state of Erebus magmas, from mantle to surface, driven by magma ascent and degassing. *Earth Planet. Sci. Lett.* **393,** 200–209.

-Mundl A., Touboul M., Jackson M. G., Day J. M., Kurz M. D., Lekic V., Helz R. and Walker R. J. (2017) Tungsten-182 heterogeneity in modern ocean island basalts. *Science* **356**, 66–69.

-Mutanen T. and Huhma H. (2001) U-Pb geochronology of the Koitelainen, Akanvaara and Keivitsa layered intrusions and related rocks. In Radiometric Age Determinations from Finnish Lapland and Their Bearing on the Timing of Precambrian Volcano-Sedimentary Sequences (ed. M. Vaasjoki). *Geol. Surv. Finl., Spec. Pap*. 33, 229–246.

-Nesbitt R. W. and Sun S.-S., (1976). Geochemistry of Archean spinifex-textured peridotites and magnesian and low-magnesian tholeiites. *Earth Planet. Sci. Lett.* **31,** 433–453.

-Nicklas R. W. and Puchtel I.S. (2016) Preservation of magma ocean redox heterogeneities: evidence from Paleoarchean komatiites. Abstract V11D-03, presented at 2016 Fall Meeting, AGU, San Francisco, California, 12–16 Dec, 2016.

-Nicklas, R. W., Puchtel I. S. and Ash R. D. (2016) High-precision determination of the oxidation state of komatiite lavas using vanadium liquid-mineral partitioning. *Chem. Geol.* **433**, 36–45.

-Nicklas R. W., Puchtel I. S. and Ash, R. D., 2018. Redox state of the Archean mantle: Evidence from V partitioning in 3.5–2.4 Ga komatiites. *Geochim. Cosmochim. Acta* **222**, 447–466.

-Nisbet E. G., Cheadle M. J., Arndt N. T. and Bickle M. J. (1993) Constraining the potential temperature of the Archaean mantle: A review of the evidence from komatiites. *Lithos* **30**, 291–307.

-Norman M. D. and Garcia M. O. (1999) Primitive magmas and source characteristics of the Hawaiian plume: Petrology and geochemistry of shield picrites. *Earth Planet. Sci. Lett*. **168**, 27–44.

-Ohtani E., Kawabe I., Moriyama J. and Yoshihiko N. (1989) Partitioning of elements between majorite garnet and melt and implications for petrogenesis of komatiite. *Contrib. Mineral. Petrol.* **103**, 263–269.

-Ono S. (2017) Photochemistry of sulfur dioxide and the origin of mass-independent isotope fractionation in Earth's atmosphere. *Ann. Rev. Earth Planet. Sci.* **45**: 301–329.

-Padron-Navarta J. A., Sanchez-Vizcaino V. L., Garrido C. J. and Gomez-Pugnaire M. T. (2011) Metamorphic record of high-pressure dehydration of antigorite serpentinite to chlorite harzburgite in a subduction setting (Cerro del Almirez, Nevado-Filabride Complex, Southern Spain). *J. Petrol.* **52**, 2047–2078.

-Parkinson I. J. and Arculus R. J. (1999) The redox state of subduction zones: insights from arc-peridotites. *Chem. Geol.* **160,** 409–423.

-Pedersen A. K., Larsen L. M., Riisager P. and Dueholm K. S. (2002) Rates of volcanic deposition, facies changes and movements in a dynamic basin: the Nuussuaq Basin, West Greenland, around the C27n–C26r transition. In The North Atlantic Igneous Province: Stratigraphy, Tectonics, Volcanic and Magmatic Processes (eds. D. W. Jolley and B. R. Bell). *Geol. Soc. London, Spec. Publ.* 197, 157–181.

-Pitcher L., Helz R. T., Walker R. J. and Piccoli P. M. (2009) Fractionation of the platinum-group elements and Re during crystallization of basalt in Kilauea Iki Lava Lake, Hawaii. *Chem. Geol.* **260**, 196–210.

-Planavsky N. J., Asael D., Hofmann A., Reinhard C. T., Lalonde S. V., Knudsen A., Wang X., Ossa Ossa F., Pecoits E., Smith A. J. B., Beukes N. J., Bekker A., Johnson T. M., Konhauser K. O., Lyons T. W. and Rouxel O. J. (2014) Evidence for oxygenic photosynthesis half a billion years before the Great Oxidation Event. *Nature Geosci.* **7**, 283.

-Polyakov G. V., Balykin P. A., Glotov A. I., Tran Q. H., Ngo T. P., Hoang H. T. and Bui A. N. (1991) Permian-Triassic association of high-magnesian volcanic rocks of the Song Da zone (north-western Vietnam). *Sov. Geol. Geophys.* **32**, 1–11

-Puchtel I. S., Blichert-Toft J., Touboul M., Horan M. F. and Walker R. J. (2016a) The coupled ^{182}W-^{142}Nd record of early terrestrial mantle differentiation. *Geochem. Geophys. Geosys.* **17**, 2168–2193.

-Puchtel I. S., Touboul M., Blichert-Toft J., Walker R. J., Brandon A. D., Nicklas R. W., Kulikov V. S. and Samsonov A. V. (2016b) Lithophile and siderophile element systematics of the Earth's mantle at the Archean-Proterozoic boundary: Evidence from 2.4 Ga komatiites. *Geochim. Cosmochim. Acta* **180**, 227–255.

-Puchtel I. S., Walker R. J., Touboul M., Nisbet E. G. and Byerly G. R. (2014) Insights into early Earth from the Pt-Re-Os isotope and highly siderophile element systematics of Baberton komatiites. *Geochim. Cosmochim. Acta* **125**, 394–413.

-Puchtel I. S., Blichert-Toft J., Touboul M., Walker R. J., Byerly G., Nisbet E. G. and Anhaeusser C. R. (2013) Insights into early Earth from Barberton komatiites: Evidence from lithophile isotope and trace element systematics. *Geochim. Cosmochim. Acta* **108**, 63–90.

-Puchtel I. S., Walker R.J., Anhaeusser C. R. and Gruau G. (2009) Re-Os isotope systematics and HSE abundances of the 3.5 Ga Schapenburg komatiites, South Africa: Hydrous melting or prolonged survival of primordial heterogeneities in the mantle? *Chem. Geol*. **262**, 355–369.

-Puchtel I. S., Brandon A. D., Humayun M. and Walker R. J. (2005) Evidence for the early differentiation of the core from Pt-Re-Os isotope systematics of 2.8-Ga komatiites. *Earth Planet. Sci. Lett.* **237**, 118–134.

-Puchtel I. S., Humayun M., Campbell A., Sproule R. and Lesher C. M. (2004) Platinum group element geochemistry of komatiites from the Alexo and Pyke Hill areas, Ontario, Canada. *Geochim. Cosmochim. Acta* **68**, 1361–1383.

-Puchtel I. S., Arndt N. T., Hofmann A. W., Haase K. M., Kröner A., Kulikov V. S., Kulikova V. V., Garbe-Schonberg C. D. and Nemchin A. A. (1998a) Petrology of mafic lavas within the Onega plateau, central Karelia: Evidence for 2.0 Ga plume-related continental crustal growth in the Baltic Shield. *Contrib. Mineral. Petrol.* **130**, 134–153.

-Puchtel I., Brügmann G. and Hofmann A. (1998b) Precise Re–Os mineral isochron and Pb–Nd–Os isotope systematics of a mafic–ultramafic sill in the 2.0 Ga Onega plateau (Baltic Shield). *Earth Planet. Sci. Lett.* **170**, 447–461.

-Revillon S., Chauvel C., Arndt N. T., Pik R., Martineau F., Fourcade S. and Marty B. (2002) Heterogeneity of the Caribbean plateau mantle source: heterogeneity of the Caribbean plateau mantle source: Sr, O and He isotopic compositions of olivine and clinopyroxene from Gorgona island. *Earth Planet. Sci. Lett.* **205**, 91–106.

-Revillon S., Arndt N. T., Chauvel C. and Hallot E. (2000) Geochemical study of ultramafic volcanic and plutonic rocks from Gorgona island, Colombia: the plumbing system of an oceanic plateau. *J. Petrol.* **41**, 1127–1153.

-Richter D. H. and Moore J. G. (1966) Petrology of the Kilauea Iki Lava Lake, Hawaii, *U.S. Geol. Surv. Prof. Pap.* 537-B.

-Rizo H., Walker R. J., Carlson R. W., Horan M. F., Mukhopadhyay S., Manthos V., Francis D. and Jackson M. G. (2016) Preservation of Earth-forming events in the tungsten isotopic composition of modern flood basalts. *Science* **352**, 809–812.

-Robillard I., Francis D. and Ludden J. N. (1992) The relationship between E- and N-type magmas in the Baffin Bay lavas. *Contrib. Mineral. Petrol.* 112, 230–241.

-Roeder P. L. and Emslie R. F. (1970) Olivine-liquid equilibrium. *Contrib. Mineral. Petrol.* **29**, 275–282.

-Sack R. O., Carmichael I. S. E., Rivers M. and Ghiorso, M. S. (1980) Ferric-ferrous equilibria in natural silicate liquids at 1 bar. *Contrib. Mineral. Petrol.* **75**, 369–376.

-Schidlowski M. (1988) A 3,800-million-year isotopic record of life from carbon in sedimentary rocks. *Nature* **333**, 313–318.

-Serrano L., Ferrari L., Martinez M. L., Petrone C. M. and Jaramillo C. (2011) An integrative geologic, geochronologic and geochemical study of Gorgona Island, Colombia: Implications for the formation of the Caribbean Large Igneous Province. *Earth Planet. Sci. Lett.* **309**, 324–336.

-Shu Q., Brey G. P., Hoefer H. E., Zhao Z. and Pearson D. G. (2016) Kyanite/corundum eclogites from the Kaapvaal Craton: subducted troctolites and layered gabbros from the Mid- to Early Archean. *Contrib. Mineral. Petrol.* 171: 11. https://doi.org/10.1007/s00410-015-1225-5

-Sinton C. W., Duncan R. A., Storey M., Lewis J. and Estrada J. J. (1998) An oceanic flood basalt province within the Caribbean plate. Earth Planet. Sci. Lett. **155**, 221– 235.

-Sizova E., Gerya T., Brown M. and Perchuk L. (2010) Subduction styles in the Precambrian: Insight from numerical experiments. *Lithos* **116**, 209–229.

-Sossi P. A., Eggins S. M., Nesbitt R. W., Nebel O., Hergt J. M., Campbell I. H., O'Neill H. St. C., Van Kranendonk M. and Davies D. R. (2016) Petrogenesis and geochemistry of Archean komatiites. *J. Petrol.* **57**, 147–184.

-Sossi P. A., Foden J. D. and Halverson G. P. (2012) Redox-controlled iron isotope fractionation during magmatic differentiation: An example from the Red Hill intrusion, S. Tasmania. *Contrib. Mineral. Petrol.* **164**, 757–772.

-Starkey N., Stuart F. M., Ellam R. M., Fitton J. G., Basu S. and Larsen L. M. (2009) Helium isotopes in early Iceland plume picrites: constraints on the composition of high $^{3}He/^{4}He$ mantle. *Earth Planet. Sci. Lett.* 277, 91–100.

-Stolper D. A. and Keller C. B. (2018) A record of deep-ocean dissolved O_2 from the oxidation state of iron in submarine basalts. *Nature* **553**, 323–327.

-Stuart F. M., Lass-Evans S., Fitton J. G. and Ellam R. M. (2003) High $^{3}He/^{4}He$ ratios in picritic basalts from Baffin Island and the role of a mixed reservoir in mantle plumes. *Nature* **424**, 57–59.

-Tonks W. B. and Melosh H. J. (1993) Magma ocean formation due to giant impacts. *J. Geophys. Res.* **98**(E3), 5319–5333.

-Touboul M., Puchtel I. S. and Walker R. J. (2012) ^{182}W evidence for long-term preservation of early mantle differentiation products. *Science* **335**, 1065–1069.

-Trail D., Watson E. B. and Tailby N. D. (2011) The oxidation state of Hadean magmas and implications for early Earth's atmosphere. *Nature* **480**, 79–82.

-Viljoen M. J. and Viljoen R. P. (1969) The geology and geochemistry of the Lower Ultramafic Unit of the Onverwacht Group and a proposed new class of igneous rocks. *Geol. Soc. S. Afr., Spec. Publ.* **2**, 55–86.

-Walker R. J., Storey M., Kerr A. C., Tarney J. and Arndt N. T. (1999) Implications of ^{187}Os isotopic heterogeneities in a mantle plume: Evidence from Gorgona Island and Curaçao. *Geochim. Cosmochim. Acta* **63**, 713–728.

-Wang C. Y., Zhou M.-F. and Qi L. (2007) Permian flood basalts and mafic intrusions in the Jinping (SW China)-Song Da (northern Vietnam) district: mantle sources, crustal contamination and sulfide segregation. *Chem. Geol.* **243,** 317– 343.

-Waters L. E. and Lange R. A. (2016) No effect of H_2O degassing on the oxidation state of magmatic liquids. *Earth Planet. Sci. Lett.* **447,** 48–59.

-Waterton P., Pearson D. G., Kjarsgaard, B., Hulbert, L., Locock, A., Parman, S. and Davis, B. (2017) Age, origin and thermal evolution of ultra-fresh ~1.9 Ga Winnipegosis komatiites, Manitoba, Canada. *Lithos* **268-271**, 114–130.

-White R. and McKenzie D. (1989) Magmatism at rift zones: The generation of volcanic continental margins and flood basalts. *J. Geophys. Res*. **94.** 7685–7729.

-Willbold M., Mojzsis S. J., Chen H. W. and Elliott T. (2015) Tungsten isotope composition of the Acasta Gneiss Complex. *Earth Planet. Sci. Lett.* **419.** 168–177.

-Williams H. M., Nielsen S. G., Renac C., Griffin W. L., O'Reilly S. Y., McCammon C. A., Pearson N., Viljoen F., Alt J.C. and Halliday A. N. (2009) Fractionation of oxygen and iron isotopes by partial melting processes: Implications for the interpretation of stable isotope signatures in mafic rocks. *Earth Planet. Sci. Lett*. **283,** 156–166.

-Williams H. M., Peslier A. H., McCammon C., Halliday A. N., Levasseur S., Teutsch N. and Burg J. P. (2005) Systematic iron isotope variations in mantle rocks and minerals: The effects of partial melting and oxygen fugacity. *Earth Planet. Sci. Lett.* **235,** 435–452.

-Wood, D. H. (1991) Oxygen barometry of spinel peridotites. Rev. Mineral. Geochem. 25, 417–432.

-Wood B. J., Walter M. J. and Wade J., 2006. Accretion of the Earth and segregation of its core. *Nature* **441,** 825–833.

-Woodland A. and Koch M. (2003) Variation in oxygen fugacity with depth in the upper mantle beneath the Kaapvaal craton, Southern Africa. *Earth Planet. Sci. Lett*. **214**. 295–310.

-Wright T. L. (1973) Magma mixing as illustrated by the 1959 eruption. Kilauea Volcano, Hawaii: *Geol. Soc. Am. Bull.* **84**, 849–858.

-Zahnle K. J., Catling D. C. and Claire M. W. (2013) The rise of oxygen and the hydrogen hourglass. *Chem. Geol.* **362,** 26–34.

Chapter 5: Re-Os Isotope and Highly Siderophile Element Abundance Systematics of 89 Ma Gorgona Komatiites

Note: All Os isotopic and HSE abundance analyses of samples Gor152-Gor160, Gor23B, and Gor47 were performed by undergraduate student Kyle Ludwig in the course of his senior thesis at UMD. These data are used here with his permission. All interpretations and text are my own.

Note: This chapter is currently being prepared for publication as following:

Nicklas, R. W., Puchtel, I. S., Ludwig, K., Bermingham, K. R., and Walker, R. J. (2019) Re-Os Isotope and Highly Siderophile Element Abundance Systematics of 89 Ma Gorgona Komatiites. To be submitted to *Earth Planet. Sci. Lett.*

Abstract for Chapter 5

Gorgona Island, Colombia, contains a rare occurrence of Phanerozoic (89 Ma) komatiites. Major, trace and highly siderophile element (HSE) abundances and Re-Os isotope systematics are reported for thirteen whole rock komatiite samples collected the island. The samples are divided into a group with broadly chondritic initial γOs values of +0.84±0.78 (2SD), termed "Group 1" and those that have previously been shown to have more radiogenic initial γOs values, termed "Group 2" (Walker et al., 1999). Group 1 komatiites have been shown to be related to each other by fractionation of olivine from a chemically homogeneous parental magma (Nicklas et al., 2019). Both groups of komatiites have HSE abundances similar to those reported in Archean komatiites with comparable MgO contents. Due to the systematic variation of HSE abundances with MgO abundance in Group 1 komatiites, it is likely that the distribution of the HSE is solely the result of igneous differentiation, and that the HSE were not remobilized in these rocks by surficial processes. Palladium, Pt and Re behaved incompatibly during differentiation of the Group 1 komatiites, while Ru, Os, and Ir abundances were probably controlled by crystallization of minor and trace phases, such as chromite and Os-Ir alloys. The calculated total HSE abundances in the mantle source of the Group 1 komatiites are within uncertainties of Bulk Silicate Earth (BSE) estimates. By contrast, the two Group 2 samples analyzed are characterized by 44±18% lower calculated total Pt and Pd abundances in their mantle source. This observation, together with the apparent decoupling of their Os and Nd isotopic systematics, likely requires early sulfide metasomatism in their mantle source region to achieve a strongly suprachondritic, long-term Re/Os in concert with a Sm/Nd ratio similar to that of the convecting upper mantle.

5.1. Introduction

Gorgona is a ~2 × 8 km island off the Pacific coast of Colombia. The high-MgO lavas of Gorgona are a rare occurrence of Phanerozoic spinifex-textured komatiites (Gansser et al., 1979). The island has been interpreted to be a remnant piece of the lowermost part of an oceanic plateau that was associated with the initial stages of the present-day Galapagos plume (Kerr *et al.*, 1996; Alvarado *et al.*, 1997; Arndt *et al.*, 1997). More than 90% of the rocks exposed on Gorgona are igneous, and the majority of those are volcanic (Echeverria, 1980). Four distinct types of volcanic rocks occur on Gorgona, including komatiites, picrites, as well as chemically enriched ("e") and depleted ("d") basalts (Kerr, 2005). Trace element and isotopic data indicate that at least three to four end member compositions are required in the mantle source region of the Gorgona lavas to account for their range in chemical and isotopic compositions (Kerr, 2005). The isotopic range of Gorgona rocks exceeds that of the much larger Ontong Java oceanic plateau. The emplacement age of these rocks has been tightly constrained by Ar-Ar dating of basalts to be 88.9 ± 1.2 Ma (Sinton et al., 1998). Both the association of the Gorgona rocks with the Galapagos plume, and melt inclusion studies showing that the komatiite magmas contained <0.9% H_2O (Shimizu et al., 2009; Gurenko et al., 2016) imply that the parental melts to the Gorgona komatiites were generated from anomalously hot and largely anhydrous mantle, likely the head of the Galapagos starting plume.

Walker et al. (1991, 1999) reported Re-Os isotopic data for Gorgona komatiites, with initial γOs values ranging from ~0 to +12. The high γOs component in the Gorgona source region was interpreted to reflect lower mantle heterogeneity left over from core formation, a possible contribution to the plume from the outer core, recycling of oceanic lithosphere, or a combination

of these options (Walker et al., 1999). Models invoking recycling of oceanic crust require prohibitively large proportions of ancient mafic material in the komatiites' mantle source, and cannot by themselves explain the high γOs component in Gorgona rocks (Walker et al., 1999). Coupling the Re-Os with the Pt-Os system showed that Gorgona komatiites plot along a mixing line between ambient mantle and a high $^{187}Os/^{188}Os$, high $^{186}Os/^{188}Os$ endmember, postulated to be the outer core (Brandon et al. 2003). Subsequent studies, (i.e. Luguet et al. 2008) however, showed that intra-mantle sulfide metasomatism can readily generate coupled high Re/Os-Pt/Os, and that outer core contribution is unnecessary to explain the data. Importantly, HSE abundance data from related Gorgona komatiites allows for the calculation of HSE abundances in their source region, which provide constraints on whether this source has had core metal added to it.

Brügmann et al. (1987) reported Au/Pd, Ir/Os, Os/Ru and Ru/Ir ratios in the Gorgona komatiites similar to those in the 2.7 Ga Alexo, Ontario, Canada komatiites, but significantly lower absolute abundances of the compatible Os, Ir and Ru. They concluded that Pd behaved incompatibly, while Ru, Ir and Os behaved compatibly during lava differentiation. The relatively high abundances of HSE and the incompatible behavior of Pd they observed led them to conclude that the Gorgona komatiites did not undergo sulfide saturation prior to eruption.

Komatiite flows on Gorgona can be traced for up to 300 m and vary in thickness between ~1 and 3 m. Their internal structures resemble those of layered Archean komatiite lava flows (e.g., Pyke et al., 1973). The Gorgona komatiite flows, from top to bottom, typically contain a 20-100 cm thick polyhedrally-jointed upper chilled margin (A_1 subzone), a 10-40 cm thick layer of random olivine spinifex grading downward into ~70 cm thick layer of oriented olivine spinifex (A_2 subzone), and a ~5-10 cm thick and often discontinuous layer of horizontal skeletal

olivine (B_1 subzone). Unlike many Archean komatiite flows, olivine cumulate layers (B_{2-4} subzones) are poorly developed in Gorgona lava flows. Where present, these layers are often discontinuous, and are never more than ~30% of the komatiite flow thickness (Kerr et al., 1996).

Previous studies have shown that the mantle source region of the Gorgona komatiites was highly depleted in incompatible lithophile trace elements, with $(Ce/Sm)_N < 0.6$ (Kerr et al. 1996; Revillon et al. 2000). Lithophile element radiogenic isotope systems reveal that the mantle source was isotopically heterogeneous. Lead isotope studies have shown that komatiites exposed on the east coast of Gorgona have similar $^{206}Pb/^{204}Pb$ ratios to cotemporaneous MORB at 18.299-18.493, while komatiites from the west coast are characterized by $^{206}Pb/^{204}Pb$ ratios that are more radiogenic at 18.581-18.608, likely due to incorporation of radiogenic plume mantle into their source (Dupre and Echeverria, 1984). Neodymium isotopic data for Gorgona komatiites are characterized by uniformly elevated εNd_T values relative to chondrites, ranging from +8.8 to +10.3, indicating long term light rare earth element (LREE) depletion in their mantle source region (Kerr, 2005). The komatiites are similarly characterized by elevated εHf_T values ranging from +17.0 to +17.7 (Thompson et al., 2003). These compositions are broadly consistent with modern mid-ocean ridge basalts (MORB), but are displaced to slightly higher εHf_T at a given εNd_T compared to the MORB array. Nevertheless, $^{87}Sr/^{88}Sr_T$ ratios range from 0.7030 to 0.7050 and are significantly more radiogenic than contemporaneous MORB. Revillon et al. (2002) reported that leached whole rocks and clinopyroxene separates yield lower initial ratios and concluded that the Sr isotope systematics of the Gorgona komatiites have been disturbed, and that even leached mineral separates likely do not reflect the true Sr isotopic composition of the mantle source. Even though several isotopic end-members are required by

the Gorgona igneous suite, the komatiites themselves display only a small part of the range shown in Gorgona, with much of the heterogeneity in Gorgona rocks hosted in picrites and basalts (Kerr, 2005). Prior studies have concluded that initial Pb, Nd and Hf isotopic ratios of Gorgona komatiites largely reflect long-term depletion of incompatible elements in their source regions, likely as a result of an earlier melting event (Dupre and Echeverria, 1984, Kerr et al. 1996, Thompson et al. 2003). Osmium isotopic systematics, however, show no correlation with the Pb, Nd, or Hf isotope systematics, indicating that the lithophile element isotope systems were decoupled from the Re-Os system in the Gorgona source (Walker et al., 1999; Thompson et al., 2003).

Despite the geochemical data available for Gorgona komatiites, a number of important issues related to their formation and composition of their mantle source are still not well understood. These include the behavior of HSE during magmatic differentiation of the komatiites and the cause of the decoupling of Os from lithophile element isotopic systematics. Notably, the highly-radiogenic Os isotopic compositions of some of the Gorgona komatiites are unusual in komatiitic lavas and overlap with compositions found in some enriched modern mantle endmembers, such as the high μ (HIMU) component (e.g., Hauri, 2002). In order to better constrain the origin of the Gorgona Os isotopic endmembers, HSE systematics of the Gorgona komatiites that can be related to one another by olivine fractionation are examined. Analysis of rocks from a single lava flow or several spatially closely associated lava flows allows for the degree of open-system behavior of the komatiites to be addressed with respect to the HSE, especially Re. Additionally, studying rocks potentially related by fractional crystallization allows assessment of the HSE content of the mantle source region(s) of the

Gorgona komatiites, and comparison of those concentrations with the estimated HSE contents of Archean komatiite source regions (e.g., Puchtel et al., 2018).

5.2. Samples.

Thirteen komatiite samples from Gorgona Island were analyzed for their Re-Os isotopic and trace element, as well as HSE systematics. Most samples were obtained from the Smithsonian Institution, National Museum of Natural History. The samples were divided into two groups, "Group 1", for which no previous Os isotopic data have been reported, and "Group 2" samples, which had been shown to have highly radiogenic Os isotopic systematics (Walker et al., 1999). Major element compositions for the Group 1 samples were recently reported in Nicklas et al. (2019) and it has been determined that these rocks are likely related to one another by olivine fractionation of a homogenous parental magma.

The Group 1 samples GOR152 – GOR160 came from the eastern-central coast of the island in the vicinity of "Punta Trinidad". These samples were collected by L. M. Echeverria (Echeverria, 1980). The Group 1 samples GOR537 – GOR540 were collected from the beach at "La Mancura" by S. Revillon and N.T. Arndt. Petrographic details regarding the latter group of samples can be found in Revillon et al. (2000). The Group 2 samples GOR23B and GOR47 were collected by L.M. Echeverria from the southwestern shores of the island (Echeverria, 1980). Petrographic details regarding the Punta Trinidad area samples are provided in the Supplemental Materials, and details regarding the Group 2 samples are provided in Echeverria (1980). Some of the samples analyzed here have previously been analyzed for Sr, Nd, Os, and Pb isotope systematics, and these data are provided in **Table 5.1**. The Os, Ir, Ru, and Pd

abundances have been previously determined in the Group 1 samples GOR156, GOR159, and GOR160 using the instrumental neutron activation analysis (INAA) technique, with concentrations ranging between 1.7-2.5, 1.6-2.3, 2.7-3.4, and 10.3-10.7 ppb, respectively (Brügmann et al., 1987).

Table 5.1. Published initial Sr, Nd, Os and Pb isotopic data for the Gorgona komatiite samples analyzed in this study

	Group 1						Group 2	
	Gor155	**Gor156**	**Gor160**	**Gor537**	**Gor538**	**Gor539**	**Gor23B**	**Gor47**
$^{87}Sr/^{88}Sr$	n.d.	0.702733[a]	0.703286[a]	0.703467[b]	0.703061[b]	0.70335[b]	n.d.	0.70356[c]
$\varepsilon^{143}Nd(T)$	n.d.	9.37[a]	n.d.	10.02[d]	10.12[d]	9.07[d]	n.d.	9.90[c]
$\gamma^{187}Os$	n.d.	n.d.	n.d.	n.d.	n.d.	n.d.	11.4[e]	12.4[e]
$^{206}Pb/^{204}Pb$	18.332[f]	n.d.	18.320[f]	n.d.	n.d.	n.d.	n.d.	18.581[f]
$^{207}Pb/^{204}Pb$	15.499[f]	n.d.	15.501[f]	n.d.	n.d.	n.d.	n.d	15.535[f]
$^{208}Pb/^{204}Pb$	37.822[f]	n.d.	37.824[f]	n.d.	n.d.	n.d.	n.d	38.207[f]

n.d. – not determined. Data sources: [a]Aitken and Echeverria (1984), [b]Revillon et al. (2002), [c]Echeverria, (1980), [d]Revillon et al. (2000), [e]Walker et al. (1999), [f]Dupre and Echeverria (1984).

5.3. Analytical Techniques

5.3.1. Analysis of major and minor elements in whole-rock samples

New powders were made for all rock samples analyzed in this study using an alumina jaw crusher, an alumina shatterbox, and an alumina disc mill. These new powders may differ somewhat from the powders of samples with the same numbers analyzed in previous studies, partly due to differences in olivine modal abundance between adjacent rock pieces. The Group 1 samples have previously been analyzed for major elements by Nicklas et al. (2019). New major element analyses of the Group 2 samples were made at Franklin & Marshall College on fused glass discs using a Phillips 2404 XRF spectrometer, following the procedure of Mertzman (2000). Typical accuracy of the analyses was ~2% relative (2SD) for major elements with

concentrations >0.5% and ~5% relative for the rest of the major and minor elements, as indicated by the analysis of the U.S. Geological Survey geochemical reference materials (GRM) BIR-1 and BCR-1 as unknowns (Puchtel et al., 2016a).

5.3.2. Analysis of trace elements

The abundances of lithophile trace elements in the whole-rock samples were determined using the standard addition solution inductively-coupled plasma mass-spectrometry technique (SAS ICP-MS) following the protocols detailed in Puchtel et al. (2016a) and Nicklas et al. (2018). The sample solutions were analyzed on a *Thermo Finnigan Element2* sector field ICP-MS at the *Plasma Laboratory (PL),* Department of Geology, University of Maryland. The external precision and accuracy (2SD) of the procedure was previously found to be ~5% for all the elements of interest based on replicate analyses of USGS GRM BIR-1 and BCR-1 (Puchtel et al., 2016a; Nicklas et al., 2018).

5.3.3. Analysis of Highly Siderophile Elements and Os Isotopes

The methods for determining HSE abundances and Os isotope ratios are similar to those detailed in Puchtel et al. (2016a). Briefly, 1.0-1.7 g of whole-rock powder, 6 mL of double-distilled concentrated HNO_3, 4 mL of triple-distilled concentrated HCl, and appropriate amounts of mixed ^{185}Re–^{190}Os and HSE (^{191}Ir, ^{99}Ru, ^{194}Pt and ^{105}Pd) spikes were sealed in internally-cleaned, chilled 25 mL Pyrex^{TM} borosilicate Carius tubes. The tubes with sample were heated to 270°C for ~72 hr. Osmium was extracted from the acid solution by CCl_4 solvent extraction (Cohen and Waters, 1996), then back-extracted into HBr and purified via microdistillation (Birck

et al., 1997). Iridium, Ru, Pt, Pd, and Re were separated and purified using anion exchange chromatography following the protocol of Rehkämper and Halliday (1997) with some modifications. The total analytical blanks (TAB) measured during the analytical campaign were (in pg): Ir – 0.16, Ru – 2.80, Pt – 95, Pd – 6.40, Re – 1.10 and Os – 0.13 (n=1). The average blank corrections for Ir, Ru, Pt, Pd, Re and Os were 0.01, 0.06, 0.47, 0.03, 0.08 and 0.005%, respectively, and were negligible for all elements.

Osmium isotopic measurements were performed via negative thermal ionization mass-spectrometry (Creaser et al., 1991). All samples were analyzed using a secondary electron multiplier detector of a *Thermo Fisher Triton* mass spectrometer at the *Isotope Geochemistry Laboratory (IGL)*, University of Maryland. The measured isotopic ratios were corrected for mass-fractionation using $^{192}Os/^{188}Os = 3.083$. The internal precision of measured $^{187}Os/^{188}Os$ for all samples was between 0.07-0.20% relative (2SE). The $^{187}Os/^{188}Os$ ratio of 300–500 pg loads of the in-house Johnson-Matthey Os standard measured during the period of data collection averaged 0.11357 ± 11 (2SD, $N = 6$). This value characterizes the external precision of the isotopic analysis (0.10%). The measured $^{187}Os/^{188}Os$ ratios were further corrected for instrumental mass bias relative to the average $^{187}Os/^{188}Os = 0.11379$ measured for the Johnson-Matthey Os standard on the Faraday cups of the *IGL Triton* (Puchtel *et al.*, 2016b). The correction factor of 1.00194 was calculated by dividing this value by the average $^{187}Os/^{188}Os$ measured for the *Johnson-Matthey* Os standard on the SEM of the same instrument.

The measurements of Re, Ir, Ru, Pt and Pd were performed at the *Plasma Lab (PL)* via inductively-coupled plasma mass-spectrometry (ICP-MS) using a *Nu Plasma* instrument with a triple electron multiplier configuration in static mode. Isotopic mass fractionation was monitored

and corrected for by interspersing samples and standards. Diluted spiked aliquots of iron meteorites were run during each analytical session as secondary standards. The results from these runs agreed within 0.5% for Re and Ir, and within 2% for Ru, Pt, and Pd, with fractionation-corrected values obtained from measurements of undiluted solutions of iron meteorites using Faraday cups of the same instrument with a signal of >100 mV for the minor isotopes. We therefore cite ±2% as the uncertainty on the concentrations of Ru, Pt, and Pd, ±0.5% as the uncertainty on the concentrations of Re and Ir, and ±0.2% as the uncertainty on the concentrations of Os. The uncertainty on the Re concentration was the main source of uncertainty for the Re/Os ratio. The uncertainty on the $^{187}Os/^{188}Os$ ratio used for isochron calculations was either the external reproducibility of the *Johnson-Matthey* Os standard run during the analytical campaign, or the in-run precision of the individual analyses, whichever was greater. The initial $\gamma^{187}Os$ values for individual samples were calculated as the percent deviation of their isotopic composition at 89 Ma relative to the chondritic reference of Shirey and Walker (1998).

5.4. Results

5.4.1. Major, Minor, and Lithophile Trace Element Concentrations

Major, minor, and trace element concentration data for whole rock samples are listed in **Table 5.2**, re-normalized for loss on ignition (LOI). The REE and other lithophile trace elements, such as Nb and Th, are strongly inversely correlated with the MgO content in Group 1 samples, indicating incompatible behavior of these elements during lava differentiation (**Supplementary Figure 5.1**). The BSE-normalized $(La/Sm)_N$ ratios for the Group 1 komatiites averaging

0.29±0.03 (2SD), indicating LREE depletion in the source region of these komatiites. The two Group 2 komatiite samples have $(La/Sm)_N$ = 0.24 and 0.36. The $(Gd/Yb)_N$ ratios of the Group 1 komatiites are also uniform, at 1.24±0.04 (2SD), while the two Group 2 samples have very different $(Gd/Yb)_N$ ratios of 0.86 and 1.23. The abundances of the major elements and the lithophile trace elements Sc, V, Cu, Ga, Y, and Zr were reported for Group 1 samples by Nicklas et al. (2019), and the abundances of these elements in Group 2 reported here are similar. Despite the decoupling of lithophile and siderophile isotopic signatures shown by the Gorgona komatiites, trace element abundances of identical sample powders are necessary to provide geochemical context for HSE and Os isotopic data.

Major element concentrations for the Group 2 samples GOR23B and GOR47 were previously reported in Echeverria (1980). In general, our results reproduce these data well, with all major elements in abundances >1% consistent within ~6% relative. Low concentration elements, such as the alkalis, vary by as much as ~50% between our results and the literature values, possibly as a result of heterogeneous re-mobilization of these elements. The REE abundances are reported in the literature for samples GOR537, GOR538, GOR539 (Revillon et al. 2000), GOR156 (Aitken and Echeverria, 1984) and GOR47 (Echeverria, 1980). Our REE concentrations agree with the literature values to within ~20%, whereas the $(La/Sm)_N$ and $(Gd/Yb)_N$ ratios replicate the literature values to within ~10%. The offset between our data and the literature data is likely the result of variations in chemical composition between different pieces of rock processed for powders in the different studies.

Table 5.2. Major and minor metal abundances in whole rock komatiite samples from Gorgona Island. Oxide concentrations are in weight %, while other element concentrations are in ppm.

	Group 1											Group 2	
Sample	**Gor152**	**Gor153**	**Gor155**	**Gor156**	**Gor157**	**Gor159**	**Gor160**	**Gor537**	**Gor538**	**Gor539**	**Gor540**	**Gor23B**	**Gor47**
SiO_2	45.3	44.1	46.3	45.0	45.7	44.5	45.1	44.3	42.9	43.9	43.5	43.3	46.0
TiO_2	0.679	0.510	0.690	0.631	0.770	0.609	0.651	0.642	0.524	0.646	0.662	0.650	0.400
Al_2O_3	12.5	9.66	12.6	11.8	13.9	11.6	11.8	12.0	9.3	12.2	12.2	11.9	12.0
Fe_2O_3	12.9	12.2	12.8	12.7	13.1	12.7	12.7	12.8	12.0	12.2	12.8	14.4	11.6
MnO	0.210	0.200	0.180	0.210	0.210	0.205	0.194	0.177	0.185	0.188	0.189	0.222	0.197
MgO	15.3	23.8	15.4	17.7	12.1	18.7	17.8	17.2	25.7	18.3	18.0	17.8	16.6
CaO	11.2	8.22	10.3	10.3	12.2	9.80	10.1	10.7	8.05	11.0	10.8	10.2	10.8
Na_2O	1.62	0.93	1.33	1.27	1.59	1.23	1.18	1.63	0.69	1.03	1.40	1.12	1.28
K_2O	0.0210	0.0050	0.0660	0.0210	0.0420	0.0200	0.0440	0.0411	0.0308	0.0834	0.0210	0.0640	0.0190
P_2O_5	0.0389	0.0320	0.0410	0.0380	0.0440	0.0360	0.0360	0.0401	0.0514	0.0625	0.0525	0.0460	0.0390
LOI	2.80	3.29	5.97	3.09	3.15	2.69	5.07	1.83	2.88	4.21	4.64	4.61	3.68
Sc	37.7	29.3	38.9	35.0	42.0	34.2	35.7	35.2	27.3	33.3	36.6	29.3	31.8
V	307	227	314	284	346	276	289	293	221	266	298	262	240
Cu	146	107	155	134	158	133	132	137	99.5	135	123	158	114
Ga	14.6	10.9	14.4	13.6	16.3	13.4	14.0	13.8	10.1	13.0	13.2	14.2	12.3
Y	15.3	11.4	15.6	14.3	17.3	13.8	14.4	14.5	10.4	13.4	13.2	14.0	12.5
Zr	33.1	24.8	31.9	30.9	36.5	29.2	30.9	29.9	21.8	28.2	26.4	29.5	16.0
Nb	0.404	0.313	0.409	0.384	0.444	0.367	0.371	0.383	0.300	0.367	0.328	0.692	0.304
La	0.685	0.490	0.666	0.618	0.849	0.599	0.611	0.610	0.453	0.616	0.491	0.756	0.313
Ce	2.35	1.71	2.19	2.13	2.51	2.00	2.02	2.06	1.54	2.09	1.82	2.31	1.05
Pr	0.487	0.355	0.489	0.446	0.538	0.440	0.455	0.444	0.319	0.435	0.378	0.431	0.210
Nd	3.12	2.30	3.18	2.92	3.50	2.84	2.97	2.85	2.06	2.85	2.62	2.76	1.44
Sm	1.43	1.06	1.50	1.37	1.64	1.30	1.35	1.37	0.97	1.31	1.22	1.31	0.81
Eu	0.619	0.466	0.627	0.588	0.705	0.563	0.577	0.586	0.412	0.572	0.535	0.565	0.388
Gd	2.33	1.74	2.32	2.20	2.67	2.08	2.21	2.11	1.54	2.00	1.93	2.08	1.49
Tb	0.423	0.313	0.426	0.398	0.481	0.375	0.389	0.390	0.283	0.375	0.347	0.398	0.313
Dy	2.84	2.12	2.94	2.69	3.31	2.58	2.73	2.61	1.89	2.55	2.45	2.66	2.24
Ho	0.590	0.446	0.615	0.564	0.692	0.545	0.572	0.559	0.402	0.548	0.509	0.550	0.497
Er	1.68	1.27	1.71	1.60	1.94	1.53	1.61	1.55	1.13	1.52	1.43	1.55	1.46
Tm	0.235	0.177	0.238	0.222	0.272	0.212	0.222	0.219	0.158	0.209	0.198	0.213	0.213
Yb	1.50	1.13	1.52	1.42	1.73	1.36	1.41	1.39	1.02	1.34	1.27	1.36	1.40
Lu	0.213	0.164	0.220	0.204	0.249	0.194	0.204	0.201	0.146	0.198	0.185	0.190	0.203
Hf	0.998	0.751	0.997	0.956	1.13	0.888	0.947	0.921	0.684	0.899	0.876	0.283	0.168
Th	0.0369	0.0235	0.0311	0.0289	0.0343	0.0279	0.0315	0.0273	0.0200	0.0282	0.0233	0.0170	0.0061
U	0.0116	0.0087	0.0126	0.0104	0.0123	0.0098	0.0254	0.0110	0.0074	0.0156	0.0104	0.0254	0.0099
$(La/Sm)_N$	0.301	0.290	0.280	0.285	0.326	0.289	0.284	0.281	0.295	0.295	0.253	0.362	0.244
$(Gd/Yb)_N$	1.25	1.25	1.24	1.26	1.25	1.23	1.26	1.23	1.22	1.20	1.23	1.23	0.86

Lithology	CM	Ol Cum	Ol Spx	Ol Spx	Ol Spx	Ol Spx	Ol Spx	Ol Spx	Ol Cum	Ol Spx	Ol Spx	Ol Spx	Ol Spx

Note- CM - chilled margin, Spx – spinifex textured komatiite, Ol Cum – olivine cumulate. N - BSE normalizing values from Hofmann (1988). LOI- loss on ignition. Major element and Sc, V, Cu, Ga, Y and Zr abundances for the Group 1 komatiites are from Nicklas et al. (2019) and were determined on the same powders used for analyses reported here.

5.4.2. HSE abundances and Re-Os isotopic systematics

The Re-Os isotopic and HSE concentration data for the whole rock samples are reported in **Table 5.3**. The komatiites are characterized by HSE abundances as follows: Os- 0.82 to 3.69, Ir- 0.56 to 2.39, Ru- 2.75 to 4.98, Pt- 12.0 to 17.8, Pd- 12.4 to 21.8 and Re 0.60 to 1.33 ppb. Highly siderophile element abundances in Group 1 samples GOR156, GOR159 and GOR160 have been previously reported by Brügmann et al. (1987). The Os, Ru and Pd abundances measured in our samples were up to 50%, 35% and 40% greater, respectively, than those previously reported, likely due to sample powder heterogeneity between the newly prepared samples powders and old sample powders, possibly due to a "nugget effect". The Ir abundances were determined to be between 20% lower to 30% greater than those reported in the Brügmann et al. (1987) study, likely for similar reasons. It is notable that the HSE are usually hosted in trace phases, such as sulfides or alloys, in silicate rocks , and, thus, the "nugget effect" for these elements can be often significant (Meisel et al. 2003).

Table 5.3. Highly siderophile element abundances (in ppb) and Re-Os isotopic data for whole rock samples from Gorgona Island.

Sample	Re	Os	Ir	Ru	Pt	Pd	$^{187}Re/^{188}Os$	±2σ	$^{187}Os/^{188}Os$	±2σ	$^{187}Os/^{188}Os(i)$	$\gamma^{187}Os(T)$
GOR 152	1.16	2.48	1.74	3.32	14.3	16.3	2.2517	0.0007	0.13077	0.00013	0.1274	0.799
GOR 153	0.917	1.42	1.08	3.38	12.1	13.3	3.1239	0.0013	0.13190	0.00017	0.1273	0.668
GOR 155	0.604	2.63	2.01	3.10	16.4	17.0	1.1035	0.0007	0.13022	0.00013	0.1286	1.71
GOR 156	1.18	2.75	1.92	3.41	15.4	16.7	2.0603	0.0007	0.13034	0.00014	0.1273	0.681
GOR 157	1.33	3.16	2.11	2.75	17.8	18.8	2.0275	0.0006	0.12992	0.00013	0.1269	0.394
GOR 159	1.20	3.69	2.33	4.78	14.4	15.8	1.5699	0.0005	0.12960	0.00013	0.1273	0.674
Replicate	1.05	3.39	2.22	4.93	14.6	15.9	1.4906	0.0005	0.12971	0.00013	0.1275	0.856
GOR 160	0.990	3.50	2.39	3.99	15.5	16.0	1.3638	0.0005	0.12863	0.00016	0.1266	0.145
GOR 537	1.05	2.43	1.75	3.68	15.7	16.9	2.1124	0.0009	0.13088	0.00013	0.1277	1.05
GOR 538	0.806	2.27	1.63	4.98	12.1	12.4	1.7584	0.0009	0.13028	0.00013	0.1277	0.992
GOR 539	1.00	2.78	2.10	3.80	17.8	21.8	1.8091	0.0008	0.13049	0.00013	0.1278	1.10
GOR 540	0.784	2.22	1.65	3.70	16.4	16.4	1.7824	0.0009	0.13035	0.00013	0.1277	1.02
GOR23B	1.25	0.820	0.781	4.14	12.0	14.2	7.3360	0.0024	0.15064	0.00024	0.1398	10.6
GOR47	0.834	0.842	0.563	2.79	13.0	14.9	4.7916	0.0022	0.15001	0.00030	0.1429	13.1

The HSE abundances are plotted against MgO in **Fig. 5.1.** Abundances of Pt, Pd and Re in the Group 1 samples plot on linear trends with varying degrees of scatter, and are inversely correlated with the MgO content. By contrast, Os, Ir, and Ru abundances do not significantly correlate with the MgO content. Highly siderophile element concentrations normalized to the CI chondrite values of Horan et al. (2003) are plotted in **Fig. 5.2**. All samples show enrichments in the more incompatible Pt, Pd and Re relative to the more compatible Ru, Os and Ir, with $(Pd/Ir)_N$ = 3.3-5.8 in the Group 1 samples, and $(Pd/Ir)_N$ = 7.9-12 in the Group 2 samples. The Re-Os isotopic data are plotted in **Fig. 5.3** along with a chondritic 89 Ma reference isochron using the parameters of Shirey and Walker (1998). The Group 1 samples scatter slightly above this reference isochron. The initial $\gamma^{187}Os$ values at 89 Ma for Group 1 average +0.8±0.8 (2SD). By contrast, the two Group 2 samples GOR23B and GOR47 have suprachondritic initial $\gamma^{187}Os$ values of +10.6 and +13.1 respectively, which are similar to the previously reported values for these samples in Walker et al. (1999) of +11.4 and +12.4, respectively.

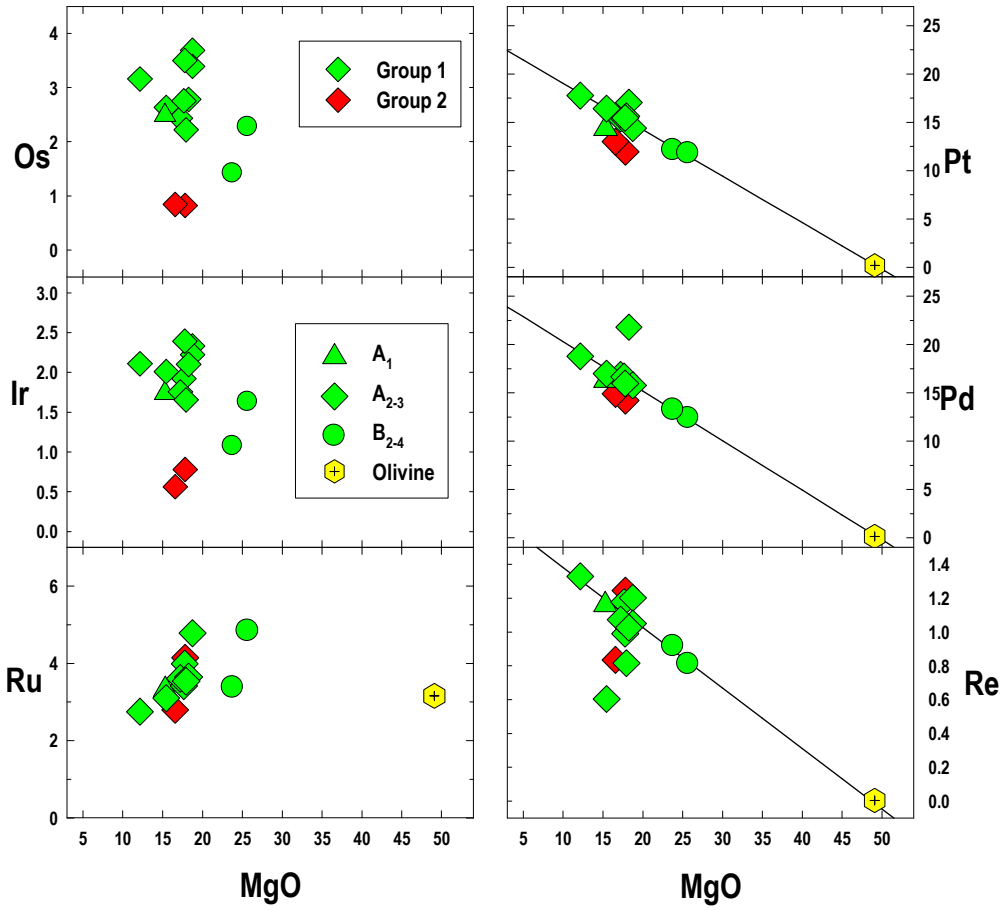

Fig. 5.1. HSE (ppb) abundances in whole-rock samples from Gorgona Island plotted against MgO contents (wt. %). Also plotted is the composition of calculated liquidus olivine with MgO = 49.1% and Pt, Pd, and Re concentrations of 0.256, 0.413, and 0.05 ppb respectively for an olivine separate sample from Puchtel et al. (2004a). A_1 – chilled margin, A_{2-3} – spinifex textured komatiite, B_{2-3} – olivine cumulate. Different colors correspond to different komatiite groups: green – Group 1, red – Group 2, and yellow – the calculated liquidus olivine composition. The lines are least-squared ISOPLOT regressions of the Group 1 komatiite HSE data. Samples Gor152 and Gor539 were excluded from the regressions for Pd and Pt. Sample Gor540 was excluded from the regression for Re. Error bars are smaller than the size of the symbols used.

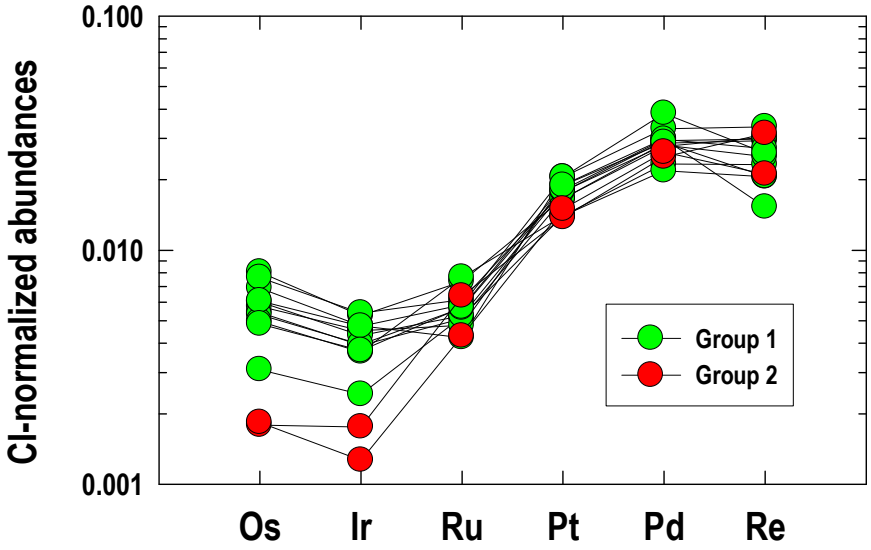

Fig. 5.2. CI chondrite-normalized HSE abundances in whole-rock Grogona komatiite samples. Normalizing values are from Horan et al. (2003).

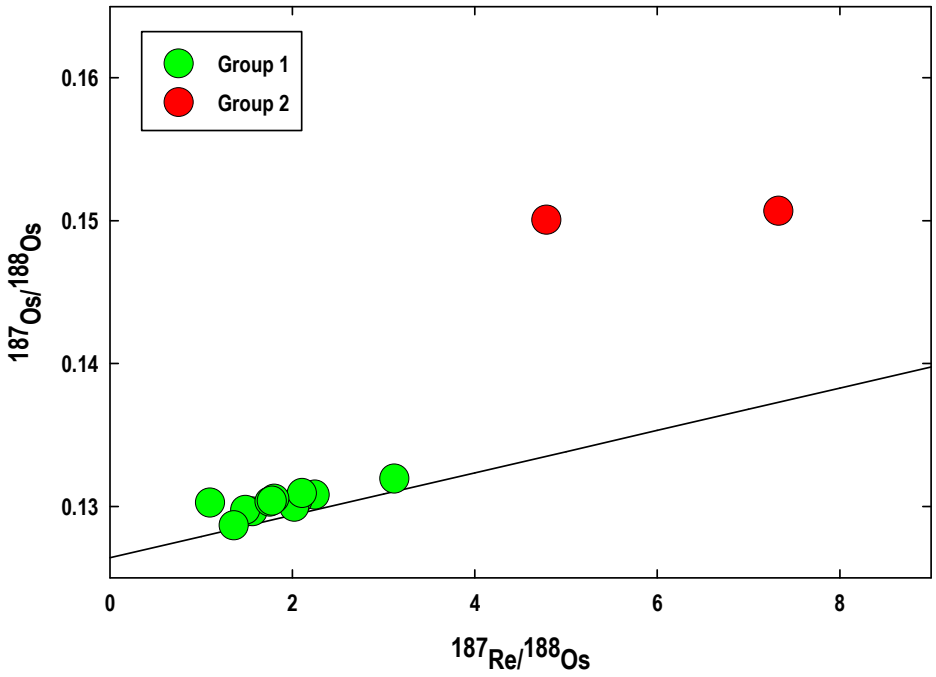

Fig. 5.3. Re-Os isochron diagram for whole rock komatiite samples from Gorgona Island. The line is an 89 Ma chondritic reference isochron.

5.5. Discussion

5.5.1. HSE abundances

Both Pd and Pt typically behave incompatibly during differentiation of sulfide-undersaturated komatiitic systems (e.g., Barnes et al., 1985), and this behavior was also observed for the Gorgona komatiites (**Fig. 5.1**). The strong correlation of Pt and Pd with an index of magmatic differentiation (MSWD = 2.5 and 3.7, respectively), such as MgO content, indicates that these elements were not mobilized in these samples after emplacement by weathering or hydrothermal alteration. Additionally, these correlations indicate that Pt and Pd were highly incompatible in olivine, the only major fractionating mineral phase during komatiite differentiation, and that the abundances of these elements follow olivine control lines.

Rhenium also shows an inverse correlation with MgO, albeit with significantly more scatter than Pt and Pd (**Fig. 5.1**) (MSWD = 32) indicating magmatic behavior of Re similar to that of Pt and Pd, with possibly some minor post-magmatic re-distribution of this element. Rhenium is typically a highly fluid-mobile element during surficial processes (Lassiter, 2003; MacKenzie and Canil, 2006) and rarely follows indices of magmatic differentiation in weathered rocks. However, the young age and excellent state of preservation of the Gorgona komatiites evidently allowed retention of magmatic Re signatures.

The incompatible behavior of these three elements indicates that the Group 1 komatiites were sulfide-undersaturated (Barnes et al., 1985), as any fractionating sulfide assemblage would have led to highly compatible behavior for all of the strongly chalcophile HSE. Platinum, Pd and Re also likely behaved incompatibly during the mantle melting that generated these komatiites,

as all three are strongly enriched relative to the more compatible Os and Ir (**Fig. 5.2)**. Additionally, the high-degree partial melting that is necessary to generate komatiites effectively consumes all low-temperature sulfide in the mantle source leading to quantitative removal of Pt, Pd and Re into the melt (Keays, 1995), allowing for calculations of the abundances of these elements in the mantle source region of komatiites (Puchtel et al., 2004).

Osmium and Ir show no correlation with MgO in the Group 1 samples (**Fig. 5.1**) indicating that the behavior of these elements was controlled by distribution of a trace phase, likely Os-Ir alloy, which has been shown to be an important Os and Ir host in sulfur-undersaturated ultramafic magmas (Brenan and Andrews, 2001). Osmium and Ir normally behave very similarly in magmatic system, and thus the Os/Ir ratio varies little between any of the Group 1 lavas (**Supplementary Figure 5.2**), with an average value of 1.42 ± 0.18 (2SD).

The Ru abundances exhibit no correlation with MgO (**Fig. 5.1**) however, the Ru and Cr concentrations in all samples are strongly positively correlated (**Fig. 5.4**), providing evidence that Ru was incorporated in a minor Cr-rich fractionating phase, most likely chromite. Indeed, small opaque chromite grains were identified in thin sections of the spinifex textured rocks in the Group 1 samples, and it has been shown that Ru is strongly compatible in chromite in other komatiitic systems (Locmelis et al. 2011). Overall, the correlations of the Ru, Pt, Pd and Re with lithophile elements in the Group 1 komatiites show that they were a largely a closed system with respect to the HSEs from emplacement to the present day.

The abundances of Pt, Pd, Ru, and Re of the Group 2 samples plot close to the regression lines defined by the Group 1 samples. By contrast, the abundances of Os and Ir in the Group 2

samples are significantly lower than those in the Group 1 samples with the similar MgO content (**Figs. 5.1-2**).

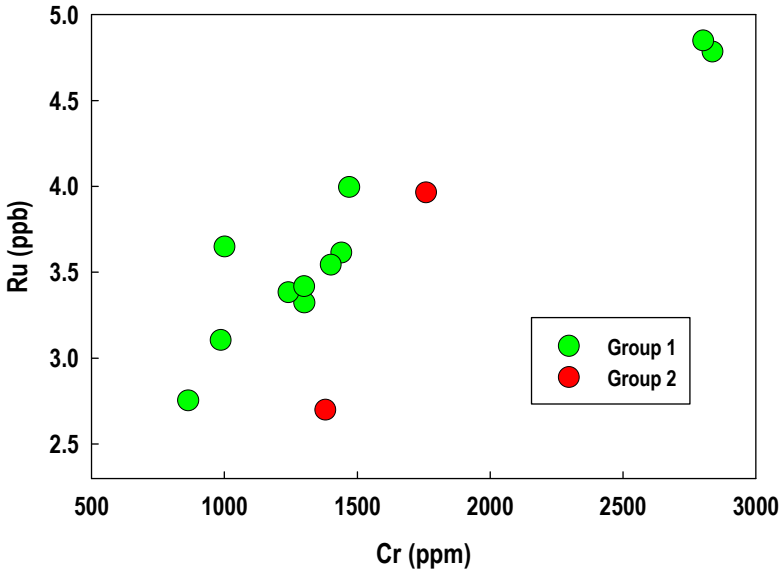

Fig. 5.4. Cr concentration in ppm as determined by XRF, plotted against Ru concentration in ppb for the whole rock komatiite samples. The strong positive correlation between Cr and Ru concentrations shows that Ru was incorporated into a Cr-rich liquidus phase, likely chromite. See text for details.

5.5.2. Re-Os isotopic data

The Group 1 komatiites have an average γ^{187}Os value of +0.84±0.78 (2SD), and plot within the chondritic evolution field, similar to the majority of previously analyzed Gorgona komatiites (Walker et al., 1999). Assuming a Solar System initial $^{187}Os/^{188}Os = 0.09517$ at 4568 Ma (Archer et al. 2014), the Group 1 komatiites source region was calculated to have evolved with a time-integrated $^{187}Re/^{188}Os$ ratio of 0.414±0.004. Although komatiites collected on the eastern and western shores of the island have been found to differ in Pb-isotopic composition (Dupre and Echeverria, 1984), Group 1 komatiites from both sides of the island were evidently derived from source regions with similar, chondritic long-term Re/Os ratios.

The elevated initial $\gamma^{187}Os$ values of the Group 2 samples may indicate long-term suprachondritic Re/Os in their source. It is also possible that Re loss, resulting from surface alteration, has led to the high apparent initial $\gamma^{187}Os$ values of the Group 2 samples. The latter possibility seems highly unlikely. In order for the Group 2 samples GOR23B and GOR47 to lie on an 89 Ma isochron consistent with long-term chondritic evolution, primary $^{187}Re/^{188}Os$ ratios of 18.60 and 18.10 respectively, would be required These calculated ratios, compared to the measured $^{187}Re/^{188}Os$ ratios would require ~61% and ~74% of recent Re loss for GOR23B and GOR47, respectively. As Re shows good correlation with MgO in the Group 1 samples (**Fig. 1.**), indicating magmatic control, it is unlikely that such strong recent Re depletion has affected any of these rocks. Therefore, we consider the elevated initial $\gamma^{187}Os$ values for the Group 2 samples to indicate a contribution from a source component characterized by long-term elevated Re/Os.

5.5.3. The HSE abundances of the Gorgona komatiite mantle source regions

Because Pt, Pd, and Re behaved incompatibly during differentiation of the Group 1 suite, and closely followed olivine control lines, these elements are useful proxies for calculating the total HSE abundances in the source regions of the Gorgona komatiites. By contrast, Ru, Ir, and Os abundances are uncorrelated with MgO content and are more problematic from which to calculate mantle source abundances.

As olivine is the only major fractionating mineral phase during komatiite differentiation, linear regression of Pt, Pd, or Re and MgO abundances in whole rock and olivine samples can be used to constrain the abundance of these elements at an appropriate MgO content in the source. Previous studies have applied this protocol, for determining the HSE abundances of the mantle

source regions of komatiites (e.g., Puchtel et al., 2014; 2016a; 2016b). We apply this method here to constrain the HSE abundances in the source region of the Group 1 samples.

Least-squares linear regressions of Pt, Pd and Re versus MgO for the Group 1 samples were calculated using ISOPLOT 3.00 (Ludwig, 2003) and shown in **Fig. 5.1.** In order to better constrain the slope in the MgO vs. HSE diagrams (**Fig. 5.1.**), a theoretical HSE composition of liquidus olivine in equilibrium with the emplaced komatiite lava was used for each regression calculation. The theoretical olivine is assumed to have had 0.0035 ppb Re, 0.132 ppb Pd and 0.193 ppb Pt based on data for an olivine separate from the Pyke Hill komatiites (Puchtel et al., 2004a) and the observation that Re, Pd and Pt concentrations in olivine are very low and vary little between komatiite flows. The MgO content for the liquidus olivine was calculated to be 49.1±0.5% MgO based on data from Nicklas et al. (2019) and the $D^{ol/melt}_{Mg\text{-}Fe}$ value of 0.30 from Beattie et al. (1991). Samples GOR152 and GOR539 were excluded from the regressions, as they plotted well off the regression lines, indicating that these samples likely experienced post-emplacement mobility of Pt and Pd, while sample GOR540 was excluded from the Re regression for the same reason. With these samples excluded, the Pt and Pd regressions have MSWD values ≤ 2.8, indicating strongly linear behavior, and the Pt and Pd abundances in a projected mantle source with a BSE MgO content of 38 wt.% (Hofmann, 1988) are calculated to be 5.6±0.7 and 6.0±0.9 ppb, respectively. The Re data are more scattered than the Pt and Pd data and a regression with an MSWD of 33 was calculated, yielding a source concentration of Re of 0.38±0.17 ppb.

The Pt and Pd concentrations of the source region of the Group 2 samples were determined by taking the regression slope for each element from the Group 1 data, and using that slope to

regress the Pd and Pt concentrations in samples GOR23B and GOR47 back to a mantle MgO of 38 wt. %. The calculated source compositions, as determined from the two Group 2 samples, were then averaged and the 2SD of the calculated source compositions was reported as the uncertainty. The calculated abundances of Pt and Pd in the Group 2 source region were 2.50±1.17 and 4.06±0.29, respectively.

The Pt and Pd abundances in each group's source region were then compared to the BSE Pt+Pd abundance, as calculated from the values of Becker et al. (2006). The % BSE Pt+Pd in the source region of Gorgona komatiites is compared to literature data for Archean komatiite source regions in **Fig. 5.5.** The source region of Group 1, at 77±7%, plots within the uncertainties of the BSE Pt+Pd value of Becker et al. (2006). The Group 2 Pt+Pd abundances of 44±18% of the BSE abundances, are markedly lower than those of the BSE. As Pt and Pd are moderately incompatible during mantle melting, it is possible that the depletion of these elements in the Group 2 komatiite source region reflects a previous melting event. This interpretation is problematic, however, as Re/Os shows long-term enrichment in the Group 2 source, which is the opposite of what is expected for a previously melt-depleted source. It is, therefore, likely that the Group 2 samples were partially or wholly derived from a distinct mantle source which may have acquired its HSE and Os isotopic signatures via different processes than the Group 1 komatiites.

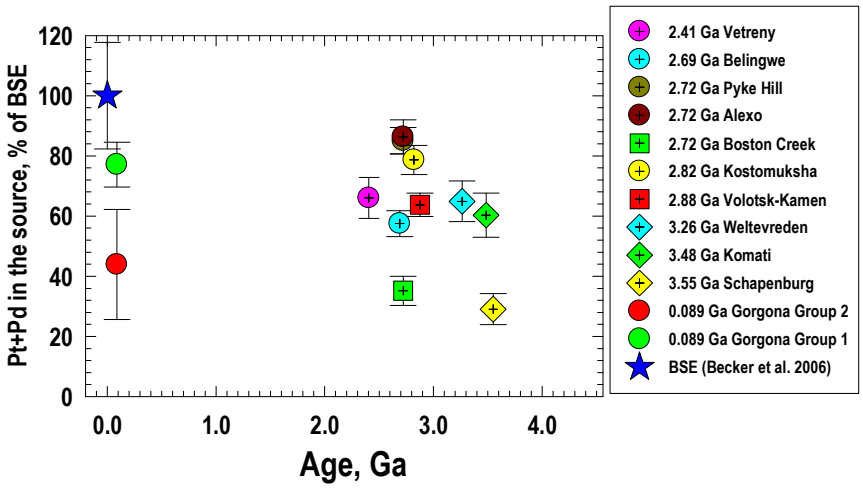

Fig. 5.5. Calculated total Pt + Pd abundances in the sources of the Group 1 and 2 Gorgona komatiites plotted as percentage of the total Pt + Pd abundances in the estimate for the modern BSE of Becker et al. (2006). The data for the Archean komatiite systems, plotted for comparison, are from Puchtel et al. (2004a,b, 2005, 2007, 2009a,b, 2014, 2016a,b, 2018) and Puchtel and Humayun (2005). Uncertainties are 2SD. See text for details.

From the calculated time-integrated Re/Os ratio in the source of the Group 1 komatiites of 0.0876±0.0006, an Os concentration of 4.3±1.9 ppb in their source is calculated. As discussed previously, the Os/Ir ratios of the Group 1 samples are very consistent, at 1.4±0.2 (2SD). This ratio does not correlate with the MgO contents (**Supplementary Figure 5.2**) indicating that the Os/Ir ratio did not fractionate during komatiite lava differentiation. This in turn suggests that Os and Ir also did not fractionate from each other during mantle melting. Using the average Os/Ir of the samples and the calculated Os abundance in the source, the Group 1 komatiite source region Ir abundance is calculated to be 3.1±1.4 ppb.

The calculated Re, Os, and Ir abundances in the Group 1 komatiite source region (**Table 5.4)** correspond to 108±48, 111±49, 87±41 respectively of these elements in the estimates for the modern BSE. The Ru concentration was not estimated due to the complicating effect of chromite fractionation during the komatiite differentiation. The total abundance of all the

measured HSE, except for Ru, is calculated to be 85±12% of those in the BSE estimates of Becker et al. (2006). The calculated HSE abundances of the Group 1 komatiite source region and the BSE estimate of Becker et al. (2006) are plotted on a CI chondrite-normalized diagram in **Fig. 6**. All elements overlap with the BSE mantle abundances, except for a slight depletion in Pt, indicating that the Group 1 source region underwent little fractionation of the HSE during its history.

Table 5.4. Calculated source HSE concentrations (ppb) for the Group 1 and 2 komatiites from Gorgona Island.

	Group 1 Source	**Group 2 Source**
MgO (wt%)	38.0	38.0
Pt	5.6±0.7	2.5±1.2
Pd	6.0±0.9	4.1±0.3
%BSE Pt+Pd	77±7	44±18
$(^{187}Re/^{188}Os)_t$	0.414±0.003	0.611±0.069
Re	0.38±0.17	n.d.
Os	4.3±1.9	n.d.
Ir	3.1±1.4	n.d.
% BSE HSE	85±12	n.d.

% BSE ΣHSE is percentage of the Bulk Silicate Earth concentration of the combined HSE excluding Ru. The BSE values are from Becker et al. (2006). See text for details.

Previous studies have reported the abundances of HSE in various reservoirs, such as modern abyssal peridotites (Luguet et al. 2001; Alard et al. 2005; Becker et al. 2006; Liu et al. 2009), the peridotite sections of ophiolites (Schulte et al. 2009; O'Driscoll et al. 2015), as well as the mantle source regions of Archean komatiites (e.g., Puchtel et al., 2014, 2018). An average abyssal peridotite HSE pattern, the projected HSE patterns of the mantle source regions of the 3.48 Ga Komati and 3.26 Ga Weltevreden komatiite suites and an average HSE pattern for peridotites from the 6 Ma Taitao ophiolite are also plotted on a CI chondrite-normalized plot in **Fig. 5.6.** It is evident that the comparatively flat HSE pattern shown in the Group 1 Gorgona

source is similar to that of abyssal peridotites, the Komati and Weltevreden source regions, and the Taitao peridotites. We conclude that the Group 1 mantle source, prior to the generation of the komatiites, had not experienced melting events sufficient to fractionate its HSE, and that its history of melt depletion does not exceed that of the bulk convecting mantle source of MORB, as sampled by abyssal peridotites and ophiolite peridotites. The HSE abundances of both the Group 1 and Group 2 source regions also effectively rule out direct contamination by outer core metal, as such a contribution would lead to HSE abundances well in excess of the BSE, which is not observed.

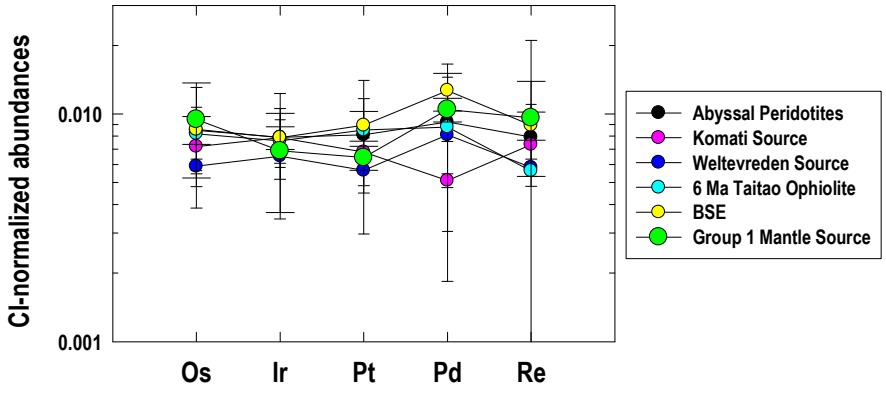

Fig. 5.6. CI chondrite-normalized HSE abundances in the calculated source region of the Gorgona Group 1 komatiites, the BSE estimate of Becker et al. (2006), average modern abyssal peridotites, calculated source regions of the Archean Komati and Weltevreden komatiite suites and average peridotite from the 6 Ma Taitao Ophiolite. Abyssal peridotite values are from Luguet et al. (2001), Alard et al. (2005), Becker et al. (2006), and Liu et al. (2009). Komati and Weltevreden source region data are from Puchtel et al. (2014). Taitao peridotite data are from Schlute et al. (2009). CI chondrite normalizing values are from Horan et al. (2003).

5.5.4. Modeling the Formation of the Gorgona Source Regions

Of the samples analyzed for Re-Os isotope systematics in this study, five have also been previously analyzed for Sm-Nd isotope systematics, including the Group 1 samples GOR537, GOR538, GOR539 (Revillon et al. 2002), and sample GOR156 (Aitken and Echeverria, 1984) and the Group 2 sample GOR47 (Echeverria, 1980). Although there are numerous other published isotopic data for Gorgona rocks, their high level of geochemical diversity calls into question whether these rocks share the same mantle source as those analyzed here. We have, therefore, chosen to direct our modeling based on the five samples, for which both the Sm-Nd and Re-Os data are available.

The chondritic initial $\gamma^{187}Os$ values of the Group 1 komatiites are in contrast to the radiogenic εNd_T values of +9.1 to +10.1. The apparent decoupling of the lithophile element isotope systematics from the Re-Os system has been previously documented in both Gorgona rocks (Walker et al. 1999) and numerous other komatiite localities (Wilson et al. 2003; Gangopadhyay et al. 2006; Puchtel et al. 2004b, 2007, 2009). The nature of this decoupling was tested by applying a mantle melting model.

Similarly to the protocol used to calculate the time-integrated Re/Os ratios, we determined the time-integrated Sm/Nd ratios for these five samples using a Solar System initial $^{143}Nd/^{144}Nd$ of 0.506686 at 4.568 Ga (Bouvier et al. 2008). Calculated time-integrated Sm/Nd and Re/Os ratios for each of these five samples are shown in **Table 5.5**.

Table 5.5. Calculated time-integrated isotopic and elemental ratios for the Gorgona komatiites.

	($^{147}Sm/^{144}Nd$)	($^{187}Re/^{188}Os$)	Sm/Nd	Re/Os	Nd Data Source
GOR537	0.2136	0.4184	0.3389	0.0885	Revillon et al. (2002)
GOR538	0.2138	0.4184	0.3392	0.0885	Revillon et al. (2002)
GOR539	0.2119	0.4201	0.3363	0.0888	Revillon et al. (2002)
GOR156	0.2125	0.4126	0.3371	0.0873	Echeverria (1980)
GOR47	0.2134	0.6143	0.3386	0.1299	Aitken and Echeverria (1984)
PUM	0.2048	0.2426	0.3250	0.0900	

Bulk Silicate Earth (BSE) values are from Hofmann (1988) for Sm/Nd and Becker et al. (2006) for Re/Os.

In contrast to Re/Os, time-integrated Sm/Nd ratios for both Group 1 and 2 samples are indistinguishable, at 0.3378±0.0028 (2SD). A mantle melting model was developed using the primitive upper mantle (PUM) Sm, Nd, Re and Os contents from Hofmann (1988) and Becker et al. (2006) as the starting point. The bulk mantle partition coefficients for Sm and Nd used were 0.037 and 0.023, respectively (Green, 1994), while the Os bulk mantle partition coefficient was taken to be 2.1 (Puchtel and Humayun, 2000). The bulk mantle partition coefficient for Re is dependent on oxygen fugacity, but a value of ~0.2 is most relevant for the modern upper mantle conditions (Mallmann et al., 2007). Batch and fractional melting calculations were performed and the results are shown in **Fig. 5.7**. Both modes of melting can easily produce the time integrated Sm/Nd and Re/Os ratios of the group 1 samples, but the melt fraction extracted must be small, on the order of 0.3%. This model assumes that the melting event occurred early, i.e. at 4.568 Ga and thus represents a lower limit on extent of melting, as later melting events would need to be larger to evolve to the measured $^{187}Os/^{188}Os$ and $^{143}Nd/^{144}Nd$ ratios.

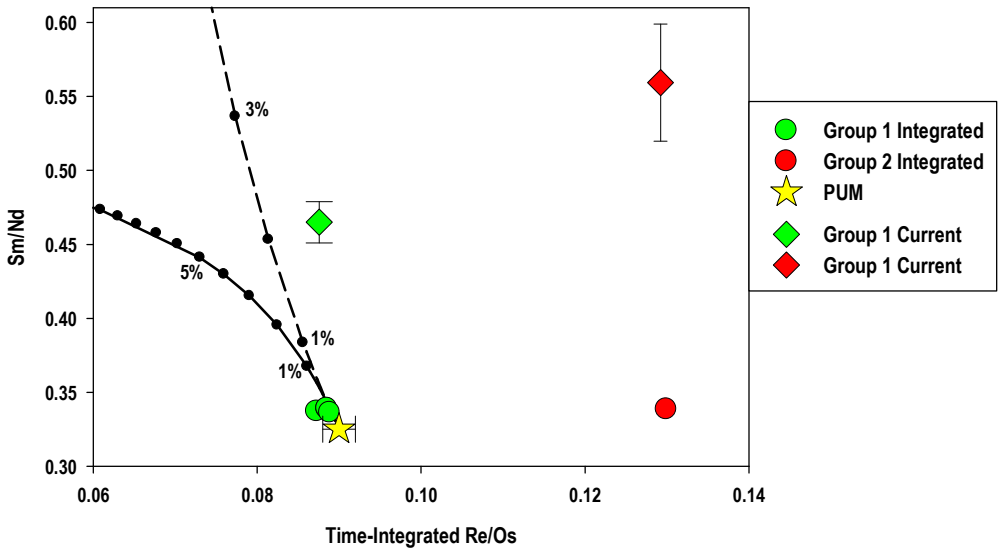

Fig. 5.7. Calculated time-integrated Sm/Nd and Re/Os ratios for the Gorgona Group 1 and 2 komatiites. Also plotted is the Hofmann (1988) and Becker et al. (2006) BSE value for these ratios, and two curves representing batch and fractional melting of the BSE as solid and dashed lines, respectively. Tick marks on the model melting lines indicate 1% melting. Circles show time integrated Re/Os and Sm/Nd for each komatiite group, while diamonds show time-integrated Re/Os and current measured average Sm/Nd for each group. The elevated measured Sm/Nd ratios show that all the source regions experienced melt depletion shortly before komatiite formation. Bulk mantle partition coefficients for Nd and Sm are from Green (1994), for Re from Mallmann et al. (2007), and for Os - from Puchtel and Humayun (2000). See text for additional details.

As Sm and Nd are both incompatible elements, it is unlikely that the Sm/Nd ratio was fractionated during the high-degree melting that produced the komatiites. We can therefore compare the measured Sm/Nd ratios of the Gorgona komatiites with their calculated time-intergrated Sm/Nd ratios. Measured Sm/Nd ratios of 0.465±0.014 (2SD), for Group 1 are significantly higher than their time-integrated ratios. This indicates these source region of the komatiites was depleted in incompatible elements shortly before komatiite formation, possibly in a dynamic melting regime within the same plume that formed the komatiites, as suggested by Arndt et al. (1997).

In contrast to the Group 1 samples, the isotopic signatures of the Group 2 sample GOR47 cannot be generated via melting of a PUM source, as the depleted Sm-Nd systematics are decoupled from the enriched Re-Os systematics. Like the Group 1 samples, the measured present-day Sm/Nd ratio of 0.465±0.014 (2SD) of GOR47 is significantly higher than the calculated time-integrated Sm/Nd of 0.2134, again indicating that LREE depletion occurred shortly before komatiite formation. The Group 2 source region probably experienced a complex history of melting and re-enrichment that de-coupled its long-lived isotopic signatures. It is difficult to model its evolution given the limited number of samples available from this group and the uncertainties regarding their relationship to each other. One possible mechanism for generating the strong decoupling of Re-Os from Sm-Nd shown in the Group 2 source region is sulfide metasomatism transporting HSE without affecting lithophile elements. A similar mechanism was proposed by Luguet et al. (2008) for generating coupled $^{186\text{-}187}Os/^{188}Os$ in plume lavas. Gorgona komatiites show coupled $^{186\text{-}187}Os/^{188}Os$ ratios (Brandon et al. 2003), offering evidence of sulfide metasomatism operating in the source of at least some Gorgona rocks. Any event that was responsible for enrichment of the Group 2 komatiite source region in Re over Os must have occurred early in Earth's history in order to allow for appreciable ingrowth of the radiogenic Os.

5.6. Conclusions

The major, trace, and highly siderophile element abundances, as well as Re-Os isotopic systematics, have been determined for an 89 Ma suite of komatiites from Gorgona Island, Colombia. Eleven samples from the Group 1 komatiites that were related by crystal-liquid

fractionation show that Pd, Pt and Re behaved incompatibly during komatiite lava differentiation, and that the abundances of the HSEs were controlled by igneous processes and not secondary alteration. The Group 1 samples have initial Os isotopic systematics similar to that of chondrites. Two samples from the Group 2 komatiites have been previously shown (Walker et al., 1999) to have highly radiogenic Os isotopic systematics relative to chondrites, and this study confirms that. All samples show largely similar chondrite-normalized HSE patterns, with depletions in Os, Ir and Ru relative to Pt, Pd and Re, and broadly chondritic $(Pd/Pt)_N$ ratios. The source region of the Group 1 komatiites was calculated to have Os, Ir, Pd and Re abundances within error of BSE values, with a slight depletion in Pt. The Group 2 komatiite samples show Pt and Pd abundances in their source region that were considerably lower than the BSE values. The Group 1 komatiite source shows apparently decoupled Nd and Os isotopic systematics that are reconciled with a previous low-degree melting event that occurred early in Earth history. In contrast, the Group 2 komatiite source shows decoupled Nd and Os isotopic systematics that cannot be explained by simple melting of a primitive mantle source and metasomatism decoupling siderophile from lithophile elements is likely required early in Earth history in order to generate the Group 2 source. Additionally, it is unlikely that any of the Gorgona komatiites sampled regions that interacted with the outer core (Brandon et al. 2003) as none of their mantle source regions shows strong enrichments in HSEs. Further work on additional samples from the Group 2 komatiites is necessary to better constrain the isotopic evolution of the Gorgona radiogenic Os endmember, as coupled $^{186\text{-}187}Os/^{188}Os$ ratios in Group 2 komatiites will provide evidence for ancient sulfide metasomatism in their source region.

Acknowledgments for Chapter 5.

This study was supported by NSF EAR 1447174 to I.S. Puchtel. This source of support is gratefully acknowledged. We also thank the Smithsonian Institution National Museum of Natural History and Nick Arndt for providing samples.

References for Chapter 5

-Aitken, B.G., Echeverria, L.M., 1984. Petrology and geochemistry of komatiites and tholeiites from Gorgona island, Colombia. Contributions to Mineralogy and Petrology **86**: 94–105.

-Alard, O., Luguet, A., Pearson, N. J., Griffin, W. L., Lorand, J.-P., Abdelmouhcine, G., Burton, K. W., O'Reilly, S. Y., 2005. *In situ* Os isotopes in abyssal peridotites bridge the isotopic gap between MORBs and their source mantle. Nature **436**: 1005-1008.

-Alvarado, G.E., Denyer, P., Sinton, C.W. 1997. The 89 Ma Tortugal komatiitic suite, Costa Rica: implications for a common geologic origin of the Caribbean and East Pacific region from a mantle plume. Geology, **25**(5): 439-442.

-Archer, G. J., Ash, R. D., Bullock, E. S., Walker, R. J., 2014. Highly siderophile element and ^{187}Re-^{187}Os isotopic systematics of the Allende meteorite: Evidence for primary nebular processes and late-stage alteration. Geochimica et Cosmochimica Acta, **131**: 402-414.

-Arndt, N. T., Kerr, A. C., & Tarney, J., 1997. Dynamic melting in plume heads: The formation of Gorgona komatiites and basalts. Earth and Planetary Science Letters, **146**(1-2): 289-301.

-Arndt, N. T., 1985. Differentiation of Komatiite Flows. Journal of Petrology, **27**(2): 279-301.

-Barnes, S.J., Hill, R.E.T., Gole, M.J., 1988. The Perseverance ultramafic complex, Western Australia: the product of a komatiite lava river. Journal of Petrology 29 (2), 305–331.

-Barnes, S-J., Naldrett, A. J., Gorton, M. P. 1985. The origin of the fractionation of platinum-group elements in terrestrial magmas. Chem. Geol. **53**: 303–23

-Beattie, P., Ford, C., Russell, D., 1991. Partition coefficients for olivine-melt and orthopyroxene-melt systems. Contributions to Mineralogy and Petrology **109** (2): 212-224.

-Becker, H., Horan, M., Walker, R., Gao, S., Lorand, J., & Rudnick, R., 2006. Highly siderophile element composition of the Earth's primitive upper mantle: Constraints from new data on peridotite massifs and xenoliths. Geochimica et Cosmochimica Acta **70**(17): 4528-4550.

-Birck J. L., Roy-Barman M. and Capman F., 1997. Re–Os isotopic measurements at the femtomole level in natural samples. Geostand. Newslett. **20**(1): 19–27.

-Bouvier, A., Vervoort, J.D., Patchett, P.J., 2008. The Lu–Hf and Sm–Nd isotopic com-position of CHUR: constraints from unequilibrated chondrites and implications for the bulk composition of terrestrial planets. Earth Planet. Sci. Lett. **273** (1): 48–57.

-Brandon, A. D., Walker, R. J., Puchtel, I. S., Becker, H., Humayun, M., Revillon, S., 2003. ^{186}Os-^{187}Os systematics of Gorgona Island komatiites: Implications for early growth of the inner core. Earth and Planetary Science Letters **206** (3-4): 411-426.

-Brandon, A.D., Walker, R.J., Morgan, J.W., Norman, M.D., Prichard, H.M., 1998. Coupled ^{186}Os and ^{187}Os evidence for Core-Mantle Interaction. Science **280**: 1570-1573.

-Brenan, J. M., Andrews, D., 2001. High-temperature stability of laurite and Ru-Os-Ir alloy and their role in PGE fractionation in mafic magmas. Can. Mineral. **39,** 341–360.

-Brügmann, G., Arndt, N., Hofmann, A., & Tobschall, H., 1987. Noble metal abundances in komatiite suites from Alexo, Ontario and Gorgona Island, Colombia. Geochimica Et Cosmochimica Acta, **51**(8): 2159-2169.

-Cohen A. S. and Waters F. G., 1996. Separation of osmium from geological materials by solvent extraction for analysis by thermal ionization mass spectrometry. Anal. Chim. Acta **332**(2–3): 269–275.

-Creaser R. A., Papanastassiou D. A. and Wasserburg G. J., 1991. Negative thermal ion mass-spectrometry of osmium, rhenium, and iridium. Geochim. Cosmochim. Acta **55**(1): 397–401.

-Dupre, B., Echeverria, L.M., 1984. Pb isotopes of Gorgona island (Colombia): isotopic variations correlated with magma type. Earth and Planetary Science Letters **67**: 186–190.

-Echeverria, L., 1980. Tertiary or Mesozoic komatiites from Gorgona Island, Colombia: Field relations and geochemistry. Contributions to Mineralogy and Petrology, 253-266.

-Gangopadhyay, A., Walker, R. J., Hanski, E., & Solheid, P. A., 2006. Origin of Paleoproterozoic Komatiites at Jeesiorova, Kittila Greenstone Complex, Finnish Lapland. Journal of Petrology, **47**(4): 773-789.

-Gansser A., Dietrich V.J., Cameron W.E., 1979. Paleogene komatiites from Gorgona Island. Nature **278**: 545-546

-Green T. H., 1994. Experimental studies of trace-element partitioning applicable to igneous petrogenesis – Sedona 16 years later. Chem. Geol. **117**: 1–36.

-Gurenko, A. A., Kamenetsky, V. S., Kerr, A. C., 2016. Oxygen isotopes and volatile contents of the Gorgona komatiites, Colombia: A confirmation of the deep mantle origin of H_2O. Earth and Planetary Science Letters. **454**: 154-165.

-Hauri, E. H., 2002. Osmium Isotopes and Mantle Convection. Phil. Trans. R. Soc. Lond. A **380**: 2371-2382

-Hofmann, A.W., 1988. Chemical differentiation of the Earth: the relationship between mantle, continental crust, and oceanic crust. Earth and Planetary Science Letters **90**: 297–314.

-Horan, M.F., Walker, R.J., Morgan, J.W., Grossman, J.N., Rubin, A.E., 2003. Highly siderophile elements in chondrites. Chemical Geology, **196**(1–4): 5–20.

-Keays, R. R. 1995. The role of komatiitic and picritic magmatism and S-saturation in the formation of ore deposits. Lithos, **34**:1-18.

-Kerr, A. C. 2005. La Isla de Gorgona, Colombia: A petrological enigma? Lithos, **84**(1-2): 77-101.

-Kerr, A. C., Marriner, G. F., Arndt, N. T., Tarney, J., Nivia, A., Saunders, A. D., & Duncan, R. A., 1996. The Petrogenesis of Gorgona Komatiites, Picrites and Basalts: New Field, Petrographic and Geochemical Constraints. Lithos **37:** 245-260.

-Lassiter, J.C., 2003. Rhenium volatility in subaerial lavas: constraints from subaerial and submarine portions of the HSDP-2 Mauna Kea drillcore. Earth and Planetary Science Letters **214**: 311-325.

-Liu, C.-Z., Snow, J. E., Brugmann, G., Hellebrand, E., Hofmann, A. W., 2009. Non-chondritic HSE budget in Earth's upper mantle evidenced by abyssal peridotites from Gakkel ridge (Arctic Ocean). Earth and Planetary Science Letters **283**: 122-132.

-Locmelis, M., Pearson, N.J., Barnes, S.J., Fiorentini M.L., 2011. Ruthenium in komatiitic chromite. Geochimica et Cosmochimica Acta, **75**: 3645-3661.

-Ludwig, K. R., 2003, ISOPLOT 3.00. A geochronological toolkit for Microsoft Excel, Berkeley Geochronol. Cent. Spec. Publ., 4, 70 pp.

-Luguet, A., Pearson, G. D., Nowell, G. M., Dreher, S. T., Coggon, J. A., Spetsius, Z. V., Parman, S. W., 2008. Enriched Pt-Re-Os Isotope Systematics in Plume Lavas Explained by Metasomatic Sulfides. Science **319**: 453-456.

-Luguet, A., Alard, O., Lorand, J. P., Pearson, N. J., Ryan, C., O'Reilly, S. Y., 2001. Laser-ablation microprobe (LAM)-ICPMS unravels the highly siderophile element geochemistry of the oceanic mantle. Earth and Planetary Science Letters **189**: 285-294.

-MacKenzie, J.M., Canil, D., 2006. Experimental constraints on the mobility of Rhenium in silicate liquids. Geochimica et Cosmochimica Acta, **70**: 5236–5245.

-Mallmann, G. & O'Neill, H. St. C., 2007. The effect of oxygen fugacity on the partitioning of Re between crystals and silicate melt during mantle melting. Geochimica et Cosmochimica Acta **71**: 2837-2857.

-Meisel, T., Reisberg, L., Moser, J., Carignan, J., Melcher, F., Brugmann, G., 2003. Re-Os systematics of UB-N, a serpentinized peridotite reference material. Chem. Geol. **201**: 161-179.

-Mertzmann, S. A., 2000. K-Ar results from the southern Oregon - northern California Cascade range. Oregon Geology **62** (4): 99-122.

-Nicklas, R.W**.**, Puchtel, I.S., Ash, R.D., Piccoli, P.M., Hanski, E., Nisbet, E.G., Waterton, P., Pearson, D.G., Anbar, A.D., 2019. Secular Mantle Oxidation across the Archean-Proterozoic Boundary: Evidence from V Partitioning in Komatiites and Picrites. *Geochimica et Cosmochimica Acta* **250**: 49-75.

-Nicklas, R.W., Puchtel, I.S., Ash, R.D., 2018. Redox State of the Archean Mantle: Evidence from V partitioning in 3.5-2.4 Ga Komatiites. Geochimica et Cosmochimica Acta **222**: 447-466

-O'Driscoll, B., Walker, R. J., Day, J. M. D., Ash, R. D., Daly, J. S., 2015. Generations of melt extraction, melt-rock interaction and high-temperature metasomatism preserved in peridotites of the ~497 Ma Leka Ophiolite Complex, Norway. Journal of Petrology **56**(9): 1797-1828.

-Puchtel, I.S. Blichert-Toft, J., Touboul, M., Walker, R.J., 2018. ^{182}W and HSE constraints from 2.7 Ga komatiites on the heterogeneous nature of the Archean mantle. Geochimica et Cosmochimica Acta, (in press)

-Puchtel, I. S., Touboul, M., Blichert-Toft, J., Walker, R. J., Brandon, A. D., Nicklas, R. W., Kulikov, V. S., and Samsonov, A. V., 2016a. Lithophile and siderophile element systematics of the Earth's mantle at the Archean-Proterozoic boundary: Evidence from 2.4 Ga komatiites. Geochimica et Cosmochimica Acta, **180**: 227–255.

-Puchtel, I. S., Blichert-Toft, J., Touboul, M., Horan, M. F., Walker, R. J., 2016b. The coupled ^{182}W-^{142}Nd record of early terrestrial mantle differentiation. Geochemistry, Geophysics, Geosystems. **17** (6): 2168-2193.

-Puchtel I. S., Walker R. J., Touboul M., Nisbet E. G. and Byerly G. R., 2014. Insights into Early Earth from the Pt–Re–Os isotope and Highly Siderophile Element abundance systematics of Barberton komatiites. Geochim. Cosmochim. Acta **125**: 394–413.

-Puchtel, I. S., Blichert-Toft, J., Touboul, M., Walker, R. J., Byerly, G., Nisbet, E. G., Anhaeusser, C. R., 2013. Insights into early Earth from Barberton komatiites: Evidence from lithophile isotope and trace element systematics. Geochimica et Cosmochimica Acta **108**: 63-90.

-Puchtel, I. S., Walker, R. J., Brandon, A. D., Nisbet, E. G., 2009. Pt-Re-Os and Sm-Nd isotope and HSE and REE systematics of the 2.7 Ga Belingwe and Abitibi komatiites. Geochimica et Cosmochimica Acta **73**(20): 6367-6389.

-Puchtel, I.S., Humayun, M., Walker, R.J., 2007. Os-Pb-Nd isotope and highly siderophile and lithophile trace element systematics of komatiitic rocks from the Volotsk suite, SE Baltic Shield. Precambrian Research **158**: 119-137.

-Puchtel, I. S., Humayun, M., 2005. Highly siderophile element geochemistry of ^{187}Os-enriched 2.8 Ga Kostomuksha komatiites, Baltic Shield. Geochimica et Cosmochimica Acta **69**(6): 1607–1618.

-Puchtel, I. S., Humayun, M., Campbell, A., Sproule, R., Lesher, C. M., 2004a. Platinum group element geochemistry of komatiites from the Alexo and Pyke Hill areas, Ontario, Canada. Geochimica et Cosmochimica Acta **68** (6): 1361-1383.

-Puchtel, I.S., Brandon, A.D., Humayun, M. 2004b. Precise Pt-Re-Os isotope systematics of the mantle from 2.7 Ga komatiites. Earth and Planetary Science Letters, **224**: 157-174.

-Puchtel, I.S., Humayun, M., 2000. Platinum group elements in Kostomuksha komatiites and basalts: Implications for oceanic crust recycling and core-mantle interaction. Geochimica et Cosmochimica Acta, **64**(24): 4227-4242.

-Pyke, D.R., Naldrett, A.J. and Eckstrand, O.R., 1973. Archean ultramafic flows in Munro Township, Ontario. Geol. Soc. Am. Bull., **84**: 955-978.

-Rehkamper M. and Halliday A. N., 1997. Development and application of new ion-exchange techniques for the separation of the platinum-group and other siderophile elements from geological samples. Talanta, **44**(4): 663–672.

-Revillon, S., Arndt, N.T., Chauvel, C., Hallot, E., 2000. Geochemical study of ultramafic volcanic and plutonic rocks from Gorgona island, Colombia: the plumbing system of an oceanic plateau. Journal of Petrology **41**: 1127–1153.

-Revillon, S., Chauvel, C., Arndt, N.T., Pik, R., Martineau, F., Fourcade, S., Marty, B., 2002. Heterogeneity of the Caribbean plateau mantle source: heterogeneity of the Caribbean plateau mantle source: Sr, O and He isotopic compositions of olivine and clinopyroxene from Gorgona island. Earth and Planetary Science Letters **205**: 91– 106.

-Roeder, P. L., Emslie, R. F., 1970. Olivine-liquid equilibrium. Contributions to Mineralogy and Petrology **29** (4): 275-282.

-Schlute, R. F., Schilling, M., Anma, R., Farquhar, J., Horan, M. F., Komiya, T., Piccoli, P. M., Pitcher, L., Walker, R. J., 2009. Chemical and chronological complexity in the convecting upper mantle: Evidence from the Taitao Ophiolite, southern Chile. Geochimica et Cosmochimica Acta **73**: 5793-5819.

-Shimizu, K., Shimizu, N., Komiya, T., Suzuki, K., Maruyama, S., Tatsumi, Y., 2009. CO_2-rich komatiitic melt inclusions in Cr-spinels within beach sand from Gorgona Island, Colombia. Earth and Planetary Science Letters **288**: 33-43.

-Shirey, S. B. and Walker, R. J., 1998. The Re–Os isotope system in cosmochemistry and high-temperature geochemistry. Annu. Rev. Earth Planet. Sci. **26**: 423–500.

-Sinton, C.W., Duncan, R.A., Storey, M., Lewis, J., Estrada, J.J., 1998. An oceanic flood basalt province within the Caribbean plate. Earth and Planetary Science Letters **155**, 221– 235.

-Sun, S.S., Nesbitt, R.W., 1978. Petrogenesis of Archaean ultrabasic and basic volcanics: evidence fromrare-earth elements. Contributions to Mineralogy and Petrology 65 (3), 301–325.

-Thompson, P. M. E., Kempton, P. D., White, R. V., Kerr, A. C., Tarney, J., Saunders, A. D., Fitton J. G. and McBirney A, 2003. Hf–Nd isotope constraints on the origin of the Cretaceous Caribbean plateau and its relationship to the Galapagos plume. Earth Planet. Sci. Lett. **217**(1–2): 59–75.

-Walker, R. J., 2016. Geochemical Perspectives: Siderophile Elements in Tracing Planetary Formation and Evolution (1st ed., Vol. 5) (T. Elliott, Ed.). Houton: European Association of Geochemistry.

-Walker, R., Echeverria, L., Shirey, S., & Horan, M., 1991. Re - Os isotopic constraints on the origin of volcanic rocks, Gorgona Island, Colombia: Os isotopic evidence for ancient heterogeneities in the mantle. Contributions to Mineralogy and Petrology: 150-162.

-Walker, R. J., Storey, M., Kerr, A. C., Tarney, J., & Arndt, N. T., 1999. Implications of 187Os isotopic heterogeneities in a mantle plume: Evidence from Gorgona Island and Curaçao. Geochimica Et Cosmochimica Acta, **63**(5): 713-728.

-Wilson, A.H., 2003. A new class of silica-enriched, highly depleted komatiites from Kaapvaal Craton, South Africa. Precambrian Research **127**: 125-141.

Supplemental Material for Chapter 5

Petrography of Eastern Komatiite Samples

Sample GOR152 shows the highest level of alteration of any sample, and consists of sparse ~1 mm thick macroscopic pseudomorphs after spinifex olivine, and also contains ~200 μm euhedral olivines replaced by serpentine. The devitrified glassy groundmass and sparse phenocrysts allow us to classify this sample as a chilled margin. Sample GOR153 contains large (~200 μm) euhedral olivine grains set in a groundmass of clinopyroxene and olivine lathes, and is thus classified as an olivine cumulate. Sample GOR155 consists of ~2 mm long olivine laths, with plagioclase and clinopyroxene laths in the groundmass. Samples GOR156, GOR159 and GOR160 are similar to sample GOR155, except that all of the olivine has been replaced by serpentine pesudomorphs. Sample GOR157 consists of (>200 μm) euhedral pyroxene phenocrysts in a groundmass of devitrified glass with subordinate pyroxene and plagioclase skeletal lathes. GOR155 – GOR160 are therefore classified as spinifex textured komatiites and contain abundant opaque mineral grains, likely chromian spinel.

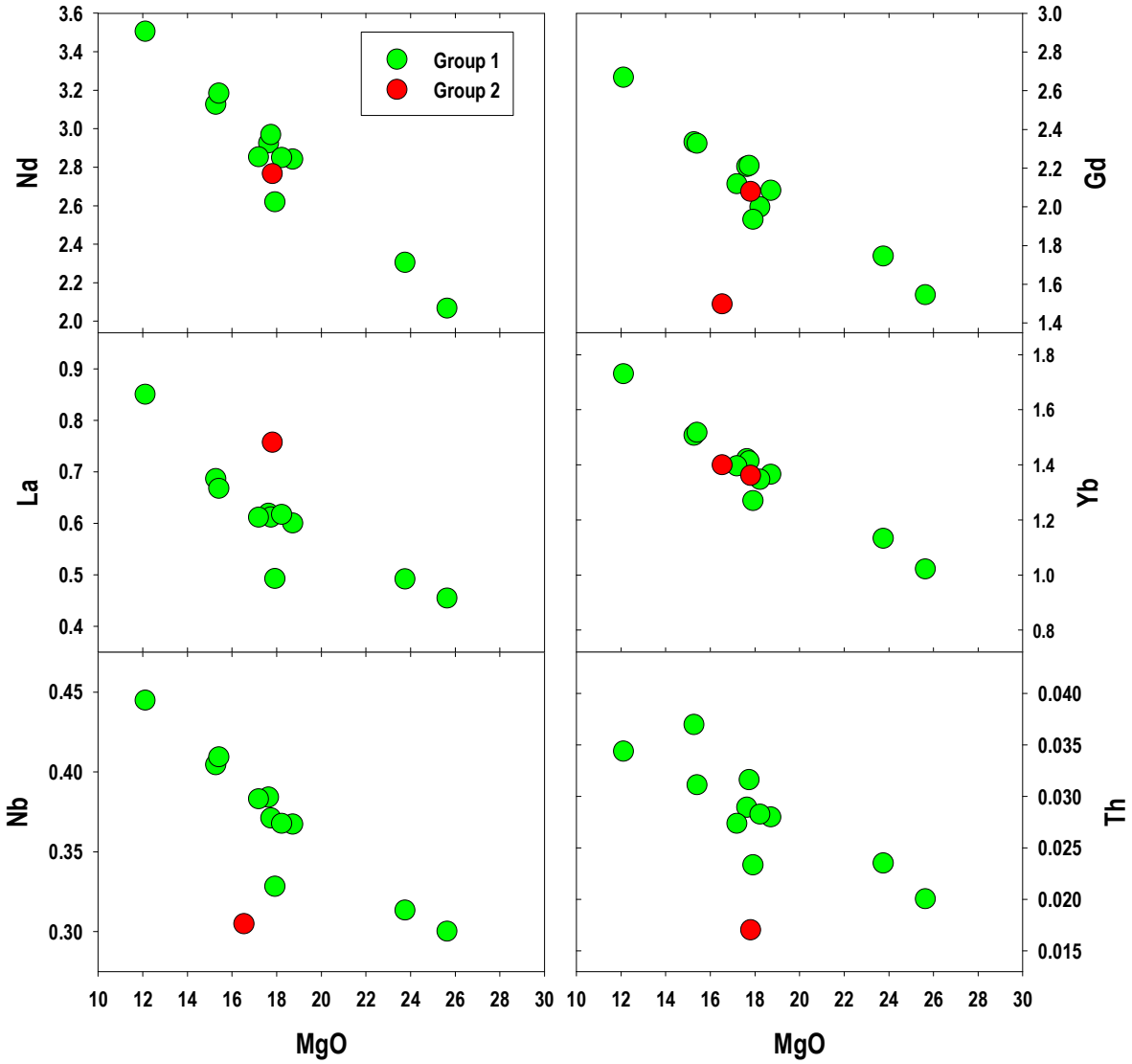

Supplemental Figure 5.1: Abundances of Nd, La, Nb, Gd, Yb, and Th (in ppm) plotted against wt. % MgO for komatiites from Gorgona Island. All these incompatible trace elements show strong negative correlations with MgO for Group 1 samples, while Group 2 samples scatter more widely. Uncertainties are smaller than the size of the symbols. Some Group 2 samples plot outside of the area shown.

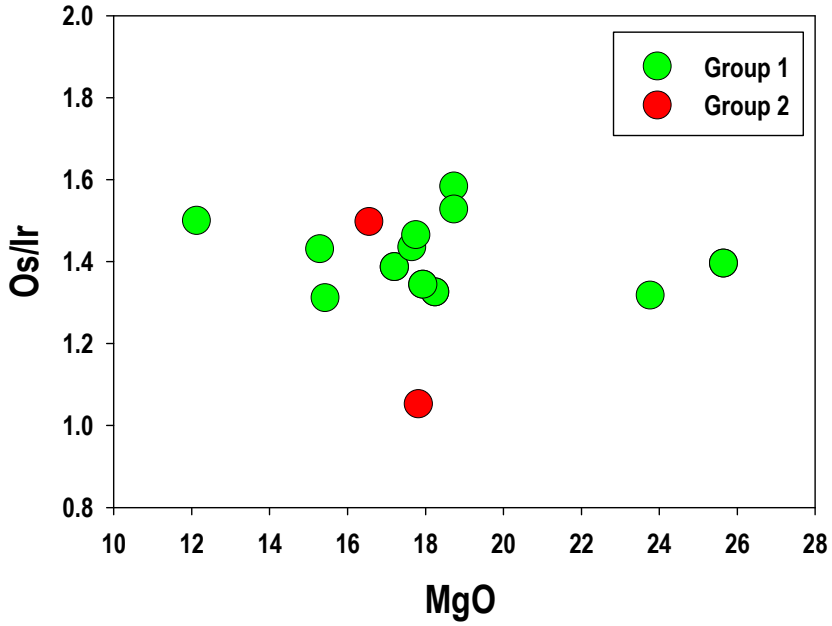

Supplemental Figure 5.2: Os/Ir ratios plotted against weight % MgO komatiites from Gorgona Island. There is no correlation between Os/Ir ratio and MgO in either of the sample sets and they are indistinguishable from each other. Os/Ir ratios for Group 1 samples cluster more closely around a mean value of 1.42 ± 0.18 (2SD).

Chapter 6: Conclusions and Future Work

6.1. Summary of Conclusions

Chapters two through four of this dissertation focused on constraining the redox evolution of the plume-source mantle using the redox-dependent partitioning of V into liquidus olivine in a set of sixteen ultramafic magmatic systems ranging in age from 3.55 Ga to modern. This V-partitioning method was refined over the course of this study to give typical precision on oxygen fugacity measurements of ~±0.30 log units relative to the fayalite-magnetite-quartz (FMQ) mineral buffer. Although a restricted set of komatiites ranging in age from 3.48-2.41 Ga all have measured oxygen fugacities overlapping within uncertainties, the full data set shows that there is a resolvable oxidation trend of 1.33±0.43 log units ΔFMQ over 1.61 Gyr of Earth's history. This oxidation trend is within errors of the 0.93±0.55 log unit difference between modern MORB and Archean MORB-like rocks shown by Aulbach and Stagno (2016). The lack of correlation of measured fO_2 with bulk lava chemistry or temperature indicates that the oxidation trend likely reflects oxidation of the accessible upper mantle. The rocks formed by hot plumes and decompression melting (Aulbach and Stagno, 2016) show a similar oxidation trend, lending strength to this conclusion.

Three possible mechanisms for the observed mantle oxidation were considered. Recycling of oxidized surficial materials and venting of oxygen from the outer core were determined to be unlikely mechanisms for explaining the trends in the data. Complete mantle mixing leading to homogenization of magma ocean-associated redox heterogeneities is the mechanism that best fits the available constraints. The strongest evidence supporting this mechanism is the relatively high oxidation state of the 3.55 Ga Schapenburg komatiite system, as

the mantle source region of this system has been shown to have resided in the lower mantle during crystallization of a terrestrial magma ocean, and was then preserved unmixed until 3.55 Ga (Puchtel et al., 2016). The oxygen fugacity of the Schapenburg system is considered to be direct evidence that early-formed redox heterogeneities persisted until at least 3.55 Ga, lending further credence to the proposed mechanism.

Chapter 5 examined the HSE and Os isotopic systematics of 89 Ma Gorgona Island komatiites, including all of the Gorgona samples studied for their oxygen fugacity in Chapter 4. The previously studied subset of komatiites were shown to have broadly chondritic Os isotopic systematics and bulk silicate earth (BSE)-like HSE abundances in their source region, validating their use to constrain the oxygen fugacity of the bulk mantle. Two komatiite samples that were not analyzed for their oxygen fugacity were confirmed to have highly radiogenic Os systematics as previously shown by Walker et al. (1999). These two samples were also shown to sample a mantle region depleted in Pt and Pd relative to BSE. A mantle melting model utilizing literature Nd isotopic data demonstrated that the chondritic komatiite group shows coupled Os-Nd isotopic systematics. In contrast, the two radiogenic samples show a strong decoupling between the two isotope systems, the reasons for which merits further study.

6.2 Suggestions for Future Work

Although the mantle oxidation trend shown by the data in this thesis is an exciting conclusion, further work is necessary to contextualize and extend this dataset. Firstly, although it has been shown that mantle oxidation by as little as ~0.50 log unit is sufficient to trigger the

GOE (Holland, 2002), rigorous atmospheric modeling using both our dataset and the Aulbach and Stagno (2016) dataset are necessary to further clarify the relationship between mantle and atmospheric oxidation.

A major issue in mantle oxidation studies is the offset between the oxidation state of lavas determined by V-partitioning into olivine and that determined by $Fe^{+3}/\Sigma Fe$ systematics, the reasons for which are currently unclear (Mallmann and O'Neill 2013). This is exemplified by the offset between the oxidation state of MORB determined by V-partitioning at +0.60±0.15 ΔFMQ (Nicklas et al., 2018) and the canonical MORB oxidation state determined by $Fe^{+3}/\Sigma Fe$ systematics of +0.1 ΔFMQ (Berry et al., 2018). A resolution to this problem will require determination of oxygen fugacity by both methods in modern, unaltered rocks, such as MORB, to determine if the offset between the two oxybarometers is systematic or random. Additionally, the MORB oxidation state determined by V-partitioning relies on only four published analyses, and a systematic survey of MORB using this oxybarometer is necessary. An important nuance of this problem is the potential for the two oxybarometers to record the oxygen fugacity of a melt at different stages in its evolution, i.e. during early olivine crystallization vs. late quenching of glass.

Although we have already determined the oxidation state of ten ultramafic systems that are Paleoproterozoic or older, there remain many Archean cratons from which no systems have been analyzed. Recognition of komatiites of low-metamorphic grade that retain unaltered olivine in Archean rocks from areas such as the Pilbara, Yilgarn, Nain, São Francisco, West

African, Amazonian, North China, South China and Dharwar cratons will supplement the current dataset and test whether the mantle oxidation trend obtained in this study is truly global in nature. Although the vast majority of Precambrian komatiites and picrites do not preserve igneous olivine, igneous olivine was found in both the Winnipegosis komatiites and Onega Plateau picrites over the course of this study. Careful examination of both surface outcrop and drill core samples may yield additional komatiites flows with a sufficiently high degree of preservation.

Finally, it is important to test whether oxidation state varies between mantle derived rocks that appear to sample different isotopic end-members, such as the canonical DMM, EM1, EM2, and HIMU of Zindler and Hart (1986). The ideal locality to test this is Gorgona Island, as the igneous rocks on the island show both an excellent state of preservation and a very high degree of isotopic variability (Kerr, 2005). Identification of the oxidation state of different mantle end-members within a single system would offer important constraints on the identity of said end-members, especially as recycled materials, such as oceanic crust or sediments, are expected to be significantly more oxidized than ambient mantle peridotite. Oxygen fugacity could serve as an important additional parameter to evaluate the origin of ocean island basalt lavas, along with the existing long- and short-lived isotope systems.

With regard to the Re-Os isotopic and HSE systematics of Gorgona island lavas, additional work on new samples is also needed. Further sampling of Gorgona komatiites with highly radiogenic Os isotopic signatures, especially those related by crystal-liquid fractionation,

will allow better constraints to be placed on their source region HSE content and will allow an evaluation of their source region's oxygen fugacity. As the mechanism for forming such highly radiogenic Os isotopic signatures remains unclear, more lithophile isotope measurements, such as Lu-Hf and U-Pb in radiogenic samples, are also necessary to constrain the origin of this signature. This work will likely require additional field work on Gorgona Island which will sample more komatiites related by crystal-liquid fractionation.

References for Chapter 6

-Aulbach, S., and Stagno, V., 2016. Evidence for reducing Archean ambient mantle and its effects on the carbon cycle. Geology **44**: 751-754.

-Berry, A. J., Stewart, G. A., O'Neill, H. St.C., Mallmann, G., Mosselmans, J.F.W., 2018. A re-assesment of the oxidation state of iron in MORB glasses. Earth Planet. Sci. Lett. **483**: 114-123.

-Holland, H.D., 2002. Volcanic gases, black smokers, and the great oxidation event. Geochimica et Cosmochimica Acta **66**(21): 3811-3826.

-Kerr, A. C. 2005. La Isla de Gorgona, Colombia: A petrological enigma? Lithos, **84**(1-2): 77-101.

-Mallmann G. and O'Neill H. St. C. (2013) Calibration of an empirical thermometer and oxybarometer based on the partitioning of Sc, Y and V between olivine and silicate melt. *J. Petrol.* **54,** 933–949.

-Nicklas, R.W., Puchtel, I.S., Ash, R.D., 2018. Redox State of the Archean Mantle: Evidence from V partitioning in 3.5-2.4 Ga Komatiites. Geochimica et Cosmochimica Acta **222**: 447-466

-Puchtel, I. S., Blichert-Toft, J., Touboul, M., Horan, M. F., Walker, R. J., 2016b. The coupled ^{182}W-^{142}Nd record of early terrestrial mantle differentiation. Geochemistry, Geophysics, Geosystems. **17** (6): 2168-2193.

-Walker, R. J., Storey, M., Kerr, A. C., Tarney, J., & Arndt, N. T., 1999. Implications of 187Os isotopic heterogeneities in a mantle plume: Evidence from Gorgona Island and Curaçao. Geochimica Et Cosmochimica Acta, **63**(5): 713-728.

-Zindler, A., Hart, S., 1986. Chemical Geodynamics. Ann. Rev. Earth Planet. Sci. **14**: 493-571.